Imperial College London

A non-classical role for polycomb repressive complex 2 in co-ordinating adherens junctions and canonical Wnt signalling in embryonic stem cells and differentiation

Ceris Ifan Owen

A thesis submitted to Imperial College London

for the degree of Doctor of Philosophy

Lymphocyte Development Group

MRC London Institute for Medical Sciences

Imperial College School of Medicine

May 2021

'Yr hen a ŵyr a'r ieuanc a dybia'

Welsh proverb meaning 'the old know what the young suspect'

"It ain't what you don't know that gets you in trouble.

It's what you know for sure that just ain't so"

Mark Twain

I, Ceris Ifan Owen, declare that this thesis is my own work and that work performed by others has been acknowledged and appropriately referenced in the text.

Abstract

Polycomb repressive complex 2 (PRC2) has a well characterised role in maintaining gene silencing and is essential for normal development, tissue homeostasis and is frequently dysregulated in cancer. The classical role of PRC2 is to catalyse post-translational modification of histone tails, with tri-methylation of Histone 3 lysine 27 strongly associated with gene silencing. Recent studies have highlighted additional non-classical roles for PRC2 including methylation of non-histone substrates, direct transcriptional activation and association with cell signalling cascades. Here I show that loss of core PRC2 components results in reduced Wnt signalling in embryonic stem cells (ESCs). Mouse ESCs that lack Suz12 show virtually undetectable canonical Wnt signalling. ESCs lacking Suz12 fail to differentiate. Intriguingly, efficient downregulation of pluripotency genes, but failure of induction of lineage specific genes is observed. In addition to the contribution to canonical Wnt signalling, β-catenin also complexes with E-cadherin at cell surface adherens junctions. Importantly, altered E-cadherin localisation is observed in PRC2 null ES cells. E-cadherin localisation is normalised at cell-cell contacts between PRC2 mutant and wild type ES cells when grown together. Normalisation of E-cadherin localisation occurs concomitant to reestablishment of canonical Wnt signalling, and rescue of neuronal differentiation.

The dual residency protein Afadin, a constituent of the intracellular adherens junction complex is also shown to have altered subcellular localisation in the absence of Jarid2 or Suz12. Taken together these results suggests a potential non-classical role for PRC2 in regulation of the adherens junctions, which in turn modifies the contribution of cadherin associated β-catenin to Wnt signalling, and differentiation.

Acknowledgments

I would like to thank both Mandy and Matthias, not only for their invaluable guidance throughout this project, but also for their compassion and understanding during a family bereavement early in my time with the lymphocyte development group. Their thoughtfulness during this difficult time will remain with me. Also, I would like to thank them for their sympathetic understanding of my bleary-eyed state following the arrival of my firstborn.

Thanks also to all members of the Lymphocyte development group, past and present for help and support. I'd particularly like to thank Andy Malinowski for taking me under his wing at the beginning of the project. Thanks also to Felix, Stephan, Sergi, Chiara, Irene, Karen, Andrew, Matt, Amelie, Alessandra, Jocelyn and Ludovica for discussions, coffee and the occasional beer. I would also like to thank the members of the flow cytometry group, Bhavik, Thomas and particularly James for his enduring support with this project and good grace when Sheffield United edged out Leeds United in the promotion race of 2018/19 (at the time of writing Leeds are firmly ensconced in the premier league, so all's well that ends well in that regard, well, for Leeds at least…). Additionally, I would like to thank the transgenic facility for their support with the blastocyst injections, particularly Zoe and Elodie. Thanks also to the Mass Spectrometry facility, especially Holger and Illyana for their help and the many patient discussions we had during this project. Thanks to Chad of the imaging facility. Thanks also to the Lamond group in Dundee for their help and for looking after me during my visit, particularly Tony, Sara and Angus. Finally, thanks to Jane, Finlay and latterly little Seren for keeping me going with hugs, laughs and espressos throughout the project and the write up.

Table of contents

Table of Contents

Figures and tables

List of Figures

List of Tables

Abbreviations

AACR	American association of cancer research
ADP	Adenosine diphosphate
Adt2	ADP/ATP translocase 2
Aebp2	Adipocyte enhancer binding protein 2
AlyRef	Aly/REF exporter protein
AML	Acute myeloid leukaemia
APC	Adenomatous polyposis coli
AR	Androgen reception
ATCC	American type culture collection
ATP	Adenosine triphosphate
ATRA	All-trans retinoic acid
Bcl9	B-cell CLL/Lymphoma protein 9
bFGF	Basic fibroblast growth factor
Brg1	Brahma related gene 1
BSA	Bovine serum albumin
Cas9	CRISPR-associated protein 9
CBP	CREB-binding protein
Cbx	Chromobox protein homologue
CGI	CpG islands
ChIP	Chromatin immunoprecipitation
CK	Casein kinase 1
CK2α	Casein kinase 2-alpha
CLL	Chronic lymphocytic leukaemia
CML	Chronic myeloid leukaemia
COMPASS	Complex proteins associated with Set1
cPRC1	Canonical polycomb repressive complex 1
CRISPR	Clustered Regularly Interspersed Palindromic Repeats
CSCs	Cancer stem cells
CTCF	CCCTC binding factor

DAPI	4’, 6-diamidino-2-phenylindole
DIPG	Diffuse intrinsic pontine glioma
DKK-1	Dickkopf 1
DLBCL	Diffuse large B-cell lymphoma
DMEM	Dulbecco’s Modified Eagles Media
DMSO	Dimethyl sulphoxide
DNA	Deoxyribonucleic acid
Dnmt3	DNA methyl-transferase
DTT	Dithiothreitol
Dvl1	Dishevelled 1
EDTA	Ethylnediaminetetraacetic acid
Eed	Embryonic ectoderm development protein
eEF1A1	Eukaryotic translation elongation factor 1 alpha 1
EGF	Epidermal growth factor
eGFP	Enhanced green fluorescent protein
EMT	Epithelial-mesenchymal transition
EpiSC	Epiblast derived stem cell
EPOP	Elongin BC and polycomb repressive complex 2 associated protein
ESC	Embryonic stem cell
Ezh1/2	Enhancer of zeste 1/2
FACS	Fluorescent activated cell sorting
FAP	familial adenomatous polyposis
FCS	Fetal calf serum
FDA	(United States) Food and Drug Administration
FDR	False discovery rate
Fgf	Fibroblast growth factor
Fl	follicular lymphoma
Frz	Frizzled
GATA4/6	GATA binding protein 4/6
GFP	Green fluorescent protein
GMEM	Glasgow’s minimal essential media
Gsk3β	Glycogen synthase kinase 3 beta

H2A	Histone 2A
H2A119ub	Histone 2A, lysine 119 monoubiquitination
H3K27me1	Histone 3 lysine 27 monomethylation
H3K27me2	Histone 3 lysine 27 dimethylation
H3K27me3	Histone 3 lysine 27 trimethylation
H3K36me2	Histone 3 lysine 36 dimethylation
H3K36me3	Histone 3 lysine 36 trimethylation
H3K4me3	Histone 3 lysine 4 trimethylation
H3S10p	Histone3 at the serine 10 residue
HDAC	Histone deacetylase
HEPES	Hydroxyethylpiperazine ethane sulphonic acid
HOTAIR	*HOX* transcript antisense RNA
HOX	Homeobox
ICM	Inner cell mass
IF	Immunofluorescence
IMDM	Iscove's modified Dulbecco's media
JAK	Janus kinase
Jarid2	Jumonji and AT-rich interacting domain 2
Kb	Kilobase
kDa	Kilodalton
Kdm2a/b	lysine demethylase 2a/b
LDS	Lithium dodecyl sulphate
Lef	lymphoid enhancer factor
LFQ	label-free-quantification
LIF	leukaemia inhibitory factor
LIMS	London Institute for Medical Sciences
lncRNA	Long non-coding RNA
Lrp5/6	low-density lipoprotein receptor-related proteins 5/6
mESCs	Mouse embryonic stem cells
Mll2	Mixed lineage leukaemia 2
MOPS	3-(N-Morpholino)propanesulfonic acid
MPNST	malignant peripheral nerve sheath tumour

MRC	Medical Research Council
mRNA	Messenger RNA
Mtf2	Metal response element binding transcription factor 2
ncPRC1	Non-canonical polycomb repressive complex 1 (ncPRC1)
NF-κB	Nuclear factor kapa-light-chain enhancer of B-cells
NHS	(United Kingdom) National Health Service
NICE	(United Kingdom) National institute of health and care excellence
NK/T-ALL	Natural killer cell/ T-cell acute lymphoblastic leukaemia
nM	Nanomolar
NMDA	N-methyl-D-aspartate
NrOb1	Nuclear receptor subfamily 0 group B member 1
Oct4	Octamer binding transcription factor 4
Otx2	Orthodenticle homeobox 2
PAGE	polyacrylamide gel electrophoresis
Pax6/7	Paired box protein 6/7
PBS	Phosphate buffered saline
PcG	Polycomb group
Pcgf	polycomb group ring finger
PCR	Polymerase chain reaction
PGK	Phosphoglycerate kinase
Phc	Polyhomeotic-like protein
Plc	Polycomb-like protein
PLZF	Promyelocytic leukaemia zinc finger protein
PRC1	Polycomb repressive complex 1
PRC2	Polycomb repressive complex 2
PRC2.1	Polycomb repressive complex 2.1
PRC2.2	Polycomb repressive complex 2.2
PREs	Polycomb response elements
PTM	Post-translational modification
Rbbp4/6	RB-binding protein 4/6
Rex1	Reduced expression protein 1
Ring1/2	Ring finger protein 1/2

RNA	Ribonucleic acid
RNA Pol II Ser2P	RNA polymerase 2, serine 2 phosphate
RNA Pol II Ser5P	RNA polymerase 2, serine 5 phosphate
RORα	Retinoic acid related orphan receptor alpha
rtPCR	reverse transcriptase PCR
Ryb	Ring1 and YY1-binding protein
SD	Standard deviation
SDS	Sodium dodecyl sulphate
SE	Standard error
SET	Su(var)3-9, Enhancer of zeste, Trithorax
Smad4	Mothers against decapentaplegic homologue 4
Smyd2	SET and MYND containing protein 2
Sox2	(sex determining region Y)-box2
STAT3	Signal transducer and activator of transcription 3
Suz12	Suppressor of zeste 12
TAD	Topological associated domain
TCA	Trichloroacetic acid
TCF	T-cell factor
TEAB	Triethylammonium bicarbonate
TGF-β	Transforming growth-factor beta
TRIS	Tris(hydroxymethyl)aminomethane
Tuj1	Neurone specific class III beta-tubulin
UIM	Ubiquitin interaction motif
USP	Ubiquitin carboxyl-terminal hydrolase-1
WT	Wild-type
Xi	X-chromosome inactivation
XIST	X-specific inactive transcript
Yaf2	YY1-associated factor 2
Zic1	Zinc finger of cerebellum family member 1

1. Introduction

The body is composed of integrated organ systems, which are themselves composed of multiple specialized cell types. Estimates of the total number of different cell types in the human body range from 200 to many thousands depending the interpretation of cell type boundaries, and the specific methodologies used (Roy and Conroy 2018). Each of these cell types must arise from a single fertilised cell, and acquire and maintain exquisitely controlled gene expression profiles during lineage commitment. That multicellular organisms are able to generate these varied cell types from an essentially invariant genome relies in part, on the capacity of cells to segregate the genome into active and repressed domains. Epigenetic mechanisms, heritable changes in gene expression which do not alter primary DNA sequence, contribute to the development and stability of cell type-specific gene expression programs, and permit these programs to be faithfully transmitted over multiple cell divisions (Fisher, Stumpf, and Merkenschlager 2017). In eukaryotes modifications such as methylation of cytosine residues (Bird 2002), post-translational modifications of histones, (Turner 2002), alterations to nucleosome spacing (Baldi 2019), and the organisation of genome folding in 3D space (Pombo and Dillon 2015) contribute to the development and maintenance of cell-type gene specific expression programmes. Furthermore, these modifications are not only critical to cell-fate decisions, differentiation and tissue homeostasis, but are also implicated in numerous disease states, and in the development of many malignancies (Virani et al. 2012).

1.1 The Polycomb Repressive Group

The Polycomb group (PcG) are a large family of evolutionarily conserved proteins which contribute to the maintenance of transcriptional repression in a cell-type specific manner catalysing post-translational modification to histone tails (Scelfo, Piunti, and Pasini 2015; Schuettengruber et al. 2017). The activity of PcG was first reported in *Drosophila melanogaster*, along with its antagonistic complex, trithorax, as regulating segmentation during early development by temporal and spatial silencing of the homeotic gene cluster (Lewis 1978; Paro 1995). The PcG has subsequently been identified in plants, insects and vertebrates (Schwartz and Pirrotta 2013). In metazoans the polycomb proteins form two distinct multiprotein complexes, Polycomb repressive complex (PRC) 1 and 2, each of which can be further subdivided on the basis of interactions with additional ancillary proteins, which are increasingly recognised to play important and distinct roles in polycomb function (Figure 1.1)

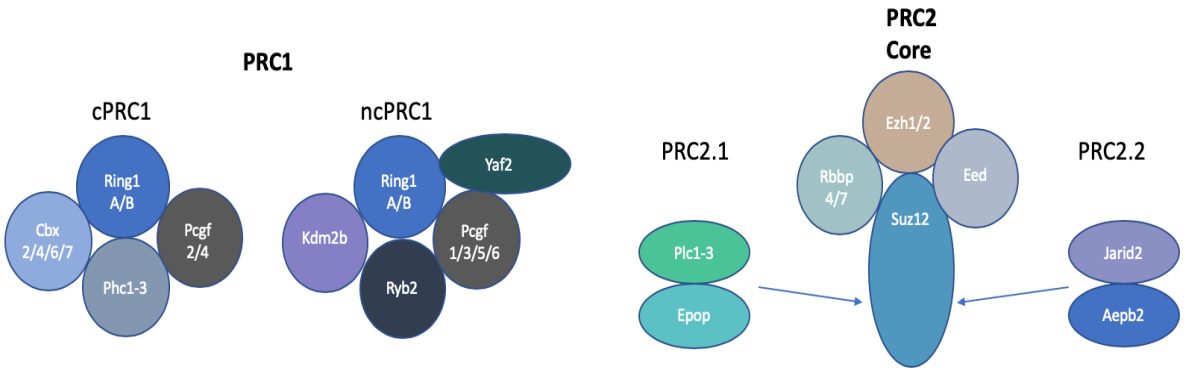

Figure 1.1. Polycomb repressive complex 1 and 2 with associated non-core sub units

Schematic representation of PRC 1, subdivided into canonical (cPRC1) and non-canonical (ncPRC1). The PRC1 E3 ubiquitin ligase core component Ring1a or Ring1B catalyses monoubiquitylation of Histone 2A, lysine 119. ncPRC1.1 shown with interacting Kdm2b, absent from other ncPRC1 complexes (i.e., ncPRC1.2, 1.5 and 1.6)

Schematic representation of core components of PRC2 with associated non-core sub units which make up PRC2.1 and PRC2.2 respectively. The PRC2 histone methylase component (Ezh1 or Ezh2), is responsible for mono-, di- and tri-methylation of Histone 3, lysine 27.

Abbreviations; Adipocyte enhancer binding protein 2 (Aebp2), Chromobox protein homologue (Cbx), embryonic ectoderm development protein (Eed), elongin BC and polycomb repressive complex 2 associated protein (Epop), enhancer of zeste1/2 (Ezh1/2), lysine demethylase 2b (Kdm2b), Jumonji and AT-rich interacting domain 2 (Jarid2), polycomb group ring finger (Pcgf), polyhomeotic-like protein (Phc), polycomb-like protein (Plc), RB-binding protein (Rbbp), Ring1 and YY1-binding protein (Ryb), Ring finger protein (Ring), Suppressor of zeste (Suz12), YY1-associated factor 2 Yaf2

Polycomb repressive complex 1 can broadly be divided into canonical (cPRC1) and non-canonical (ncPRC1) groups. All PRC1 complexes contain either Ring1a or Ring1b, the core catalytic E3 ubiquitin ligase, which catalyses ubiquitination of histone 2A at lysine 119 (H2A119ub) (Chittock et al. 2017). Canonical PRC1 complexes encompass a Cbx chromodomain containing sub-unit (either Cbx2/4/6/7/8), in addition to Pcgf2/4 and a polyhomeotic homologous protein (Phc1-3) (Gao et al. 2012; Schuettengruber et al. 2017). In contrast, Non-canonical PRC1 consists of Ring 1A or 1B, complexed with Ryb2, its paralogue Yaf2, and either Pgcf1, 3, 5 or 6 to form ncPRC1.1, 1.3, 1.5 and 1.6 respectively (Vidal and Starowicz 2017). ncPRC1.1 complexes with the histone demethylase Kdm2b in place of the Cbx subunit seen in cPRC1, resulting in altered chromatin targeting (Farcas et al. 2012). Furthermore, ncPRC1 complexes interact with additional proteins in substoichomtertic ratios, further adding complexity (Schuettengruber et al. 2017; Kang and Chun 2020).

The core components of PRC2 are conserved from Drosophila to mammals, and comprise enhancer of zeste homologue 1 or 2 (Ezh1/2), suppressor of zeste 12 (Suz12), embryonic ectoderm development protein 1 (Eed) and retinoblastoma binding protein 46 or 48 (Rbbp4/7) (Schuettengruber et al. 2017). The conserved SET (Su(var)3-9, Enhancer of zeste, Trithorax) domain of Ezh1/2 is the catalytic core of the PRC2 complex, functioning as a lysine methyl-transferase, which methylates histone 3 at lysine 27 (H3K27me) (Cao et al. 2002). The catalytic activity of Ezh2 is autoinhibited, and requires interaction with Eed and Suz12 *in vivo* for stabilisation and catalytic activity (Wu et al. 2013; Antonysamy et al. 2013). Additionally, the core PRC2 complex associates with additional accessory proteins at sub-stoichiometric ratios. Comprehensive proteomic analysis of PRC2 has identified two mutually exclusive PRC2 assemblies; PRC2.1 associated with one of three polycomb-like homologues (Pcl1-3, also referred to as PHF1, MTF2 and PHF19 respectively) together with Epop or Pali1, and PRC2.2

associated with both Jarid2 and Aebp2 (Hauri et al. 2016). Recent studies have contributed to the understanding of the role of PRC2 subcomplexes in the regulation of PRC2 chromatin targeting and regulation of catalytic activity (van Mierlo et al. 2019).

The most intensively characterised role of polycomb complexes are to catalyse post translational modifications to exposed histone tails. Post-translational modifications to histone tails correlate with transcriptional activity; specifically, ubiquitination of histone 2A lysine 119 (H2A119ub) catalysed by PRC1, and trimethylation of Histone 3 lysine 27 (H3K27Me3) catalysed by PRC2, are strongly associated with maintaining gene silencing (Jones and Wang 2010; Blackledge, Rose, and Klose 2015; Schuettengruber et al. 2017). PRC2 is the only known methyltransferase with activity at lysine 27 of histone 3, and disruption of PRC2 results in total ablation of H3K27 adornments (Hojfeldt et al. 2018; Oksuz et al. 2018). PRC2 can catalyse mono-, di- and tri-methylation (H3Kme1/2/3) in a stepwise fashion at H3K27 (Laugesen, Højfeldt, and Helin 2019). PRC2 shows greatest efficiency for mono- and di-methylation steps, with the trimethylation step requiring a greater chromatin occupancy time (Sneeringer et al. 2010). Additionally, the different methylation levels (H3Kme1/2/3) show characteristic genomic distributions (Laugesen, Højfeldt, and Helin 2019). Mono-methylation at lysine 27 is enriched within gene bodies of actively transcribed genes, and is present on 5-10% of all histone 3 proteins in mouse embryonic stem cells. Lysine 27 di-methylation is most broadly distributed, adorning at least 50% of histone 3 proteins, and enriched throughout intra- and intergenic regions. Trimethylation of histone 3, lysine 27 overlaps with genomic PRC2 binding sites, and is strongly associated with maintenance of PRC2 mediated gene repression. Given the critical role of gene silencing in development, significant efforts have focussed on elucidating the role of alternate Polycomb subcomplexes and the mechanisms that govern polycomb recruitment and enzymatic

activity. Recently, additional novel roles for polycomb complexes in development and cancer have been proposed (Chan and Morey 2019). This study focusses predominantly on PRC2 and its interacting partner Jarid2, and examines their role in ESC differentiation and early development.

1.1.1. PRC2.2 and Jarid2

Multiple PRC2 interacting proteins have been identified, that occur in sub-stoichiometric ratios (Hauri et al. 2016). The PRC2.2 component Jarid2 is of particular interest to our group, not least because our group were among the first to report the interaction between Jarid2 and PRC2 (Landeira et al. 2010). Jarid2 was first reported as a regulator of neural tube formation in mice (Takeuchi et al. 1995). It shares homology with the Jumonji family of histone demethylases, however amino acid changes to the catalytic domain of Jarid2 are predicted to ablate the demethylase activity (Klose, Kallin, and Zhang 2006). Jarid2 deficiency is embryonically lethal with developmental defects of the heart, neural tube, liver and spleen (Jung, Mysliwiec, and Lee 2005). An interaction between Jarid2 and PRC2 in mESCs was reported by several groups independently around a decade ago (Landeira et al. 2010; Pasini et al. 2010; Shen et al. 2009; Li et al. 2010; Peng et al. 2009). Jarid2 is highly expressed in mESCs, with a reported down-regulation in lineage committed cells (Zhang et al. 2011). However, a recent study has implicated a novel truncated form of Jarid2 in lineage committed keratinocytes, with a reported role in activation of polycomb target genes during differentiation (Al-Raawi et al. 2019).

Jarid2 was implicated in PRC2 recruitment to chromatin, as mESCs lacking Jarid2 demonstrate reduced occupancy of PRC2 on chromatin (van Mierlo et al. 2019). Jarid2 has weak non-

sequence-specific DNA binding properties *in vitro*, however the importance of this *in vivo* is yet to be determined (Patsialou, Wilsker, and Moran 2005). Additionally, Jarid2 can bind H2AK119ub through its ubiquitin interacting motif (UIM) domain, suggesting that Jarid2 may have a role in recruitment of PRC2 targeted by PRC1 (Cooper et al. 2016). This is supported by the observation that PRC2 recruitment in X inactivation is preceded by PRC1 deposition of H2AK119ub (Żylicz et al. 2019). Furthermore, recent crystallographic structures of PRC2 complexed with Jarid2 indicate that methylated Jarid2 activates Ezh2 via the WD40 domain of Eed (Kasinath et al. 2018). It has been suggested that this binding results in activation of PRC2 activity, in a mechanism analogous to H3K27me3 binding by EED WD40 domain (Chen, Jiao, et al. 2018). Intriguingly however, loss of Jarid2 from mESCs results in mild and inconsistent changes in H3K27me3 deposition (Landeira and Fisher 2011). Notably, while some reports have shown depleted H3K27me3 deposition (Landeira et al. 2010; Pasini et al. 2010), other reports show increased deposition (Shen et al. 2009) and one report shows unchanged global levels but altered targeting of H3K27me3 deposition (Peng et al. 2009). Furthermore, PRC2 components can still be recruited their genomic targets in Jarid2-null mESCs (Landeira and Fisher 2011). This has led to the suggestion that Jarid2 may have a role outside the context of PRC2-mediated methylation of histones. Recent studies have also shown potential redundancy between PRC2.1 and PRC 2.2. The loss of either Jarid2 or Mtf2 results in only mild changes to H3K27me3, but double knockout of Jarid2 and Mtf2 resulted in ablated PRC2 recruitment to target genes (Oksuz et al. 2018). It has been suggested that Mtf2 and Jarid2 are responsible for targeting PRC2.1 and PRC2.2 to chromatin respectively (van Mierlo et al. 2019).

A recent report from our group has also implicated Jarid2 in co-ordination of Nanog and canonical Wnt signalling in mESCs (Landeira et al. 2015). Jarid2-null cells readily able to self-

renew, but are severely compromised in their ability to differentiate, with extensive cell death induced by withdrawal of leukaemia inhibitory factor (LIF). Jarid2-null mESCs were shown to express uniformly elevated levels of Nanog, with markedly supressed canonical Wnt signalling and defective E-cadherin localisation (Landeira et al. 2015). Unusually Jarid2 null mESCs generate multiple inner cell masses (ICMs) when injected into E3.5 mouse blastocysts (Landeira et al. 2015). Co-culture of Jarid2 null mESCs with wild type mESCs rescues canonical Wnt signalling activity, enabling Jarid2 null cells to overcome their differentiation block. This highlights a role for Jarid2 in regulating a core pluripotency and Wnt signalling circuits, important for mESC differentiation and pre-implantation development. Additionally, the ability of Jarid2 null mESCs to generate independent ICMs suggests that perturbation of epigenetic machinery results in altered integration of cell surface signals, and altered cellular behaviours in this context. The mechanism by which Jarid2 is associated with supressed canonical Wnt signalling, and altered cell-cell interactions however, remains to be elucidated, and represents a significant area of investigation for this study.

1.2. Polycomb Recruitment to genomic targets

The recruitment and regulation of the polycomb group has been intensively investigated (Laugesen, Højfeldt, and Helin 2019; Schuettengruber et al. 2017). Initially a hierarchical model for the sequential recruitment PRC2, followed by PRC1, was proposed based on the observations that PRC1 and PRC2 largely co-localise across the genome, and the cPRC1 Cbx subunit has high affinity for H3K27me3 (Cao et al. 2002). This model suggested that PRC2 was targeted to specific loci, deposits H3K27Me3, which in turn acts as a signal for PRC1.1 recruitment via the Cbx subunit, resulting in chromatin compaction as a consequence of

ubiquitination of histone 2A at lysine 119 (H2AK119ub) (Wang et al. 2004). However, as ablation of PRC2 components only modestly depletes mESCs of the H2AK119ub mark (Leeb et al. 2010), at least a subset of PRC1 can be recruited to chromatin in the absence of PRC2 (Tavares et al. 2012). Furthermore, PRC1 can deposit H2AK119ub in the absence of either PRC2 or H3K27me3 (Blackledge et al. 2014); specifically the ncPRC1.1 complex, which lacks the Cbx subunit, can be targeted to unmethylated CGIs via the CXXC domain of Kdm2b (Farcas et al. 2012; He et al. 2013; Wu, Johansen, and Helin 2013), depositing the H2AK119ub1 mark. Additionally, PRC2.2 encompassing Jarid2 has been reported to be recruited to H2AK119ub1 marked histones via the Jarid2 UIM, promoting deposition of H3K27me3 (Kalb et al. 2014; Blackledge et al. 2014; Cooper et al. 2014). These observations suggest a more complex interplay between PRC1 and PRC2 than the initial hierarchical model would suggest (Cooper et al. 2016). Although the mechanism by which polycomb proteins are recruited to chromatin targets remains only partially understood, DNA sequence, chromatin context and non-coding RNA's are all reported to contribute (van Kruijsbergen, Hontelez, and Veenstra 2015).

1.2.1. Features of Polycomb bound DNA elements

In *Drosophila* polycomb group are targeted to specific *cis*-acting regulatory elements termed polycomb response elements (PREs), lengthy DNA sequences with binding sites for transcription factors which recruit PcG proteins (Kassis and Brown 2013). Mammalian PRC1 and PRC2 display widespread and largely overlapping genomic binding patterns, but mammalian elements analogous to the *Drosophila* PREs have proven difficult to identify (Bauer, Trupke, and Ringrose 2016). Chromatin immunoprecipitation studies of polycomb

group proteins have however shown a strong preference for GC rich elements (Boyer et al. 2006), and ectopic sequences with high CpG content will recruit polycomb group proteins *in vivo* (Mendenhall et al. 2010). This has led to the proposal that CpG Islands (CGIs) are the mammalian *cis* elements targeted for polycomb recruitment (Blackledge, Rose, and Klose 2015). CpG islands are small genomic elements, usually 1-2-kb in length, with high density of CpG residues, typically >50%, which are located close to transcriptional start sites (Deaton and Bird 2011). Unmethylated CGIs are bound by the PRC1.1 interacting partner Kdm2b, which may contribute to PcG targeting (Farcas et al. 2012). This mechanism does not however fully explain PRC1 recruitment to CGIs as ablation of Kdm2b does not result in complete loss of PRC2 recruitment (Blackledge, Rose, and Klose 2015). PRC2 is also recruited to CGIs. Experimentally, PRC2 is recruited to inactivated promoters of active genes, either following excision of activating motifs (Hosogane et al. 2016), or after drug induced transcriptional arrest (Riising et al. 2014). Recently, 'nucleation' sites for PRC2 within CpG rich elements have been identified using a model whereby Eed is re-expressed in Eed null mESCs (Oksuz et al. 2018). Embryonic stem cells lacking Eed are without PRC2 mediated histone adornments, but these are recapitulated upon expression of Eed. Expression of an Eed mutant with disruption of the WD40 domain, which will target PRC2 but is deficient in the 'spreading' of H3K27me3, has identified the initial genomic sites targeted in de-novo histone methylation, termed nucleation sites (Oksuz et al. 2018). These nucleation sites were reported to be enriched for GA rich regions, and GCN tandem repeats, and correspond to bivalent promoters. It has been proposed that nucleation sites act as cis-acting elements which are key to PRC2 de-novo targeting (Yu, Lee, et al. 2019). Additionally, the PRC2.2 interacting protein Jarid2 has a low affinity DNA binding domain, which preferentially interacts with GC rich DNA motifs, and this may also contribute to PcG chromatin targeting (Li

et al. 2010). An important feature of PRC2 CGI targets is that they are hypomethylated, and hypermethylation of CGIs interrupts PRC2 binding (Holoch and Margueron 2017). Disruption of DNA methylation patterns at pre-existing methylated CGIs results in *de novo* deposition of the H3K27me3 mark (Reddington et al. 2013), although the mechanism by which DNA methylation restricts PRC2 activity is yet to be fully elucidated. Intriguingly, DNA methylation *per se*, does not necessarily preclude PRC2 recruitment and H3K27me3 deposition, as PRC2 can be recruited during X-inactivation (Brockdorff 2017), or imprinted genes (Wang et al. 2015), and the PRC2.2 component Aepb2 binds methylated DNA *in vitro* (Wang et al. 2017).

1.2.2. Chromatin landscapes of Polycomb recruitment

In addition to DNA features, polycomb recruitment is influenced by chromatin context and pre-existing histone tail modifications (Laugesen, Højfeldt, and Helin 2019). It is well recognised that cPRC1 recognises pre-existing H3K27me3 through the Cbx subunit, discussed in the hierarchical polycomb recruitment model (Comet and Helin 2014). Additionally, PRC2 complexes bind H3k27me3 through the WD40 domain of Eed and results in stabilisation, and potentiates the catalytic activity of Ezh2 (Margueron et al. 2009). PRC2 is therefore able to 'read' pre-existing histone modifications, and 'write' histone modifications (Hyun et al. 2017). This could enable repressive histone marks to be conserved following DNA synthesis, with pre-existing H3K27me3 deposition guiding PRC2 to methylate newly-incorporated nucleosomes (Zhang, Cooper, and Brockdorff 2015; Hansen et al. 2008). In contrast to this, pre-existing methylation at lysine 36 of histone 3 (H3K36), a histone modification present at actively transcribed genes, is reported to constrain PRC2 activity (Holoch and Margueron 2017). H3K27me3 is rarely observed on the same histone as H3K36me2/3, and PRC2 activity

is inhibited by the H3K36me2/3 mark (Yuan et al. 2011). Furthermore, overexpression of histone H3K36 methylase has been reported in multiple myeloma cells which exhibit globally reduced H3K27me3 deposition (Popovic et al. 2014). Pre-existing histone marks seemingly play an important role in conservation and transmission histone modifications to daughter cells in cell division, however recent studies have shown that pre-existing H3K27 methylation is not required for *de novo* PRC2 targeting to repressed genes in mESCs. It is well recognised that mESCs lacking core PRC2 components (Suz12, Eed or Ezh1/Ezh2 double knockout) demonstrate globally ablated H3K27 methylation patterns (Pasini et al. 2007; Oksuz et al. 2018; Lavarone, Barbieri, and Pasini 2019). Two separate studies have shown rescue of PRC2 components Suz12 and Eed in mESCs lacking these components rapidly and accurately re-establishes *de novo* global H3K27 methylation patterns (Hojfeldt et al. 2018; Oksuz et al. 2018). This highlights that PRC2 binding and deposition of H3K27 methylation can occur independently of pre-existing H3K27 methylated nucleosomes, and demonstrates cells lacking H3K27 methylation retain the mechanisms to accurately target PRC2.

1.2.3. The role of RNA in PRC recruitment

Long non-coding RNA's (lncRNA) have also been implicated in targeting PRC2 to genomic loci. Specifically, lncRNA *XIST* has been reported to target PRC2 during X-inactivation (Zhao et al. 2008; Brockdorff 2017). Additionally, the lncRNA HOTAIR has been implicated in the recruitment of PRC2 and deposition of H3K27Me3 marks at the *HOXD* locus (Rinn et al. 2007) and Kcnq1ot1 has been reported to recruit PRC2 via interaction with Ezh2, to maintain allelic repression of the *KCNQ1* locus (Zhang, Zeitz, et al. 2014). However, in addition to evidence of lncRNAs targeting PRC to specific genomic sites, evidence of widespread promiscuous and

apparent non-specific PRC2:RNA interactions have been reported (Yan et al. 2019). Specifically, RNA immunoprecipitation studies have revealed that PRC2 components Ezh2 and Suz12 interact with many actively transcribed and housekeeping mRNAs (Kaneko et al. 2014; Davidovich et al. 2013; Zhao et al. 2010). Previous studies have shown that RNA interaction with PRC2 can reduce its methyltransferase activity (Kanhere et al. 2010; Herzog et al. 2014). However, a recent study has shown Ezh2 autocatalytic activity is unaffected by RNA binding (Wang et al. 2017). As a result of these findings a more general model of promiscuous PRC2: RNA interaction, rather than targeted lncRNA mediated chromatic targeting has been proposed. Specifically, antagonistic RNA and chromatin binding at PRC2, with mRNA completing for PRC2 binding at actively transcribed genes, may contribute to PRC2 recognition of transcriptional activity (Beltran et al. 2016; Almeida, Bowness, and Brockdorff 2020). Recent studies have highlighted an essential role for ncPRC1 targeting of PRC2 in X-inactivation. It has been reported that PRC2 recruitment by XIST to the inactive X-chromosome (Xi) is entirely dependent on prior H2AK119ub deposition by XIST targeted ncPRC1 (Almeida et al. 2017) PRC2.2 has been shown to be targeted to XIST ncPRC1 deposition sites through the UIM motif of Jarid2, and PRC2 recruitment to Xi is strongly abrogated by Jarid2 knockout (Brockdorff, 2017). These studies highlight the complex interplay between polycomb complexes and RNA species.

1.2.4. 3D genomic architecture and polycomb boundaries

Recent studies have shown that 3D architecture of the genome plays a critical role in transcriptional regulation and development (Rowley and Corces 2018). Chromosome folding within the nucleus can permit intra- and interchromosomal contacts over large distances of

the linear genome in mESCs, resulting in events such as enhancer: promotor interactions (Denholtz et al. 2013; Joshi et al. 2015). Chromosome folding is envisaged as partitioning the genome into associated domains, the largest of these being chromosomal territories (Sexton and Cavalli 2015), with each of these further divided into topologically associated domains (TADs), typically megabase in size and bounded by structural proteins such as CTCF (Gibcus and Dekker 2013). At the sub-TAD scale, recently described Polycomb domains can be viewed as looped 3D structures typically containing only one or two genes (approximately 110 kb size) (Dowen et al. 2014; Pachano, Crispatzu, and Rada-Iglesias 2019). Polycomb domains are abundant in embryonic stem cells, with 350 such domains identified in mESCs (Dowen et al. 2014). These 3D multilooped structures are enriched for both polycomb proteins and H3K27me3, bounded by CTCF and cohesion, and contain at least one developmentally repressed lineage-specific gene (Mas and Di Croce 2016). Furthermore, clusters of polycomb domains may localise within the nucleus to form PcG foci (Vieux-Rochas et al. 2015). Importantly, these long-range interactions are not H3K27 methylation dependent, as they are maintained in Eed deficient mESCs, however PRC1 is essential to their formation, as double knockout of Ring1A and Ring1B results in loss of these long-range interactions in mESCs (Schoenfelder et al. 2015). Additionally, spreading of polycomb repressive marks over large genomic distance has also been reported from the recently described PRC2 nucleation sites (Oksuz et al. 2018; Yu, Lee, et al. 2019). The function of polycomb proteins in the regulation of 3D genomic organisation remains an active area of research. Recent studies have demonstrated the importance of insulating boundaries between active and repressed polycomb regions (Yu, Lee, et al. 2019). Specifically, the *HOX* gene cluster is developmentally repressed with H3K27me3 adornment. Upon differentiation, Hoxa1-6 are expressed, lose H3K27me3 and gain histone marks of active transcription (H3K4me3), with Hoxa7 insulated

by a CTCF binding site, and retaining gene repression and H3K27me3 adornment. Deletion of this CTCF binding site results in activation of Hoxa7, and replacement of H3K27me3 with active H3K4me3, suggesting active chromatin can spread into repressed domains, unless they are insulated by CTCF binding (Narendra et al. 2015).

1.2.5. Non-classical roles of PRC2

The methyltransferase activity of PRC2 at histone 3 lysine 27 is increasingly well understood (Bracken, Brien, and Verrijzer 2019). In addition, a number of recent reports have implicated PRC2 in the methylation of non-histone substrates (summarised in table 1.1) (Chan and Morey 2019). A putative target recognition peptide sequence for PRC2 on the basis of the H3K27 site has been reported and 339 potential non-histone PRC2 methylation targets were reported (Ardehali et al. 2017). Furthermore, using an Ezh2-affinity mass spectrometry approach, a number if interesting Ezh2 non-histone methylation targets were recently reported (Sbirkov et al. 2017). Importantly this study identified methylation of known Ezh2 targets histone 3 and automethylation of Ezh2, validating the approach as robust. Additional non-histone substrates included Suz12, Cbx3, Adt2, eEF1A1 and AlyRef (Sbirkov et al. 2017) Methylation of non-histone targets plays a critical role in PRC2 function itself. Ezh2 automethylates at lysine residues K510, K514 and K515, on an evolutionarily conserved flexible loop of Ezh2. These post translational modifications have been convincingly detected by both biochemical and mass spectrometry studies (Wang et al. 2019; Lee et al. 2019). Importantly, mutation of K510, K514 and K515 to alanine residues results in significant impairment of *de novo* histone methyltransferase activity of PRC2, suggesting Ezh2 automethylation is important for PRC2 activity.

Target	Residue	Moiety	Cell type	Evidence	Reference
RORα	Lysine 38	Monomethylation	Human embryonic kidney (HEK293)	RORα co-Immunoprecipitates with EZH2, Mass spectrometry in vitro methylated RORα K 38 fragment, custom antibody to methylated RORα	(Lee et al. 2012)
Gata4	Lysine 299	Monomethylation	Mouse heart extracts	Antibody to methylated lysine stains immunoprecipitated flag-bio-epitope tagged Gata4, confirmed monomethylation of K299 by mass spectrometry, *in vitro* methylation	(He et al. 2012)
STAT3	Lysine 180	Not specified	Glioblastoma stem cells	STAT3 co-Immunoprecipitates with EZH2. Antibody to pan-methylated lysine stains immunoprecipitated STAT3	(Kim, Kim, et al. 2013)
STAT3	Lysine 49	Dimethylation	Colorectal adenocarcinoma cell line (DLD1)	Mass spectrometry of flag-tagged immunoprecipitated STAT3	(Dasgupta et al. 2015)
Jarid2	Lysine 116	Dimethylation	mESC (E14)	*In vitro* methylation, custom antibody to di and trimethylated Jarid2 peptides	(Sanulli et al. 2015b)
β-catenin	Lysine 49	Trimethylation	Liver cancer stem cells (Hep3B)	EZH2 co-Immunoprecipitates with β-catenin and lnc-β-Catm. Antibody to tri-methylated lysine stains immunoprecipitated β-catenin; in vitro methylation assay	(Zhu et al. 2016)
β-catenin	Lysine 49	Trimethylation	mESCs (W)	PRC2 core components/ Jarid2 co-Immunoprecipitates with β-catenin. Custom monoclonal antibody to *in vitro* methylated B-catenin K49me3 peptide	(Hoffmeyer et al. 2017)
Elongin-A	Lysine 754	Monomethylation	mESC (CJ57)	In vitro methylation assay, custom antibody to monomethylated Elongin A	(Ardehali et al. 2017)
PLZF	Lysine 430	Not specified	Mouse NK cells + HEK293 cells	PLZF co-Immunoprecipitates with EZH2. Antibody to pan-methylated lysine stains immunoprecipitated PLZF	(Vasanthakumar et al. 2017)
ADT2	Lysine 52	Trimethylation	FAB-M2 HL-60 Human AML cell line	EZH2 affinity-purification mass spectrometry and confirmation with pan-methyl-K immunostaining	(Sbirkov et al. 2017)
eEF1A1	Lysine 55 Lysine 165	Dimethylation for both sites	FAB-M2 HL-60 Human AML cell line	EZH2 affinity-purification mass spectrometry and confirmation with pan-methyl-K immunostaining	(Sbirkov et al. 2017)
Ezh2	Lysine 510 Lysine 514 Lysin 515	Monomethylation reported for all sites	mESCs (strain not given)	Mass spectrometry of purified PRC2 from mESCs. In vitro methylation assays. Mass spectrometry of human recombinant PRC2.	(Wang et al. 2019; Lee et al. 2019)
Talin	Lysine 2454	Trimethylation	HEK293T	EZH2 co-Immunoprecipitates with Vav1 and Talin. Antibody to trimethylated lysine stains immunoprecipitated Talin. In vitro methylation assay, confirmed by MS	(Gunawan et al. 2015; Venkatesan, Wong, Tan, Chung, Yau, Cukuroglu, Allahverdi, Nordenskiold, et al. 2018)

Table 1.1. Reported non-histone substrates of polycomb repressive complex 2

Table summarises reported non-histone targets of PRC2 showing methylated residues, degree of methylation reported, origin of samples and techniques used to identify methylation of substrate and supporting literature.

Ezh2 has been shown to catalyse monomethylation of lysine residue 116 of the PRC2.2 component Jarid2 (Sanulli et al. 2015b). Methylation of lysine 116 mimics the methylated H3K27 histone tail, with binding by the Eed aromatic cage resulting in allosteric activation of PRC2 (Kasinath et al. 2018).

Intriguingly, PRC2 has been reported to methylate a number of important cell signalling proteins and transcription factors. This suggests a possible, but unappreciated regulatory role of PRC2 in control of cell signalling and transcription. Importantly, Ezh2-mediated methylation of transcription factors has been shown to either enhance or diminish transcriptional activity (Chan and Morey 2019). Stat3 has been reported to be trimethylated at lysine 180 (Kim, Kim, et al. 2013), and dimethylated at lysine 49 (Dasgupta et al. 2015), by Ezh2. Both these PTMs have been reported to potentiate Stat3 activity, and increase expression of Stat3 target genes. In contrast reduced expression of retinoic acid related orphan receptor alpha (RORα) target genes is observed after Ezh2 methylation of RORα at lysine 38. This methylation results in RORα being recognised by a DCAF-1-containing E3-ubiquitin ligase complex resulting in degradation of RORα and loss of expression of RORα target genes (Lee et al. 2012). Additional PRC2 substrates include Gata4 lysine 229 (He et al. 2012), Elongin-A lysine 754 (Ardehali et al. 2017), Talin lysine 2454 (Gunawan et al. 2015; Venkatesan, Wong, Tan, Chung, Yau, Cukuroglu, Allahverdi, Nordenskiold, et al. 2018), promyelocytic leukaemia zing finger protein (Plzf) lysine 430 (Vasanthakumar et al. 2017), androgen receptor (AR) lysine 600/632 (Xu et al. 2012) and β-catenin lysine 49 (Hoffmeyer et al. 2017; Zhu et al. 2016). Methylation of β-catenin at lysine 49 is of particular interest to our group, as we have previously reported repressed canonical Wnt signalling in mESCs lacking the PRC2.2 component Jarid2. β-catenin is the transcriptional effector of the canonical Wnt signalling pathway, discussed later in detail (MacDonald, Tamai, and He 2009). Several

previous studies have implicated Ezh2 in the positive regulation of canonical Wnt signalling, and although the mechanism of regulation was undetermined, direct interaction between Ezh2 and β-catenin was reported in several studies (Li et al. 2009; Shi et al. 2007; Jung et al. 2013; Zhang and He 2013). Notably, two recent studies have highlighted the possibility of direct methylation of β-catenin at the lysine 49 by Ezh2 may regulate β-catenin stability and function (Hoffmeyer et al. 2017; Zhu et al. 2016). Zhu et al report that the long non-coding RNA *lnc-β-Catm* co-immunoprecipitates with both β-catenin and Ezh2 in liver cancer stem cells, and Ezh2 methylates β-catenin at lysine 49. This methylation event promotes β-catenin stability and potentiates canonical Wnt signalling, and expression of *lnc-β-Catm* is associated with cancer progression and poor prognosis. Hoffmeyer et al demonstrated that β-catenin is methylated again at lysine 49 in mESCs. It was also reported that methylated β-catenin co-Immunoprecipitates with all PRC2 core components and Jarid2 and is enriched at repressed developmental genes (Hoffmeyer at al. 2017). A further study suggested a role for the lysine demethylases Kdm2a/b in regulation of β-catenin stability, highlighting the possibility that methylation of β-catenin may impair ubiquitination, resulting in increased stability and potentiating canonical Wnt signalling (Lu et al. 2015).

Ezh2 has been reported to act as a direct activator of transcription when phosphorylated at tyrosine residue 244 by Jak3, suggesting that PRC2 components may have an additional non-classical role in activating gene expression in addition to the well characterised role in maintenance of transcriptional repression (Yan et al. 2016; Burmeister 2016). The recent description of additional polycomb substrates and non-classical polycomb activity suggests that PcG might have a broader role than previously appreciated (Chan and Morey 2019),

notably in the co-ordination of cell signalling cascades and potentiation of gene expression (Kim et al. 2018; Aubert, Egolf, and Capell 2019) (Figure 1.2).

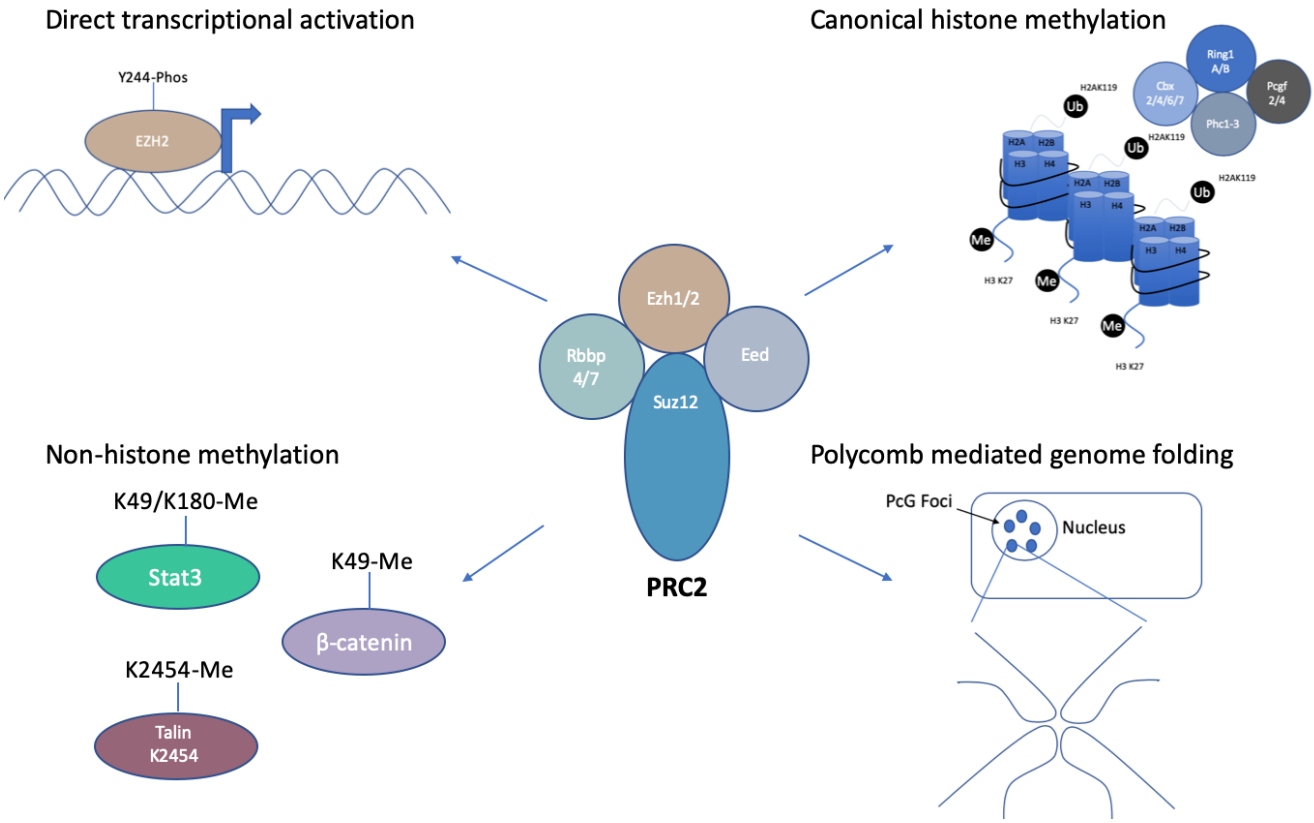

Figure 1.2. Polycomb repressive complex 2; classical and non-classical roles

Schematic representation of reported classical and non-classical roles of PRC2. The canonical role for PRC2 is well established, and involves recruitment to polycomb sites, typically GC rich domains including CpG islands, and maintenance of transcriptional repression through trimethylation of Histone3 lysine 27.

Polycomb proteins are involved in regulation of genomic architecture, mediating looping *cis*-interactions of regulatory elements, and also accumulating in PcG foci within the nucleus to regulate long-range interactions between repressed polycomb domains.

Non-classical roles of PRC2 have recently been delineated. PRC2 has been reported to methylate non-histone substrates to modulate their function and/or stability. Three examples of such non-histone methylation events include Stat3, Talin and β-catenin are shown. Ezh2 has also been reported to act as a direct transcriptional activator, either in complex with other proteins (e.g., PAZ and β-catenin), or individually as shown in the schematic when phosphorylated at serine residue Y244 by Jak.

1.2 Role of PRC2 in pluripotency and differentiation

The Polycomb group are essential to mammalian embryonic development. Loss of any PRC2 core component (Faust et al. 1995; O'Carroll et al. 2001; Pasini et al. 2004) or Ring1B of PRC1 is embryonically lethal in mice (de Napoles et al. 2004; Voncken et al. 2003). Additionally, loss of the ncPRC1 component Kdm2b (Fukuda et al. 2011), the PRC2.1 component Mtf2 (Rothberg et al. 2018) and the PRC2.2 components Jarid2 or Aepb2 (Takeuchi et al. 1995; Grijzenhout et al. 2016) also result in embryonic lethality.

Embryonic stem cells represent an important model for early development, derived from cells of the inner cell mass of mouse blastocysts. They are characterised by indefinite self-renewal in vitro, and pluripotency; the ability to generate cells of all three germ layers, both *in vitro* and *in vivo* (Davidson, Mason, and Pera 2015). Pluripotency is governed by the network of a triad of core transcription factors, Oct4, Sox2 and Nanog (Niwa 2007), with low levels of Nanog associated with differentiation, i.e. exit from pluripotency (Chambers et al. 2007). Embryonic stem cells can be further divided into naïve and primed pluripotency, with altered functional and molecular characteristics and growth requirements (Nichols and Smith 2009). Naïve stem cells were first derived from the inner cell mass of the pre-implantation blastocyst of mouse strain 129 (Martin 1981; Evans and Kaufman 1981), and retain characteristics of the pre-implantation inner cell mass cells. Specifically, they require the presence of leukaemia inhibitory factor in growth media (LIF, a JAK/Stat3 pathway activator), retain hypomethylated DNA, do not exhibit X-inactivation, express naïve markers Rex1, NrOb1 and Fgf4, express surface E-cadherin, and will contribute to ICM formation upon injection into blastocysts (Weinberger et al. 2016; Nichols and Smith 2009). In contrast primed pluripotent stem cells represent an alternative pluripotency state, with characteristics of the post-implantation EpiSC cells. Primed pluripotent stem cells are dependent on Fgf/Erk

and TGF-β or activin A signalling, but not LIF/Stat3, demonstrate DNA hypermethylation and X-inactivation, do not express naïve markers but instead express primed markers Otx2 and Zic1, express surface N-cadherin, and do not contribute to ICM formation on blastocyst injection (Weinberger et al. 2016; Nichols and Smith 2009). The epigenetic landscape of embryonic stem cells is vital to pluripotency and differentiation (Tee and Reinberg 2014). Mouse embryonic stem cells lacking any individual core PRC2 component can be generated and PRC2 is not essential for stem cell self-renewal, however these cells exhibit defective differentiation (Azuara et al. 2006; Aloia, Di Stefano, and Di Croce 2013; Pasini et al. 2007; Lee et al. 2006; Chamberlain, Yee, and Magnuson 2008).

Many key developmental regulators are targets of PRC2 in embryonic stem cells, with Ezh2 occupying 95% of developmentally regulated genes (Yu, Lee, et al. 2019). Repressive H3K27me3 modification are often found in combined with the activating histone modification, trimethylation of Histone 3 lysine 4 (H3K4me3), a histone modification catalysed by the COMPASS family member Mll2 (Hu et al. 2013; Denissov et al. 2014). This characteristic histone signature is termed bivalency (Bernstein et al. 2006; Azuara et al. 2006). Embryonic stem cells are enriched for bivalent domains (Mas et al. 2018). Bivalent domains are associated with the initiating (RNA Pol II Ser5P), but not elongating form of RNA polymerase II (RNA Pol II Ser2P) (Stock et al. 2007). Initial evidence of bivalent domains relied on bulk population data and as such the presence of opposing histone marks may represent cellular heterogeneity, however recent sequential ChIP experiments have recently catalogued 3868 bivalent domains in mESCs (Mas et al. 2018). Furthermore, visualisation of bivalent domains in single live cells using genetically encoded chromatin sensing multivalent probes, specific to H3K4me3 and H3K27me3 marked histones has recently been reported (Delachat et al. 2018). It was shown that ~35% of all mouse genes in mESCs demonstrate

bivalent chromatin, which were found to cluster together within the mouse nucleus. Furthermore, bivalent domains were minimally detected in differentiated cells, and treatment of mESCs with the polycomb inhibitor UNC1999 largely ablated bivalency (Delachat et al. 2018).

Bivalent domains are often located at promotors poised for activation upon differentiation cues, with CG rich regions commonly associated (Blanco et al. 2020). Additionally, bivalent histone marks have also recently been reported at enhancer regions in mESCs, termed poised enhancers (Caglio, Torlai Triglia, and Pombo 2017). It has been proposed that genes with bivalent promotors are poised either for activation or repression upon differentiation cues (Voigt et al. 2012). This is reflected by the high frequency of bivalent domains in stem cells compared to their scarcity in differentiated cells (Voigt, Tee, and Reinberg 2013; Delachat et al. 2018). Bivalency can be stably resolved into silenced domains with propagation of repressive histone modifications and CpG island DNA methylation, or remain active with removal of repressive histone marks, during lineage commitment (Voigt, Tee, and Reinberg 2013; Piunti and Shilatifard 2016). Bivalent domains have recently been reported *in vivo* in pre- and post-implantation stage mouse blastocysts (Liu et al. 2016; Zheng et al. 2016). Intriguingly, bivalency is not exclusive to early development and embryonic stem cells, with several reports of adult stem cells and to a lesser extent adult tissues retaining bivalency (Weiner et al. 2016; Mazzarella et al. 2011). Persistent bivalency has been observed in haematopoietic lineage committed cells, suggesting that lineage committed cells retain some epigenetic plasticity (Mazzarella et al. 2011; Cui et al. 2009), and sequential ChIP experiments have shown bivalency in adult human $CD4^+$ T Cells (Kinkley et al. 2016). These recent findings have led to the suggestion that bivalency is a mechanism that distinguishes between cell

types rather than a gene expression programme established exclusively in early development and stem cells (Blanco et al. 2020).

Recent studies have implicated genomic architecture as having a role in the regulation of bivalent domains (Pachano, Crispatzu, and Rada-Iglesias 2019). Genomic contacts have been shown to occur preferentially between regions of chromatin with similar features (Denholtz et al. 2013). Bivalent domains are located in regions of open chromatin, and have been demonstrated to participate in both intra- and inter-chromosomal interactions, and have been shown to dynamically change between naïve and primed pluripotency (Joshi et al. 2015). Embryonic stem cells lacking either core polycomb components or Mll2 have altered interactions between bivalent regions, but maintained genome organisation at TAD and chromosomal levels (Blanco et al. 2020). It has been proposed that bivalency has a role in the regulation of long-range genomic interactions, and modulation of developmental gene expression, in addition to the recognised role in poising genes for either expression or repression (Mas et al. 2018).

A recent intriguing study has implicated a non-classical role for PRC2 in differentiation. Hoffmeyer et al reported non-histone methylation of the lysine 49 (K49) residue of β-catenin by PRC2, and were able to generate a custom monoclonal antibody to this PTM. The authors reported that methylated β-catenin co-immunoprecipitates with all core PRC2 components and Jarid2 in mESCs. Lysine 49 is also a target of CREB-binding protein (CBP), which mediates acetylation of K49 (Wolf et al. 2002). Methylated β-catenin has a distinct set of genomic targets, mutually exclusive to those acetylated β-catenin, with methylated β-catenin enriched at repressed genes, and acetylated β-catenin enriched at activated genes during mesodermal differentiation. The authors suggest that post translational modification of K49 of β-catenin represents a switch to regulate either gene repression or activation during differentiation

(Hoffmeyer et al. 2017). This study highlights a non-classical role for PRC2 in mESCs and differentiation, suggesting a broader role of polycomb group in development than previously thought.

1.3 The role of PRC2 in cancer

Malignancies are characterised by extensive global epigenetic aberrations including changes to DNA methylation patterns (Ehrlich 2002), altered histone modifications (Plass et al. 2013) and disrupted genome architecture (Corces and Corces 2016). The application of massive parallel sequencing technologies to cancer cells has revealed that epigenetic modifiers are among the most frequently mutated classes of genes observed in cancer, with a reported 50% of cancer harbouring mutations to chromatin modifiers, and epigenetic modifiers representing a significant proportion of driver mutations (Flavahan, Gaskell, and Bernstein 2017; Vogelstein et al. 2013). Solid tumours exhibit marked tumour heterogeneity, with a small sub-population of cancer stem cells (CSCs) which demonstrate stem-like qualities and have been implicated in chemo-resistance, recurrence and metastasis (Visvader and Lindeman 2012). It has been reported that polycomb group are essential to maintain stem-like characteristics in adult stem cells, and EZH2 is reported to be highly expressed in CSCs derived from multiple tumour types including colorectal, breast, pancreatic, ovarian and liver cancers (Comet et al. 2016). EZH2 overexpression has also been reported to increase the proliferation rate of tumour cells, and promote tumour growth and metastasis in malignant tumour models (Gan et al. 2018). Indeed, numerous studies have shown overexpression of PRC2 components in multiple human cancers, including breast, prostate, endometrial, hepatocellular, ovarian and melanoma (Varambally et al. 2002; Bachmann et al. 2006; Jia et

al. 2014; Sudo et al. 2005; Zingg et al. 2015; Lu et al. 2010; Chen, Yang, et al. 2018). However, PRC2 expression is coupled to the cell cycle, and cancer cells typically have an increased proliferative potential, so it remains unclear whether overexpression of polycomb components is a cause, or consequence of malignancy (Comet et al. 2016; Laugesen, Højfeldt, and Helin 2016; Wassef and Margueron 2017). Increased copy number of Ezh2 has been reported in several cancers, including breast, prostate, non-small cell lung cancer and melanoma ('AACR Project GENIE: Powering Precision Medicine through an International Consortium' 2017; Saramäki et al. 2006). Additionally, Ezh2 and Eed have been shown to give a proliferation advantage when overexpressed *in vitro* (Bracken et al. 2003) and *in vivo* (Béguelin et al. 2013). Taken together these findings suggest that EZH2 overexpression may be indeed be advantageous to malignant cells. Massively parallel sequencing studies have revealed multiple mutations affecting Ezh2 and other PRC2 core and ancillary components, notably Jarid2 and Aebp2 (Comet et al. 2016; Olsson et al. 2016; Puda et al. 2012). However, the role of PRC2, has proven to be complex as both hyperactivating, and loss of function mutations as well as PRC2 substrate mutations have been identified. This highlights a multifaceted, context-dependent role for PRC2 in malignancy, and PRC2 cannot readily be classified as either an oncogene or tumour suppressor gene (Pasini and Di Croce 2016). Both loss of (Böhm et al. 2019), and hyperactivating EZH2 mutations have been reported to correlate to adverse prognosis in several cancer types. The mechanisms by which PRC2 is understood to contribute to malignancy are outlined in figure 1.3.

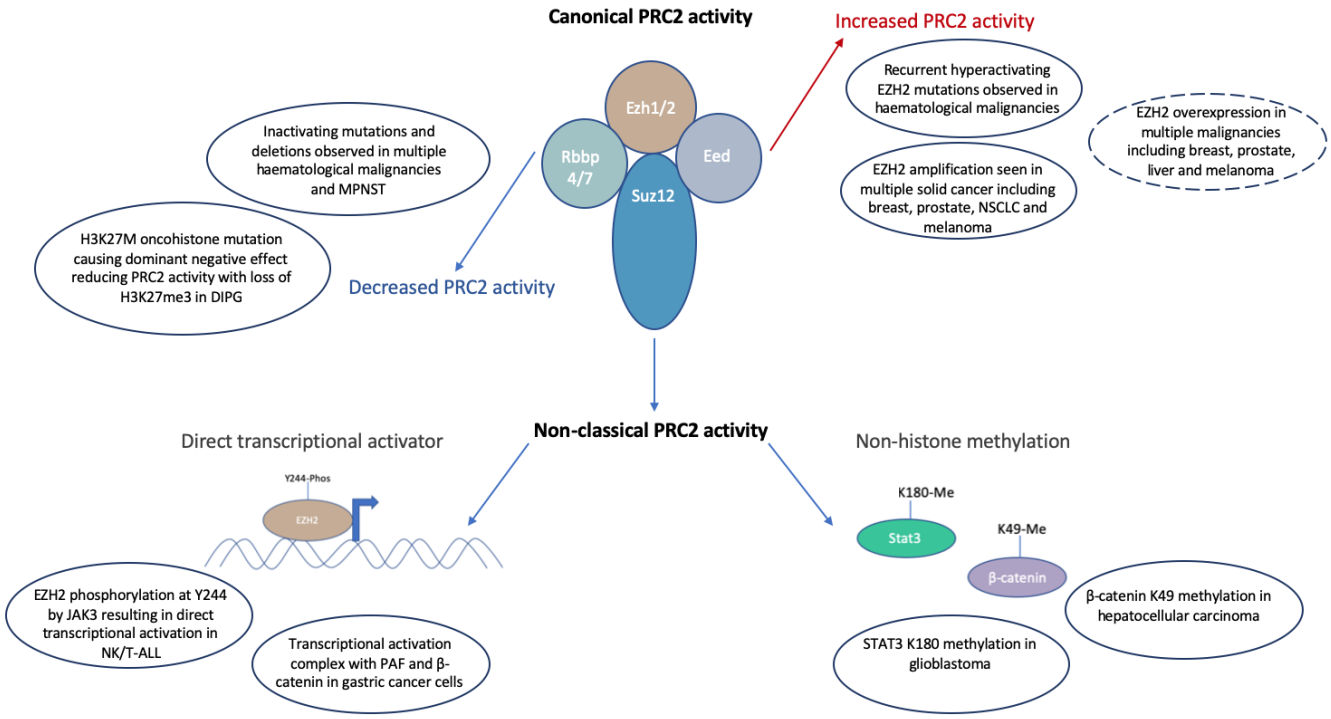

Figure 1.3. Polycomb repressor complex 2 and caner

Schematic representation of reported PRC2 activity in cancer. Aberrations in canonical PRC2 activity have been reported in multiple malignancies, with both loss of function and hyperactivating events reported. Inactivating mutations and deletions have been reported in multiple malignancies. Recurrent hyperactivating mutations have been reported, notably in haematological malignancies, and melanoma. EZH2 overexpression is also reported in many solid malignancies, however there remains debate over whether EZH2 overexpression is a cause or effect of malignancy (dashed circle to reflect this).

EZH2 has been reported to act as a direct transcriptional activator when phosphorylated by JAK3 in acute lymphomas.

Multiple reports have also implicated non-histone PRC2 mediated methylation in various malignancies, notably the methylation of β-catenin in hepatocellular carcinoma shown above, which is associated with potentiated Wnt signalling and adverse prognosis.

Abbreviation used; diffuse intrinsic pontine glioma (DIPG), malignant peripheral nerve sheath tumour (MPNST), natural killer cell/ T-cell acute lymphoblastic leukaemia (NK/T-ALL)

1.3.1 Hyperactivating Ezh2 mutations

Recurrent missense mutations in the catalytic SET domain of EZH2 have been reported in haematological malignancies. Specifically, missense mutations affecting tyrosine residue 646 (Y646F/N/S/H/C) of EZH2 have been reported in up to 25% of cases of diffuse large B-cell lymphoma (DLBCL) and 25% of follicular lymphomas (FL) (Morin et al. 2011; Okosun et al. 2014; Bödör et al. 2011). This substitution results in greatly increased efficiency of conversion of H3K27me2 to the trimethylated form, and occurs exclusively as a heterozygous mutation with a wild-type copy of EZH2. The wild type EZH2 catalyses mono and di-methylation of histone 3, with the mutant Ezh2 catalysing extensive conversion to the trimethylated form, resulting in greatly increased deposition of H3K27me3 (Sneeringer et al. 2010; Yap et al. 2011; McCabe, Graves, et al. 2012). Hyperactivating mutations affecting tyrosine 646 (Y646N/F/S) have also been identified in melanoma, but no other solid tumour (Zingg et al. 2015). Additional hyperactivating missense mutations affecting residues alanine 686 (A682G) (McCabe, Graves, et al. 2012) alanine 692 (A692V) have also been reported, although less frequently in DLBCL and FL, with the A692V mutation also seen in non-Hodgkin's lymphoma and acute B-cell lymphoblastic leukaemia (Majer et al. 2012; Ott et al. 2014). The mechanism by which enhanced Ezh2 catalytic activity, and deposition of H3K27me3 contributes to malignancy is unclear. Indeed, knockin of the Ezh2-Y646N allele into mice does not give rise to lymphoma, however in conjunction with sustained Bcl activation results in the development of germinal centre lymphomas (Béguelin et al. 2013). Additionally, expression of this allele in Eμ-Myc mice results in an observed increased lymphoma rate (Berg et al. 2014). This is in keeping with the multi-hit cancer model, where several driver mutations collaborate in the development of cancer (Tomasetti et al. 2015). It has been postulated that the hypermethylated state maintains cells in a more stem-like state, resulting in a more

anaplastic state favouring proliferation, with PRC2 functioning physiologically to balance differentiation and self-renewal in the stem cell compartment (Laugesen, Højfeldt, and Helin 2016).

1.3.2. Loss of function PRC2 mutations

The findings of Ezh2 overexpression, Ezh2 amplification and hyperactivating missense mutations are associated with haematological malignancies and melanomas would be consistent with PRC2 acting as an oncogene. However, multiple examples of loss of functions mutations, including deletions, frame shift mutations and inactivating missense mutations affecting core PRC2 components and PRC2.2 interacting protein Jarid2 have been documented, implicating PRC2 as having a tumour suppressive role. Specifically, inactivating Ezh2 mutations have been reported in myeloid malignancies including chronic myelomonocytic leukaemia (CML) and acute myeloid leukaemia (AML) (Lindsley et al. 2015; Score et al. 2012; Jankowska et al. 2011). Additionally, inactivating Eed mutations have been reported in haematological malignancies including T-cell acute lymphoblastic leukaemia and myeloproliferative neoplasia (Zhang et al. 2012; Score et al. 2012), as well as solid tumours including melanoma, glioblastoma multiforme and malignant peripheral nerve sheath tumours (MPNST) (De Raedt et al. 2014; Lee et al. 2014). Similarly, Suz12 inactivating mutations have been reported in haematological malignancies including acute T-cell lymphoblastic leukaemia (ATLL) and myeloproliferative neoplasia (Ntziachristos et al. 2012; Score et al. 2012; Zhang et al. 2012), as well as solid tumours including melanoma, glioblastoma multiforme and MPNST (De Raedt et al. 2014; Lee et al. 2014; Zhang, Wang, et al. 2014). Jarid2 mutations are also reported in myeloproliferative neoplasia and ATLL (Celik

et al. 2018; Puda et al. 2012). Intriguingly, there are reports of both monoallelic, and biallelic PRC2 component mutations, which entirely abrogate PRC2 function. In the case of MPNST 79% of cancers with NF1 microdeletions are homozygous for loss of either Suz12 or Eed, and in the *Nf1*$^{+/-}$*; Trp53*$^{+/-}$ MPNST mouse model, loss of Suz12 results in accelerated tumour development (De Raedt et al. 2014). Additionally, heterozygous deletion of Suz12 in Eμ-Myc mice results in an observed increased lymphoma rate (Lee et al. 2014). The mechanism by which compromise of PRC2 activity contributes to malignancy remains unclear, however a model whereby PRC2 acts as a tumour suppressor gene by negatively regulating expression of proliferative pathways such as the NOTCH1 pathway has been proposed (Dorfman and Tian 2016), although efforts to identify common gene expression profiles in PRC2 inactivated tumours have not yielded consistent results (Laugesen, Højfeldt, and Helin 2016).

1.3.3 PRC2 substrate mutation

Missense mutations affecting the Histones H3.3 and H3.1 resulting in a lysine to methionine substitution at the PRC2 target residue (K27M) have been reported in the 30% of paediatric glioblastomas and 60% of diffuse intrinsic pontine gliomas (DIPG), and have been termed oncohistones (Wan, Liu, and Chan 2018; Schwartzentruber et al. 2012; Wu et al. 2012). H3K27M is present in only 3-17% of nucleosomes in affected cells (Lewis et al. 2013). However, presence of the H3K27M mutation exerts a dominant-negative effect on PRC2, with globally reduced H3K27me3 deposition, and these mutations have been suggested to primarily contribute to cancer development through repression of PRC2 activity (Laugesen, Højfeldt, and Helin 2016). Reduced DNA methylation and perturbation of the chromatin landscape has been reported in cells harbouring the H3K27M substitution and is postulated

to result in aberrant transcriptional activation which may contribute to tumourigenesis. Additionally, these mutations have been reported to arrest cells in a primitive state, refractory to differentiation cues (Weinberg, Allis, and Lu 2017). Additional oncohistone mutations have also been reported affecting Histone 3.1 (K36M) and Histone 3.3 (K36M) in primary bone malignancies (Behjati et al. 2013; Sarungbam et al. 2016), and Histone 1 in haematological malignancies (Okosun et al. 2014).

1.3.4. Non-classical PRC2 activity and cancer

In addition to the contribution of PRC2 to malignancy through alterations in histone methylation described above, novel roles for PRC2 components in cancer have been described. Recent studies have implicated methylation of non-histone targets, and a direct transcriptional activator activity of Ezh2 as contributing to cancer development (Dorfman and Tian 2016). Several recent studies have highlighted the role of PRC2 mediated methylation of non-histone substrates in contributing to the development of cancer. Co-immunoprecipitation studies have shown that Ezh2 interacts with STAT3 in glioblastoma cells, resulting in methylation at lysine residue 180 of STAT3 (STAT3-K180me). Methylation of STAT3 is reported to result in increased STAT3 target gene expression and contribute to glioblastoma malignancy (Kim, Kim, et al. 2013). A further non-histone PRC2 methylation target, Talin has also been implicated in the development of neoplastic transformation and metastasis through elevated focal adhesion remodelling (Venkatesan, Wong, Tan, Chung, Yau, Cukuroglu, Allahverdi, Nordenskiöld, et al. 2018; Gunawan et al. 2015)
Importantly, β-catenin has also been identified as a non-histone target of Ezh2 methylation mediated by the long non-coding RNA lnc-β-Catm in hepatocellular malignancy. Ezh2 and β-catenin both co-immunoprecipitate with lnc-β-Catm, and β-catenin methylation has been

shown in liver cancer stem cells and primary hepatocellular cancer tissues. Methylation at lysine 49 was shown by *in vitro* methylation, and methylation efficiency of β-catenin is enhanced by the presence of lnc-β-Catm. The methylated form of β-catenin shows increased stability, as a result of reduced ubiquitination, and results in potentiated canonical Wnt signalling. Both expression of lnc-β-Catm and elevated canonical Wnt signalling are associated with disease progression, and correlate to adverse prognosis in hepatocellular cancer (Zhu et al. 2016; Mai et al. 2019). In a separate study elevated levels of Ezh2 protein in hepatocellular carcinoma are associated with elevated active-β-catenin and are correlated with disease progression and adverse prognosis (Song et al. 2018). A number of additional lines of evidence implicate a non-classical role for PRC2 in the regulation of canonical Wnt signalling. Interrogation of the cancer genome atlas reveals Ezh2 expression levels positively correlate with the expression of Wnt target genes in colorectal cancer samples (Weinstein et al. 2013). Also, overexpression of Ezh2 correlates with elevated expression of canonical Wnt signalling targets in tumour derived cell lines, and conversely Ezh2 knockdown inactivates the Wnt signalling pathway in these cell lines (Wen et al. 2017). Ezh2 has been shown to interact directly with oestrogen receptor α and β-catenin to activate expression of validated Wnt target genes c-Myc and Cyclin D1 (Shi et al. 2007; Ramakrishnan and Cadigan 2017). A complex of proliferating cell nuclear antigen associated factor (PAF), Ezh2 and β-catenin, has been shown to potentiate canonical Wnt signalling and drive tumourigenesis in colorectal cancer cells, in a methyltransferase independent fashion (Jung et al. 2013; Zhang and He 2013). Further evidence for a non-classical role for PRC2 in co-ordination of canonical Wnt signalling has been shown by treatment of human gastric cancer cells *in vitro* with the Ezh2 inhibitor DZNep. Drug treatment results in reduced total β-catenin, and supressed canonical Wnt signalling in gastric cancer cell lines (Huang, Jin, et al. 2019). Taken together, this

evidence demonstrates an overlap between a non-classical role of PRC2 and canonical Wnt signalling, a pathway critical to development and recognised to play a role in multiple malignancies, notably colorectal cancer. Given our groups previous publication implicating the PRC2.2 component Jarid2 in the co-ordination of canonical Wnt signalling, the interface between PRC2 and canonical Wnt signalling represents a significant area of interest to this study. As such the role of β-catenin and canonical Wnt signalling in mESCs and cancer is discussed in greater detail in section 1.4.

Further to the role for methylation of non-histone substrates, a potential role for Ezh2 as a direct activator of transcription has also been reported to contribute to malignancy (Dorfman and Tian 2016; Chan and Morey 2019). Further to the methyltransferase independent transcriptional activator role as part of the PAF-EZH2-β-catenin complex outlined above, EZH2 has been shown to form ternary complex with RelA and RelB to promote expression of NF-κB targets, independent of methyltransferase activity in triple negative breast cancer (Lee et al. 2011). An additional study has implicated the long non-coding RNA TELNEC2 as scaffolding an interaction between EZH2 and $P57^{KIP2}$ resulting in potentiation expression of p-p38 and NF-κB target genes breast cancer cells (Qiao et al. 2019). Expression of EZH2 with ablated methyltransferase activity confers a growth advantage, implicating a methyl-transferase independent role for EZH2 (Yan et al. 2013). A further study by the same authors has shown that Jak3 mediated phosphorylation of Ezh2 at tyrosine residue 244 results in dissociation from PRC2, with EZH2 acting independently as a transcriptional activator. This results in upregulation of multiple gene targets including genes associated with cell cycle progression, DNA replication, 'stemness' and invasive behaviours in NK/T-cell lymphomas (Yan et al. 2016; Burmeister 2016). Treatment of these cells with Jak3 kinase inhibitors, but not EZH2 methyltransferase inhibitors results in loss of expression of these target genes,

suggesting the role of transcriptional activator is independent of methyltransferase activity. In prostate cancers phosphorylation of EZH2 at the serine 21 (Ser21) residue by AKT kinase results in recruitment to active chromatin, devoid of both Eed and Suz12, but enriched for active histones marks and RNA polymerase II (Xu et al. 2012). Also, a very recent study has identified a partially disordered transactivation domain of EZH2 that resembles the protypical acidic transactivation domain of p53 and VP16. This domain is sufficient to activate transcription using a GAL4 reporter gene assay, interacts with components of active transcription machinery, and recruits and activates gene expression in a p300 dependent manner (Jiao et al. 2020).

1.3.5. Exploiting PRC2 in the treatment of cancer

Research efforts showing upregulation, amplification, and hyperactivating mutations, along with studies reporting that cancer cells frequently rely on PRC2 activity for proliferation (Albert and Helin 2010) has driven the development of specific PRC2 inhibitors with the objective of treating various cancers (Kim and Roberts 2016). In January 2020 a first in class approval for the use of EZH2 inhibitors in the treatment of cancer was granted by the United States Food and Drug Administration (FDA). Specifically, tazemetostat was licenced for treatment of adults with locally advanced or metastatic epithelioid sarcoma harbouring an hyperactivating EZH2 mutation, not amenable to total resection (Hoy 2020). This decision followed the results of the EZH-202 study, which demonstrated complete response in 1.6%, and partial sustained response in 13% patients (Italiano 2020) according to RECISTv1.1 criteria (Schwartz et al. 2016). Subsequently in June 2020, the FDA granted accelerated approval for tazemetostat in the treatment of relapsed or refractory follicular lymphoma in

patients with or without hyperactivating EZH2 mutation. This followed the publication of the follicular lymphoma cohort of the E7438-G000-101 study, which demonstrated overall response in refractory or relapsed lymphoma of 69%, with complete response of 12% and partial response of 57%, and a mean duration of response of 11 months in patients with EZH2 mutation, and an overall response rate of 34% with complete response in 4% and partial response in 30% and mean duration of response of 13 months in patients without EZH2 mutation (Italiano et al. 2018). Additionally promising interim results have been reported for the treatment of DLBCL (Morschhauser et al. 2017). In the United Kingdom the national institute of care excellence (NICE) is currently undertaking a technology assessment for this medication, however at the time of writing this medication is not funded by the national health service (NHS). Additional phase I and II trials into the use of tazemetostat in paediatric haematological malignancies, adult DLBCL and solid tumours are ongoing (Gulati, Béguelin, and Giulino-Roth 2018). Also, phase I studies are ongoing for the small molecule EZH2 inhibitors CPI-1205 in the treatment of non-Hodgkin's lymphoma (Vaswani et al. 2016) and GSK126 in the treatment of non-Hodgkin's lymphoma, multiple myeloma and DLBCL (McCabe, Ott, et al. 2012; Huang, Wang, et al. 2019). Furthermore, multiple additional small molecule EZH2 inhibitors (Stazi et al. 2017) , simultaneous inhibitors of both EZH1 and EZH2 (Yamagishi et al. 2016; Xu, On, et al. 2015) and inhibitors of PRC2 stability (Kim, Bird, et al. 2013; Qi et al. 2017) are in preclinical development. Therapeutic targeting of PRC2 in cancer yielded a new class of drug therapy, with the potential to improve the outcomes in numerous cancers, particularly haematological malignancies. Current treatments and promising agents under investigation are EZH2 inhibitors and are most effective in cancer with hyperactivating EZH2 mutations, although activity is also seen in cancers with wild type EZH2. However, as PRC2 has a tumour suppressor function in some malignancies the use of EZH2 inhibition must

be carefully interrogated for appropriate cancer types and populations. The possibility of PRC2 related treatment strategies in patients with inactivating PRC2 mutations, or the targeting of non-classical roles of PRC2 remains as yet unexploited.

1.4 Canonical Wnt signalling and PRC2

As discussed above, a number of lines of evidence suggest a correlation between PRC2, and β-catenin activity. Specifically, our group has shown that the PRC2.2 component Jarid2 co-ordinates canonical Wnt signalling and core pluripotency circuits and mESCs lacking Jarid2 demonstrate supressed canonical Wnt signalling (Landeira et al. 2015). Additionally, two recent reports have highlighted direct non-histone methylation of β-catenin by Ezh2, in both embryonic stem cells and cancer stem cells, with this methylation event acting as a switch for gene activation or repression, or a mechanism for increasing β-catenin stability respectively (Hoffmeyer et al. 2017; Zhu et al. 2016).Furthermore, Ezh2 activity correlates to expression of Wnt targets in various malignancies (Wen et al. 2017), and treatment of cells with targeted Ezh2 inhibition results in supressed canonical Wnt signalling (Huang, Jin, et al. 2019). The interplay between PRC2, Jarid2 and β-catenin represents a major focus of investigation in this study, and therefore a more detailed review of Wnt signalling and β-catenin is warranted.

The canonical Wnt signal pathway is a well characterised signal transduction cascade, critical to development, and also closely associated with cancer (Clevers and Nusse 2012; Nusse and Clevers 2017b; Zhan, Rindtorff, and Boutros 2017). The first report of a component of the Wnt signalling pathway was Wingless, which was identified in a mutagenesis screen for phenotypes affecting developmental pattering in Drosophila (Nusse and Varmus 1982). Subsequently studies have identified many components of the Wnt family of signalling

proteins, which are evolutionarily conserved in animals (Nusse and Varmus 2012; Verkaar, Cadigan, and van Amerongen 2012). Wnt signalling can be activated through the β-catenin dependent 'canonical' pathway, or the β-catenin independent planar cell polarity and calcium dependent pathways (Komiya and Habas 2008).

Beta-catenin has dual function, and is a constituent of the adherens junctions at the cell surface, a role discussed in greater detail later. Canonical Wnt signalling is initiated by binding of a secreted Wnt ligand to the cell surface receptor Frizzled (Frz) and the co-receptor low-density lipoprotein receptor-related proteins 5/6 (Lrp5/6). Receptor occupancy results in recruitment of Dishevelled (Dvl1), which interacts directly with Axin of the β-catenin destruction complex, inhibiting phosphorylation of β-catenin by casein kinase 1 (Ck1) and glycogen synthase kinase 3β (Gsk3β). This results in stabilisation of active β-catenin, which then translocates to the nucleus and binds transcription factors T-cell specific transcription factor (Tcf), and lymphoid enhancer biding factor (Lef), to drive Wnt responsive gene expression patterns (Nusse and Clevers 2017a) (Figure 1.4). Non-canonical Wnt signalling is defined by β-catenin independent signal transduction, either via Wnt/PCP signalling through Wnt activation of ROR-frizzled receptor complex and signal transduction via Dvl or Vangl mediated activation of Rho kinase and Janus Kinase; or through the calcium dependent pathway in which G-protein coupled phospholipase C activity drive intracellular calcium fluxes which result in transcriptional and cytoskeletal responses (Zhan, Rindtorff, and Boutros 2017).

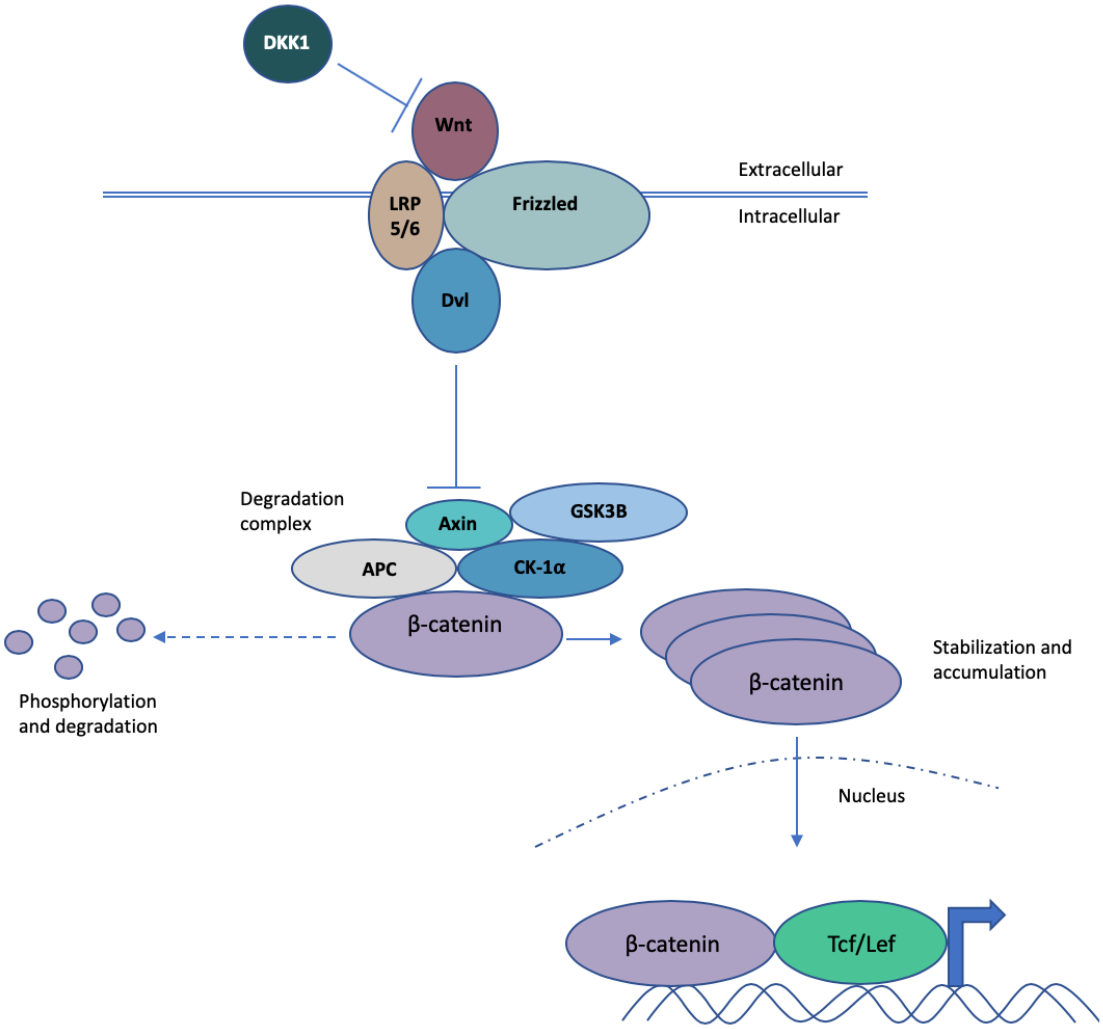

Figure 1.4. Canonical Wnt/β-catenin signalling pathway in vertebrates

Schematic representation of canonical Wnt signalling pathway. In the absence of Wnt ligand, the β-catenin destruction complex comprised of the scaffolding protein Axin1, APC, GSK3β an CK-1α phosphorylate β-catenin, which permits subsequent ubiquitination by β-TrCP and proteasomal degradation. In the absence of nuclear β-catenin a repressive complex of Tcf/Lef and TLE/Groucho recruits HDACs to repress target genes. In the presence of Wnt ligand (such as Wnt3a or Wnt1) at the Frizzled/LRP co-receptor results in LRP phosphorylation by GSK3β and CK-1α, and Dvl recruitment to the cell surface membrane. Active Dvl disables the β-catenin destruction complex, allowing accumulation of cytoplasmic β-catenin. Nuclear translocation of β-catenin allows formation of the Tcf/Lef-β-catenin transcriptional activator, also allowing recruitment of active histone modifiers such as CBP/p300, BRG1 and BCL9. Transcription of downstream Wnt targets governs multiple cell processes. DKK-1 is a secreted Wnt antagonist, which sequesters the LRP6 co-receptor, preventing Wnt ligand signal transduction.

Abbreviation used; adenomatous polyposis coli (APC), B-cell CLL/Lymphoma protein 9 (BCL9), Brahma related gene 1 (BRG1), casein kinase 2-alpha (CK2α), CREB-binding protein (CBP), dickkopf 1 (DKK-1) dishevelled (Dvl) glycogen synthase kinase 3-beta (GSK3β), Histone deacetylase (HDAC), low density lipoprotein related protein (Lrp), lymphoid enhancer factor (LEF), T-cell factor (Tcf)

1.4.1. Wnt signalling in stem cells and development

The role of canonical Wnt signalling in mESC pluripotency and differentiation remains contentious (Sokol 2011; Serio 2014; de Jaime-Soguero, Abreu de Oliveira, and Lluis 2018). Wnt signalling has been implicated in the seemingly opposing processes of stem cell self-renewal and differentiation (Sineva and Pospelov 2014). Initially, activation of Wnt signalling through suppression of Gsk3β was reported to maintain mESC pluripotency in the absence of leukaemia inhibitory factor (LIF) (Sato et al. 2004), and Wnt signalling was proposed as being necessary for stem cell self-renewal. Multiple subsequent studies have implicated canonical Wnt signalling in ESC self-renewal (Hao et al. 2006; Miyabayashi et al. 2007; Wagner et al. 2010; ten Berge et al. 2011). However, the prevailing view that canonical Wnt signalling is essential to self-renewal has been challenged by the generation of mESCs lacking β-catenin (Okumura et al. 2013; Lyashenko et al. 2011; Wray et al. 2011) . Furthermore, dominant interfering TCF proteins which block expression of Wnt target genes do not inhibit the ability of mESCs to self-renew (Kelly et al. 2011), and mESCs lacking porcupine, a protein essential to secretion of all Wnt ligands, also display normal self-renewal properties (Biechele et al. 2013). In keeping with this view, mESCs lacking Jarid2 have supressed canonical Wnt signalling, will readily self-renew but fail to differentiate. Canonical Wnt signalling has also been implicated in differentiation, both in mouse embryos *in vivo*, and in mESCs Wnt signalling has been reported to be required for commitment to mesodermal differentiation (Lindsley et al. 2006; Bakre et al. 2007; Atlasi et al. 2013). The contradictory role of β-catenin in both self-renewal and differentiation has been suggested to be reconciled by the interrogation of the role of canonical Wnt signalling in naïve and primed state (Steinhart and Angers 2018). Studies in naïve embryonic stem cells show a role in self renewal and pluripotency (Xu et al. 2016; ten

Berge et al. 2011), with canonical Wnt signalling preventing transition in primed ES cells (Davidson et al. 2012; Kurek et al. 2015).

It is clear that canonical Wnt signalling is essential to early development and is instrumental for development of dorsoventral and anteroposterior body axes patterning in multiple animal species (Niehrs 2010). Spatiotemporal activation of Wnt signalling is critical to body patterning, with anterior repression of Wnt signalling resulting in development of the head, and active Wnt signalling posteriorly driving development of tail structures (Green et al. 2015). These studies have highlighted that effects of Wnt activity depend on the cellular context during development, and complex downstream consequences result from this interplay. Additionally, canonical Wnt signalling is also essential to normal tissue homeostasis (Steinhart and Angers 2018). In adult tissues Wnt signalling is essential to maintenance of the stem cell niche in multiple tissues, where Wnt signalling promotes self-renewal of tissue specific progenitor stem cells, notably in gut epithelia (Clevers 2013), bone (Baron and Kneissel 2013), and skin (Veltri, Lang, and Lien 2018). Importantly, as canonical Wnt signalling is required for normal tissue homeostasis, aberrant canonical Wnt signalling is observed in many malignancies, although the precise mechanism and frequency of dysregulation has been found to be tissue specific (Jackstadt, Hodder, and Sansom 2020) .

1.4.2. Canonical Wnt signalling in cancer

Colorectal cancer is the most extensively investigated cancer with respect to dysregulation of Wnt signalling, as dysregulation of canonical Wnt signalling was first identified in the hereditary cancer syndrome familial adenomatous polyposis (FAP), with patients heterozygous for an APC mutation (Kinzler et al. 1991; Nishisho et al. 1991). Subsequent

studies have shown APC mutations to be widespread in sporadic colorectal cancer with up to 80% cancers harbouring biallelic APC loss (Sanchez-Vega et al. 2018; Wood et al. 2007). Additionally, a small number of cancers harbour activating β-catenin mutations (Segditsas and Tomlinson 2006), or mutations to the degradation complex scaffold protein Axin2 (Liu et al. 2000), in colorectal cancers with normal APC alleles, further implicating Wnt signalling in neoplastic transformation. Deleterious mutation of APC results in reduced degradation of β-catenin, increased β-catenin stability, and formation of constitutive complexes with TCF resulting in constitutively activated Wnt signalling (Korinek et al. 1997; Rubinfeld et al. 1996). The development of colorectal cancer from adenomatous polyps provides a conceptual framework for the multistep model of malignancy, with multiple adenomas forming in patient with FAP as a result of a second hit to the non-mutated APC allele. Subsequent accumulation of additional mutations in adenomas affecting genes such as K-ras, p53 and Smad4 result in neoplastic transformation of adenomas to adenocarcinomas, and the development of invasive disease (Reya and Clevers 2005). In addition to colorectal cancer, dysregulated Wnt signalling is also seen in hepatocellular (Longerich et al. 2019), gastric (Radulescu et al. 2013), pancreatic (Sano et al. 2016), endometrial cancer (Liu et al. 2014), acute and chronic leukaemias (Staal et al. 2016) and childhood neuroblastomas (Szemes et al. 2018; Becker and Wilting 2019). In view of the broad range of malignancies with dysregulated Wnt signalling, targeting β-catenin, or other components of the canonical Wnt signalling pathway has been intensively investigated for the possible treatment of numerous cancers. Initial safety concerns seem unfounded (Kahn 2014) and a large number of pre-clinical and phase I trials are ongoing targeting Wnt signalling in malignancy, with two phase II of WNT947, targeting Porcupine in metastatic head and neck squamous cell carcinoma, and PRI-724, a direct β-catenin antagonist in acute and chronic myeloid leukaemias (Jung and Park

2020). At the time of writing, no drug targeting the Wnt signalling pathway has been licenced for use worldwide, however encouraging animal model and safety profiles have been reported (Harb, Lin, and Hao 2019).

In addition to the role as the end effector of canonical Wnt signalling, β-catenin also has a fundamental role at the cell surface linking adherens junctions to the cytoskeleton.

1.4.3. The role of β-catenin at Adherens junctions

In addition to the critical role in canonical Wnt signalling transduction, β-catenin is also an essential component of cell surface adherens junctions (Shapiro and Weis 2009). Cell-cell junctions are critical to the morphogenesis and maintenance of tissues, cell polarity, and cell-cell communication (Green et al. 2010). Vertebrates possess three classes of intercellular junction systems; Gap junctions, forming intercellular channels allowing direct cell-cell communication by passage of small molecules and metabolites; tight junctions which act as the primary cellular determinant of the epithelial barrier; anchoring junctions, including adherens junctions and adherens junctions which link the cell surface to the cytoskeleton and mediate cell behaviours (Tian et al. 2011). Ultrastructural studies show that cells are linked by multiple junctional complexes, with tight junctions located most apically, adherens junctions immediately posteriorly to tight junctions, and desmosomes and gap junctions located more basally (Campbell, Maiers, and DeMali 2017). Adherens junctions are composed of two families of transmembrane adhesive receptors, Cadherins and Nectins (Harris and Tepass 2010). The extracellular domains of both Nectins and cadherins homodimerise with adjacent cells, mediating cell-cell adhesion, with the intracellular domains of both cadherins and recruiting additional proteins. Intracellularly Nectin interacts with the dual residency protein

Afadin, whereas Cadherins interact with α-, β-, γ-catenin and P120, which link cadherins to the actin cytoskeleton (Campbell, Maiers, and DeMali 2017; Ozawa, Baribault, and Kemler 1989) (Figure 1.5).

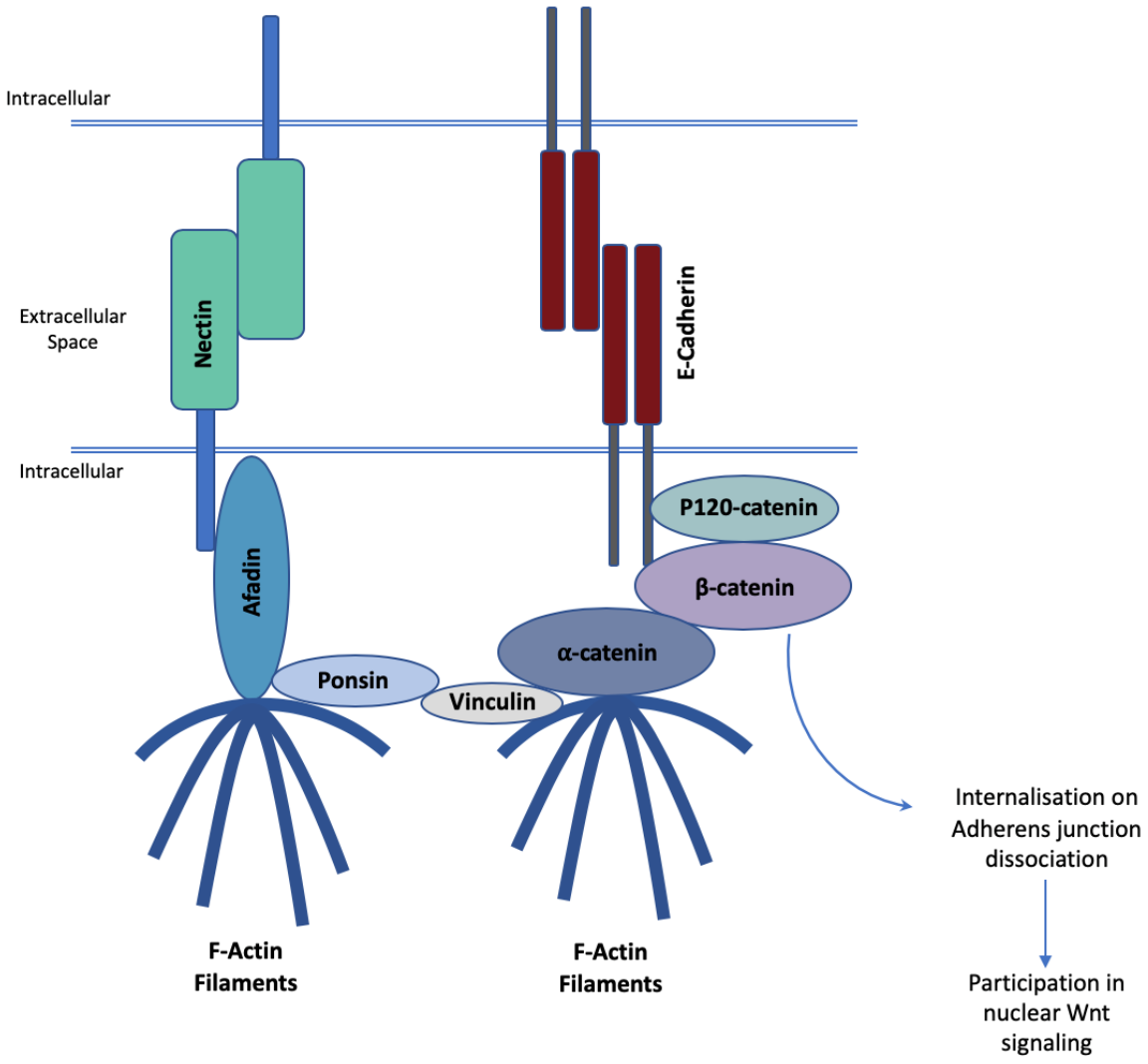

Figure 1.4. The adherens junction

Schematic representation of the adherens junction. Adherens junction are formed of both Nectin based adhesions and Cadherin based adhesions. The extracellular domain of Cadherins homodimerize in a calcium dependent fashion. The internal domain of Cadherin recruits β-catenin which binds to α-catenin, which links the cell surface complex to the F-actin skeleton. Similarly, the extracellular domain of Nectins homodimerize, with the intracellular tail interacting with Afadin, which links to the F-actin skeleton. The Nectin and Cadherin components are liked intracellularly by the linking proteins Ponsin and Vinculin (Mandai et al. 1999). Both Afadin and β-catenin can localise to the nucleus upon dissociation of the adherens complex.

The classical Cadherins constitute a large family of cell surface proteins, with a single transmembrane domain, which participate in calcium dependent cell-adhesion (Oda and Takeichi 2011). E-cadherin is the core transmembrane protein of adherens junctions. Protein interactions at the C-terminal intracellular domain of E-cadherin are regulated by phosphorylation of both E-cadherin and β-catenin. Phosphorylation of E-cadherin at serine residues (residues S684, S686 and S692) increases β-catenin binding, whereas phosphorylation of tyrosine residues of β-catenin disrupts E-cadherin (residues Y489 and Y654) and α-cadherin (Y142) interactions (Hartsock and Nelson 2008).

E-cadherin is essential to the formation of polarised epithelia, and is the major cadherin expressed in embryonic stem cell (Pieters and van Roy 2014). Furthermore, E-cadherin is essential to preimplantation development, mediating compaction of the pre-implantation blastocyst (Larue et al. 1994). Embryonic stem cell lacking E-cadherin have been generated, and demonstrate LIF independent self-renewal, with β-catenin essential to reversal of this phenotype (Soncin et al. 2009). Additionally, E-cadherin expression is frequently lost in multiple cancer types by both mutation and promotor hypermethylation (Yu, Yang, et al. 2019), although E-cadherin expression has been reported to be maintained in metastatic deposits (Petrova, Schecterson, and Gumbiner 2016; Canel et al. 2013).

Emerging evidence is showing interplay between the Wnt associated and cadherin associated pools of β-catenin (Nelson and Nusse 2004). It has been suggested that the presence of β-catenin in both these pathways suggests a mechanistic link, integrating spatial organisation of cells with gene expression through Wnt signalling. Evidence for the intersection of these fundamental cellular processes has been demonstrated by time-lapse microscopy of GFP-tagged β-catenin showing that cadherin bound β-catenin is internalised with E-cadherin upon

adherens junction dissociation, and can be translocated to the nucleus on Wnt stimulation (Kam and Quaranta 2009). Additionally, E-cadherin associated β-catenin has been shown to be internalised upon epithelial-mesenchymal transition, a process that results in dissociation of adherens junctions, and contributes to activation of Wnt signalling independently of cytoplasmic β-catenin. Additionally, Cadherins have also been shown to be required for augmentation of Wnt signalling *in vivo* (Howard et al. 2011).

Intriguingly, PRC2 has been implicated in transcriptional repression of E-cadherin in cancer (Cao et al. 2008). Additionally, mESCs lacking the PRC2.2 component Jarid2 demonstrate both aberrant E-cadherin expression and localisation, and reduced canonical Wnt signalling (Landeira et al. 2015), perhaps suggesting a mechanistic link between non-classical polycomb activity, cadherin associated β-catenin and Wnt signalling.

1.5. Aims of this study

The critical importance of PRC2 in tissue homeostasis, development and cancer is widely recognised. The polycomb group regulate chromatin and maintenance of gene silencing through covalent modification of histone tails and are implicated in the regulation genomic architecture. The PcG also have non-classical activities as a methylase of non-histone substrates and as a direct transcriptional activator. Multiple lines of evidence suggest an intersection between PRC2 activity and several key cell signalling pathways. Of particular interest is the relationship between PRC2 and canonical Wnt signalling that we have reported *in vitro*, and may be important in both development and in neoplasia. This study aims to interrogate the role of PRC2 in regulation of Wnt signalling in differentiation, by broadening our previous studies on Jarid2 null mESCs to investigate if mESCs lacking core PRC2 components show dysregulated Wnt signalling. Furthermore, this study aims to delineate the mechanism by which canonical Wnt signalling and differentiation can be rescued by co-culture with wild type mESCs.

2. Materials and Methods

2.1 Cell Lines

E14	Mouse ESC line deficient for *Hprt* derived from Lesch-Nyhan mouse embryos (Smith and Hooper 1987).
E14eGFP	Mouse ESC line generated by lentiviral transformation of E14 mESC line with the PL-SIN-PGK-eGFP plasmid (Adgene plasmid #21316 (Hotta et al. 2009)). Generated in house by Ceris Owen as part of this study.
JM8	Mouse embryonic stem cell line derived from C57BL6/N mouse embryo.
E8	Jarid2 null mESC line generated using targeted gene-trap strategy, MRC London Institute for Medical Sciences (Landeira et al., 2010).
Jarid2$^{fl/fl}$/Jarid2$^{-/-}$	Jarid2$^{fl/fl}$ mESC line was derived from fl/fl chimeric mice (Jarid2 floxed 129/Sv mESCs x C57BL/C6). Jarid2$^{-/-}$ mESC line was generated by Cre-recombinase treatment (Shen et al. 2009). Kindly provided by S. Orkin (Boston, USA)
Jarid2^{CRISPR}	Mouse ESC Jarid2-null line generated using CRISPR-Cas9 targeting in E14tg2A mESCs, in house by Hackan Bagci (Landeira et al. 2015).

B1.3 Eed$^{-/-}$	Mouse ESC line, derived from an eed3354SB mutant mouse (C5Bl/6) obtained from the Oak Ridge National Laboratory (Azuara et al. 2006)
Suz12$^{-/-}$	Mouse ESC line, derived from a superovulated Suz12$^{+/-}$ mutant mouse (C5Bl/6), kindly gifted by D. Pasini, Centre for Epigenetics and BRIC, University of Copenhagen (Pasini et al. 2007)
Suz12$^{-/-}$eGFP	Mouse ESC line generated by transformation of Suz12$^{-/-}$ mESC line with the PL-SIN-PGK-eGFP plasmid (Adgene plasmid #21316 (Hotta et al. 2009)). Generated in house by Ceris Owen as part of this study.
Ezh2$^{fl/fl}$/EZH2$^{-/-}$	Mouse ESC line, derived from Ezh2$^{fl/+}$Mx-Cre mice (Su et al. 2003). Kindly gifted by J. Pereira, Gurton Institute, University of Cambridge (Pereira et al. 2010).
C1 (E-cadherin$^{-/-}$)	Mouse ESC E-cadherin-null line generated using CRISPR-Cas9 targeting in E14tg2A mESCs in house by Andy Malinowski.
E14 H2AmCherry	Mouse ESC line with mCherry embedded in Histone 2A generated by lentiviral transformation with the mCherry_H2A plasmid (Adgene plasmid #55024) into E14 mESC line. Generated in house by Hackan Bagki.

HEK293	Human embryonic kidney cell line transformed using Adenovirus 5 DNA, obtained from ATCC (CRL-1573) (Graham et al., 1977).
Hep3B	Human hepatoma cell line transformed using human hepatitis B virus. Kindly gifted by Angela Woods, Cellular Stress Group, London Institute for Medical Sciences (Aden et al. 1979).

The cell lines used in this study were free from Mycoplasma infection.

2.2 Antibodies

2.2.1 Primary Antibodies

α-tubulin	Sigma T9026
Active β-catenin	Millipore 05-665
β-catenin	BD biosciences BD61054; Abcam AB32572
Connexin 45	EMD Millipore AB1745
E-cadherin	BD biosciences BD61081
GATA-6	R+D Systems AF1700-SP
Green fluorescent protein	Life technologies A11122; Abcam AB5450
Histone-3	Abcam AB1791
Histone3-lysine27-Me^3	Millipore 07-449
L-Afadin	Abcam AB11337
Lamin-B	Santa Cruz SC6216
Nanog	ReproCELL AB001P
Nestin	Abcam AB6142
Oct 4	Abcam AB27985
Pan-methylated-lysine	Novus NB600-824
Tuj 1	Biolegend 801202

2.2.2 Secondary Antibodies

Alexa488-conjugated donkey-anti-Rabbit	Life technologies A21206
Alexa568-conjugated donkey-anti-mouse	Life technologies A11057
Alex680-conjugated Goat-anti-mouse	Life technologies A21057
Alexa680-conjugated goat-anti-rabbit	Life technologies A21109

2.3 Tissue culture

2.3.1 Mouse embryonic stem cell line tissue culture

mESCs were grown on 0.1% gelatine treated 10cm plates, to 60-75% confluence, and typically passaged 1:10-1:15 every 48 hours, with daily media change. JM8, E8 Jarid2 -/- (Landeira et al. 2010), E14 and C1 E-cadherin -/- mESCs were maintained in knockout Dulbecco's Modified Eagles Media (DMEM, Gibco #10829-018) supplemented with 10% Embryonic stem cell fetal calf serum (ES-FCS, Gibco #10439-024), 2mM L-glutamine (Gibco #25030-024), 100 U/ml penicillin + 100µg/ml streptomycin (Gibco #15140-122), non-essential amino acids (Gibco #11140-035), 50µM 2-mercaptoethanol (Gibco #31350-010) and 1000 IU/ml leukaemia inhibitory factor (LIF).

Suz12 -/- mESCs (Pasini et al. 2007) were maintained in Glasgow's minimal essential media (GMEM) BHK21 (Gibco #21710-025) supplemented with 10% ES-FCS, 1mM sodium pyruvate (Gibco #11360-039), 100 U/ml penicillin + 100µg/ml streptomycin, non-essential amino acids, 50µM 2-mercaptoethanol and 1000 IU/ml LIF.

Eed -/- mESCs (Azuara et al. 2006) were maintained in GMEM-BHK21 media supplemented with 10% ES-FCS, 100 U/ml penicillin + 100µg/ml streptomycin, non-essential amino acids, 1mM sodium pyruvate, 0.2% Sodium Bicarbonate (Gibco 25080-060), 50µM 2-mercaptoethanol and 1000 IU/ml LIF.

Ezh2-/- mESCs (Pereira et al. 2010) were maintained in knockout DMEM supplemented with 10% ES-FCS, 5% knockout serum replacement (Gibco #10828-028), 2mM L-glutamine, 100 U/ml penicillin + 100µg/ml streptomycin, non-essential amino acids, 1mM sodium pyruvate, 50µM 2-mercaptoethanol and 1000 IU/ml LIF.

2.3.2 Human cell line tissue culture

Human HEK293T cells were maintained in Iscove's modified Dulbecco's media (IMDM, Gibco #21980-032), supplemented with 10% FCS, 2mM L-glutamine, 50µM 2-mercaptoethanol and 100 U/ml penicillin + 100µg/ml streptomycin.

Hep3B cells were maintained in complete DMEM supplemented with 10% FCS, 50µM 2-mercaptoethanol and 100 U/ml penicillin/100µg/ml streptomycin.

2.3.3 Hep3B Tissue culture and oncosphere formation

Hep3B cells (ATCC Hb-8064) cells were maintained in complete DMEM supplemented with 10% FCS, 50µM 2-mercaptoethanol and 100 U/ml penicillin/100µg/ml streptomycin. To form oncospheres, 500,000 Hep3B cells were seeded into 50ml Oncosphere media (complete DMEM supplemented with N2B27, 50µM 2-mercaptoethanol, 100 U/ml penicillin/100µg/ml streptomycin, 20ng/ml bFGF and 20ng/ml EGF) on Corning ultralow® adherence T75 flasks (Sigma #CLS3814). Oncospheres were incubated at 37ºC, 5% CO_2, 3% O_2 for 10 days. Oncosphere formation was confirmed by phase contrast microscopy.

2.3.4 Embryonic stem cell co-culture protocol

Exponentially growing cultures of E8 -/- and JM8 +/+ mESCs, or Suz12-l- and E14 mESCs were harvested, mixed 1:4 (wild-type to knockout), and grown in DMEM supplemented with 10% ES-FCS, 2mM L-glutamine, 100 U/ml penicillin + 100µg/ml streptomycin, non-essential amino acids, 50µM 2-mercaptoethanol and 1000 IU/ml LIF, on 0.1% gelatine treated nunclon T75cm flasks. Co-cultured cells were grown for 24 hours before FACS for neuronal differentiation and 24 or 72 hours prior to FACS for TOPFLASH assay.

In addition, co-culture experiments were undertaken in the presence of the gap-junction inhibitor carbenoxolone (Sagar and Larson 2006). Cells were grown in media as above supplemented with 100µM carbenoxolone for 24 hours prior to FACS sorting, and subsequent neuronal differentiation.

2.3.5. Alkaline phosphatase studies

Triplicates of 200 or 400 cells were plated onto 0.1% gelatinised 6-well plates and grown for seven days prior to alkaline phosphatase staining using the Sigma-Aldrich alkaline phosphatase staining kit (#86R 1KT), as per manufacturer's instructions.

2.4 Lentiviral transformation of mESCs

Human HEK293T cells (ATCC CRL-3216) were plated to a density of $1x10^5$ cell/cm^2, and grown for 24 hours in Iscove's modified Dulbecco's media (IMDM, Gibco #21980-032), supplemented with 10% FCS, 2mM L-glutamine, 50µM 2-mercaptoethanol and 100 U/ml penicillin + 100µg/ml streptomycin. Two hours prior to transfection cells were switched to media without antibiotic. Cells were transfected with PL_SIN_PGK_eGFP (Veeman et al. 2003), PAX2 (Pfisterer et al. 2011) and VZVg plasmids (Stewart et al. 2003) (5:2:1 ratio), using Lipofectamine® 2000 reagent (Invitrogen #11668-019). Cells were grown for 24 hours before changing to mESC media. Virus was harvested at +24 and +48 hours after switch to ES media, centrifuged 1200rpm for 5 minutes and passed through a 45µM filter. Viral suspensions were then added directly to mESCs plated at $1x10^5$ cell/cm^2, in the presence of 8µg/ml Polybrene (hexadimethrine bromide, Sigma #107689), following each lentivirus harvest. Infected mESCs

were grown for 96 hours with daily media changes prior to selection by fluorescent activated cell sorting to obtain homogeneous levels of enhanced green fluorescent protein (eGFP) expression.

Lentiviral infected mESCs were trypsin harvested, washed in phosphate buffered saline (PBS, Gibco #14190-094), and Resuspended in FACS sorting buffer (PBS supplemented with 1% FCS, 1mM EDTA (Invitrogen #15575-038) and 25mM HEPES buffer pH 7.6 (Sigma #H0887)) at $3x10^6$ cells/ml. Cells were then sorted on the basis of enhance green fluorescent protein (eGFP) signal by the MRC London Institute for Medical Sciences flow cytometry facility (BD FACSAria II and BD FACSAria III cell sorting machines). Cells were sorted into collection buffer (45µM filtered PBS supplemented with 10% FCS), centrifuged at 1200 rpm for 5 minutes, and seeded onto 0.1% gelatine treated plates, in appropriate mESC media. Enhanced GFP expression was confirmed by confocal microscopy.

2.5 Blastocyst injections

Blastocyst injections were undertaken by the MRC London Institute for Medical Sciences transgenic facility. Day 2.5 C57Bl/6 embryos were thawed, and grown for 24 hours in KSOM Media (Merck #MR-121-D). 10-15 eGFP expressing mESCs were injected into the inner cell mass (ICM) of day 3.5 blastocysts (separate injections in triplicate for Suz12-/-eGFP mESCs, and in duplicate for E14eGFP and C1eGFP E-cadherin -/- cell lines). Injected blastocysts were grown for 18 hours in KSOM media prior to fixation with 2% w/v paraformaldehyde and immunofluorescence analysis.

2.6 Neuronal differentiation

mESCs were suspended in neuronal differentiation media (1:1 mix Neurobasal media (Gibco #21103-049) and DMEM/F12 media (Gibco #21331-020), supplemented with N2 (Gibco #17502-048), B27(Gibco #17504-044), 2mM L-glutamine, 100 U/ml penicillin + 100µg/ml streptomycin, non-essential amino acids and 50µM 2-mercaptoethanol, at 25,000 cells/ml and grown in non-adherent conditions (Corning ultralow® adherence T75 flasks (Sigma #CLS3814)) for 5 days.

Cell aggregates were harvested by gravity for 15 minutes and plated on 0.1% gelatine treated nunclon T75 flasks (Fisher scientific #10538931) in neuronal differentiation media supplemented with 10ng/ml epidermal growth factor (EGF, Peprotech #315_09) and 10ng/ml basic fibroblast growth factor (h-bFGF, Peprotech #450_33) for a further three days. Cells were then plated as a monolayer in neuronal differentiation media supplemented with hFGF-2 and hEGF, on 0.1% gelatine plates/cover slips for a further 48 hours prior to processing for either RNA harvest, western analysis of immunofluorescence.

2.7 TOPFlash reporter assay

mESCs were grown to 80-90% confluence on 0.15 gelatine treated nunclon 6-well plates (ThermoFisher #140675). Cells were co-transfected with 4 µg of TOPFlash (M50 Super 8x TOPFlash, Addgene plasmid #12456, gift from R. Moon (Veeman et al. 2003)) and 0.4 µg constitutive *Renilla* luciferase (pRL-TK, Promega #E2231) plasmids using Lipofectamine 2000 reagent (ThermoFisher #11668019), in antibiotic free media. Transfected cells were grown for 48 hours prior to cell lysis. Canonical Wnt signalling activity was assessed as relative Firefly/Renilla luciferase enzymatic activity using the Dual Luciferase Reporter Assay System

(Promega #E1910), according to the manufacturer's instruction. For co-culture experiments, Suz12-l-eGFP mESCs were co-cultured with E14 mESCs (1:4 ratio) for 24 and 72 hours prior to FACS-on the basis of eGFP expression. Cells were then seeded onto 0.1% gelatine treated nunclon 6-well plates for plasmid transfection and TOPFlash assay as above. For drug inhibition experiments, 50,000 E14 mESCs were seeded onto 0.1% gelatine treated nunclon 6-well plates, and treated with 100 nM GSK 343, (Ezh2 inhibition, kindly provided by Andrew Diamond, Lymphocyte Development Group, MRC London Institute for Medical Sciences), UNC1999 (Ezh1/Ezh2 co-inhibition, 100nM, Tocris biosciences #4904) and 100nM Daminozide (KDM2A/B inhibition, Tocris biosciences #4684) for 48 hours prior to plasmid transfection and TOPFlash assay.

2.8 Nuclear/Cytoplasmic fractionation

Mouse embryonic stem cells were trypsin harvested and washed in PBS, then resuspended in ice cold fractionation buffer (10mM HEPES, 10mM KCl, 1.5 mM $MgCl_2$, 0.34M sucrose, 10%v/v glycerol, 1mM DTT, 0.1%v/v Triton X-100 and cOmplete protease inhibitor cocktail), and incubated on ice for eight minutes. Samples were then centrifuged at 1200g for 5 minutes, cytoplasmic supernatant was retained and spun 12,000g for 5 minutes. Nuclear pellets were washed in fractionation buffer. For mass spectrometry, samples were flash frozen in liquid nitrogen, and couriered on dry ice to the mass spectrometry facility (Lamond Group, University of Dundee). Samples for western blot analysis were diluted in Laemmli buffer (2% w/v sodium dodecyl sulphate (SDS), 10% v/v glycerol, 0.002% bromophenol blue, 0.06M TRIS HCl pH 6.8, 5%v/v 2-mercaptoethanol), incubated at 95ºC for 5 minutes prior to

prior to SDS polyacrylamide gel electrophoresis (PAGE). Nuclear samples were probed for lamin-B, and cytoplasmic samples for α-tubulin to confirm effective fractionation.

2.9 Immunofluorescence analysis

For mESCs; 100,000 cells were seeded onto 0.1% gelatine treated glass coverslips and grown for 24-48 hours, prior to fixation with 2% w/v paraformaldehyde for twenty minutes, followed by a five-minute incubation in permeabilization buffer (PBS + 0.4% Triton X-100). Cells were then incubated for 30 minutes in blocking buffer (PBS supplemented with 2.5%w/v BSA Fraction V, 0.05% TWEEN 20 and 10% FCS), prior to primary antibody incubation (typically diluted 1:50 to 1:500 depending on primary antibody, diluted in blocking buffer) for 90 minutes in a humidified chamber. Secondary antibodies were diluted 1:400 in blocking buffer and centrifuged at 12,000g for 10 minutes at 4ºC prior to incubation in a dark humidified chamber for 60 minutes. Slides were mounted using Vectasheld (Vector laboratories #H-1200) with 4', 6-diamidino-2-phenylindole (DAPI).

Blastocysts were fixed in 2% w/v paraformaldehyde for 15 minutes, then incubated in blastocyst permiabilisation buffer for five minutes prior to incubation in blocking buffer for 45 minutes. Blastocysts were incubated in primary antibody diluted in blocking buffer for 2 hours in a humidified chamber. Secondary antibodies were diluted 1:400 in blocking buffer and centrifuged at 12,000g for 10 minutes at 4ºC prior to incubation in a dark humidified chamber for 60 minutes. Blastocysts were mounted using Vectasheld with DAPI.

Immunofluorescence images were obtained using Leica TCS SP5-II confocal microscope.

2.10 Western blot analysis

Protein extracts were quantified using the Qubit® system as per manufacturer's instructions. Typically, 15µg protein were run per lane on 10% 15 well mini-protean TGX^{TM} polyacrylamide gels (Biorad #456-1036). Samples were run for 60 minutes at 180V, 25mA. Gels were transferred to Immobilon®-FL transfer membrane (Merck #IPFL00010), using the semi dry method and blocked with 5% milk in TRIS buffered Saline + 0.1% TWEEN 20 (TBST). Primary antibody was diluted in 5% milk/TBST and incubated overnight at 4ºC on rocking platform. Membranes were then washed in TBST, prior to secondary incubation at room temperature for 45 minutes. Fluorescent western blots were imaged using Studiolite® software.

2.11 Quantitative polymerase chain reaction

Cells were counted and 5x10^5 cells were washed in PBS and pelleted. RNA was extracted from mESC pellets using the Qiagen RNA Easy mini kit (Qiagen #74106) according to manufacturer's instructions. RNA was quantified using the ThermoFisher NanoDrop system. 1.5µg RNA was DNAse treated using the Ambion TURBO-DNA free kit, (#AM1907) according to manufacturer's instructions. RNAs were reverse transcribed using the Invitrogen SuperScript III kit (#18080051).

Primers (Table 2.1) were designed using the NCBI primer BLAST tool (https://www.ncbi.nlm.nih.gov/tools/primer-blast/). Amplification efficiencies of primers were calculated on serial dilutions of positive control cDNA and primers with amplification efficiencies close to 2 were used. qPCR analysis was carried out on Opticon DNA engine using Biorad CFX manager software. PCR reactions contained Quantitech ® SYBR®Green PCR

Mastermix (Qiagen #1020722), 300 nM primers and 2 µl of template in a 12 µl reaction volume. Cycling conditions were as follows: 95°C for 15 min, then 40 cycles of 94°C for 15 sec, 60°C for 30 sec, 72°C for 30 sec. A reaction without DNA template was included to control for formation of primer-dimers. Reactions were performed as technical duplicates and data was normalised to mUBC expression. The relative abundance of transcripts was calculated using ΔΔC(T) method.

2.12 Mass spectrometry

2.12.1 Crude cellular extract proteomic analysis

Monolayer mESCs (JM8 and E8), cells were grown to 75% confluence on 0.1% gelatine treated 14cm nunclon plates. Cells were washed in PBS, and collected by cell scraper in 2ml ice cold PBS supplemented with cOmplete® EDTA free protease inhibitor cocktail (Roche #19543200), and pooled and pelleted by centrifugation at 1200 rpm for 5 minutes. Hep3B oncospheres were harvested by gravity over 15 minutes, washed in PBS supplemented with protease inhibitor and pelleted by centrifugation at 1200 rpm for 5 minutes. Pellets were resuspended in 3x volumes Pierce IP cell lysis buffer (Thermo-Fisher #87787, composed of 25mM Tris-HCl pH 7.4, 150nM NaCl, 1mM EDTA, 1% NP40 and 5% glycerol) supplemented with 25IU/ml universal nuclease for cell lysates (Pierce #88701), 1x cOmplete protease inhibitor cocktail and 1x PhosSTOP phosphatase inhibitor cocktail (Roche #04-906-837-001). Samples were crushed with ten passes of the tight Dounce homogeniser and then incubated on rotating platform for 90 minutes at 4ºC. Cellular debris removed by centrifugation at 12,000g for 15 minutes at 4ºC. Protein concentrations were quantified using the Qubit® system. Lysate samples were flash frozen in liquid nitrogen and stored at -80°C prior to use.

2.12.2 Immunoprecipitation of target proteins

Immunoprecipitating antibody was bound to Protein-G dynabeads (Novex #1400G), for 30 minutes at room temperature on rotating wheel. Antibody cross linking using BS^3 cross-linking reagent (Thermo-Fisher #21580) was undertaken according to manufacturer's instructions if stated. Cross linking was quenched with 50mM TRIS buffer.

Antibody bound beads were incubated with whole cell lysates for 90 minutes at 4ºC on a rotating wheel. The beads were then washed five times in 500µl ice cold IP wash buffer (20mM HEPES pH7.6, 150mmol NaCl, 1.5mM $MgCl_2$ 0.2mM EDTA, 0.02% NP40 alternate) prior to elution. For Mass spectrometry samples, bound proteins were eluted in 100mM Glycine pH 2.3 for 15 minutes at room temperature. Immunoprecipitates were flash frozen in liquid nitrogen and stored at -80ºC prior to clean up and mass spectrometry. For immunoblotting, proteins were eluted into 1x Laemmli buffer and incubated at 95ºC for 5 minutes, prior to SDS PAGE and western blot analysis.

2.12.3 Immunoprecipitation clean up

Alternate clean-up methodologies were trialled and optimised;

2.12.3.1 SP3 bead clean-up

Eluates were defrosted on ice, mixed with Sera-mag® beads, and acidified to pH <2.0 with formic acid. Samples were then incubated at 25ºC for 8 minutes, then sequentially washed

with 70% ethanol and 100% acetonitrile before being eluted in 100mM triethylammonium bicarbonate (TEAB) prior to endopeptidase digestion

2.12.3.2 Trichloroacetic acid/acetone precipitation

Eluates were defrosted on ice, and mixed 1:1 with trichloroacetic acid (TCA) and incubated on ice for 5 minutes. Samples were centrifuged at 17,000g for 15 minutes at 4ºC. The pellet was washed twice in ice cold 100% acetone, then resuspended in 100mM TEAB.

2.12.3.3 In-gel digest

Eluates were defrosted on ice. NuPage LDS buffer (4:1 dilution, ThermoFisher #NP0008) was added, and samples were incubated at 65ºC for 10 minutes. Samples were then loaded onto a pre-set 10% NuPage gel with 3-(N-Morpholino)propanesulfonic acid (MOPS) buffer (Sigma-Aldrich #NP0302) for electrophoresis. Bands corresponding to expected size of β-catenin were visualised on a light box and cut out using a scalpel. The gel fragments were dehydrated in 100% acetone for 5 minutes at room temperature, before resuspension in 100mM TEAB.

2.12.4 Endopeptidase Digest

Endopeptidases used for these analyses; Trypsin endopeptidase (Pierce #90307), GluC (Pierce #90054), AspN (Pierce #90053). Following clean-up Immunoprecipitates were sequentially digested for 4 hours at 37ºC as per manufacturer's instructions, prior to TCA precipitation, and vacuum drying.

2.12.5 Mass Spectrometry

Mass spectrometry (MS) was kindly undertaken by two independent MS facilities (MS Facility, MRC London Institute for Medical Sciences and the Lamond Group, School of Life Sciences, University of Dundee). High pressure liquid chromatography and MS was undertaken using a 2-hour gradient on Q-Exactive prior to MS. Both MaxQuant (Tyanova et al. 2015) and MASCOT (Brosch et al. 2009) algorithms were used for lysine methylation searches, with the kind assistance of both the MRC MS facility, and the Lamond group. MaxQuant analysis alone was undertaken for co-immunoprecipitation studies. The proteomic method used in this study is termed '*bottom up proteomics'*, whereby peptide digest fragments are identified by a database search algorithm, then assembled into proteins through protein inference (Huang et al. 2012). Both MASCOT and MaxQuant use such a database search strategy, with a probabilistic peptide scoring model for the analysis of tandem mass spectrometry data (Perkins et al. 1999; Cox and Mann 2008). This study utilises 'label free quantification', a technique that allows for quantification of protein levels between sample conditions (for example jarid2 WT vs. Jarid2 null mESCs), without peptide labelling (Cox et al. 2014). Briefly this technique normalises paired datasets to each other based on the abundance of peptides that do not change in expression levels between samples, and a normalisation algorithm controls for systematic artefacts in peptide intensity values between samples. Peptides with significant differences in abundance between the samples can then be identified. Both MASCOT and MaxQuant utilise a false discovery rate (FDR) control, employing a target-decoy database search strategy (Wang et al. 2009).This process provides a means for controlling the numbers of expected false positive identifications in a given dataset. Data analysis and figure preparation was undertaken by myself using Perseus version 1.6.14.0 (Tyanova et al. 2016).

Table 2.1 Primers used in this study

Mouse target	Primer name	Sequence 5'-3'
Nanog	Nanog_F	GAACTATTCTTGCTTACAAGGGTCTGC
	Nanog_R	GCATCTTCTGCTTCCTGGCAA
Gata6	Gata6_F	GGTCTCTACAGCAAGATGAATGG
	Gata6_R	TGGCACAGGACAGTCCAAG
Rex1	Rex1_F	CTCCTAGCCGCCTAGATTTCC
	Rex1_R	CGTGTCCCAGCTCTTAGTCCATT
Gata4	Gata4_1F	TCTAAGACGCCAGCAGGTC
	Gata4_1R	TGCTGCTGCTGCTAGTGG
Ubiquitin C	Ubc_F	AGGAGGCTGATGAAGGAGCTTGA
	Ubc_R	TGGTTTGAATGGATACTCTGCTGGA
Connexin 43	Cx43_F2	CTTTCATTGGGGGAAAGGCG
	Cx43_R2	CTGGGCACCTCTCTTTCACTT
Connexin 45	Cx45_F1	GAGTTCTGGTGAACAGGGCA
	Cx45_R1	ACAATCAGCACAGTGAGCCA
Connexin 31	Cx31_F3	CTGCTGTTCCCTAGTCAGCG
	Cx31_R3	GTGCCCACAGTCAGCGG
Sox2	Sox2_Mus_F	CACAACTCGGAGATCAGCAA
	Sox2_Mus_R	CTCCGGGAAGCGTGTACTTA
Pax6	Pax6_Mus_F	AGGGGGAGAGAACACCAACT
	Pax6_Mus_R	TTTGGCCCTTCGATTAGA
Nestin	Nestin_Mus_F	AGGCTGAGAACTCTCGCTTG
	Nestin_Mus_R	ATTAGGCAAGGGGGAAGAGA
Oct4	Oct4_Mus_F	CGTGGAGACTTTGCAGCCTG
	Oct4_Mus_r	GCTTGGCAAACTGTTCTAGCTCCT

Axin	Axin_1_F	GAGAGTGAGCGGCAGAGC
	Axin_1_R	CGGCTGACTCGTTCTCCT
Lef1	Lef1_1_F	TGGTTAACGAGTCCGAAATCA
	Lef_1_R	AGAGGACGGGGCTTGTCT
Tcf	Tcf1_1_F	GCTGCCTGAGGTCAGAGAAT
	Tcf1_1_R	CCCCAGCTTTCTCCACTCTA
Sp5	Sp5_1_F	ACCGGGACACTTTCGAGGCCACTCC
	Sp5_1_R	CAGCAGCGACTCCCACAAGCAAGG

Chapter 3. Characterising altered Wnt signalling in mESCs lacking PRC2 activity

PRC2 has been shown to interact with Jarid2 in embryonic stem cells (Landeira et al. 2010; Shen et al. 2009; Li et al. 2010; Peng et al. 2009; Pasini et al. 2010). The roles of Jarid2 for regulating PRC2 remain uncertain and are an active area of research. Jarid2 also has a role beyond PRC2 mediated histone methylation and has been implicated in the regulation of canonical Wnt signalling in mouse embryonic stem cells (Landeira et al. 2015). ESCs lacking Jarid2 demonstrate supressed canonical Wnt signalling as assessed by both TOPflash assays, and western blot analysis using antibodies specific to the unphosphorylated, active form of beta-catenin (Landeira et al. 2015). In addition, reduced expression of validated Wnt targets was also reported in Jarid2-deficient mESCs. These cells can readily self-renew, but have altered cell and colony morphology, and show a severe differentiation block, so that exposure to differentiation cues results in widespread cell death. ESCs lacking Jarid2 displayed reduced and patchy E-cadherin expression. Interestingly, upon injection into E3.5 blastocysts initiate formation of multiple inner cell masses. This unusual phenotype suggests that perturbation of the core epigenetic machinery results in changes in cell-cell communication so that individual mESCs seed ICMs independently, rather than contributing to a single ICM.

3.1. Mouse embryonic stem cells lacking core PRC2 components show reduced canonical Wnt signalling

As reduced canonical Wnt signalling has previously been demonstrated in mESCs lacking Jarid2 (Landeira et al. 2015), it is important to ask whether this is a property unique to Jarid2, or whether other PRC2 complex components also contribute to suppression of canonical Wnt signalling. To investigate this a panel of mESC lines lacking core PRC2 components (Ezh2-/- (Pereira et al. 2010), Eed deficient B1.3 (Azuara et al. 2006) and Suz12-/- (Pasini et al. 2007)),

were interrogated for canonical Wnt signalling activity using the TOPFlash assay (Korinek et al. 1997) (experiment undertaken with Dr Andy Malinowski, Lymphocyte Development Group, MRC London Institute for Medical Sciences, Figure 3.1.a.). Briefly, PRC2 null and matched parental mESCs were transiently co-transfected with a TOPFlash reporter plasmid (where the firefly luciferase lies downstream of seven tandem Wnt target TCF/LEF elements), and a constitutive expressing *Renilla* luciferase plasmid to control for variability in cell numbers and transfection efficiency. ESCs lacking each of the individual core PRC2 components demonstrated reduced canonical Wnt signalling, but to a variable degree. ESCs lacking Suz12 showed dramatically reduced Wnt signalling similar to that observed in Jarid2 -/- mESCs, whereas mESCs lacking EED or EZH2 showed reduced canonical Wnt signalling but to a lesser extent.

To validate that reduced canonical Wnt signalling is a feature of PRC2-defficient mESCs expression of a panel of validated, positively regulated Wnt target genes (Sp5 (Huggins et al. 2017), Tcf1 (Roose et al. 1999), Lef1 (Filali et al. 2002) and Brachyury (Arnold et al. 2000)) was examined using quantitative rtPCR. In these experiments Suz12 null and parental mESC cultures were compared for target gene expression normalised to expression of Ubiquitin C expression (Figure 3.1.b). Reduced expression of each of the panel of Wnt targets was observed, consistent with the supressed canonical Wnt signalling observed in Suz12-/- mESCs.

To further investigate the relevance of PRC2 activity for Wnt signalling, wild type E14 mESCs were treated with small molecule inhibitors to Ezh2 (GSK-343 (Verma et al. 2012)), Ezh1 and Ezh2 (UNC1999 (Konze et al. 2013)), and to the lysine demethylase Kdm2a (Daminozide (DZD) (Rose et al. 2012)), which has previously been reported to stabilise nuclear β-catenin (Lu et al. 2015). Cell cultures were drug treated for 48 hours prior to assessment of canonical

Wnt signalling activity by TOPFlash assay. To confirm that treatment with these drugs did not induce differentiation, mRNA expression of pluripotency markers (Nanog, Sox2, Oct4) were compared with untreated cells, along with immunostaining for Oct4 expression (Figure 3.1.c-d). Drug treated cells continued to express pluripotency markers, at both the mRNA and protein level, showing that changes in Wnt signalling were not due to drug treatment driving differentiation. Drug treated cells were interrogated for canonical Wnt signalling activity using TOPFlash assay (Figure 3.1.e). mESCs treated with Ezh2 inhibitors showed significantly reduced canonical Wnt signalling activity, and the reverse was true of cells treated with lysine demethylase inhibitor which showed elevated canonical Wnt signalling. Drug inhibition of the methyltransferase activity of PRC2 supressed canonical Wnt signalling, providing additional evidence of a role for PRC2 in the activity of canonical Wnt signalling.

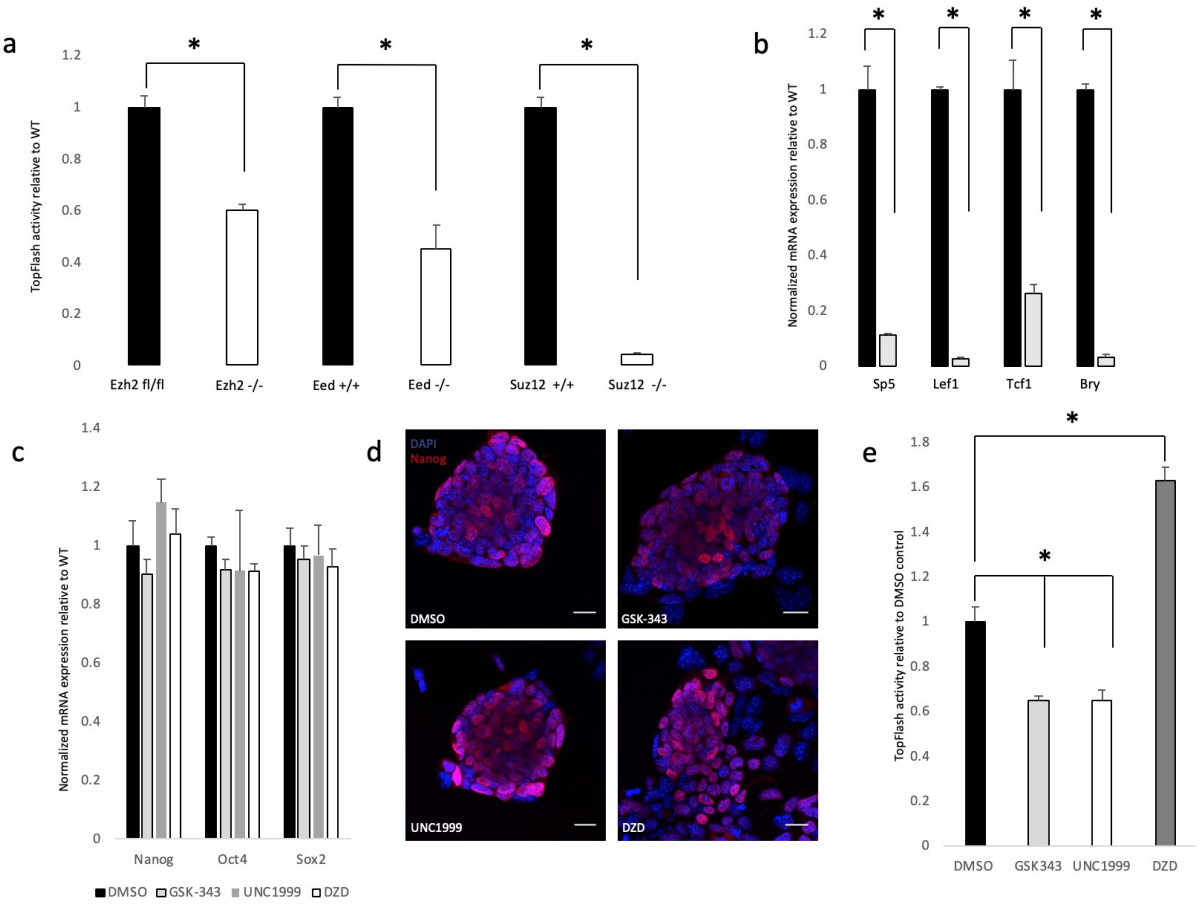

Figure 3.1. mESCs lacking core PRC2 components show reduced canonical Wnt signalling

a. β-catenin activity, evaluated by luciferase-based TOPFlash assays comparing matched wild type (black bars) and PRC2 null (white bars) mESCs: Ezh2 fl/fl:Ezh2-/- (left), Eed+/+:Eed deficient B1.3 (labelled -/-, middle), Suz12+/+:Suz12-/- (right). Activity relative to WT. Mean ± SE of three experiments shown; asterisks denote $p<0.05$ (students t-test). Experiment undertaken with Dr Andy Malinowski.

b. Quantitive-PCR analysis of validated positively regulated canonical Wnt target genes expressed by wild type (Suz12+/+, black bars) and Suz12 null (Suz12-/-, light grey bars). Expression normalised to Ubiquitin C; Expression relative to wild type. Mean ± SE of three experiments shown; asterisks denote $p<0.05$ (students t-test).

c. RT-PCR analysis of pluripotency genes (Nanog, Oct4 and Sox2 (Orkin et al. 2008)) expressed by wild type (E14) mESCs treated with 48 hours DMSO control (black bars) and 100 μM GSK-343 (light grey bars), 100μM UNC1999 (dark grey bars) of daminozide (DZD, white bars). Expression normalised to Ubiquitin C; Expression relative to DMSO control. Mean ± SE of three experiments shown; asterisks denote $p<0.05$ (students t-test).

d. Confocal images showing Nanog (Red) immunolabelling of E14 mESCs treated with 48 hours DMSO control (top left) and 100 μM GSK-343 (top right), 100μM UNC1999 (bottom left) of daminozide (DZD, bottom right). Counterstained with 4',6-diamidino-2-phenylindole (DAPI). Scale bar 20μm.

e. β-catenin activity, evaluated by luciferase-based TOPFlash assays comparing wild type (E14) mESCs treated with 48 hours DMSO control (black bar) and 100 μM GSK-343 (light grey bar), 100μM UNC1999 (white bar) of daminozide (DZD, dark grey bar). Activity relative to WT. Mean ± SE of three experiments shown; asterisks denote $p<0.05$ (students t-test).

3.2. Mouse ESCs lacking Suz12 fail to execute neuronal differentiation

As canonical Wnt signalling was drastically impaired in Suz12 null mESCs, these ES cells were selected for further functional studies. mESCs lacking Suz12 were initially generated from Suz12-/- inner cell mass outgrowth isolated from E3.5 blastocysts from heterozygote Suz12+/- crosses (Pasini et al. 2007). Suz12-/- mESCs were reported to have a global loss of H3K27me3. These ES cells self-renew in media containing serum + LIF but fail to execute lineage specification, when treated with all-trans-retinoic acid (ATRA) to induce differentiation into neural precursors (Fraichard et al. 1995). When treated with ATRA Suz12-/- mESCs demonstrated inefficient repression of pluripotency gene expression and failed to activate neuronal lineage specific genes (Pasini et al. 2007).

Suz12-/- ES cells were kindly provided to us by the Centre for Epigenetics and BRIC, University of Copenhagen. Initially I confirmed that the Suz12-/- mESCs did not express Suz12 by western blot analysis (figure 3.2.a – upper panel). Additionally, the H3K27me3 modification was also undetectable (figure 3.2.a – middle panel), as compared to robust detection in Suz12+/+ wild-type controls. In order that mutant Suz12-/- cells could be tracked in co-culture experiments and in blastocyst injection experiments, Suz12-/- mESC and matched parental controls were transfected to stably express enhanced green fluorescent protein (eGFP) under the constitutive PGK promotor (Hotta et al. 2009), using a lentiviral infection strategy (Dull et al. 1998). Stable expression of eGFP was confirmed by immunofluorescent confocal microscopy (Figure 3.2.b). To test the capacity of Suz12-/- mESCs to give rise to neuronal precursors, a monolayer differentiation approach was used (Ying et al. 2003).

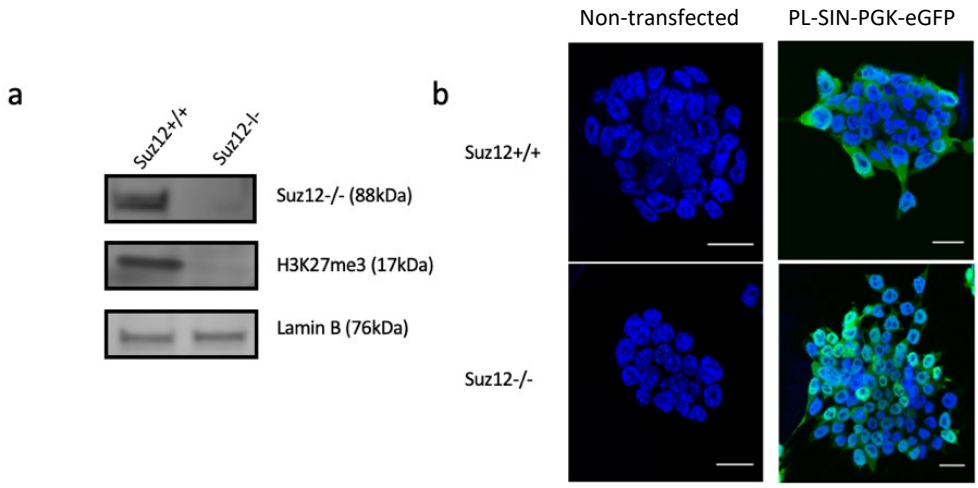

Figure 3.2. mESCs lacking Suz12 lose PRC2 mediated H3K27Me3, and will express eGFP after lentiviral transfection

a. Western blot analysis of Suz12-/- and matched parental ES cell cultures. Suz12-/- confirmed to be deficient in Suz12 expression (88kDa), with robust expression seen in matched parental cells (upper panel). Suz12-/- cells lack PRC mediated histone modification H3K27me3 (17kDa), present in matched parental cells (middle panel). Loading control Lamin B (76kDa).

b. Confocal microscopy of immunolabelled Suz12-/- (lower panels) and matched parental samples (upper panels) following lentiviral transfection of the PL-SIN-PGK-eGFP plasmid confirming eGFP expression (right), and non-transfected control mESCs (left). Scale bar 25 μm.

Briefly, undifferentiated Suz12-/- and matched parental ES cultures maintained in media supplemented with serum and LIF were detached and grown in non-adherent conditions in media supplemented with N2B27, prior to harvesting, and expansion as a monolayer on gelatine plates in media supplemented with N2B27, basic fibroblast growth factor (bFGF), and epidermal growth factor (EGF) as outlined in figure 3.3.a.

To track differentiation, the expression of pluripotency markers and neural precursor markers was assessed by quantitative rt-PCR (figure 3.3.b) and immunofluorescence confocal microscopy (figure 3.3.c). In wild-type (Suz12+/+) mESCs, Oct4, Sox2, Rex1 and Nanog expression was extinguished over time. In Suz12-/- mESCs a similar loss of pluripotency markers was seen (figure 3.3.b, upper panels). Indeed, accelerated dynamics of repression of pluripotency markers was identified for Nanog and Sox2 by quantitative rt-PCR, with repression of Oct4 and Rex1 comparable to wild type also observed. Immunofluorescence

confocal microscopy revealed that both Suz12 deficient and wild type ES cells demonstrate undetectable Oct4 expression following 12 days of neural differentiation protocol, compared to robust expression observed in undifferentiated controls (figure 3.2.b,c,d). However, mESCs lacking Suz12 failed to express markers of neural precursors, such as Nestin and Tuj1, compared to robust expression observed in matched parental controls (figure 3.2.c,d). Immunofluorescence analysis did not detect Nestin or Tuj1 expression by Suz12-/- cells following monolayer neural differentiation (figure 3.2.c,d). Additionally, I also noted that inactivation of eGFP expression occurred in a proportion of wild type and Suz12-/- ES cells following the differentiation protocol (figure 3.3.c,d lower panels). Loss of expression of PGK promotor driven GFP following neural differentiation of lentiviral transfected GFP expressing mESCs has previously been reported (Wang et al. 2008) and is not unexpected, but is relevant to co-culture experiments described later in this chapter.

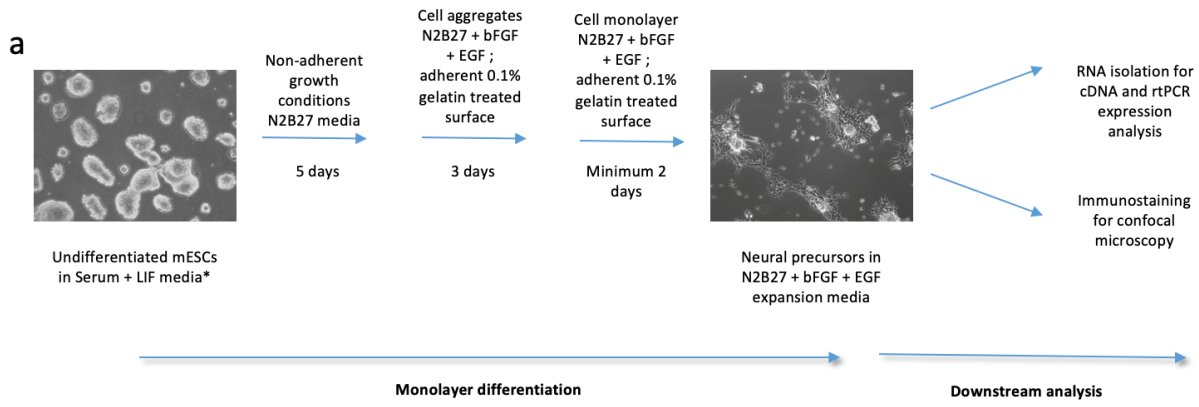

(Figure continued on next page)

b

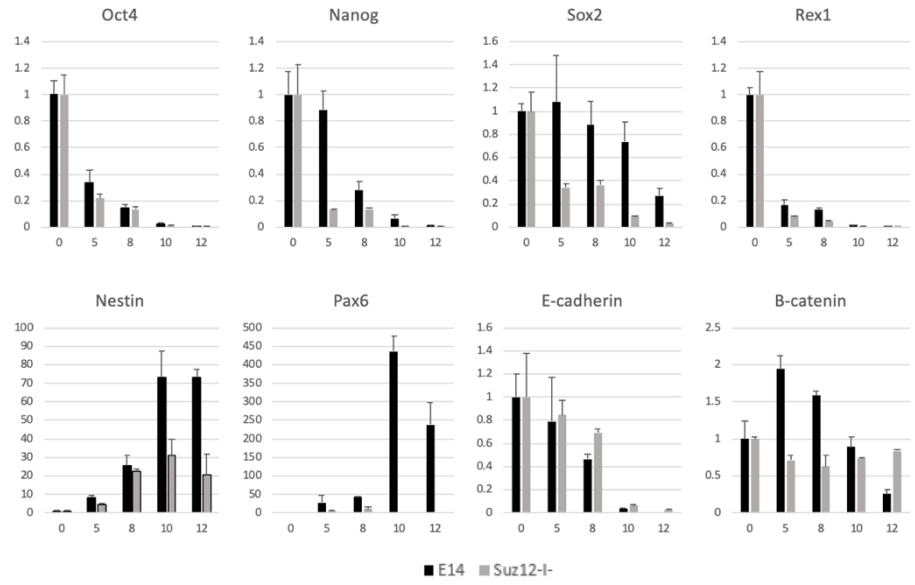

c

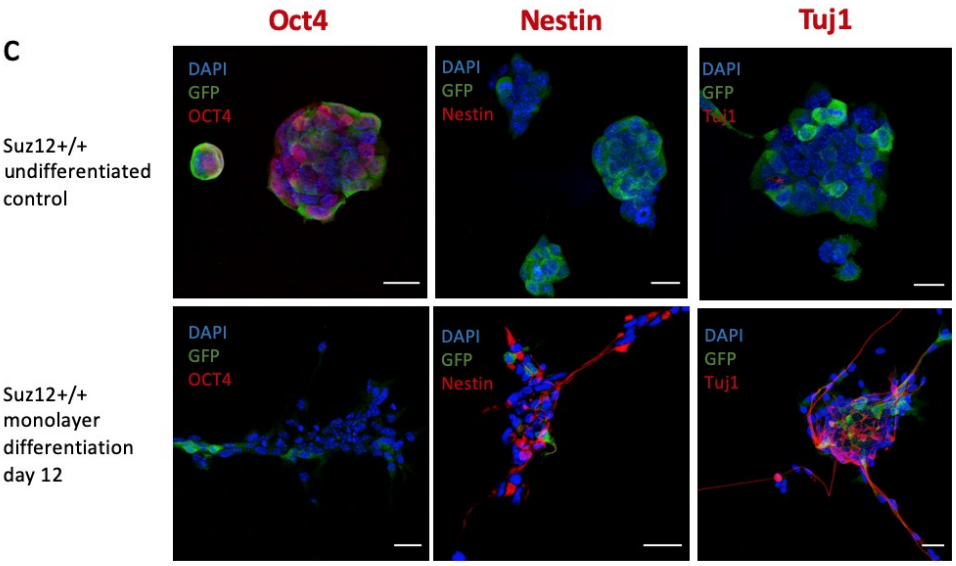

d

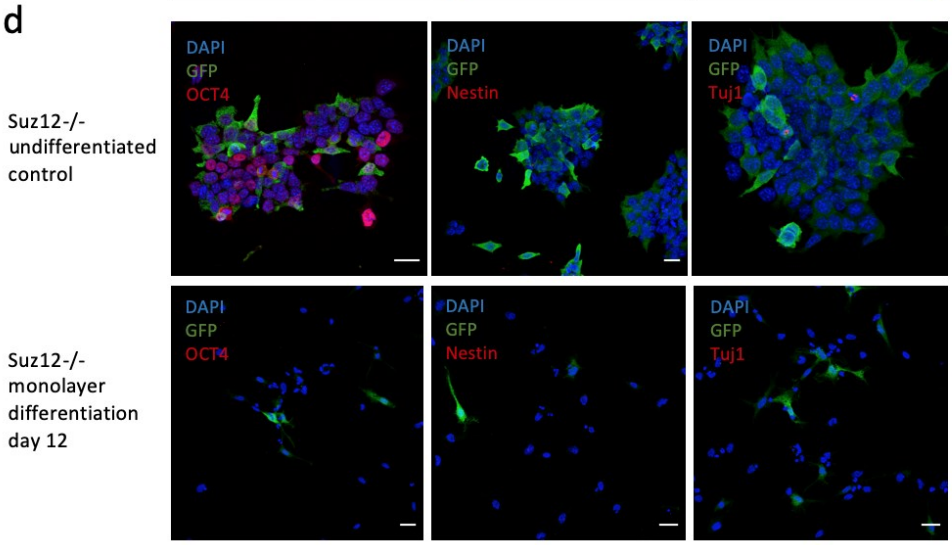

(Legend on next page)

I also examined β-catenin and E-cadherin gene expression in monolayer neural differentiation cultures; expression of E-cadherin by Suz12-/- cells was similar to parental controls, however expression of β-catenin remained stable in Suz12-/- ES cells over time course without a burst of expression between 5-8 days that was observed in parental control mESCs.

In summary, Suz12-/- mESCs failed to execute neural differentiation when exposed to a monolayer neural differentiation protocol. In contrast to the results of pluripotency gene expression previously reported for ATRA neural differentiation (Pasini et al. 2007), efficient downregulation of pluripotency genes was observed. Failure to express neural lineage markers was observed in keeping with previous reports, and a failure of a burst of β-catenin mRNA expression observed in wild type cells was also seen. Additionally, dropout of PGK driven eGFP expression was observed in a proportion of both Suz12-/- and wild type cells.

Figure 3.3. Suz12-/- mESCs fail to execute monolayer neural differentiation (Continued)

a. Schematic of monolayer neural differentiation protocol; undifferentiated mESCs are grown in non-adherent conditions in N2B27 media for five days to form aggregates, before seeding in neural expansion media, and plating into a monolayer after 72 hours. Neural progenitors were confirmed by expression of neural markers Nestin and Tuj1.

b. RT-PCR analysis of pluripotency (Oct4, Nanog, Sox2, Rex1 (Son et al. 2013)), Neural progenitor (Nestin, Pax6), and E-cadherin and β-catenin expression at timepoint 0, 5, 8, 10 and 12 days of monolayer neural differentiation protocol. Expression normalised to Ubiquitin C; Expression relative to wild type. Mean ± SE of three experiments shown.

c. Confocal images showing immunolabelling for Oct4 (red, left panels), Nestin (red, middle panels) or Tuj (red, right panels) and GFP (green), of undifferentiated Suz12+/+ ES cells (upper panels) and Suz12+/+ ES cells following 12 days of monolayer neural differentiation (lower panels). Counterstained with 4′,6-diamidino-2-phenylindole (DAPI); Scale bar 25μm. Loss of expression of the pluripotency marker Oct 4, with concomitant robust expression of neural progenitor markers Nestin and Tuj 1 was observed.

d. Confocal images showing immunolabelling for Oct4 (red, left panels), Nestin (red, middle panels) or Tuj (red, right panels) and GFP (green), of undifferentiated Suz12-/- ES cells (upper panels) and Suz12-/- ES cells following 12 days of monolayer neural differentiation (lower panels). Counterstained with 4′,6-diamidino-2-phenylindole (DAPI); Scale bar 25μm. Loss of expression of the pluripotency marker Oct 4, with concomitant failure to express neural progenitor markers Nestin and Tuj 1 was observed.

3.3. Co-culture of Suz12-/- mESCs with wild type cells partially restores canonical Wnt signalling and rescues neuronal differentiation

Previous experiments using Jarid2 null mESCs have shown constitutively supressed canonical Wnt signalling, and a severe differentiation block (Landeira et al. 2015). Intriguingly, however both canonical Wnt signalling (figure 3.4.c, experiment undertaken by Dr Andy Malinowski) and neural differentiation could be partially rescued following co-culture with the matched parental wild type ES cultures. The mechanism underlying this observation have yet to be elucidated. Given the differentiation block and supressed canonical Wnt signalling observed in Suz12-/- ES cells, co-culture experiments were undertaken to investigate whether rescue of canonical Wnt signalling and neural differentiation is a feature of both Jarid2-/- and Suz12-/- mESCs following co-culture with matched parental mESC cultures.

Initially Suz12-/- mESCs expressing eGFP under the PGK promotor (eGFP+, figure 3.2.b) were co-cultured in a 1:4 ratio with matched parental wild type cells (eGFP-) for 24 hours prior to fixation and immunostaining for GFP expression (figure 3.4.a). Clusters of eGFP+ and eGFP- cells were readily detected demonstrating interacting cells as previously observed in the Jarid2 co-culture experiments. Co-culture experiments were then undertaken to assess rescue of canonical Wnt signalling and neural differentiation. Briefly, Suz12-/-eGFP+ cells were cultured in a 1:4 ratio with parental Suz12+/+eGFP- cells, and grown in media containing fetal bovine serum and LIF. Following co-culture cells were isolated by fluorescent activated cell sorting (FACS) on the basis of GFP expression, with only GFP+ cells retained (schematic figure 3.4.b). GFP+ cells were then interrogated for β-catenin activity using TOPFlash assay (Figure 3.4.d), and for capacity to differentiate by subjecting to monolayer neural differentiation conditions. Neural precursor cells were confirmed by immunostaining for Nestin and Tuj1 (figure 3.4.e,f).

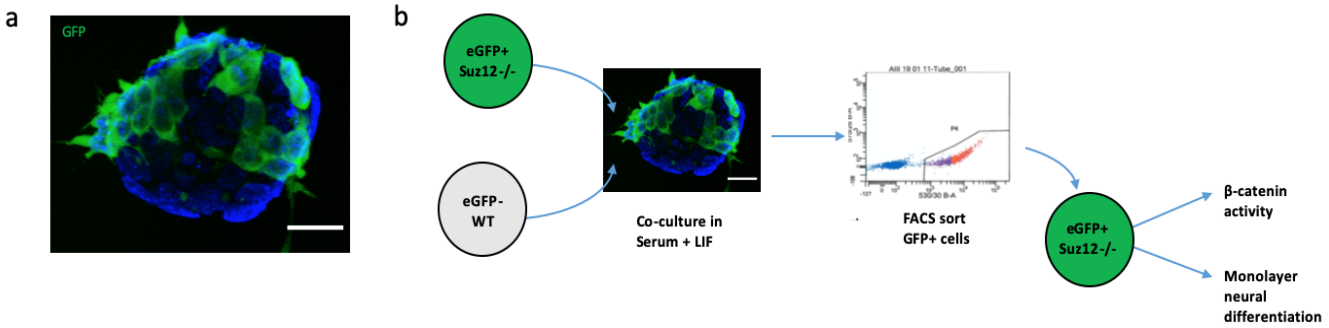

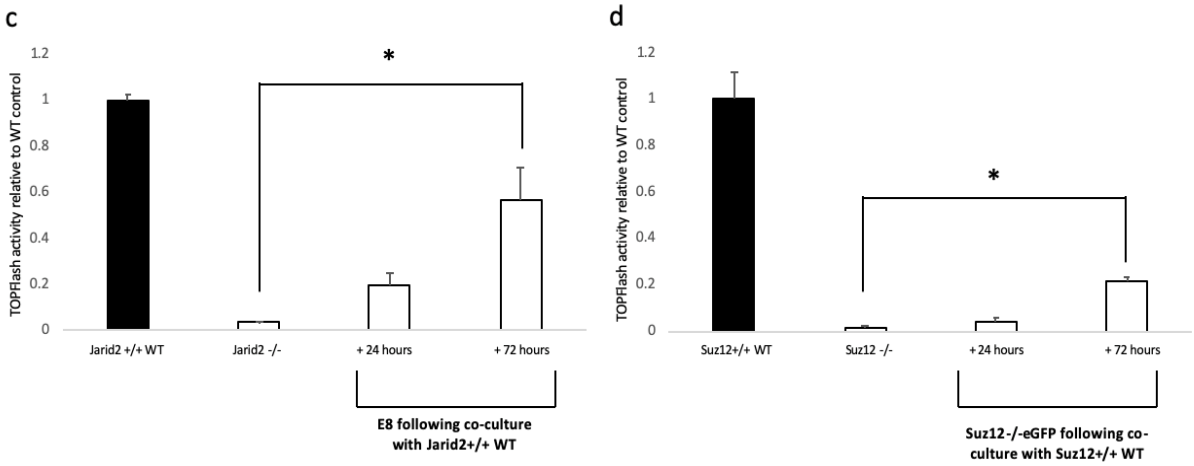

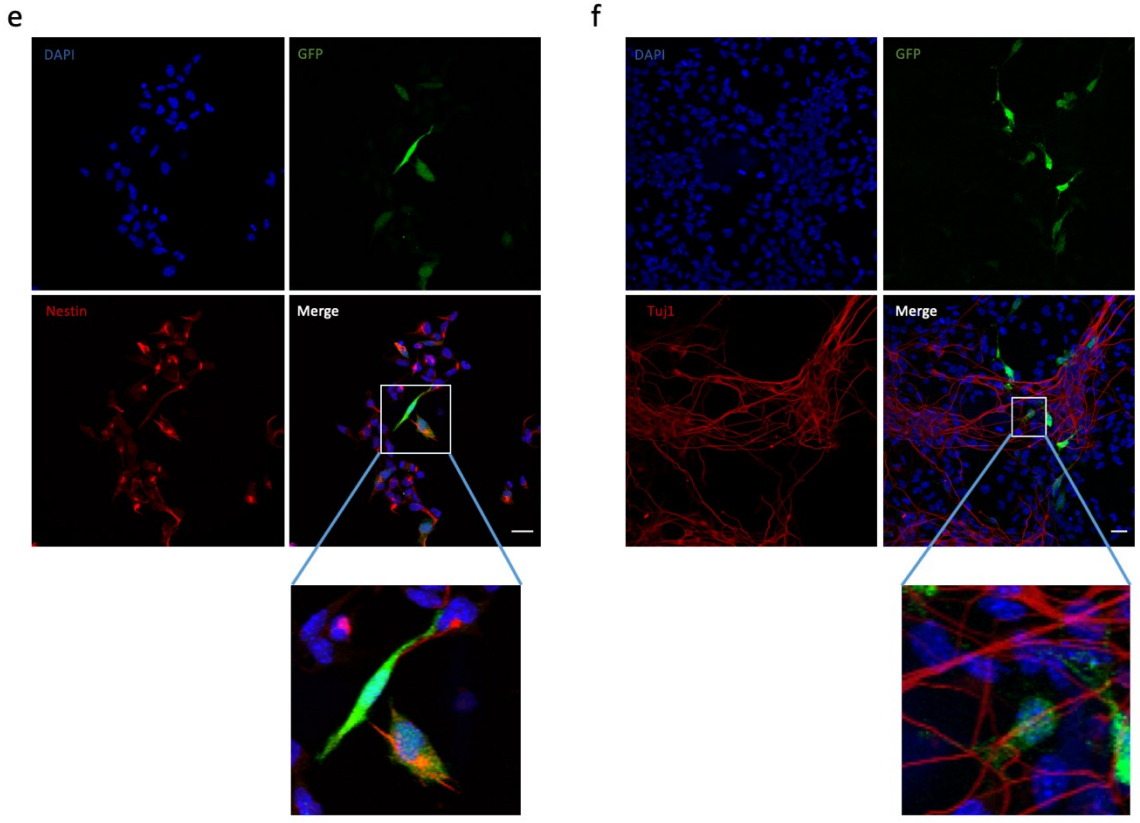

(Legend on next page)

Following co-culture canonical Wnt signalling activity was partially restored to Suz12-null mESCs, although to a lesser extent than had been observed in Jarid2-/- co-cultured ES cells (figure 3.4.c,d). In addition, competency of neural differentiation in monolayer neural differentiation conditions was also partially restored. However, as observed with the wild-type neural differentiation (figure 3.3.c), inactivation of eGFP expression is widely observed, although clear examples of Suz12-/- mutant eGFP+ ES cells expressing Nestin and Tuj1 were seen (inset figure 3.4.d,e). However, an alternative explanation for the observed eGFP- cells following differentiation could also be that a small population of GFP- cells evade FACS sorting (in cell doublets for example, although doublet discrimination is routinely undertaken), resulting in mixed colonies. Due to the prolonged neural differentiation protocol a small population of wild type cells could conceivably expand into a significant proportion of the cell culture, particularly if they have a growth advantage in neural differentiation conditions.

Figure 3.4. Canonical Wnt signalling and neural differentiation is restored in Suz12-/- mESCs following co-culture with wild type parental mESCs

a. Confocal images showing immunolabelling for GFP (green) in mixed Suz12-/-:Suz12+/+ cultures. Counterstained with 4',6-diamidino-2-phenylindole (DAPI); Scale bar 25μm. Imaging demonstrates interaction between GFP+ and GFP- cells.
b. Schematic of experimental design; GFP + suz12-/- cells are grown in mixed cultures with GFP- WT cells (ratio 1:4), sorted for eGFP expression by FACS, for downstream analysis with either TOPFlash assay to assess β-catenin activity, or monolayer neural differentiation and immunostaining for markers of neural differentiation.
c. β-catenin activity, evaluated by luciferase-based TOPFlash assays comparing matched wild type (black bars) and Jarid2 null ES cell cultures, at baseline and after 24 or 72 hours of co-culture with wild-type parental ES cultures and FACS sorting. Activity relative to wild-type. Mean ± SE of three experiments shown; asterisks denote $p<0.05$ (students t-test). Experiment undertaken by Dr Andy Malinowski, data used with permission
d. β-catenin activity, evaluated by luciferase-based TOPFlash assays comparing matched wild type (black bars) and Suz12 null ES cell cultures, at baseline and after 24 or 72 hours of co-culture with wild-type parental ES cultures and FACS sorting. Activity relative to wild-type. Mean ± SE of three experiments shown; asterisks denote $p<0.05$ (students t-test).
e. Confocal images showing immunolabelling for Nestin (Red, bottom left) and GFP (green, top right), Suz12-/- ES cells following 24-hour co-culture with wild-type ES cells, and 12 days of monolayer neural differentiation. Counterstained with 4',6-diamidino-2-phenylindole (DAPI); Scale bar 25μm. Inset; magnified confocal imaging of GFP+ cell expressing Nestin
f. Confocal images showing immunolabelling for Tuj1 (Red, bottom left) and GFP (green, top right), Suz12-/- ES cells following 24-hour co-culture with wild-type ES cells, and 12 days of monolayer neural differentiation. Counterstained with 4',6-diamidino-2-phenylindole (DAPI); Scale bar 25μm. Inset; magnified confocal imaging of GFP+ cell expressing Tuj1

To exclude this possibility, I designed an alternative strategy to distinguish Suz12-/- ES cells. Co-culture experiments were undertaken using modified E14 cells, which express mCherry embedded in histone H2A (kindly provided by Dr Hakan Bagci, Lymphocyte development group, MRC London Institute for Medical Sciences). In principle the modified H2AmCherry should remain resident in the E14 cells during differentiation, allowing discrimination of E14mCherry and Suz12-/-eGFP cells, and controlling for inactivation of eGFP expression in the Suz12-/- ES cells. Initially E14mCherry ES cell cultures were interrogated for mCherry expression both in the undifferentiated state and following monolayer neural differentiation, confirmed by Nestin expression (Figure 3.5.a). Robust mCherry signal overlying DAPI was detected in both conditions.

Subsequently repeat co-culture experiments were undertaken using E14 H2AmCherry in place of parental wild type ES cells. Briefly Suz12-/-eGFP+ cells were cultured in a 1:4 ratio with E14H2AmCherry ES cells in place of matched parental ES cells, and grown in media containing FCS and LIF. Following co-culture cells were isolated by multicolour FACS, sorting GFP+/mCherry- ES cells. Sorted ES cells then underwent monolayer neural differentiation, and neural differentiation was confirmed by immunostaining and confocal microscopy for Nestin and Tuj1 (experimental design schematic figure 3.5.b). Additionally, immunostaining was undertaken for Suz12, with secondary staining with Alexa Fluor 568nm, corresponding to mCherry excitation spectrum, i.e., cells without excitation in this spectrum are negative for both mCherry and Suz12, confirming the identity as Suz12-/- cells. This evidence suggests that co-culture of both Suz12 and Jarid2 null mESCs with parental wild type controls can partially rescue both canonical Wnt signalling and overcome differentiation block. Subsequent experiments focus on understanding the mechanism underlying this intriguing observation.

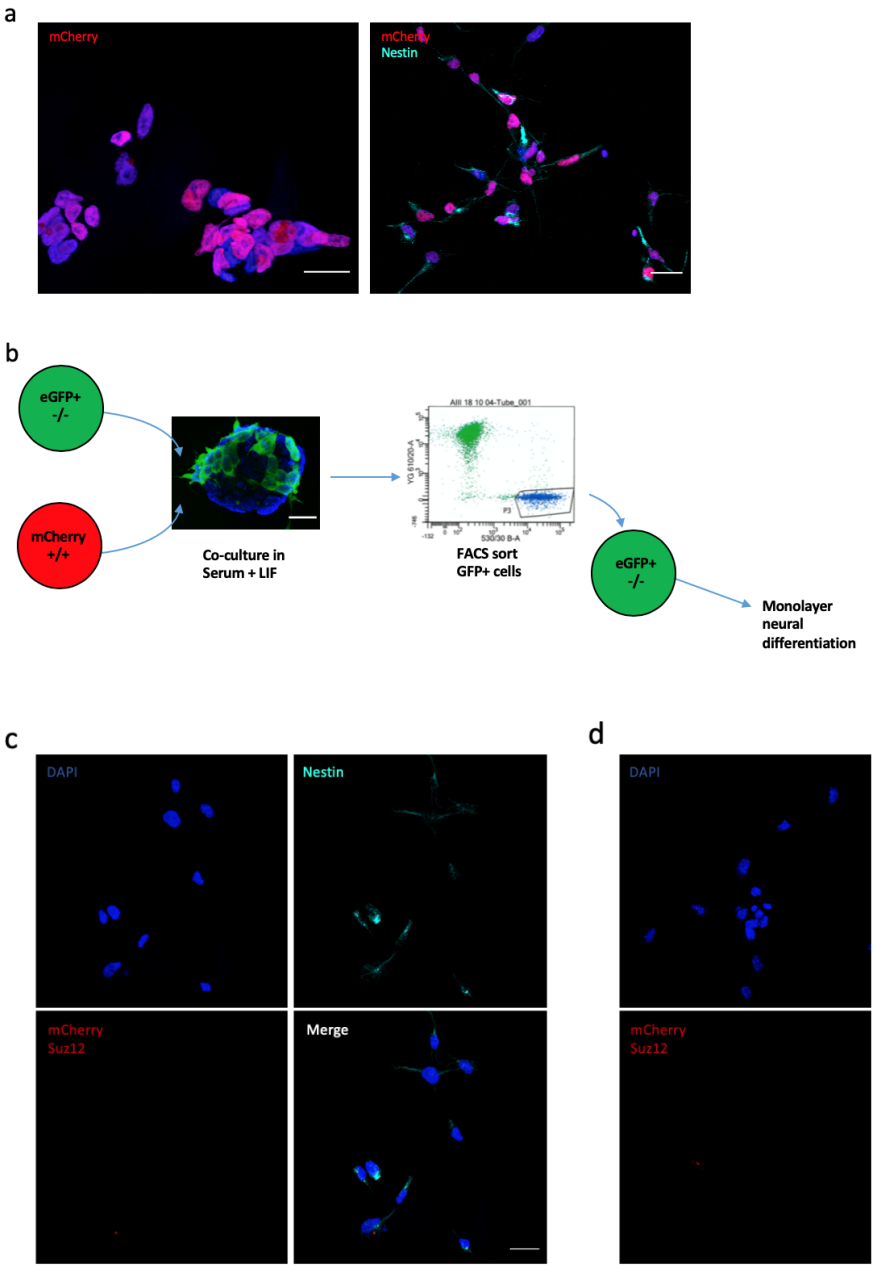

Figure 3.5 Coculture of Suz12-/-eGFP cells with H2AmCherry expressing wild type cells confirms identity of neural precursors as Suz12-/- after neural differentiation

a. Confocal images showing excitation for mCherry (Red) and immunolabelling for Nestin (cyan, right panel) in undifferentiated (Left panel), and monolayer neural differentiation day 12 E14H2AmCherry cells (right panel). Counterstained with 4′,6-diamidino-2-phenylindole (DAPI); Scale bar 25μm. Imaging demonstrates mCherry signal readily detectable in both undifferentiated and in Nestin expressing neural precursor cells.

b. Schematic of experimental design; GFP + Suz12-/- cells were grown in mixed cultures with E14H2AmCherry ES cells (ratio 1:4) for 24 hours, sorted for eGFP expression by FACS, for downstream monolayer neural differentiation and immunostaining for markers of neural differentiation.

c. Confocal images showing excitation for DAPI (blue, upper left panel), mCherry/immunolabelling for Suz12 (Red, lower left), immunolabelling for Nestin (cyan, upper right panel) in Suz12-/- ES cells following co-culture with E14H2mCherry cells, subsequent FACS sorting for eGFP expression, and monolayer neural differentiation (images taken at +day 12). Scale bar 25μm. Imaging demonstrates expression of neural lineage marker Nestin in cells lacking mCherry/Suz12 immunostaining.

(Legend continued next page)

3.4. Growth of Suz12-/- ES cultures in wild type conditioned media does not rescue neural differentiation

To investigate whether a diffusible factor may be responsible for rescuing differentiation of Suz12-/- mESCs, experiments using conditioned media were undertaken. Suz12-/- ESCs were grown in conditioned media (i.e., media taken from wild type parental ES cultures after 24 hours growth), for 24 hours prior to neural differentiation. I observed no rescue of neural differentiation using conditioned media (Figure 3.6.a, figure shown on next page), suggesting that physical interaction of cells may be required for rescue of differentiation.

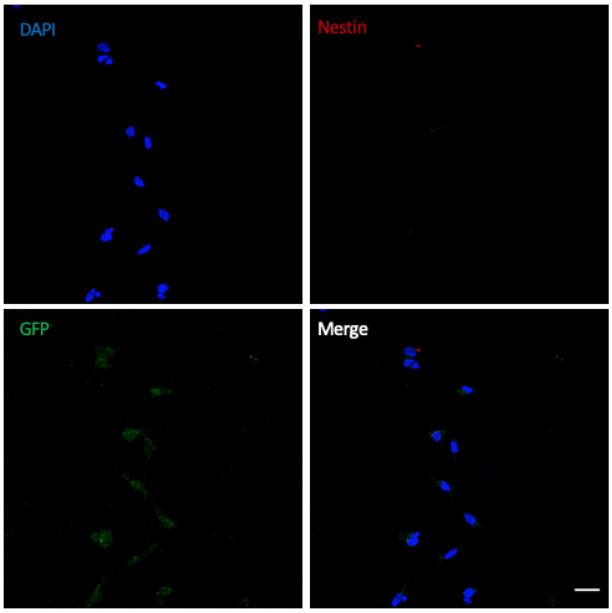

Figure 3.6. Growth of Suz12-/- ES cell cultures in wild type conditioned media does not rescue neural differentiation

a. Confocal images showing immunolabelling for Nestin (red, upper right), GFP (green, lower left panel), DAPI (blue, upper left panel) and merged images (lower right panel) of conditioned media treated Suz12-/- ES cells following monolayer neural differentiation. Scale bar 25μm. Imaging demonstrates failure to express neural lineage marker Nestin in cells with conditioned media treatment

---

Figure 3.5. Coculture of Suz12-/-eGFP cells with H2AmCherry expressing wild type cells confirms identity of neural precursors as Suz12-/- after neural differentiation (continued)

d. Confocal images showing excitation for DAPI (blue, upper left panel), mCherry/immunolabelling for Suz12 (Red, lower left), immunolabelling for Tuj1 (cyan, upper right panel) in Suz12-/- ES cells following co-culture with E14H2mCherry cells, subsequent FACS sorting for eGFP expression, and monolayer neural differentiation (images taken at +day 12). Scale bar 25μm. Imaging demonstrates expression of neural lineage marker Tuj1 in cells lacking mCherry/Suz12 immunostaining.

3.5. Co-culture in the presence of Gap junction inhibition does not affect rescue of neural differentiation following co-culture of Suz12-/- ES cells

Mouse ES cells have previously been demonstrated to express gap junctions, composed of Connexin proteins (Worsdorfer et al. 2008). Gap junctions form aqueous pores between the cytosol of adjacent cells allowing passage of small metabolites, conventionally thought to range up to 1.5kDa in size (Krysko et al. 2005), however recent reports have implicated gap junctions in the passage of larger molecules including small RNA species (Lemcke, Steinhoff, and David 2015). Gap junction expression was first confirmed in Suz12-/- and parental ES cell cultures by immunostaining for Connexin 43 (figure 3.7.a,b). Initially Suz12-/- and parental ES cell cultures underwent monolayer neural differentiation in the presence of 100μM carbenoxolone, a widely used non-selective gap junction inhibitor (Davidson, Baumgarten, and Harley 1986). This indicates that drug treatment does not alter neural differentiation in these ES cell cultures (i.e., drug treatment alone does not rescue neural differentiation in Suz12-/- deficient mESCs (figure 3.7.b)). Subsequently, co-culture experiments as outlined in the schematic figure 3.4.b were undertaken, with the addition of 100μM carbenoxolone during the 24-hour period of co-cultured growth. Neural differentiation was assessed by immunostaining for neural lineage markers Nestin and Tuj1 (figure 3.7.c). Importantly, neural differentiation of Suz12-/- ES cell cultures was not prevented by co-culture in the presence of the non-selective gap junction inhibitor carbenoxolone, suggesting that transfer of small molecular weight species between cells via gap junction communication is not essential for rescue of neural differentiation.

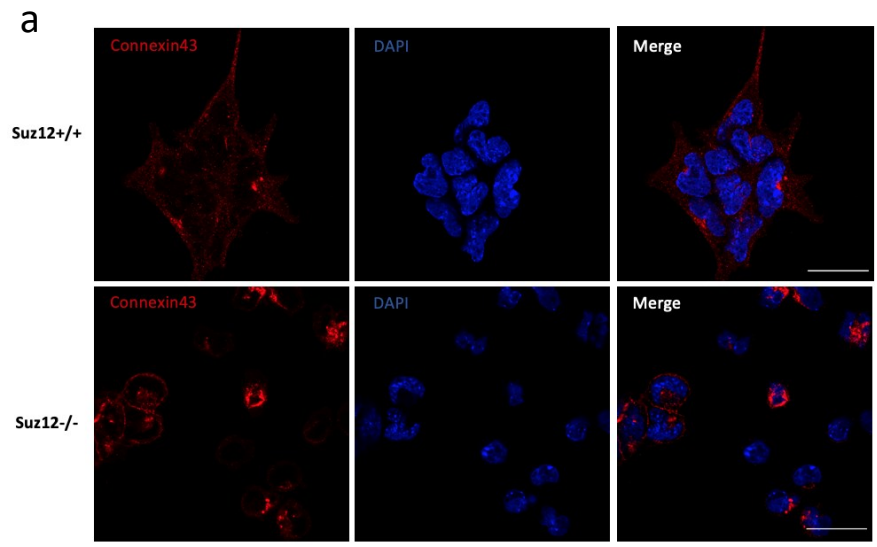

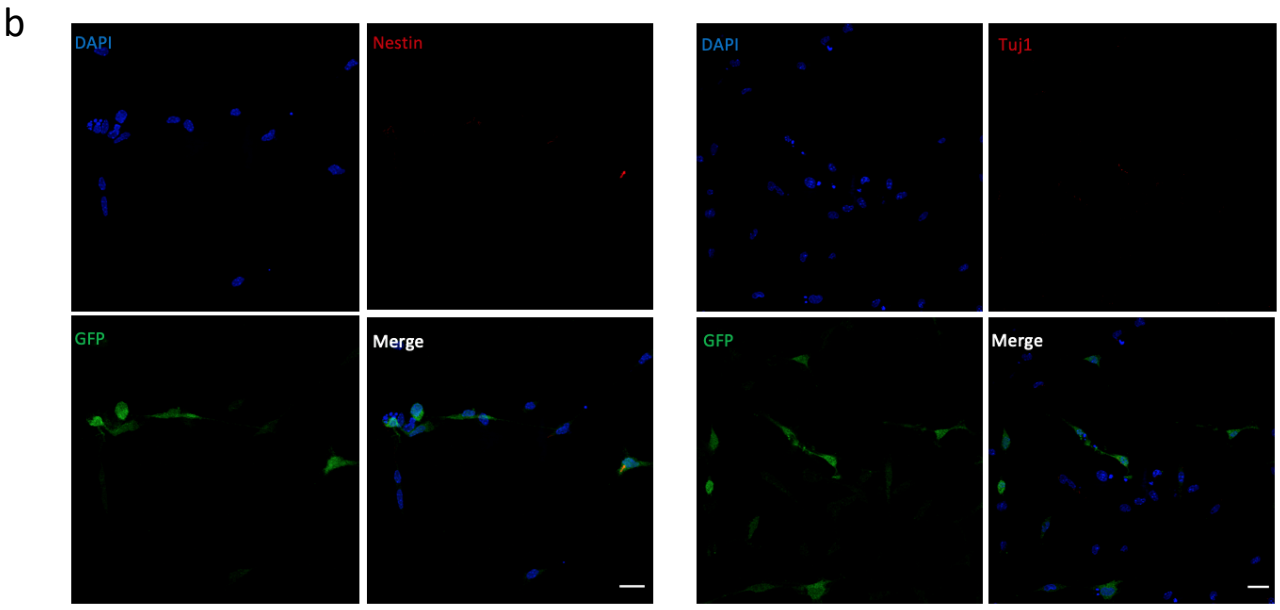

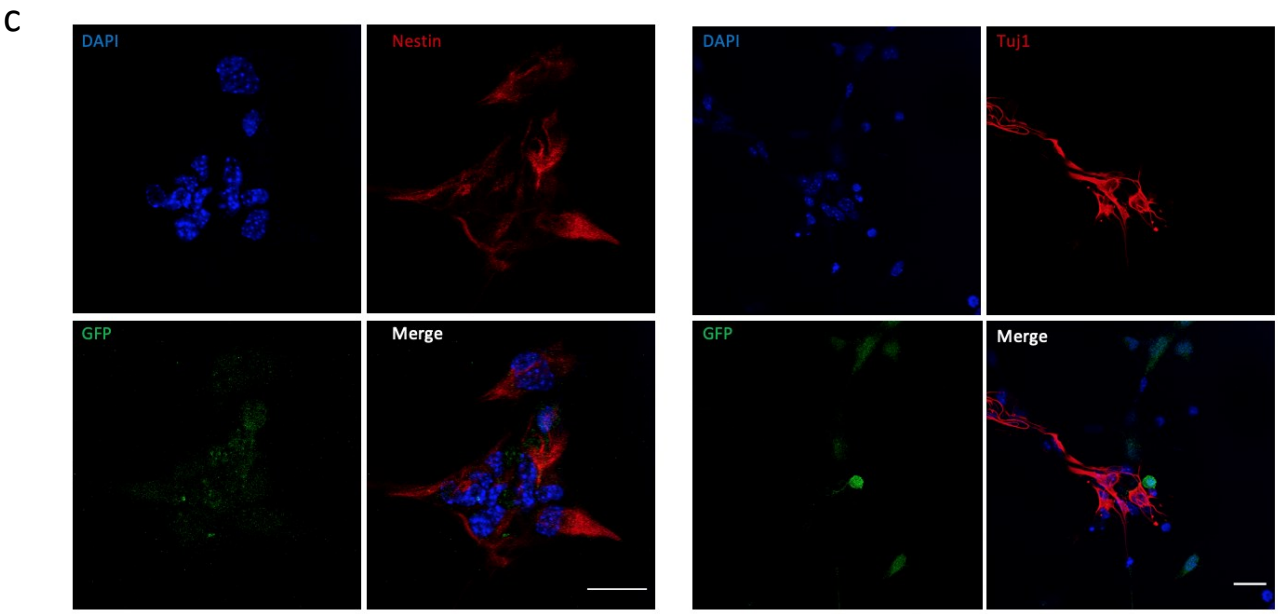

(Legend on next page)

3.7. Embryonic stem cells lacking core PRC components Eed and Suz12 show aberrant E-cadherin expression

Previous studies have suggested that E-cadherin, a protein which complexes with β-catenin at cell surface adherens junctions (Niessen and Gottardi 2008), is aberrantly localised in Jarid2-null mESCs. (Landeira et al. 2015) To see whether aberrant E-cadherin expression and localisation is unique to Jarid2 null ESCs, or is common to ES cells lacking other core PRC2 components I examined a panel of ES cells lacking other core PRC2 components; Ezh2-/- (Pereira et al. 2010), Eed deficient B1.3 (Azuara et al. 2006) and Suz12-/- (Pasini et al. 2007) alongside Jarid2-/- mESCs (Landeira et al. 2010), by immunostaining for E-cadherin (Figure 3.6.a-d). ES cells lacking Suz12 or Eed show much reduced E-cadherin labelling and a patchy distribution, compared to matched wild type controls.

Figure 3.7. Co-culture of Suz12-/- ES cells with parental wild type ES cells in the presence of gap junction inhibition does not preclude rescue of neural differentiation

- **a.** Confocal images showing immunolabelling for Connexin43 (red, left panels), DAPI (blue, middle panels) and merged images (right panels) in undifferentiated Suz12+/+ (upper panels) and Suz12-/- (lower panels) ES cell cultures; scale bar 25μm. Imaging demonstrates expression of Connexin 43 in both ES cell cultures
- **b.** Confocal images showing immunolabelling of neural lineage markers Nestin and Tuj1 (red, upper right panels respectively), DAPI (blue, upper left panels), GFP (green, lower left panels) and merged images (lower right panels) following monolayer neural differentiation of Suz12-/- ES cultures in the presence of 100μM carbenoxolone; scale 25μm. Images shows failure to induce neural lineage markers, showing carbenoxolone treatment alone does not induce neural differentiation.
- **c.** Confocal images showing immunolabelling of neural lineage markers Nestin and Tuj1 (red, upper right panels respectively), DAPI (blue, upper left panels), GFP (green, lower left panels) and merged images (lower right panels) following monolayer neural differentiation of Suz12-/- following co-culturing with parental ES cells in the presence of 100μM carbenoxolone; scale 25μm. Images shows expression of neural lineage markers, showing carbenoxolone treatment does not prevent rescue of neural differentiation.

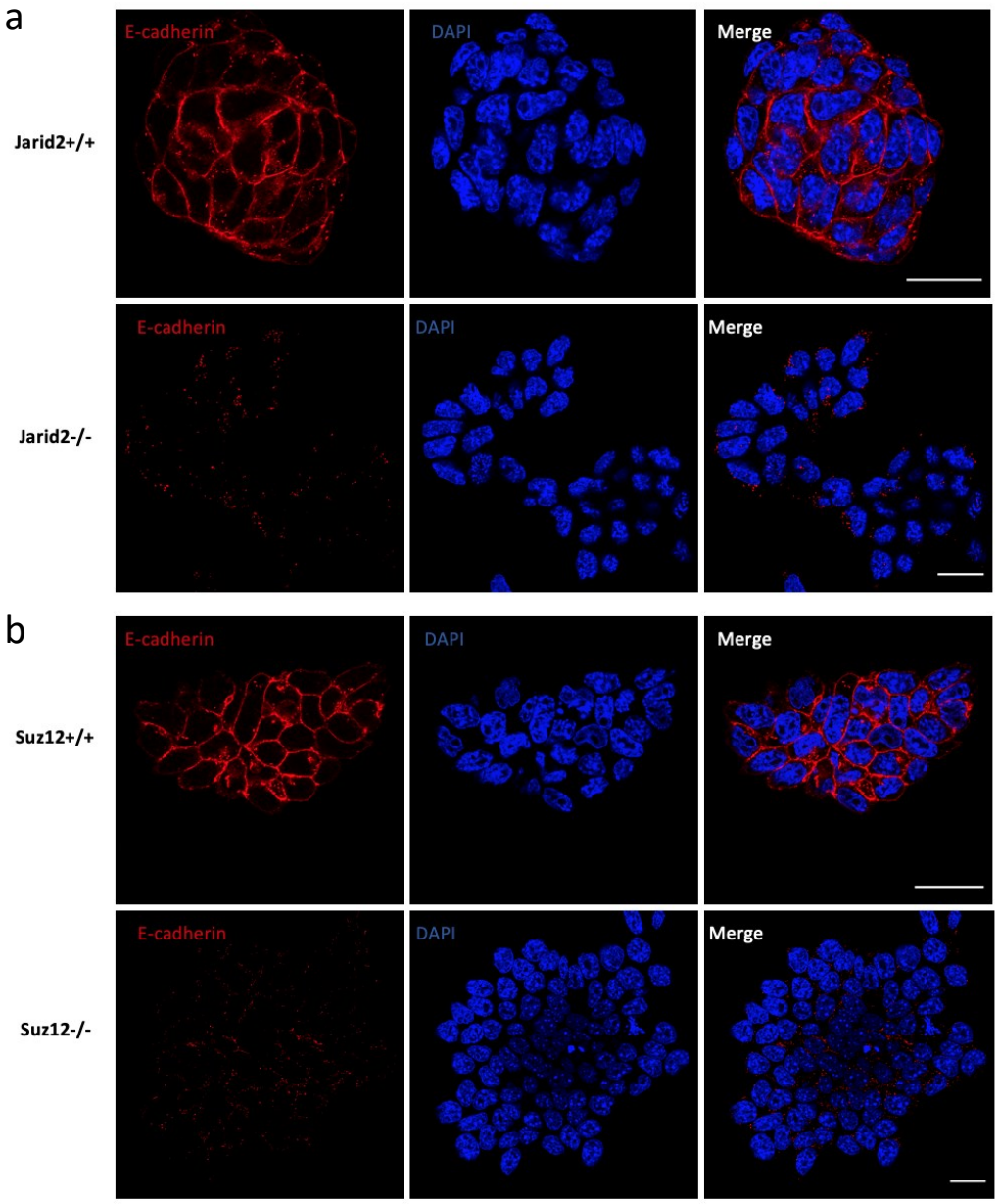

(Figure continued on next page)

Figure 3.8. Jarid2 -/-, Suz12-/- and Eed-/- mESCs exhibit aberrant E-cadherin localisation

a. Confocal images showing immunolabelling for E-cadherin (red, left panels), DAPI (blue, middle panels) and merged images (right panels) ES cell cultures grown in media with serum and LIF, comparing Jarid2 null ES cells (lower panels) with matched parental wild type ES cells (upper panels) Scale bar 25μm. Imaging demonstrates reduced and patchy E-cadherin staining in Jarid2 null cells compared to wild type.

b. Confocal images showing immunolabelling for E-cadherin (red, left panels), DAPI (blue, middle panels) and merged images (right panels) ES cell cultures grown in media with serum and LIF, comparing Suz12 null ES cells (lower panels) with matched parental wild type ES cells (upper panels) Scale bar 25μm. Imaging demonstrates reduced and patchy E-cadherin staining in Suz12 null cells compared to wild type.

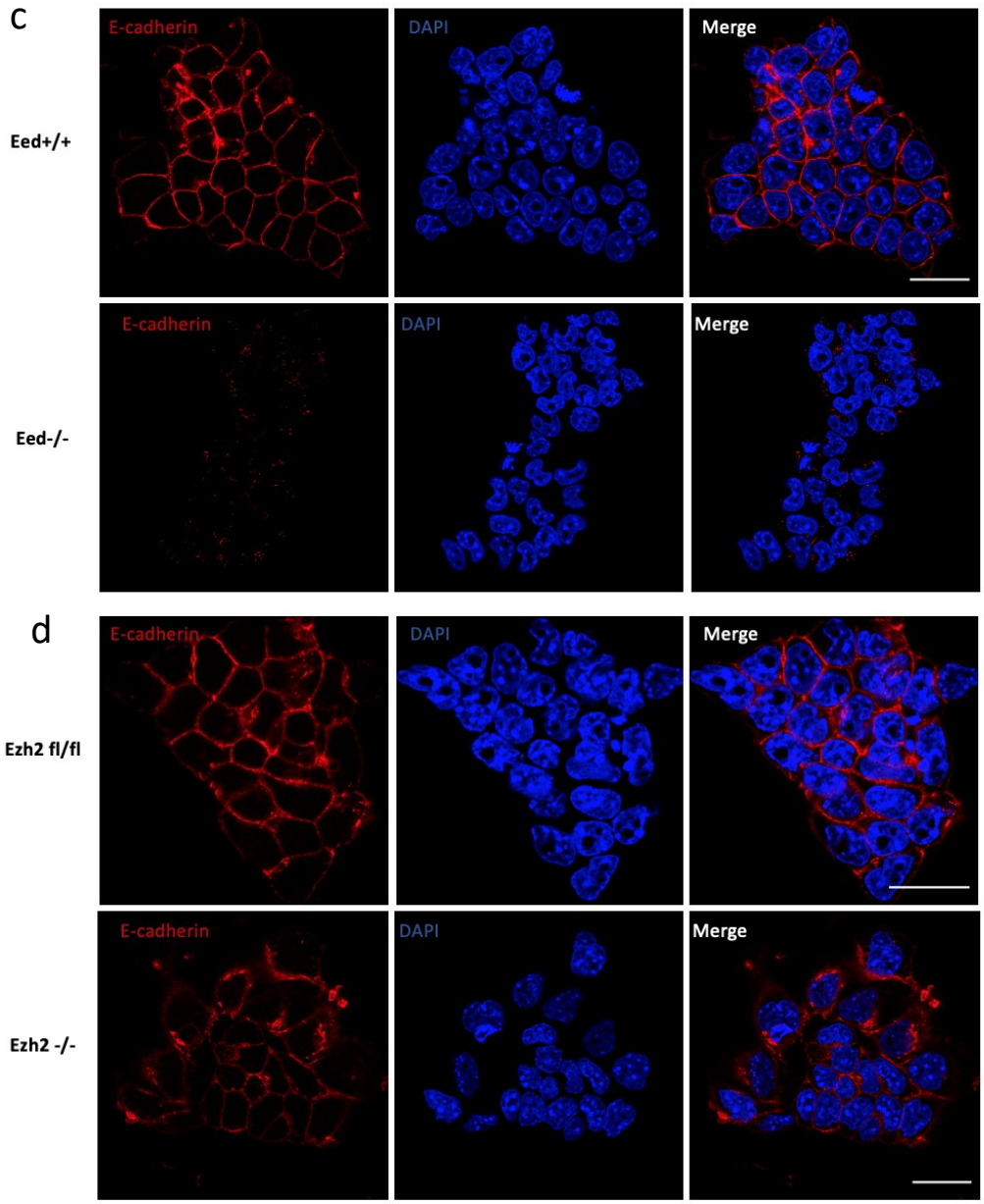

Figure 3.8. Jarid2, Suz12 and Eed null ES cell cultures exhibit aberrant E-cadherin staining

c. Confocal images showing immunolabelling for E-cadherin (red, left panels), DAPI (blue, middle panels) and merged images (right panels) ES cell cultures grown in media with serum and LIF, comparing Eed null ES cells (lower panels) with matched parental wild type ES cells (upper panels) Scale bar 25μm. Imaging demonstrates reduced and patchy E-cadherin staining in Eed null cells compared to wild type.

d. Confocal images showing immunolabelling for E-cadherin (red, left panels), DAPI (blue, middle panels) and merged images (right panels) ES cell cultures grown in media with serum and LIF, comparing Ezh2 null ES cells (lower panels) with matched parental wild type ES cells (upper panels) Scale bar 25μm. Imaging demonstrates essentially normal E-cadherin staining in Ezh2 null cells compared to wild type.

Interestingly ES cells lacking the enzymatic component of PRC2 Ezh2, had a distribution of E-cadherin proteins that were much more similar to wild-type controls (Ezh2 fl/fl, Figure 3.8.d). Ezh1 has previously been reported to compensate for loss of Ezh2 function, and this finding may reflect functional redundancy of Ezh1 in mESCs. It is also possible that these results indicate that the mechanism by which E-cadherin is altered is Ezh2 independent. To address this question, it would be of interest to perform E-cadherin analysis in Ezh1/Ezh2 double knockouts.

3.8. Expression of E-cadherin by co-culture partner cells is essential to rescue of both canonical Wnt signalling and neural differentiation in Suz12-/- mESCs

Landeira et al reported co-culture of Jarid2 null ES cells with parental wild type cells restores coherent colony formation, with normal E-cadherin staining observed at Jarid2 null: wild type ES cell interfaces (Figure 3.9a, experiment undertaken by Dr Andy Malinowski, figure used with permission (Landeira et al. 2015)). In view of the suggestion that cell interactions are required for rescue of neural differentiation, further investigation of whether E-cadherin is essential for coherent colony formation and properties was undertaken.

E-cadherin null mESCs were generated (Cell line termed C1, was generated using CRISPR/Cas9 targeting exon 5 of E-cadherin gene, by Dr Andy Malinowski (figure 3.9.b), and ES cells used with his kind permission). Initially the E-cadherin targeted cells were examined for E-cadherin protein expression by western blot analysis. This confirmed loss of E-cadherin expression (Figure 3.9.b, upper panel), with normal pluripotency gene expression being retained (Nanog, figure 3.9.b, middle panel). E-cadherin null mESCs were characterised in

terms of growth rate and alkaline phosphatase positive colony unit formation efficiency (Figure 3.9.c,d). This showed similar characteristics to the parental E14 ES cell line.

To assess whether E-cadherin is required to rescue of neuronal differentiation, co-culture experiments as outlined in the schematic figure 3.4.b were undertaken using E-cadherin null (C1) ES cells, in place of the wild type cells used in the original experiment. Neural differentiation was assessed by immunostaining for neural lineage markers Nestin and Tuj1 (figure 3.10.a.b).

Co-culture with E-cadherin null mESCs fails to rescue neural differentiation in Suz12-/- ES cells (Figure 3.10.a,b, matched positive controls using E14 WT cells demonstrated rescue of monolayer neural differentiation, data not shown). This confirms an essential role for E-cadherin in rescue of neural differentiation.

Landeira et al. previously proposed that, as β-catenin activity has been reported as necessary for ES cell differentiation (Atlasi et al. 2013; Lyashenko et al. 2011), Jarid2 null ES cells may be unable to differentiate due to low β-catenin activity (Landeira et al. 2015). E-cadherin is an interacting partner of β-catenin, and it is conceivable that E-cadherin interaction may contribute to the partial normalisation of β-catenin activity observed following co-culture, which permits ES differentiation. To investigate this possibility, β-catenin activity was assessed by TOPFlash assay, following co-culture with mESCs lacking E-cadherin for both Jarid2-/- (E8), and Suz12-/- ES cells (figure 3.10.c,d). Importantly, β-catenin activity was not restored following co-culture with E-cadherin null mESCs, showing that E-cadherin interaction may be essential to rescue of canonical Wnt signalling. These findings suggest a new model whereby E-cadherin interaction between mutant and wild type cells overrides a block in β-catenin activity, and enables Jarid2-null or Suz12-null mutant ES cells to overcome differentiation block.

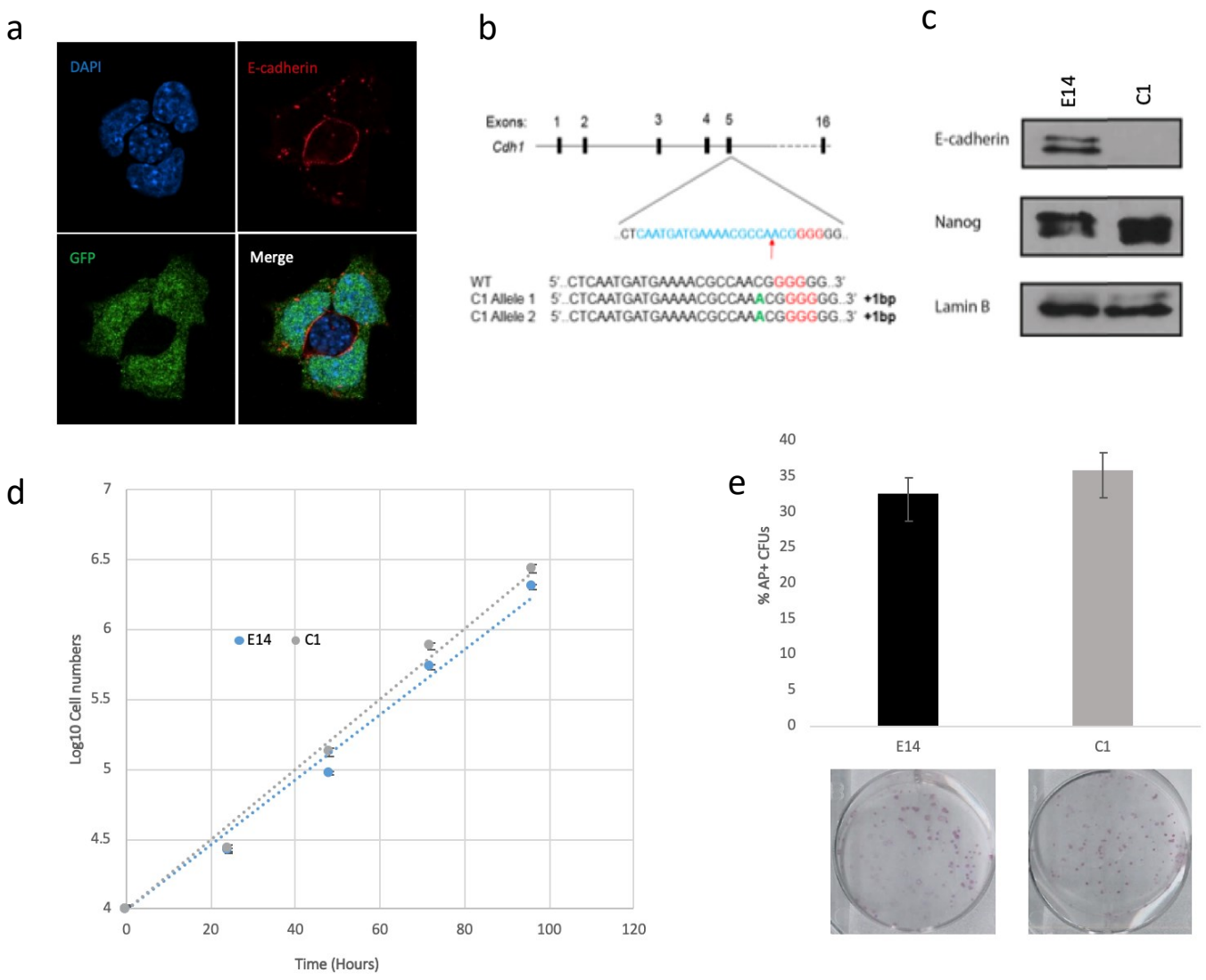

Figure 3.9. Generation and characterisation of E-cadherin null ES cells

a. Confocal images showing immunolabelling for E-cadherin (red, upper right), DAPI (blue, upper left), GFP (lower left) and merged images (lower right panels) of mixed cultures of JM8 (unlabelled) and Jarid2-/- (E8, GFP expressing). Imaging demonstrates reduced and patchy E-cadherin staining in E8l cells, with normal E-cadherin staining observed at interface with the wild type cell. Experiment undertaken by Dr Andy Malinowski, figure used with permission

b. Schematic representation of CRISPR/Cas9 targeting to E-cadherin gene at exon 5; nucleotides in red represent the PAM sequence for Cas9; nucleotides in blue depict sgRNA binding sites; red arrow shows site of double strand cleavage on CRISPR/Cas9 activation.

c. Western blot of CRISPR/Cas9 generated E-cadherin null (C1) mESCs and, matched parental cell line (E14) for E-cadherin, and Nanog expression; Lamin B loading control. Confirms loss of expression of E-cadherin, with maintain expression of pluripotency gene Nanog in C1 cell line.

d. Logarithmic scale growth curve of E14 and C1 ES cell lines over 96 hours. Samples repeated in triplicate; standard error bars shown.

e. Efficiency of alkaline phosphatase positive colony formation in E14 and C1. Samples repeated in triplicate; standard error bars shown. Example plates shown in lower panels.

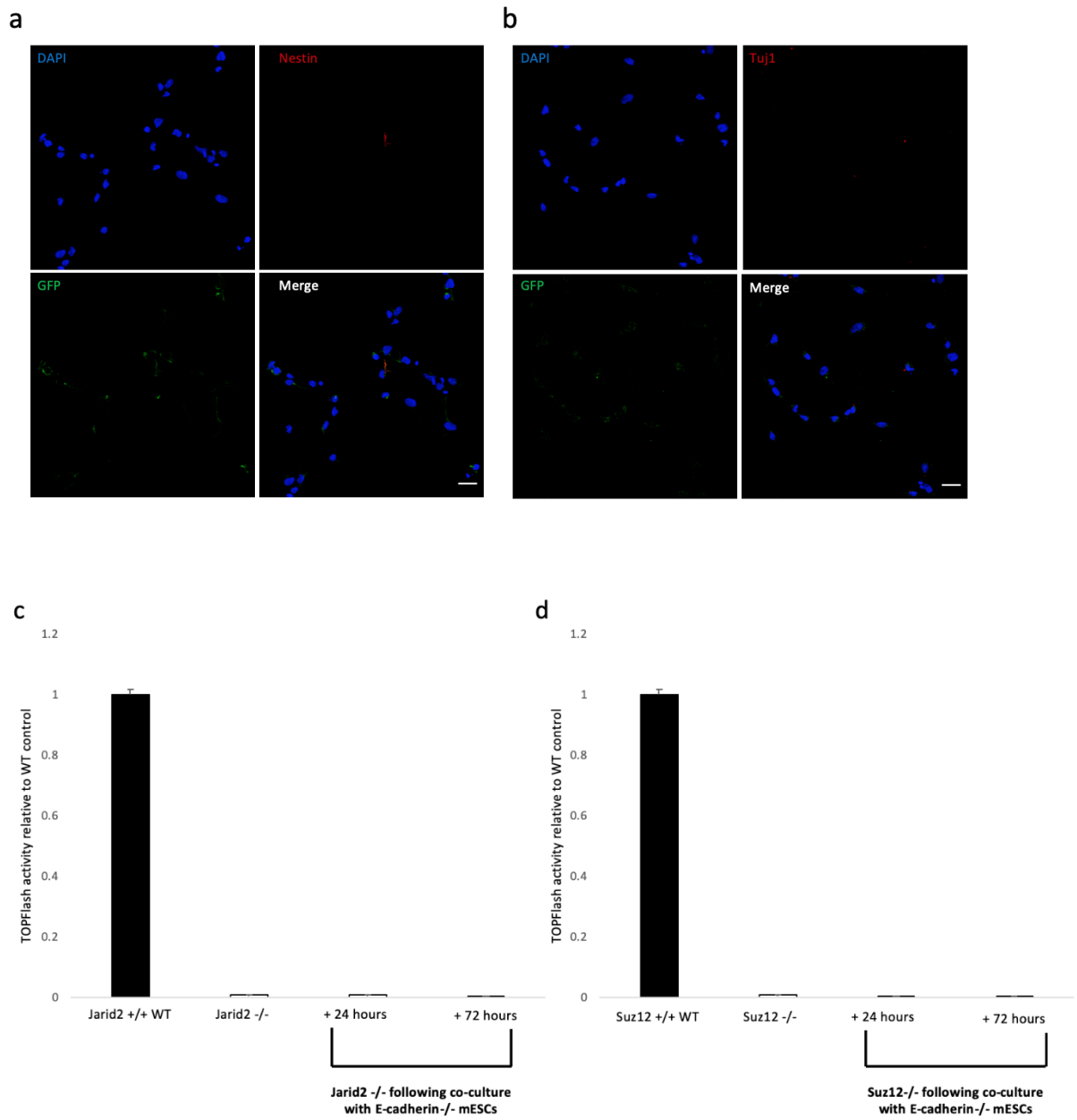

Figure 3.10. Co-culture of Jarid2-/- or Suz12-/- ES cells with mESCs lacking E-cadherin fails to rescue monolayer neural differentiation or canonical Wnt signalling

- **a.** Confocal images showing immunolabelling of neural lineage markers Nestin (red, upper right panels), DAPI (blue, upper left panels), GFP (green, lower left panels) and merged images (lower right panels) following monolayer neural differentiation of Suz12-/- ES cultures after 24 hours co-culture with E-cadherin null ES cells; scale 25μm.
- **b.** Confocal images showing immunolabelling of neural lineage markers Tuj1 (red, upper right panels), DAPI (blue, upper left panels), GFP (green, lower left panels) and merged images (lower right panels) following monolayer neural differentiation of Suz12-/- ES cultures after 24 hours co-culture with E-cadherin null ES cells; scale 25μm. Images shows failure to induce neural lineage markers, suggesting E-cadherin expression is essential to rescue of neural differentiation.
- **c.** β-catenin activity, evaluated by luciferase-based TOPFlash assays comparing matched wild type (black bars) and Jarid2 null ES cell cultures, at baseline and after 24 and 72 hours of co-culture with E-cadherin null ES cultures and FACS sorting. Activity relative to wild-type. Mean ± SE of three experiments shown;
- **d.** β-catenin activity, evaluated by luciferase-based TOPFlash assays comparing matched wild type (black bars) and Suz12 null ES cell cultures, at baseline and after 24 and 72 hours of co-culture with E-cadherin null ES cultures and FACS sorting. Activity relative to wild-type. Mean ± SE of three experiments shown;

3.9. mESCs lacking Suz12 form greater than one inner cell masses upon injection into mouse blastocysts

It has been previously shown that mESCs lacking Jarid2 have the capacity to generate multiple ICMs following injection into Black 57 E3.5 blastocysts (Landeira et al. 2015). Additionally, expression of the early primitive endoderm marker Gata6 (Schrode et al. 2014) is seen in cells surrounding each individual ICM, implying interplay between chromatin regulation and cell signalling. Multiple ICM formation is a rare phenotype, and was not observed in 90 control injections using matched parental mESCs. Furthermore, single ICMs were observed following blastocyst injection ES cells lacking the core PRC2 component Eed. Importantly Landeira et al. highlighted that regulation of canonical Wnt signalling is critical for pre-implantation development, as it appears to permit discrimination of developing blastocysts resulting in a single inner cell mass. Importantly, mESCs lacking Eed retain moderate canonical Wnt signalling activity.

To investigate whether multiple ICM formation is unique to ES cells lacking Jarid2, Bl57 E3.5 blastocysts were injected with ES cells lacking Suz12, which also demonstrate supressed canonical Wnt signalling and aberrant E-cadherin expression. Initially uninjected control blastocysts were fixed and immunostained for Gata6 and Nanog, to highlight the native inner cell mass, to demonstrate the normal appearance of an E4.5 blastocyst (Figure 3.11.a). Mouse ES cells lacking Suz12, but expressing eGFP were injected into Bl57 E3.5 blastocysts (10-15 cell per blastocyst, injections kindly undertaken by LMS Transgenic Facility). Injected blastocysts were grown for 24 hours in KSOM media, prior to fixation and immunostaining for GFP to highlight injected ES cells, and Gata6 (figure 3.11.b, additionally a blastocyst injected with ES cells lacking Jarid2 is also shown for comparison, taken from Landeira et al. 2015 with permission). Notably, ES cells lacking Suz12 are also capable of forming multiple ICMs on

blastocyst injection, although with reduced efficiency when compared to blastocysts injected with ES cells lacking Jarid2 (Table 3.1). Importantly, ES cells lacking E-cadherin expression with intact PRC2 machinery, do not form multiple ICMs on blastocyst injection (figure 3.11.c), although these cells do have an increased failure rate of contribution to ICM of E-cadherin null mESCs was observed compared to parental mESC injections (Table 3.2). In addition to the observed failure of Eed deficient cells to form multiple ICMs, this suggests that aberrant E-cadherin expression is not sufficient to induce multiple ICM formation.

mESC	Number of Blastocysts analysed	Number blastocysts with >1 ICM
Jarid2+/+	90	0
Jarid2-/-	39	16 (41%)
E14 WT	110	0
Suz12-/-	78	11 (14%)
Eed deficient Bl3	27	0
E-cadherin -/-	44	0

Table 3.1. Multiple ICMs are induced in E3.5 Bl57 mouse blastocysts injected with mESCs lacking Jarid2 or Suz12, but not paired WT parental cells, or mESCs lacking Eed or E-cadherin

Data from three biological replicates for injections using Suz12-/- and E14 WT mESCs, and 2 biological replicates for injections using either Jarid2-/-, Eed deficient B1.3 or E-cadherin-/- mESCs. Data from Suz12-/- and E-cadherin-/- and matched parental controls (E14 cell line parental control for both Suz12-/- and E cadherin-/- lines) combined with previously published data of Jarid2-/- and Eed deficient B1.3 injections (Landeira et al. 2015)

	Total blastocysts injections	Failure to induce ICM formation
E14 WT	110	12 (11%)
E-cadherin -/-	44	34 (77%)
Suz12 -/-	78	13 (17%)

Table 3.2. Rate of failure to form inner cell mass following injection of E3.5 Bl57 mouse blastocysts with mESCs

Data from three biological replicates for injections using Suz12-/- and E14 WT mESCs, and two replicates using E-cadherin-/- mESCs. Data for Jarid2 wild-type (JM8) and Jarid2-/- (E8) and Eed deficient B1.3 injection unavailable.

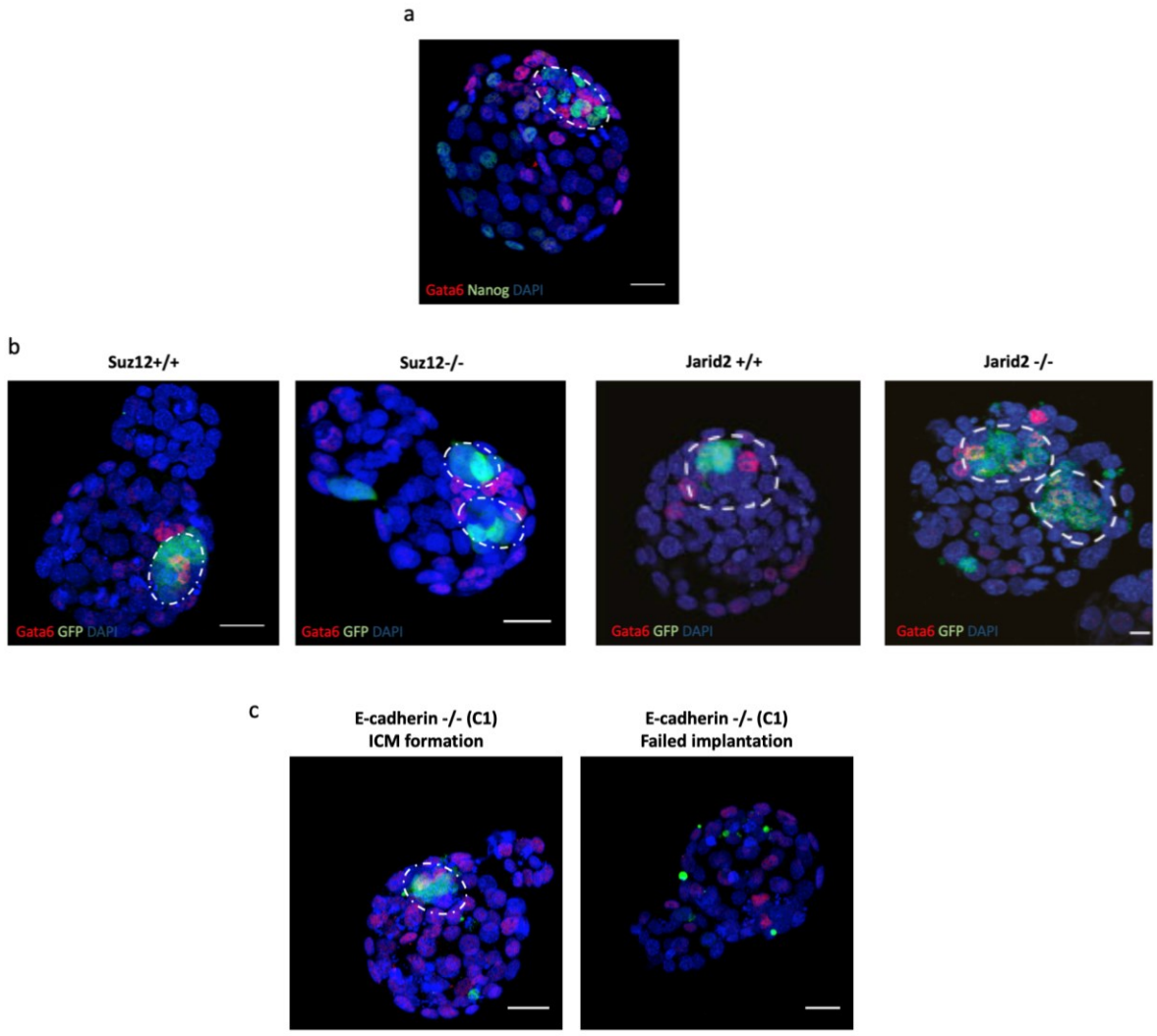

Figure 3.11. mESCs lacking either Jarid2 or Suz12 induce formation of multiple inner cell masses upon injection into E3.5 Bl57 mouse blastocysts

a. Confocal immunofluorescence image showing and uninjected E4.5 Bl57 mouse blastocyst stained for Nanog (Green) and Gata6 (Red), counterstained with 4',6-diamidino-2-phenylindole (DAPI); Scale bar 25μm. Dashed white line highlights the inner cell mass (ICM), showing a normal distribution of Nanog high expressing ICM cells, surrounded by the primitive endoderm as defined by high Gata6 expression

b. Confocal immunofluorescence image showing E4.5 Bl57 mouse blastocyst following injection of either Suz12-/- and matched parental controls, or Jarid2-/- and matched parental controls, stained for eGFP (Green) to highlight injected cells and Gata6 (Red) to define the primitive endoderm surrounding the ICM(s). Counterstained with 4',6-diamidino-2-phenylindole (DAPI); Scale bar 25μm. Dashed white line highlights the injected ICM(s). Representative images demonstrating that mESCs lacking either Jarid2 or Suz12 are capable of inducing multiple ICM formation. Jarid2 experiments images taken from Landeira et al. 2015, with kind permission.

c. Confocal immunofluorescence image showing E4.5 Bl57 mouse blastocyst following injection mESCs lacking E-cadherin, stained for eGFP (Green) to highlight injected cells and Gata6 (Red) to define the primitive endoderm surrounding the ICM. Counterstained with 4',6-diamidino-2-phenylindole (DAPI); Scale bar 25μm. Dashed white line highlights the injected ICM(s). The left image demonstrates successful ICM formation, with the image on the right representative of failed ICM formation which was noted to occur at higher frequency than either matched parental controls, or injections using mESCs lacking PRC2.2 machinery (table 3.2)

3.10. Discussion and future perspectives

Previous studies have suggested that the PRC2.2 component Jarid2 has a role outside the context of canonical histone modification (Landeira and Fisher 2011). Specifically Jarid2 has been implicated in the co-ordination of Nanog expression, canonical Wnt signalling, and E-cadherin localisation, with Jarid2 null mESCs capable of inducing multiple ICM formation on blastocyst injection (Landeira et al. 2015). Here I show that, in addition to Jarid2 null mESCs, mESCs lacking core PRC2 components Ezh2, Eed or Suz12 demonstrate reduced canonical Wnt signalling acticity, with Suz12 null mESCs showing constitutivey low canonical Wnt signalling analogous to that seen in Jarid2 null mESCs. Further, Suz12 null mESCs also demonstrate a block in differentiation, but in contrast to previous reports, are able to efficiently downregulate expression of pluripotency genes (Oct4, Nanog, Sox2 and Rex1) albeit under different differentiation conditions. However, Suz12-/- mESCs were unable to upregulate the expression of neuronal-lineage specific markers as has been previosuly reported (Pasini et al. 2007). Importantly co-culture of Suz12-/- mESCs with parental wild-type mESCs can partially rescue both canonical Wnt activity and neuronal differentiation. The role of canonical Wnt signalling in pluripotency and differentiation remains controversial (Sokol 2011; Serio 2014; de Jaime-Soguero, Abreu de Oliveira, and Lluis 2018), with seemingly contradictory reports suggesting that Canonical Wnt signalling is essential to pluripotency and ESC self renewal (Miyabayashi et al. 2007; Anton, Kestler, and Kühl 2007; ten Berge et al. 2011) while other reports implicate canonical Wnt signalling in lineage commitment and differentiation (Bakre et al. 2007; Lindsley et al. 2006). This study is in keeping with the latter, with activation of canonical Wnt signalling observed coincident with rescue of neuronal lineage commitment. My experiments also begin to elucidate the mechanism by which canonical Wnt signalling and neuronal lineage commitment are, to some extent restored

following co-culture with parental wild-type cells. Failure of Suz12 null mECSs exposed to wild-type ESC conditioned media to differentiate, along with succesful differentiation in the presence of a non-selective gap junction inhibitor suggests that neither endocrine nor paracrine secretion of small molecules is responsible for the observed restoration of canonical Wnt signalling and neuronal lineage commitment. Intruigingly however, co-culture with parental mESCs modified to ablate E-cadherin expression results in a failure to induce canonical Wnt signalling and neuronal lineage commitment. Furthermore, aberrant expression and localisation of E-cadherin is observed in mESC lacking either Jarid2 or Suz12, and co-ordination of E-cadherin at the WT:Jarid-/- cell interface has been reported in co-cultured colonies (Landeira et al. 2015). Cytoplasmic β-catenin binds to the intracellular domain of E-cadherin in mESCs, linking adherens junctions to the cytoskeleton (Niessen and Gottardi 2008). Loss of E-cadherin mESCs by genetic knockout results in mESCs which retain self renewal in absence of LIF, and maintain an undifferentiated phenotype when exposed to differentiation inducing conditions (Soncin et al. 2009). Additionally, Soncin et al. reported that the E-cadherin:β-catenin interaction is essential to lineage commitment as reversal of the E-cadherin null phenotype is dependent on the presence of the cytoplamic β-catenin binding domain of E-cadherin in ectopically expressed E-cadherin. Additionally, the authors report that β-catenin null mESCs also demonstrate the same phenotype of maintainance of pluripotency in the absence of LIF. E-cadherin has been reported as required for the increase in cytosolic β-catenin and play an instructive role in providing a pool of β-catenin for canonical Wnt signalling (Howard et al. 2011). Our observation are in keeping with the finding that E-cadherin is essential to rescue of canonical Wnt signalling and differentiation. A model whereby an inteaction between WT and Suz12-/- mESCs results in restoration of E-cadherin architecture, allowing replenishment of the pool of available β-catenin and rescue of active

Wnt signalling, requisite for lineage commitment, could potentially explain the observed restoration of lineage commitment in mESCs lacking either Suz12 or Jarid2.

Perhaps most intriguingly, rescue of neuronal lineage in Suz12-/- mESCs suggests that transition from pluripotency to early neuronal lineage commitment, and perhaps lineage commitment generally, may occur in the absence of PRC2 mediated histone H3K27me modifications. It is well recognized that mESCs lacking Suz12 demonstrate global loss of H3K27 methylation (Pasini et al. 2007; Hojfeldt et al. 2018). A recent study has shown that ectopic expression of Suz12 in mESCs lacking Suz12 will accurately and rapidly establish *de novo* H3K27 methylation (Hojfeldt et al. 2018), and it is possible but very unlikely that PRC2 mediated histone methylation occurs following co-culture, through an as yet unknown mechanism, perhaps with an alternative histone methyltransferase. To exclude this possibility a future avenue of research would be to isolate the nuclei of Suz12 null cells driven to neuronal differentiation following co-culture, to interogate for PRC2 mediated histone modifications, as this would elucidate whether PRC2 mediated histone methylation is in itself requisite for lineage commitment.

Chapter 4. Proteomic analysis of Jarid2 null mESCs

4.1. Whole cell extract proteomic analysis of Jarid2 null mESCs

Jarid2-deficient ESCs have altered Wnt-signalling and altered expression on non-canonical Wnt signalling pathways (Landeira et al. 2010, Landeira at al. 2015). To assess changes in the ES cell proteome that are associated with Jarid2 loss, we performed Mass Spectrometry (MS) analysis of Jarid2-null versus wild-type mESCs. Whole cell extracts were obtained in triplicate for Jarid2-/- (E8 cell line) and matched parental mESCs (JM8 cell line), during log phase growth, maintained in media supplemented with serum and leukaemia inhibitory factor (LIF) (performed by Andy Malinowski, Lymphocyte Development group, MRC LMS). A standard TCA precipitation and trypsin digest followed by high pressure liquid chromatography and mass spectrometry using a 2-hour gradient on Q-exactive prior to MS was performed (in collaboration with Dr Tony Ly, Lamond Group, University of Dundee). Overall label-free-quantification (LFQ) were obtained for 6168 proteins. 3061 proteins were detected sufficiently (>2 replicates in each sample), to allow comparison of relative abundancies. Scatter plot and principle component analysis demonstrate good reproducibility between biological replicates (Figure 4.1.a,b). Unsupervised hierarchical clustering separates Jarid2-/- and parental mESC cell line, although there was significant overlap between these two mESC lines (Figure 4.1.c).

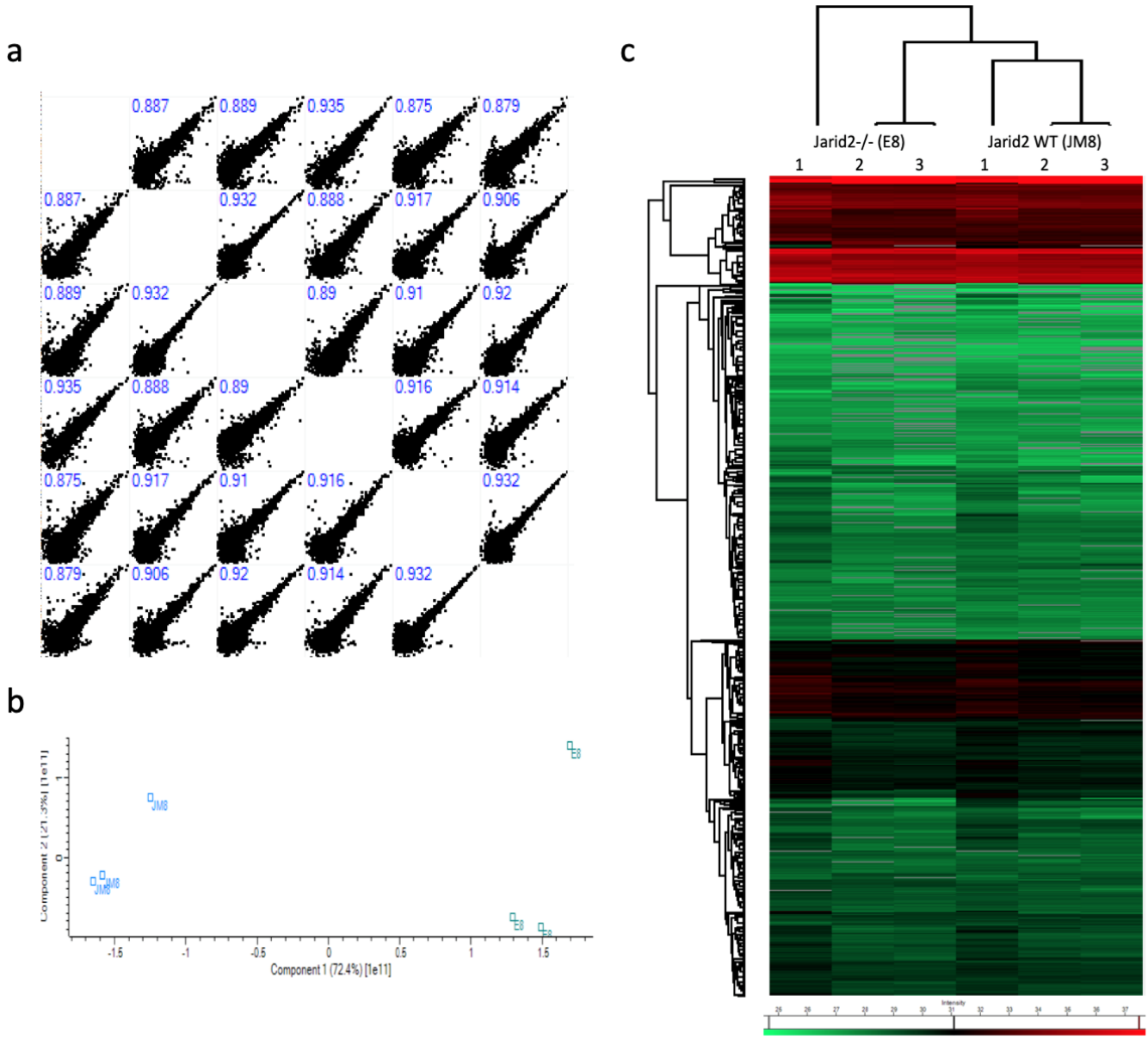

Figure 4.1. Proteins identified as having significantly increased or decreased abundance in Jarid2 null mESCs relative to wild type mESCs

a. Scatterplot analysis of proteomic data comparing biological replicates of Jarid2-null (E8) mESC vs. matched Jarid2 +/+ parental control mESC whole cell extract. Pearson rank co-efficient shows significant correlation (range +0.875-0.932)

b. Principle component analysis of Jarid2 -/- (E8) and matched parental controls (JM8), showing discrete clustering of each cell type

c. Heatmap showing intensity of biological replicates of Jarid2-/- mESCs and WT mESCs for each protein. Unsupervised hierarchical clustering separates Jarid2-/- and matched parental replicates.

Volcano plot analysis with a crude cut off (ANOVA p<0.5 and fold change >2 change) demonstrates 42 proteins with reduced relative abundance and 25 proteins with increased relative abundance in Jarid2-/- mESCs relative to matched parental controls. This is further reduced to 17 proteins with reduced abundancy and 11 with increased abundancy when a false discovery rate of 0.05 is applied (Elias and Gygi 2007) (Figure 4.2.a,b; Table 4.1).

Protein	Gene	Log2 mean Jarid-/- LFQ intensity	Log2 mean Jarid WT LFQ intensity	Δ Log2 LFQ intensity Jarid-/-:WT	P-value
Alpha-internexin	Ina	30.11	27.57	2.55	0.0093
Coactosin-like protein	Cotl1	29.70	28.12	1.57	0.0212
Fatty acid-binding protein, heart	Fabp3	32.33	30.94	1.39	0.0111
Equilibrative nucleoside transporter 1	Slc29a1	29.61	28.41	1.19	0.0006
E3 ubiquitin-protein ligase NEDD4-like	Nedd4l	29.41	28.39	1.03	0.0109
RNA-binding motif protein, X-linked like 2	Rbmxl2	30.79	29.79	1.00	0.0018
Adenylate kinase 4, mitochondrial	Ak4	29.94	28.97	0.97	0.0085
Centromere protein V	Cenpv	29.70	28.73	0.97	0.0359
Glutathione S-transferase A4	Gsta4	33.56	32.65	0.92	0.0034
Core histone macro-H2A.2	H2afy2	29.83	28.98	0.84	0.0170
Heterogenous nuclear ribonucleoprotein H3	Hnrnph3	29.45	28.74	0.72	0.0143
Ubiquitin-conjugating enzyme E2 Z	Ube2z	27.96	28.69	-0.73	0.0105
NIF3-like protein 1	Nif3l1	28.85	29.66	-0.81	0.0189
Protein lin-28 homolog A	Lin28a	29.35	30.24	-0.88	0.0157
Myosin light polypeptide 6	Myl6	30.47	31.38	-0.90	0.0020
Annexin;Annexin A7	Anxa7	28.01	28.94	-0.93	0.0020
Asparagine--tRNA ligase, cytoplasmic	Nars	30.68	31.68	-0.99	0.0281
D-3-phosphoglycerate dehydrogenase	Phgdh	31.17	32.22	-1.06	0.0130
Tubulin beta-3 chain	Tubb3	28.77	29.91	-1.14	0.0363
Glycine dehydrogenase, mitochondrial	Gldc	28.64	29.95	-1.32	0.0182
Septin-9	Sep-09	28.73	30.08	-1.35	0.0426
Phosphoserine aminotransferase	Psat1	31.70	33.11	-1.41	0.0329
DNA (cytosine-5)-methyltransferase 3B	Dnmt3b	28.89	30.31	-1.42	0.0079
Laminin subunit beta-1	Lamb1	26.15	27.59	-1.44	0.0298
Synaptosomal-associated protein 47	Snap47	26.94	28.60	-1.65	0.0328
Transgelin-2	Tagln2	29.48	31.29	-1.81	0.0110
DNA (cytosine-5)-methyltransferase 3-like	Dnmt3l	28.58	30.89	-2.31	0.0350
Catenin beta-1	Ctnnb1	28.15	30.88	-2.72	0.0046

Table 4.1. Proteins identified as having significantly increased or reduced abundance by LFQ proteomic analysis of whole cell extracts of Jarid2 null mESCs vs. wild type mESCs

Listed in descending order from protein with greatest relative abundance (α-internexin), to least relative abundance (β-catenin). P-value by one-way ANOVA.

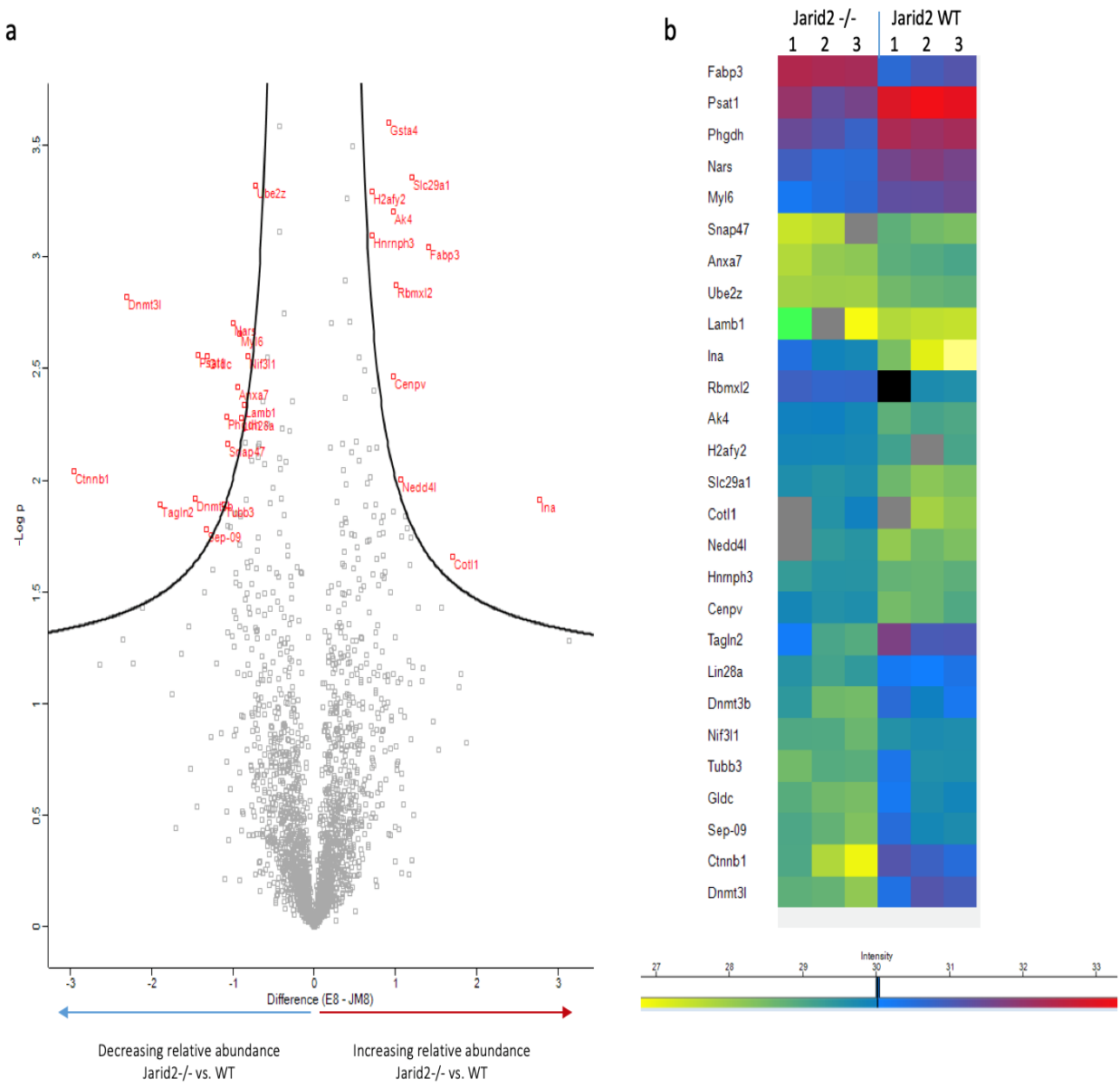

Figure 4.2. Proteins identified as having significantly increased or decreased abundance in Jarid2 null mESCs relative to wild type mESCs

a. Volcano plot showing log2 difference in mean LFQ abundance in Jarid2-/- mESCs (E8) versus WT (JM8) (x-axis), against -log10 p-value (y-axis). Proteins with FDR>0.05 highlighted in red, non-significant proteins in grey. Reduced relative abundance to left of zero, increased relative abundance to right of zero. Twenty-eight proteins identified, with 17 with reduced relative abundance, and 11 with increased relative abundancy.

b. Multi-colour heatmap showing intensity of biological replicates of Jarid2-/- mESCs and WT mESCs for each protein with FDR<0.05

A striking observation from the whole cell extract MS data is that β-catenin is the protein demonstrating the greatest reduction in relative abundance in Jarid2-/- mESCs relative to matched parental controls (Δlog mean intensity -2.72, p=0.0046) (Figure 4.3.a). This result was reproducible across all three biological replicates (Figure 4.3.b,c). Previous studies have indicated reduced activity of β-catenin in Jarid2-/- mESCs (Landeira et al. 2015), and reduced β-catenin abundance would be consistent with this observation.

Two previous studies have highlighted the intriguing possibility that direct methylation of β-catenin at the lysine 49 residue can regulate β-stability and function (Hoffmeyer et al. 2017; Zhu et al. 2016). Zhu et al reported that the long non-coding RNA lnc-β-Catm co-immunoprecipitates with both β-catenin and Ezh2 in liver cancer stem cells. Using both an anti-pan-methyl-lysine antibody-based approach and an *in vitro* methylation assay, it was suggested that Ezh2 can methylate β-catenin at lysine 49, and that methylation promotes β-catenin stability. A further report demonstrated that β-catenin is methylated in mESCs (Hoffmeyer et al. 2017). Using a custom-made rat monoclonal antibody raised against a methylated peptide corresponding to the region surrounding β-catenin lysine 49. It was also reported that methyl-β-catenin co-Immunoprecipitates with all PRC2 core components and Jarid2. Furthermore, methylated β-catenin was claimed to be enriched at repressed developmental genes, and also in association with E-cadherin at the cell surface adhesion complex (Hoffmeyer at al. 2017). A further study has also highlighted the role of the lysine demethylases KDM2A in regulation of β-catenin stability, highlighting the possibility that methylation of β-catenin impairs ubiquitination, resulting in stabilisation and increased abundancy of β-catenin, potentiating canonical Wnt signalling (Lu et al. 2015). Because these reports suggest that PRC2 could methylate β-catenin at lysine 49, and thereby stabilize activity, it is important to verify these observations, although we have been unable to acquire

the bespoke anti-K49me β-catenin antibody. Given the potential significance of PRC2 mediated methylation of β-catenin for developmental and cancer biology, further efforts were made to identify endogenous β-catenin methylation using mass spectrometry approaches.

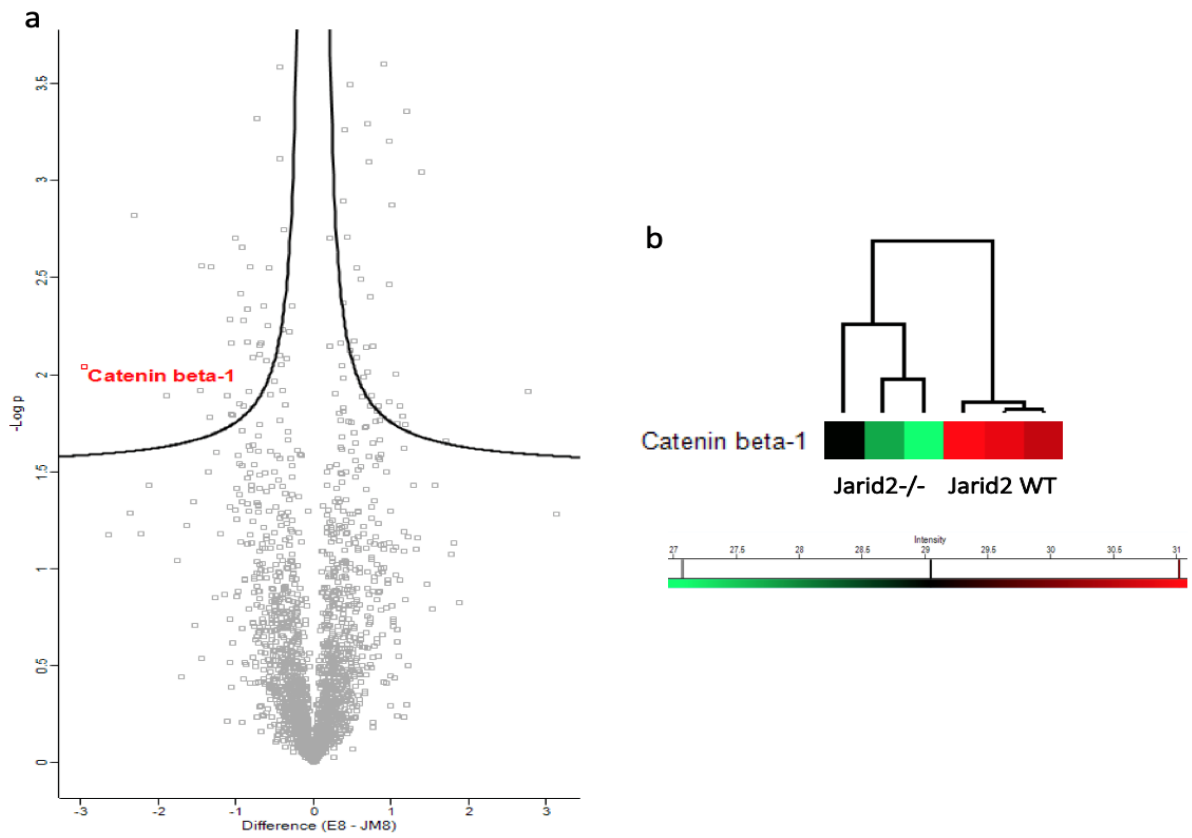

Figure 4.3. Beta-catenin demonstrates significantly reduced abundance in Jarid2 null mESCs compared to Jarid2 wild-type mESCs

a. Volcano plot showing log2 difference in mean LFQ abundance in Jarid2-/- mESCs (E8) versus WT (JM8) (x-axis), against -log10 p-value (y-axis). Beta-catenin (Labelled Catenin beta-1) highlighted in red, showing reduced relative abundance in Jarid2-/- mESCs when compared to matched parental Jarid2 WT mESCs

b. Individual heatmap showing unsupervised hierarchical clustering of intensity of biological replicates of Jarid2-/- mESCs and WT mESCs for each β-catenin. Jarid2-/- and WT replicated form separate clusters.

4.2 Mass spectrometry search for evidence of β-catenin lysine 49

A literature search has shown no current publications in which endogenous methylation of β-catenin at lysine 49 was evident using mass spectrometry-based approaches. Hoffmeyer et al. also reported that attempts to identify methylation by mass spectrometry were unsuccessful, and this was attributed to a reduced trypsin digest efficiency at methylated lysine residues (Hoffmeyer et al. 2017). Indeed, a MaxQuant search for methylated peptides from the crude Jarid2-/- and wild type extracts did not identify methylated β-catenin peptides containing lysine 49 (representative MS fragmentation spectrum corresponding to unmethylated K49 fragment; figure 4.4.a). Following detailed discussions with the Lamond group, University of Dundee and with the MRC LMS Mass Spectrometry group (lead by Dr Holger Kramer), an immunoenrichment strategy to detect endogenous β-catenin was designed. This approach is frequently employed when seeking to detect specific post-translational protein modifications (Kim, Zhong, and Pandey 2016; Zhao and Jensen 2009). Initially lysates from wild type ES cells were used to attempt to reproducibly identify this methylation event, before assessing any change between wild-type and PRC2 mutant cells.

To maximise the probability of identifying methylated β-catenin fragments, β-catenin was immunoenriched using two different antibodies so as to exclude the possibility that the methylated form of β-catenin was not bound. Additionally, antibodies used bind the C-terminal of β-catenin, distant to the reported lysine 49 methylation event, thus reducing the likelihood of methylation affecting antigen binding (BD biosciences BD 61054 and Cell Signalling Technology CST9587 antibodies used). Furthermore, as this methylation event was reported in both mESCs and oncospheres formed from liver cancer stem cells, immunoenrichments were generated from lysates of both wild type JM8 mESCs and liver

cancer cell line (Hep3b) treated to form oncospheres to enrich for resident liver cancer stem cells (as used in the study by Zhu et al., oncosphere formation shown figure 4.4.b). Finally, because the lysine demethylase KDM2A might be responsible for demethylation of β-catenin, lysates were prepared in the presence and absence of the KDM2A demethylase specific inhibitor, Daminoxide (Rose et al. 2012).

To address the possibility raised by Hoffmeyer et al. that trypsin/GluC endopeptidase digests fail to digest at methylated lysine-49, alternate AspN digests were also prepared and analysed. In total MS experiments were undertaken on 16 different conditions in biological and technical replicate, to comprehensively interrogate endogenous β-catenin for its methylation profile (experimental design schematic shown Figure 4.4.c).

Beta-catenin immunoprecipitation was optimised for each antibody, with BS^3 cross linking at 0.25mM for the BD 61054 antibody, and no cross linking used for the CST9587 antibody, as this dramatically reduced of yield of target immunoprecipitate. Immunoprecipitates were interrogated with anti-β-catenin to confirm successful immunoprecipitation, as well as anti-pan-methyl-K antibody to confirm antibody detected methylation of β-catenin as previously reported. Western blot analysis of Immunoprecipitates with anti-β-catenin antibody demonstrated robust immunoprecipitation of target protein (Figure 4.4.d). Interrogation of Immunoprecipitates with anti-pan-methyl-K antibody demonstrated a low to moderate methylation signal in both JM8 mESC and Hepb3 oncosphere lysates (Figure 4.4.d), in contrast to the strong signal reported using a similar technique previously reported by others (Zhu et al. 2016, Hoffmeyer et al. 2017). Efforts were made to optimise yield of methylated β-catenin, by shortening the lysis and pulldown protocols and trialling different lysis buffers, with little apparent effect on either yield of immunoprecipitated β-catenin, or the detection of lysine methylation. The presence of daminoxide during the cell lysis protocol seemingly

had minimal effect on the strength of methylation signal (data not shown). Despite this we decided to continue with the planned experimental design, assuming mass spectrometry may be able to detect differences in methylation that might not be easily observed using an antibody-based approach.

4.3.2. Optimisation of Mass Spectrometry protocol of immunoenriched β-catenin

Initial β-catenin Immunoprecipitates using BD 61054 antibody were used to optimise the clean-up of samples. In gel digest, trichloroacetic acid (TCA) and SP3 bead (Hughes et al. 2019) clean up techniques were compared. All techniques revealed strong enrichment, between with mean β-catenin signal intensity greater than 30% across the three preparations. The in-gel digest technique yielded the greatest enrichment of β-catenin (close to 55% peptide enrichment). However, the TCA clean up approach yielded the greatest intensity of β-catenin peptide MS signal. Subsequent MS experiments samples were prepared in biological replicates, using the optimised immunoprecipitation protocols, and TCA clean up prior to MS.

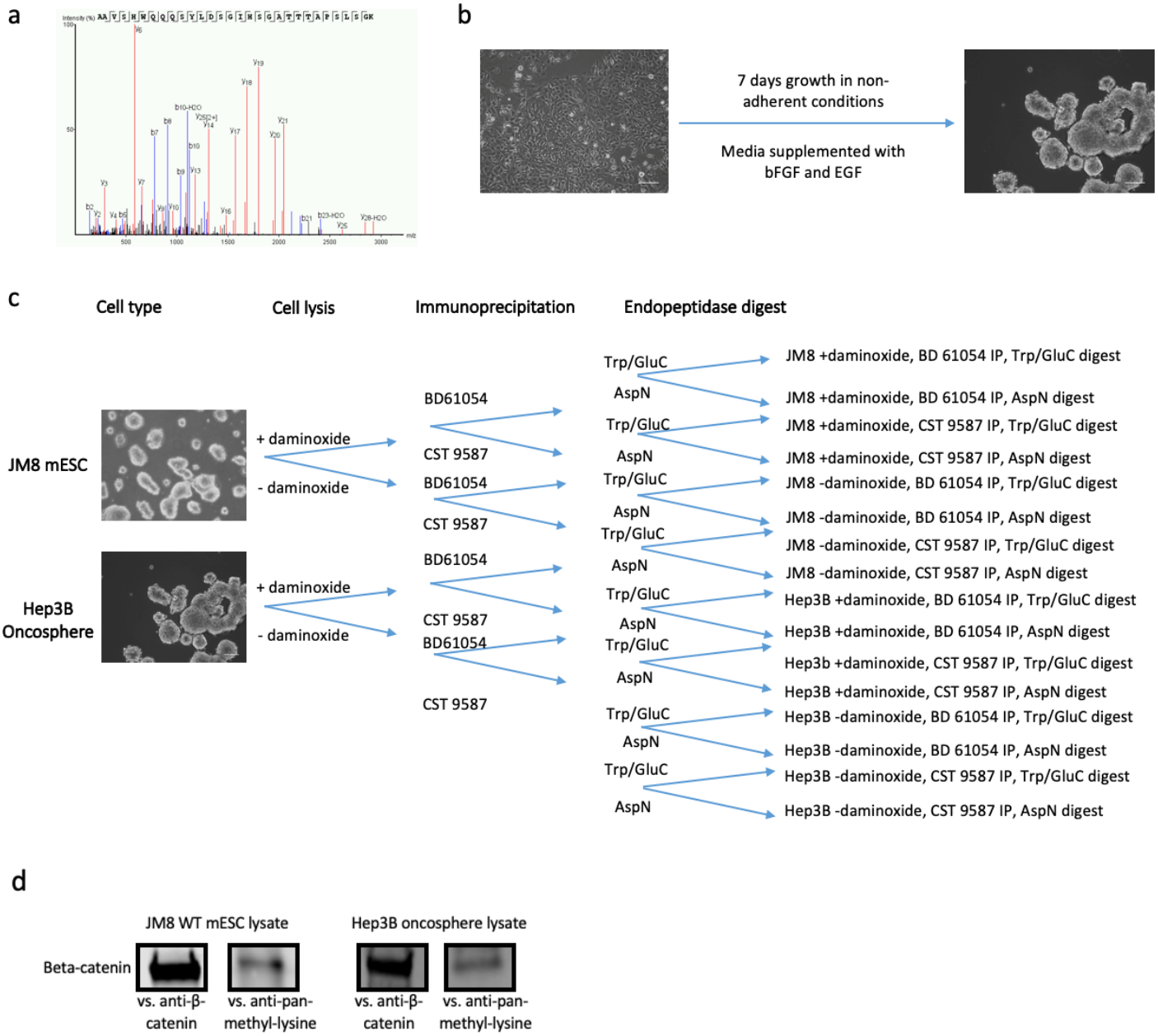

Figure 4.4. Experimental design and optimisation of efforts to identify methylation at residue lysine 49 methylation of β-catenin

a. Representative MS fragmentation spectrum corresponding to β-catenin K49 Trypsin/GluC digest fragment. No methylation was identified in biological replicates of either Jarid2 WT mESCs or Jarid2-/- mESCs.

b. Schematic representation of Hep3B oncosphere formation protocol, to enrich for resident liver cancer stem cells. Successful oncosphere formation confirmed by phase contrast microscopy. Representative image of Hep3B oncosphere on right.

c. Schematic representation of experimental design for β-catenin lysin 49 methylation search. Both JM8 and HepB3 lysates prepared in the presence and absence of Daminoxide, Immunoprecipitation with two separate antibodies (BD 61054 and CST9587), and digested with either GluC/Trypsin or AspN. In total 16 different condition, in biological replicate.

d. Representative western blot analysis showing successful immunoprecipitation of β-catenin using BD61054 (left panel in pairs). Counter-staining with anti-pan-methyl-lysine antibody shows modest staining in both JM8 and Hep3B oncosphere lysates. Similar results obtained for CST9587 not shown.

4.3.3. Mass spectrometry analysis of immunoenriched β-catenin did not reveal evidence for mono- or tri-methylation at lysine 49

Biological replicates were interrogated for immunoprecipitations using separate antibodies, on two separate lysates, in the presence or absence of daminoxide, using two separate endopeptidases. In total eight separate mass spectrometry experiments were repeated in duplicate for each endopeptidase digest (i.e., JM8 lysate vs two antibodies, each +/- daminoxide and Hep3b oncosphere lysate vs. two antibodies, each +/- daminoxide; in total 32 individual MS experiments were undertaken for this methylated peptide search).

The predicted peptide fragments containing lysine 49 following Trypsin/GluC digest are shown figure 4.5a. MS following trypsin/GluC endopeptidase digest of immunoenriched β-catenin yielded peptide good coverage of β-catenin (typically >75% peptide coverage, Figure 4.5.b), with exceptional signal reported for the lysine 49 containing fragment. No detectable methylation at lysine 49 was identified for either antibody using both MaxQuant and MASCOT searches, either in the presence or absence of daminoxide (representative MS fragmentation spectrum corresponding to unmethylated K49 Trypsin/GluC digest fragment; figure 4.5.c). Trypsin cleavage occurs at the C-terminal side of lysine and arginine residues, and as such the β-catenin peptide fragment containing lysine 49 is cleaved directly at the C-terminal of lysine 49. It has been reported that trypsin digest efficiency is reduced at methylated lysine residue (Snijders et al. 2010). If cleavage at this site is inefficient, a peptide fragment of a predicted size of 3484Da should be generated. A search was undertaken for this peptide fragment, but we did not find evidence of either the methylated or unmethylated form, suggesting that either digestion was efficient, or that the generated peptide was present but not detected by MS protocol used. It has been suggested that highly

changed fragments may be retained on the MS column, and are then absent in the MS spray (A. Lamond, personal communication). Quantification of the K49 fragment versus the whole protein and remaining peptides did not identify a 'missing peptide' quantity, suggesting that loss of the methylated K49 fragment by column binding is unlikely. However, to confirm that reduced efficiency of digest at methylated lysine peptides by trypsin was not contributing to the failed detection of methylated β-catenin, further MS was undertaken on immunoprecipitated β-catenin treated with AspN endopeptidase (predicted lysine 49 fragment sequence given figure 4.5.d). Typically, these digests were less efficient, and yielded peptide coverage of β-catenin of 35-50% (Figure 4.5.e), however good signal was reported for the lysine 49 containing fragment. Again, no detectable methylation was identified using MaxQuant or MASCOT search at lysine 49 for either antibody, either in the presence or absence of daminoxide (representative MS fragmentation spectrum corresponding to unmethylated K49 AspN digest fragment; figure 4.5.e). This analysis has shown that lysine 49 methylation of β-catenin is not detectable by mass spectrometry on β-catenin, either in whole cell lysates, or endogenous immunoprecipitated β-catenin enriched from either embryonic stem cells or enriched liver cancer stem cells, using two separate immunoprecipitating antibodies, and in the presence or absence of specific KDM2A demethylase inhibition. This calls into question the validity of previous claims that have been based solely on antibody specificity (for K49-methylated β-catenin), particularly as we have not been able to assess the antibody in question for an assessment of reproducibility.

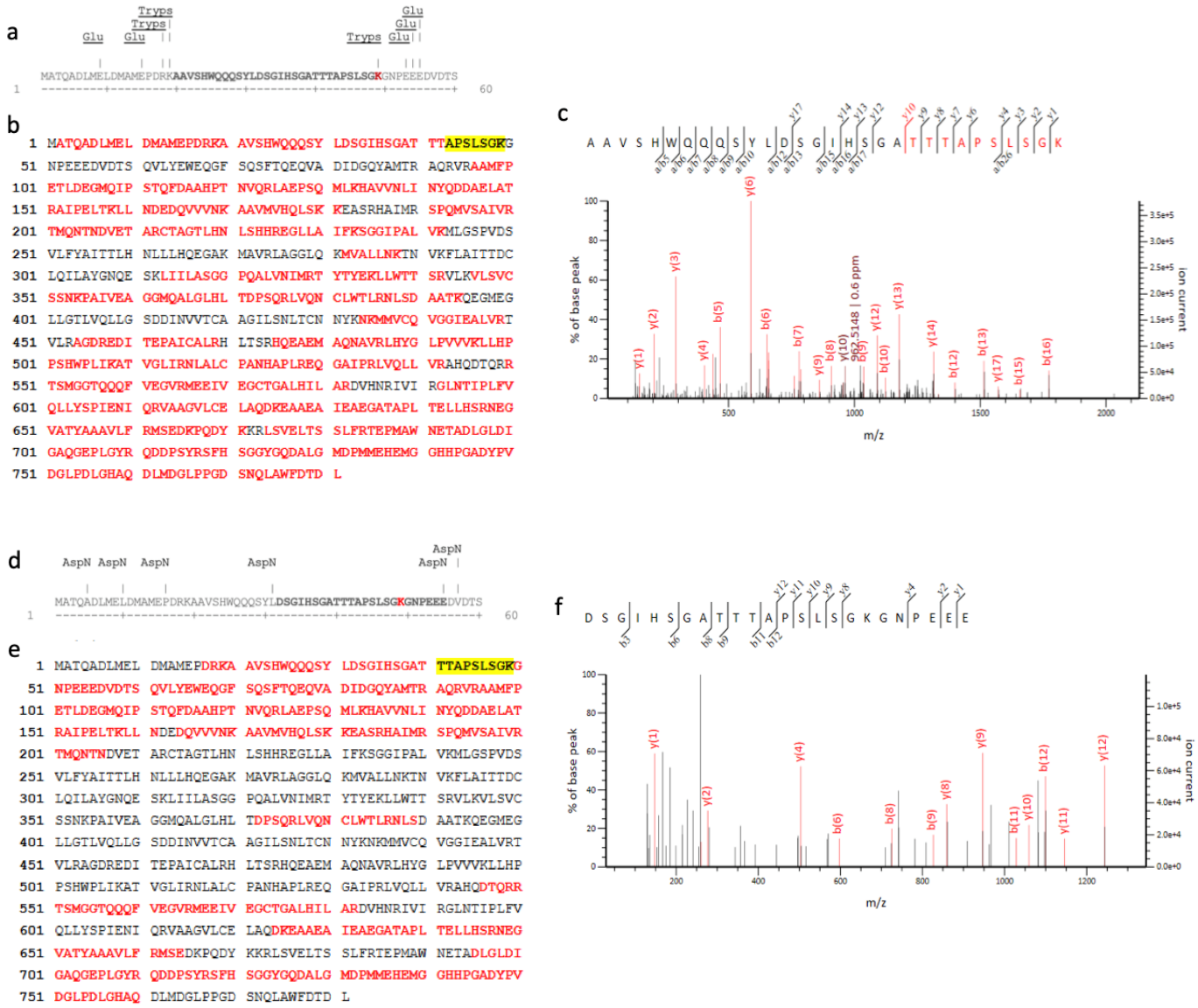

Figure 4.5. Comprehensive mass spectrometry analysis of immunoenriched β-catenin fails to identify methylation of lysine 49

a. Predicted Trypsin/GluC digest of β-catenin (amino acid sequence 1-60). Fragment containing lysine 49 residue in bold, lysine 49 highlighted in red. Fragment has estimated molecular weight of 3484 Da in unmethylated form.

b. Representative protein sequence coverage of immunoenriched β-catenin following Trypsin/GluC digest. Matched sequence in red. Excellent peptide abundance of lysine 49 fragment reported. Total protein coverage 77%.

c. Representative MS fragmentation spectrum corresponding to β-catenin K49 Trypsin/GluC digest fragment. No methylation was identified in any of biological replicates of eight conditions that underwent trypsin/GluC digest.

d. Predicted AspN digest of β-catenin (amino acid sequence 1-60). Fragment containing lysine 49 residue in bold, lysine 49 highlighted in red. Fragment has estimated molecular weight of 2342 Da in unmethylated form.

e. Representative protein sequence coverage of immunoenriched β-catenin following AspN digest. Matched sequence in red. Satisfactory peptide abundance of lysine 49 fragment reported. Total protein coverage 44%.

f. Representative MS fragmentation spectrum corresponding to β-catenin K49 AspN digest fragment. No methylation was identified in any of biological replicates of eight conditions that underwent AspN digest.

4.3.4. Mass spectrometry analysis of immunoenriched β-catenin identifies mono- and tri-methylation at lysine 133

Lysine 133 methylation has been reported for β-catenin (Deng et al. 2017), which is SMYD2 dependent rather than PRC2 mediated. This PTM was reported to be critical for nuclear localisation of β-catenin. In this case the authors were able to identify methylated lysine 133 using mass spectrometry, following *in vitro* methylation of β-catenin by recombinant SMYD2. This study however, did not show lysine 133 methylation of endogenous β-catenin. Clearly it is important to validate *in vitro* methylation assays and identify methylated endogenous peptides, since *in vitro* methylation assays are non-physiological, and high concentrations of both enzyme and target residue may result in non-specific methylation (Zhao and Jensen 2009). Importantly I detected both mono- and tri-methylation of β-catenin at lysine residue 133 in samples digested with both trypsin and AspN digests (figure 3.6.c,f). Lysine 133 methylation was observed in nine of sixteen trypsin digests MS experiments, and six of sixteen AspN digest MS experiments. Lysine methylation was detected in both samples with or without the addition of daminoxide. I believe that this is the first report of the lysine 133 methylation of endogenous β-catenin, and augments the previous report by Deng et al. Although this is an important result that warrants further investigation, unfortunately this was beyond the timescale of this research project. Significantly, the identification of K133 methylation may explain why methylation was observed using an anti-pan-methyl-lysine antibody on immunoprecipitated β-catenin samples. Additionally, that methylation is detectable at lysine 133, provides reassurance that a methylation event at lysine 49 ought also to be detected.

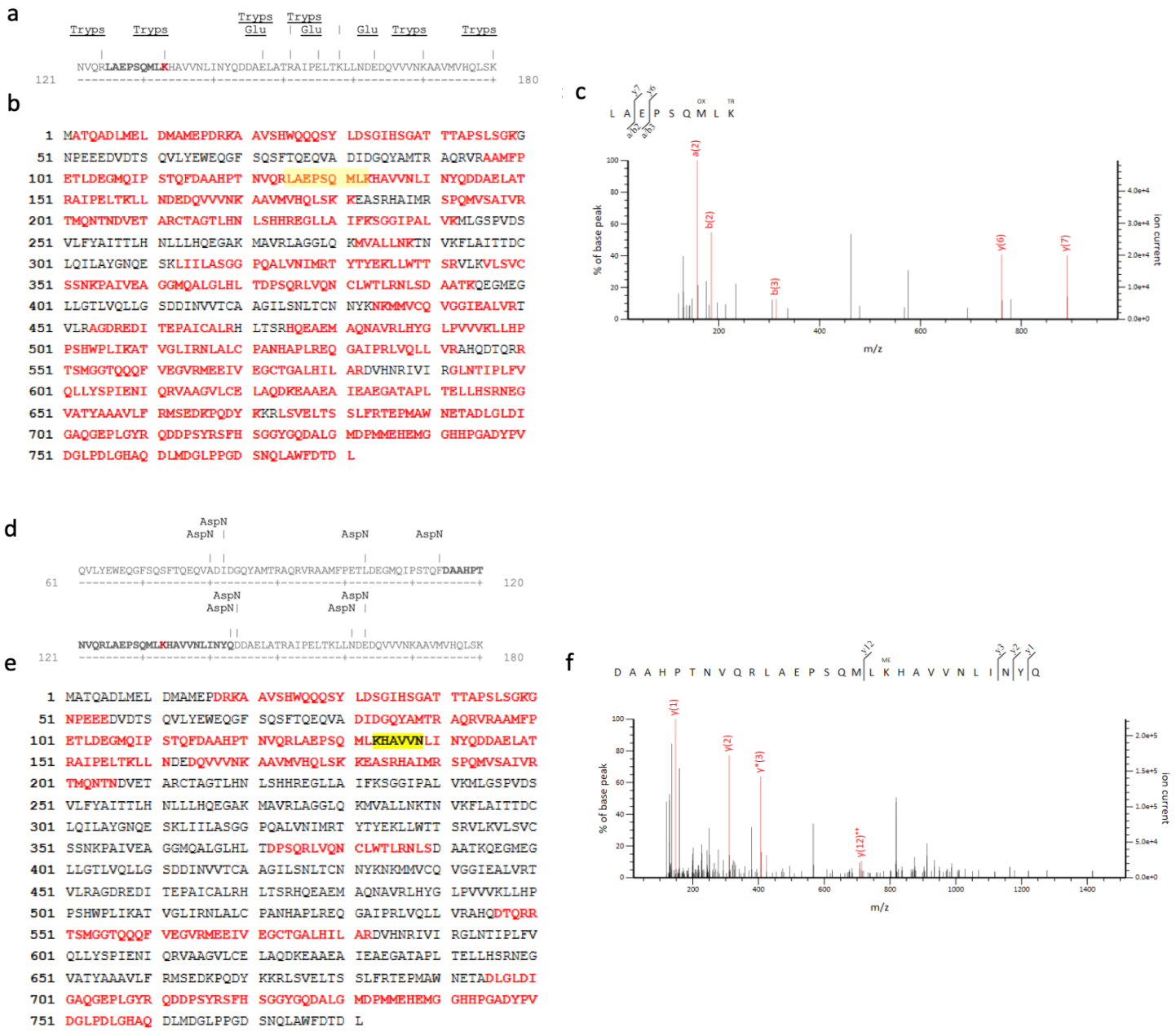

Figure 4.6. Comprehensive mass spectrometry analysis of immunoenriched β-catenin identifies methylation of lysine 133

a. Predicted Trypsin/GluC digest of β-catenin (amino acid sequence 121-180). Fragment containing lysine 49 residue in bold, lysine 49 highlighted in red. Fragment has estimated molecular weight of 1016 Da in the unmethylated form, 1030 Da in the lysine mono-methyl form, and 1059 Da in the lysine tri-methyl form.

b. Representative protein sequence coverage of immunoenriched β-catenin following Trypsin/GluC digest. Matched sequence in red. Excellent peptide abundance of lysine 49 fragment reported. Total protein coverage 77%.

c. Representative MS fragmentation spectrum corresponding to β-catenin K49 Trypsin/GluC digest fragment, showing tri-methyl lysine.

d. Predicted AspN digest of β-catenin (amino acid sequence 61-121). Fragment containing lysine 49 residue in bold, lysine 49 highlighted in red. Fragment has estimated molecular weight of 3259 Da in the unmethylated form, 3273 Da in the lysine mono-methyl form, and 3303 in the lysine tri-methyl form.

e. Representative protein sequence coverage of immunoenriched β-catenin following AspN digest. Matched sequence in red. Satisfactory peptide abundance of lysine 49 fragment reported. Total protein coverage 38%.

f. Representative MS fragmentation spectrum corresponding to β-catenin K49 AspN digest, showing mono-methyl lysine

3.4 Discussion and future perspectives

Here a comprehensive proteomic analysis of Jarid2 null mESCs is presented, which yields a number of interesting results. Label free quantification allows accurate and reproducible quantification of samples (Asara et al. 2008), permitting a direct comparison of different samples. Comparison of Jarid2 null and wild-type mESCs shows that there is great similarity between the Jarid2 null and wild type mESCs, with just 28 of 3026 (<1%) proteins showing significantly increased or decreased abundance when false discovery rate of <0.05 was applied. It is important to note that peptides which were below the detection threshold in greater than one sample in either Jarid2-/- or wild type-mESCs were excluded from the analysis, and as such proteins which have very low expression in either Jarid2 null or WT mESCs are potentially missed from this investigation. However, a number of important candidate proteins were identified as having either increased or decreased abundancy. Notably, both DNA methyl transferases Dnmt3b and Dnmt3l both demonstrate significant reduction in abundance in Jarid2 null mESCs. This is an intriguing finding, as PRC2 H3K27me3 profiles often correspond to CpG islands (Blackledge and Klose 2011), and Jarid2 null mESCs have been reported to have aberrant PRC2 targeting (either increased, reduced, or globally similar levels with altered chromatin targeting (Landeira and Fisher 2011). Mouse embryonic stem cells lacking Dmnt3b have been generated and are able to self-renew, and will differentiate into all three germ layers, but progressively lose DNA methylation as the cells are passaged. Significantly, differentially methylated regions in Dnmt3-/- mESCs show strong enrichment for both Ezh2 and Suz12 DNA binding sites as determined by ENCODE (Liao et al. 2015). This observation may provide further insight into the complexities of PRC2 targeting in Jarid2 null mESCs, linking DNA methylation, with observed changes in PRC2 targeting mESCs lacking Jarid2.

A further exciting observation was that β-catenin is the protein demonstrating the greatest reduction in abundancy in Jarid2-/- mESCs relative to wild type, a finding in keeping with previously reported reduced canonical Wnt signalling observed in Jarid2 null mESCs. Given our interests in the overlap between epigenetic machinery and cell signalling this important result was investigated further. A recently proposed mechanism whereby PRC2 regulated β-catenin stability and Wnt signalling is through direct non-canonical lysine methylation of β-catenin at lysine 49 (Hoffmeyer et al. 2017; Zhu et al. 2016). Despite extensive efforts this modification was not detected in endogenous β-catenin, in either whole cell extracts of following immunoenrichment, although a previously reported SMYD2 mediated lysine 133 methylation event was shown for the first time in endogenous β-catenin samples. This is the second report of failure to detect lysine 49 methylation using mass spectrometry (Hoffmeyer et al. 2017), and is at odds with reported detection using antibody based methodologies. This finding may support the observation that E-cadherin interaction between Jarid2 null and wild-type mESCs results in potentiated canonical Wnt signalling, possibly through a mechanism which increases the β-catenin pool in the Jarid2 null cells. Examination of total β-catenin abundance and localisation following the co-culture protocol would be of great value.

Chapter 5. Jarid2 dependent localisation of the dual residence protein Afadin

A significant advantage of global proteomic analysis is that it allows investigation not only of protein abundance, but also interrogation of sub-cellular location (Orre et al. 2019). There are many examples of cell signalling cascades, where proteins are present in the cytoplasm, until activated to translocate to the nucleus. A notable example is β-catenin, where translocation to the nucleus enables β-catenin to complex with transcriptional activating partners LEF and TCF to drive canonical Wnt target gene expression (Kretzschmar and Clevers 2017). We have shown that mESCs lacking Jarid2 have a reduced abundance of β-catenin in whole cell fractions. To investigate whether β-catenin, or indeed other cell signalling proteins, have altered cellular localisation in Jarid2 null mESCs, proteomic analysis was performed on isolated nuclear and cytosolic fractions from Jarid2 null and wild type mESCs.

5.1. Separation of Jarid2 null and wild type mESCs into nuclear and cytoplasmic fractions

Jarid2-/- and matched parental mESCs were grown in media supplemented with LIF, and separated into nuclear and cytoplasmic fractions using a standard fractionation buffer (fractionation performed by Andy Malinowski, lymphocyte Development Group, MRC LMS). Western blot analysis of nuclear and cytoplasmic fractions revealed good fractionation, with robust detection of the cytosolic resident protein α-tubulin in the cytosolic fraction, absent from the nuclear fraction, and conversely detection of the nuclear envelope protein Lamin B in the nuclear fraction, but absent from the cytoplasmic fraction (Figure 5.1.a). This confirms that the fractionation had enriched the cytosolic and nuclear fractions appropriately. A standard TCA precipitation and trypsin digest followed by high pressure liquid chromatography and mass spectrometry using a 2-hour gradient on Q-exactive prior to MS

was undertaken in biological triplicate, and technical replicate in collaboration with Dr Tony Ly (Lamond Group, University of Dundee). Comparison of relative abundancies of proteins in the nuclear and cytoplasmic fractions showed anticipated enrichment of histone proteins in the nuclear fraction in both Jarid2-/- and wild type mESCs, validating successful fractionation (Figure 5.1.b-d).

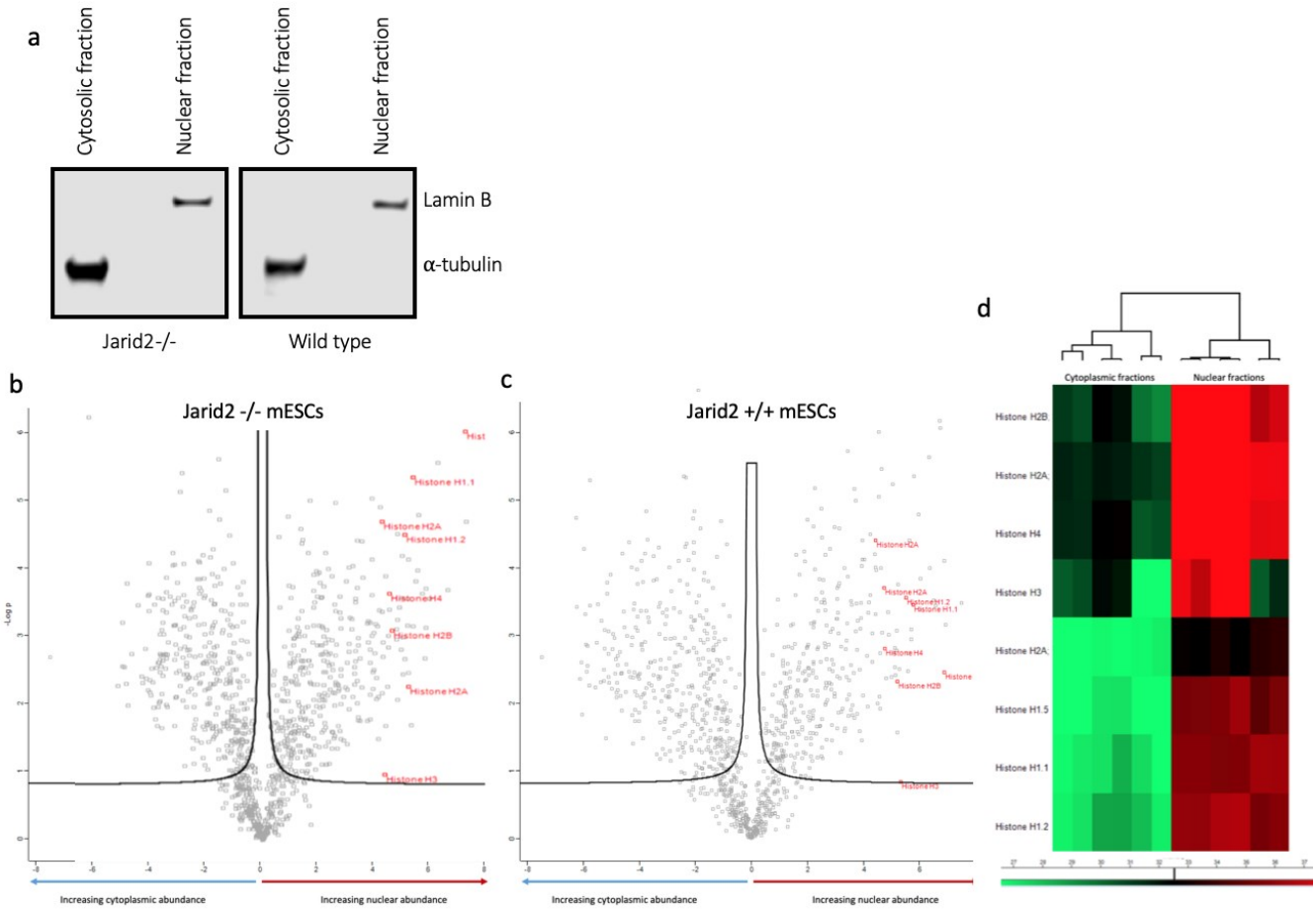

Figure 5.1. Validation of successful separation of cytoplasmic and nuclear fractions of Jarid2 null and wild type mESCs

- **a.** Western blot analysis of fractionated blot analysis of Jarid2/- and matched parental wild type mESCs. Lamin B (66 kDa) is a nuclear envelope protein and indicates nuclear fraction. Alpha-tubulin (50 kDa) is a microtubule protein indicating cytosolic fraction.
- b. Volcano plot comparing relative abundancies in nuclear and cytosolic fractions of Jarid2 null mESCs (FDR <0.5). Detected histones highlighted in red. Increasing nuclear abundance >0
- c. Volcano plot comparing relative abundancies in nuclear and cytosolic fractions of wild type mESCs (FDR <0.5).Detected histones highlighted in red. Increasing nuclear abundance >0
- d. Heatmap showing unsupervised clustering of histone abundances into cytoplasmic (left) and nuclear (right) fractions of combined Jarid2-/- and wild type samples.

5.2 Interrogation of global nuclear and cytoplasmic fractions between Jarid2 null and wild type mESCs

Global analysis of protein abundancies comparing nuclear fractions and cytoplasmic fractions between Jarid2 null and WT mESCs was undertaken. This revealed overlap with the proteins showing reduced abundancy in the whole cell extracts global proteomic analysis. This agreement provided reassurance that the observed results in both the whole cell extract and fractionated extract experiments are robust and reliable. The abundance of β-catenin was reduced abundance in both the cytosolic and nuclear fractions of Jarid2-/- mESCs relative to wild type (69.8% reduction in relative nuclear abundance p=0.051, 33.4% reduction in relative cytosolic abundance p=0.006).

5.3. Interrogation of relative nuclear to cytoplasmic abundancies between Jarid2 null and wild type mESCs

To assess changes in the sub-cellular localization of protein between Jarid2 null and wild type mESCs, the relative nuclear to cytoplasmic abundance was calculated for each protein, and compared between Jarid2 null and matched parental wild type samples (Figure 5.2.a). Global analysis revealed a shift predominantly from nuclear to cytosolic localization, with 1208 of the 1746 (69.2%) comparable proteins showing greater relative cytoplasmic abundance in Jarid2 null mESCs when compared to wild-type cells. The remaining 538 protein showing increased nuclear abundancy in Jarid2-/- mESCs relative to wild type. Applying a cut off of >2-fold change in relative nuclear to cytoplasmic abundance and p-value <0.5, identifies 50 proteins as having significant change in sub-cellular localization. An increased relative cytoplasmic intensity was shown in 41 of these proteins, with nine showing increased relative nuclear abundance in Jarid2-/- mESCs when compared to wild type mESCs (Figure 5.2.b).

Proteins showing a significant change in sub-cellular location (fold change >2, p<0.05) are shown in Table 5.1.

a

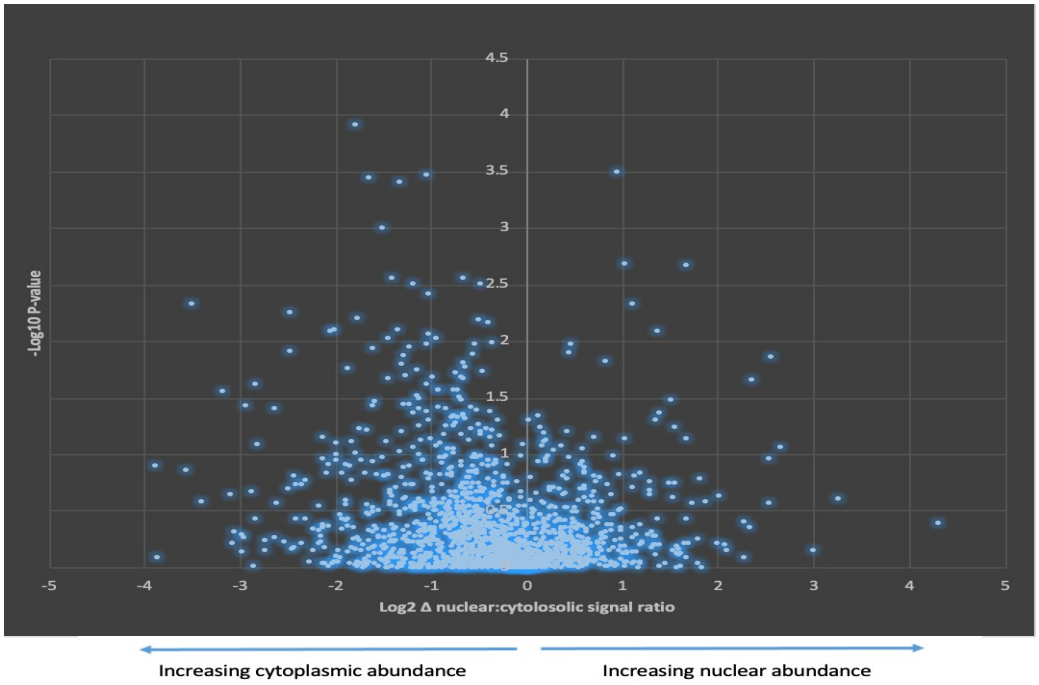

b

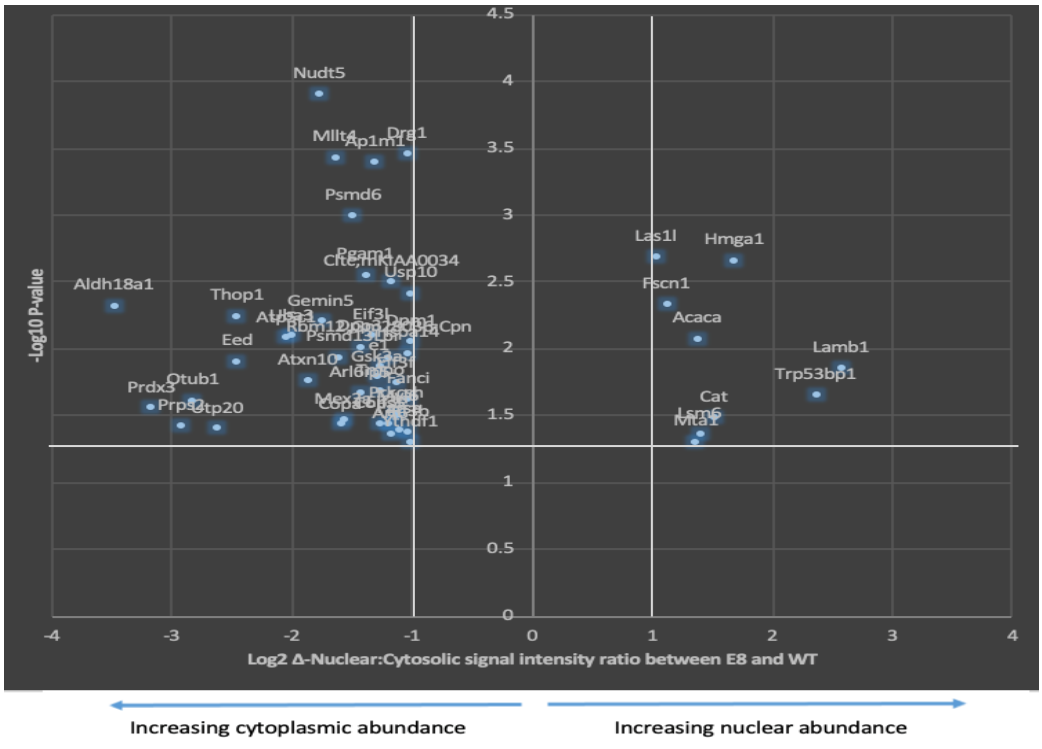

Figure 5.2. Proteins demonstrating preferential cytosolic and nuclear localisation in Jarid2 null mESCs relative to wild-type

a. Global distribution of relative protein localisation of protein in Jarid2 mESCs compared to matched parental wild mESCs. Greater relative cytoplasmic abundance in Jarid2-/- compared to wild type to left (<0), and greater relative nuclear abundance to right (>0)

b. Proteins identified with greater than 2-fold change in localisation and p-value <0.05, in Jarid2 mESCs compared to matched parental wild mESCs. Greater relative cytoplasmic abundance in Jarid2-/- compared to wild type to left (<0), and greater relative nuclear abundance to right (>0). Vertical grey lines represent 2 fold cut off, horizontal grey line represents p-value <0.05 (Proteins labelled with gene ID, protein IDs given in table 5.3)

Protein Identification	Gene Identification	Jarid-/- Mean Nuclear intensity	Jarid2-/- Mean Cytosoloc Intensity	Jarid2-/- Nuclear to Cytosolic Intensity Ratio	WT Mean Nuclear intensity	WT Mean Cytosoloc Intensity	WT Nuclear to Cytosolic Intensity Ratio	Relative nuclear:cytosolic Intensity Change Jarid-/-:WT	Log2 Relative nuclear:cytosolic Intensity Change Jarid-/-:WT	-Log10 P-value
Delta-1-pyrroline-5-carboxylate synthase	Aldh18a1	2.23E+09	1.67E+08	13.379	5.52E+09	3.68E+07	149.895	0.089	-3.486	2.337
Thioredoxin-dependent peroxide reductase, mitochondrial	Prdx3	5.53E+07	3.64E+08	0.152	3.61E+08	2.64E+08	1.370	0.111	-3.173	1.568
Ribose-phosphate pyrophosphokinase 2	Prps2	5.56E+07	3.26E+09	0.017	3.50E+08	2.70E+09	0.129	0.132	-2.923	1.435
Ubiquitin thioesterase OTUB1	Otub1	2.77E+07	2.79E+09	0.010	2.52E+08	3.59E+09	0.070	0.141	-2.826	1.624
Small subunit processome component 20 homolog	Utp20	6.72E+09	2.34E+08	28.669	7.13E+09	4.03E+07	177.032	0.162	-2.626	1.412
Thimet oligopeptidase	Thop1	5.06E+07	5.50E+09	0.009	2.64E+08	5.22E+09	0.051	0.182	-2.458	2.257
Polycomb protein EED	Eed	2.19E+09	3.28E+08	6.667	1.89E+09	5.15E+07	36.625	0.182	-2.458	1.921
ATP synthase subunit gamma;ATP synthase subunit gamma, mitochondrial	Atp5c1	4.35E+09	1.82E+08	23.820	5.68E+09	5.75E+07	98.641	0.241	-2.050	2.091
NEDD8-activating enzyme E1 catalytic subunit	Uba3	2.35E+07	6.18E+08	0.038	1.10E+08	7.17E+08	0.153	0.249	-2.008	2.107
Ataxin-10	Atxn10	1.26E+08	2.51E+09	0.050	6.93E+08	3.77E+09	0.184	0.273	-1.870	1.772
ADP-sugar pyrophosphatase	Nudt5	5.01E+07	2.25E+09	0.022	1.20E+08	1.56E+09	0.076	0.292	-1.775	3.917
Gem-associated protein 5	Gemin5	3.63E+08	2.39E+09	0.152	1.79E+09	3.47E+09	0.515	0.294	-1.765	2.214
Afadin	Mllt4	1.18E+09	2.58E+09	0.458	1.61E+09	1.12E+09	1.434	0.320	-1.646	3.445
26S proteasome non-ATPase regulatory subunit 13	Psmd13	2.74E+08	5.81E+09	0.047	8.99E+08	6.27E+09	0.143	0.329	-1.605	1.947
Coatomer subunit alpha;Coatomer subunit alpha;Xenin;Proxenin	Copa	3.66E+08	3.83E+09	0.095	1.15E+09	3.98E+09	0.290	0.329	-1.603	1.443
Mex3 RNA binding family A	Mex3a	3.29E+07	8.44E+07	0.390	3.59E+07	3.09E+07	1.163	0.335	-1.576	1.478
26S proteasome non-ATPase regulatory subunit 6	Psmd6	2.30E+08	5.56E+09	0.041	6.83E+08	5.85E+09	0.117	0.355	-1.494	3.009
Dipeptidyl peptidase 3	Dpp3	7.95E+07	3.86E+09	0.021	2.65E+08	4.74E+09	0.056	0.368	-1.441	2.028
PRA1 family protein 3	Arl6ip5	8.20E+07	1.71E+08	0.479	1.05E+08	8.14E+07	1.296	0.369	-1.437	1.682
Phosphoglycerate mutase 1	Pgam1	9.37E+08	2.90E+10	0.032	2.60E+09	3.07E+10	0.085	0.381	-1.391	2.567
Eukaryotic translation initiation factor 3 subunit L	Eif3l	7.30E+08	8.01E+09	0.091	1.93E+09	8.35E+09	0.231	0.394	-1.345	2.113
AP-1 complex subunit mu-1	Ap1m1	2.34E+08	4.92E+08	0.476	5.49E+08	4.66E+08	1.179	0.404	-1.309	3.408
Glycogen synthase kinase-3 alpha	Gsk3a	4.96E+07	1.04E+08	0.476	5.98E+07	5.12E+07	1.168	0.407	-1.296	1.798
RNA-binding protein 12	Rbm12	1.75E+08	3.62E+08	0.482	3.49E+08	2.98E+08	1.169	0.412	-1.278	1.876
COP9 signalosome complex subunit 5	Cops5	9.46E+07	1.31E+09	0.072	2.49E+08	1.43E+09	0.174	0.414	-1.272	1.446
Lamina-associated polypeptide 2, isoforms alpha/zeta	Tmpo	1.04E+10	3.13E+08	33.313	8.90E+09	1.11E+08	80.187	0.415	-1.267	1.697
Eukaryotic translation initiation factor 3 subunit E	Eif3e	4.37E+08	4.23E+09	0.103	1.24E+09	5.17E+09	0.239	0.432	-1.210	1.453
Lamin-B receptor	Lbr	9.58E+09	1.36E+08	70.373	1.34E+10	8.24E+07	162.616	0.433	-1.208	1.950
ADP-ribosylation factor 6	Arf6	1.02E+08	2.47E+08	0.413	9.28E+07	9.89E+07	0.939	0.440	-1.184	1.368
Clathrin heavy chain 1	Cltc1	1.21E+10	2.09E+10	0.580	1.93E+10	1.47E+10	1.309	0.443	-1.173	2.514
Eukaryotic translation initiation factor 3 subunit F	Eif3f	4.10E+08	5.19E+09	0.079	9.86E+08	5.66E+09	0.174	0.454	-1.139	1.752
Glucosidase 2 subunit beta	Prkcsh	6.61E+07	2.41E+09	0.027	1.19E+08	1.98E+09	0.060	0.456	-1.134	1.526
Myosin light polypeptide 6	Myl6	5.40E+08	2.38E+09	0.227	1.66E+09	3.36E+09	0.494	0.460	-1.121	1.506
Phenylalanine--tRNA ligase alpha subunit	Farsa	6.58E+08	3.32E+09	0.198	1.80E+09	4.20E+09	0.429	0.462	-1.113	1.407
Developmentally-regulated GTP-binding protein 1	Drg1	4.90E+08	1.05E+09	0.467	8.64E+08	8.95E+08	0.966	0.484	-1.047	3.472
Heat shock 70 kDa protein 14	Hspa14	4.91E+08	1.44E+09	0.341	8.44E+08	1.21E+09	0.700	0.488	-1.035	1.979
Eukaryotic translation initiation factor 3 subunit B	Eif3b	1.19E+09	9.86E+09	0.120	2.34E+09	9.52E+09	0.246	0.488	-1.035	1.385
Fanconi anemia group I protein homolog	Fanci	1.61E+08	3.72E+08	0.431	3.22E+08	3.65E+08	0.882	0.489	-1.033	1.630
YTH domain-containing family protein 1	Ythdf1	1.52E+08	2.25E+08	0.676	2.39E+08	1.75E+08	1.367	0.495	-1.015	1.311
Ubiquitin carboxyl-terminal hydrolase 10	Usp10	7.19E+08	1.78E+09	0.403	1.38E+09	1.69E+09	0.813	0.495	-1.014	2.428
Dolichol-phosphate mannosyltransferase subunit 1	Dpm1	5.80E+07	2.40E+08	0.242	8.05E+07	1.65E+08	0.487	0.497	-1.009	2.069
Ribosomal biogenesis protein LAS1L	Las1l	2.76E+09	1.14E+08	24.134	2.37E+09	2.00E+08	11.836	2.039	1.028	2.695
Fascin	Fscn1	2.49E+09	2.91E+09	0.857	1.39E+09	3.52E+09	0.396	2.165	1.114	2.340
Metastasis-associated protein MTA1	Mta1	5.31E+09	1.04E+08	50.948	2.44E+09	1.23E+08	19.817	2.571	1.362	1.316
Acetyl-CoA carboxylase 1;Biotin carboxylase	Acaca	2.75E+08	2.67E+09	0.103	9.88E+07	2.48E+09	0.040	2.590	1.373	2.089
U6 snRNA-associated Sm-like protein LSm6	Lsm6	7.30E+08	2.72E+08	2.688	6.55E+08	6.39E+08	1.026	2.621	1.390	1.371
Catalase	Cat	1.34E+08	3.96E+09	0.034	4.26E+07	3.60E+09	0.012	2.851	1.511	1.492
High mobility group protein HMG-I/HMG-Y	Hmga1	1.09E+10	1.03E+08	106.146	6.84E+09	2.07E+08	33.092	3.208	1.682	2.676
Tumor suppressor p53-binding protein 1	Trp53bp1	2.56E+09	1.80E+07	142.130	1.91E+09	6.89E+07	27.704	5.130	2.359	1.666
Laminin subunit beta-1	Lamb1	1.70E+08	4.43E+07	3.847	1.26E+08	1.94E+08	0.648	5.936	2.570	1.867

Table 5.1. Proteins identified as having significant change in cellular localisation in Jarid2 null mESCs compared to wild-type

Proteins with greater cytoplasmic: nuclear abundance in Jarid2 null mESCs compared to wild type highlighted in green. Proteins with greater nuclear: cytoplasmic abundance in Jarid2 null mESCs compared to wild type highlighted in blue. -log10 p-value shown (i.e. -log10 p-value > 1.301)

This analysis reveals a number of attractive candidate proteins that differentially localize in the absence of Jarid2. Notably the PRC2 component Eed demonstrates a 5.5-fold increased cytosolic abundance in Jarid2-/- mESCs relative to wild type cells, showing there is a substantial shift in Eed localization towards the cytoplasmic compartment in the absence of Jarid2. Jarid2 has been reported to interact directly with Eed, and is thought to promote enzymatic activity of PRC2 (Sanulli et al. 2015a). Additionally, Eed interaction with Ezh2 is required for H3K27 methylation, as Ezh2 is autoinhibitory in the absence of Eed (Wu et al. 2013), and Eed is implicated in maintenance of gene silencing through targeting of PRC2 to existing H3K27me3, through recognition of H3K27me3 via its WD40 domain (Jiao and Liu 2015). It is intriguing to observe a shift away from the nuclear compartment in the absence of Jarid2, as the targeting and activity of PRC2 in the absence of Jarid2 remains ambiguous.
An additional candidate of interest is the dual residency protein Afadin, which shows a 3.1-fold increase in relative cytoplasmic abundance in the absence of Jarid2. The role of Afadin in the nucleus is unclear, although a role in post translational modifications of histones has been reported (VanLeeuwen et al. 2014; Sellers et al. 2018). In the cytoplasmic compartment Afadin links adherens junction protein Nectin to F-actin (Harris and Tepass 2010). Interestingly, both E-cadherin and β-catenin are adherens junction proteins, and have been recently reported to interact with Afadin through αE-catenin at adherens junctions. Importantly this study has identified Afadin, E-cadherin and β-catenin as all displaying altered localization and/or abundance in mESCs lacking Jarid2, highlighting the possibility that Jarid2 may in some way regulate adherens junction activity. Additionally, altered cell morphology and the ability to participate in multiple ICM formation on blastocyst injections is in agreement with possible disruption of cell-cell interface in cells lacking Jarid2 or Suz12. In view of this, Afadin was selected for further investigation.

5.4. Afadin shows preferential cytoplasmic localization in the absence of Jarid2

The proteomic data demonstrates Afadin has increased cytoplasmic abundance in jarid2 null mESCs. This is confirmed by examining Afadin abundancies in both Jarid2 null and wild type mESCs (figure 5.3.a,b,c). Wild type mESCs show significant (FDR<0.05) nuclear enrichment, as opposed to the significant cytoplasmic enrichment seen in Jarid2 null mESCs.

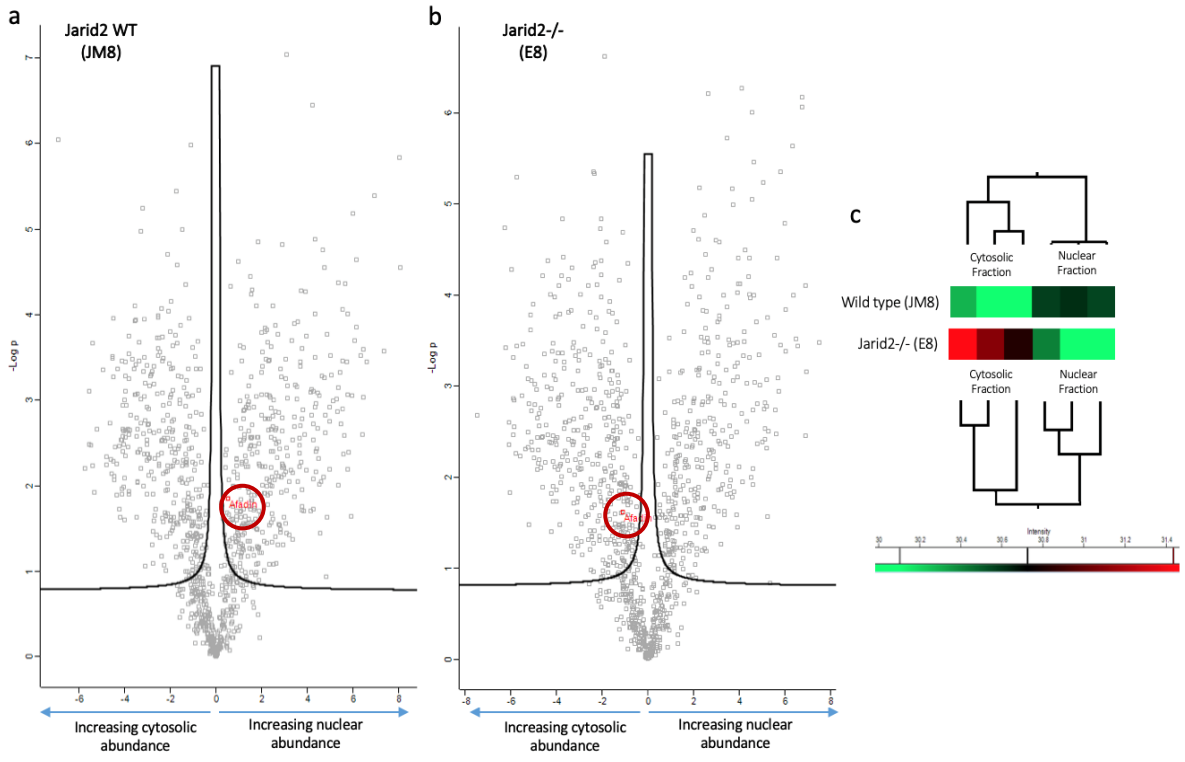

Figure 5.3. Proteomic analysis reveals shift from nuclear to cytosolic Afadin in Jarid2 null mESCs

a. Volcano plot comparing relative protein abundancies in nuclear and cytosolic fractions of wild type mESCs (FDR <0.5). Afadin highlighted in red, showing increased nuclear abundance relative to cytoplasmic abundance. Increasing nuclear abundance to the right (>0).

b. Volcano plot comparing relative protein abundancies in nuclear and cytosolic fractions of jarid2 null mESCs (FDR <0.5). Afadin highlighted in red, showing increased cytoplasmic abundance relative to nuclear abundance. Increasing cytoplasmic abundance to the left (<0)

c. Heatmap of Afadin in wild type and jarid2 null mESCs. Unsupervised hierarchical clustering into cytosolic (left) and nuclear (right) fractions. Wild type cells show increased nuclear abundance, conversely Jarid2 null mESCs show increased cytoplasmic abundance.

To validate this data, immunofluorescence microscopy and western blot analysis was performed using antibodies to Afadin (Figure 5.4.a-f). Increased cytosolic Afadin signal intensity was demonstrated indicated by the mean peak cytosolic Afadin intensities from 50 individual cells of either Jarid2-/- and wild type cells. A significant increase in peak (grey value) intensity for surface Afadin staining was detected in Jarid2-/- mESCs compared to wild-type (Figure 5.4.c, 2.46-fold greater mean peak grey value, $p=1.87E^{-14}$ (Students T-test); representative confocal images and grey value surface plots given figure 5.4.a,b). Furthermore, this result was replicated by examining an independently derived Jarid2 depletion ESC line (Shen et al. 2009) (Figure 5.4.c, 1.92-fold greater mean peak grey value in $Jarid2^{-/-}$ compared to $Jarid2^{fl/fl}$ mESC, $p=7.20E^{-10}$ (Students T-test)).

Semi-quantitative western blot analysis again shows an approximate two-fold increase in staining signal for Afadin (normalized to α-tubulin) in the cytosolic fraction in mESCs lacking Jarid2 compared to wild type mESCs (Representative blot shows figure 5.4.d). Quantification of Afadin staining a 2.26-fold increase in normalized cytoplasmic staining of Afadin in Jarid2 null mESCs compared to parental control (Figure 5.4.e, p=0.0028 (Students T-test)). Additionally, this result is also observed in Jarid2 deplete mESCs, with a 1.86-fold increase in normalized cytoplasmic staining in $Jarid2^{-/-}$ relative to $Jarid2^{fl/fl}$ mESCs (figure 5.4.f, p=0.0012; Students T-test). Nuclear Afadin staining was readily detectable in both mESCs lacking Jarid2 and wild-type cells (Figure 5.4.d). A trend towards reduced nuclear signal of Afadin (normalized to Lamin-B) was detected but did not reach significance in either Jarid2 null or Jarid2 deplete mESCs when compared to wild type (JM8/E8; 0.79-fold decrease in normalized nuclear staining in E8 relative to JM8, p=0.22; Jarid2 fl/fl, Jarid2-/-; 0.94-fold decrease in Jarid2-/- relative to Jarid2 fl/fl, p=0.85 (Students T-test).

These findings act to validate the proteomic data, as both the confocal microscopy, and fractionated western blot analysis are in agreement with the altered localization of Afadin shown in the fractionated proteomic data. Taken together, these data show robust evidence that Afadin does indeed show preferential cytoplasmic localization in the absence of Jarid2, and highlights a possible novel role for Jarid2 in coordinating nuclear localization of Afadin.

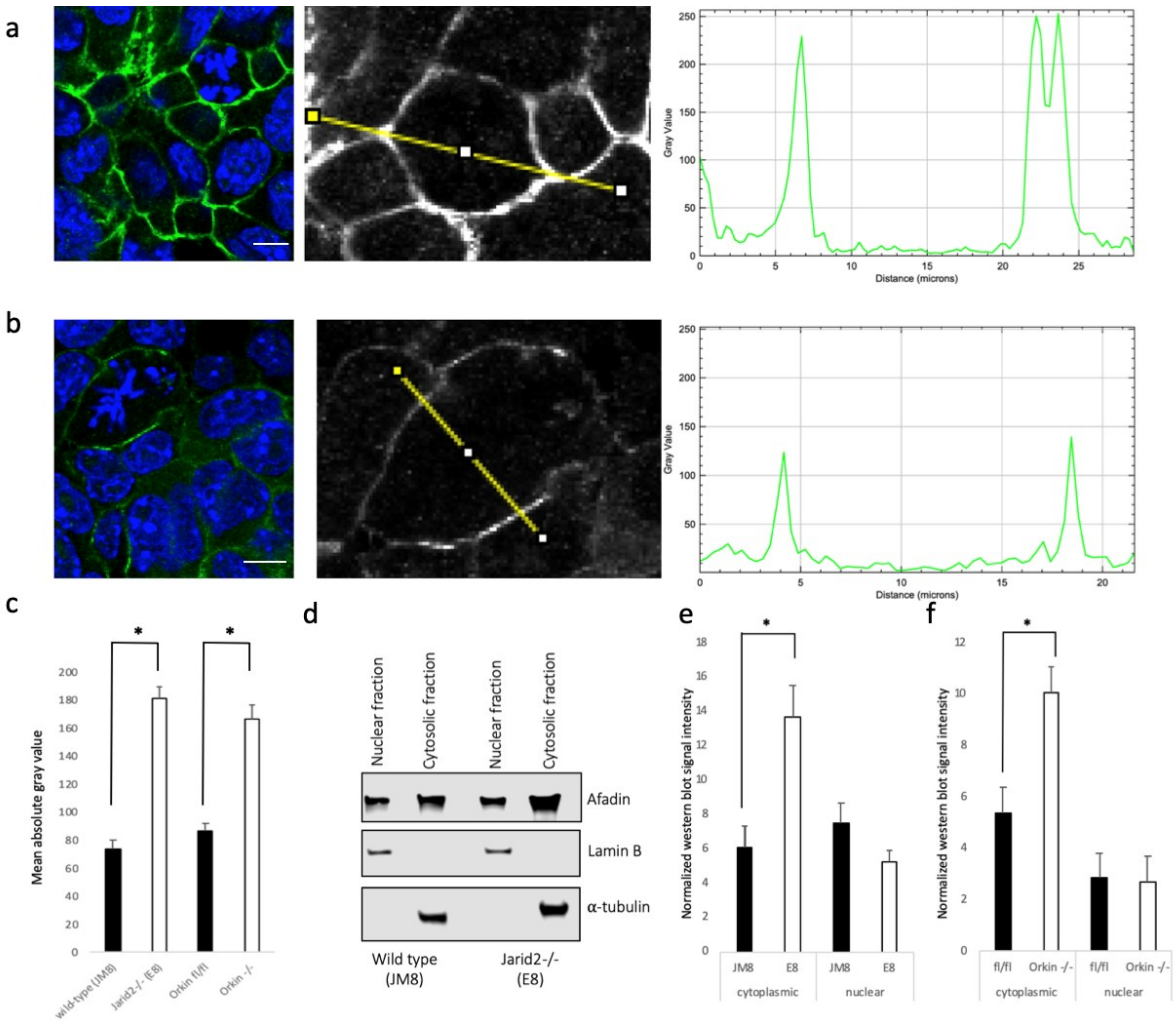

Figure 5.4. Confocal microscopy and fractionated western blot confirm preferential cytoplasmic abundance of Afadin in mESCs lacking Jarid2

a. Representative confocal microscopy image of Jarid2 null mESCs (E8, left image) stained for Afadin (green), counterstained with DAPI (blue). Scale bar 10μM. Greyscale image of Afadin staining an individual cell (middle), with surface mapping for grey value scoring (yellow line). Graphical representation of highlighted grey value (right).

b. Representative confocal microscopy image of Jarid2 wild type mESCs (JM8, left image) stained for Afadin (green), counterstained with 4',6-diamidino-2-phenylindole (DAPI, blue), scale bar 10μM. Greyscale image of Afadin staining only individual cell (middle), with surface mapping for grey value scoring (yellow line). Graphical representation of highlighted grey value (right).

(Legend continues on following page)

5.4. Afadin co-Immunoprecipitates with Jarid2 and core polycomb repressor complex 2 components

To investigate whether Jarid2 and PRC2 interact with Afadin, co-immunoprecipitation experiments were undertaken. Initial experiments using western blot analysis showed readily detectable Jarid2 staining following immunoprecipitation of Afadin. Additionally, weak but detectable Afadin signal was also observed following Jarid2 immunoprecipitation (Figure 5.5.a, b). To investigate this further, Afadin immunoprecipitations were scaled up and analyzed using mass spectrometry to identify interacting proteins. A tri[chloro]acetic acid (TCA) 'clean up' and trypsin digest was undertaken, prior to high pressure liquid chromatography using a 2-hour gradient on Q-exactive prior to mass spectrometry (Experiment undertaken in collaboration with Dr Holger Kramer, Mass spectrometry group, MRC LMS). Good enrichment of Afadin was achieved, and robust detection of Jarid2 as well as core PRC2 Suz12, Ezh2, Eed and Aebp2 was detected in wild-type mESCs. In order to identify whether loss of Jarid2 significantly changes which proteins are co-immunoprecipitated with Afadin, immunoprecipitations using Jarid2 null mESCs were undertaken.

Figure 5.4. Confocal microscopy and fractionated western blot confirm preferential cytoplasmic abundance of Afadin in mESCs lacking Jarid2 (cont…)

c. Mean peak grey value intensity of fifty individual cells stained for Afadin, comparing Jarid2 null (E8) and wild type (JM8), and Jarid2 deplete (Orkin-/-) and parental mESCs (Orkin fl/fl). Mean + standard error bars shown. Asterix denotes significance ($p<0.05$). Shows significant increase in peak Afadin grey value for mESCs lacking Jarid2, demonstrating preferential cytosolic localisation of Afadin.

d. Representative western blot showing nuclear and cytosolic fractions of Jarid2 null (E8), and wild-type mESCs. Lamin-B staining (66 kDa) shows nuclear fraction, and α-tubulin (50kDa) shows cytosolic fraction. Afadin (207 kDa) staining is increased in the cytosolic fraction of Jarid2 null mESCs, when compared to wild type.

e. Comparison of normalised Afadin signal intensity in cytoplasmic and nuclear fractions using semi-quantitative western, in Jarid2 null (E8) and wild type (JM8) mESCs. Mean + standard error bars shown. Asterix denotes significance ($p<0.05$).

f. Comparison of normalised Afadin signal intensity in cytoplasmic and nuclear fractions using semi-quantitative western, in Jarid2 deplete (Orkin-/-) and Parental (fl/fl) mESCs. Mean + standard error bars shown. Asterix denotes significance ($p<0.05$).

These immunoprecipitations were compared to wild type mESC Afadin immunoprecipitations (Figure 5.6.a,b). Strikingly, all core PRC2 components show reduced abundance in the absence of Jarid2, with Aepb2 and Suz12 showing the greatest reduction in abundance of all detected proteins (Aebp2; 98.6% reduction (p=0.003), Suz12-/-; 96.4% reduction ($p=4.5x10^{-5}$), Ezh2; 77.2% reduction (p=0.004), Eed; 37.2% reduction (p=0.02), full list of Afadin co-precipitants with significantly reduced abundance given in appendices)

A review of the whole cell proteomic analysis of Jarid2 null vs. wild type mESCs demonstrated no difference in abundance of PRC2 proteins, with the exception of a modest increase in Eed observed in Jarid2 null mESCs (Aebp2; 16.3% increased abundance (p=0.39), Suz12-/-; 10.9% reduced abundance (p=0.55), Ezh2; 26.9% reduced abundance (p=0.77), Eed; 16.2% increased abundance (p=0.01)). This suggests that the reduced abundance seen following Afadin immunoprecipitation from mESCs lacking Jarid2 is not due to a reduced pool of PRC2 proteins in Jarid2 null mESCs extracts. This could suggest that PRC2 interacts with Afadin, and Jarid2 as essential to this interaction. In view of this, a speculative methylation search was undertaken from the wild type Afadin data, to look for a possible non-canonical PRC2 methylation targets, but no methylated Afadin peptides were identified in this search, however this search was not optimized in a similar way to the search for methylated β-catenin peptides outlined in Chapter four. Although acceptable peptide coverage was achieved (66.4% protein coverage overall), the majority of lysine residues were not in peptides detected by mass spectrometry in this experiment (69 of 115 lysine residues not detectable in this mass spectrometry experiment). As such the possibility remains that Afadin is a non-histone target of PRC2 mediated methylation, and this may act as a nuclear localization signal. Afadin Immunoprecipitates were interrogated with western blot analysis using anti-pan-methyl-lysine antibody, and low but detectable staining was observed in wild-

type mESCs (figure 5.5.d), with a possible slight reduction in staining observed in Jarid2 null mESCs (figure 5.5.d). However, a more robust mass spectrometry-based interrogation of Afadin and *in vitro* methylation assays should be undertaken to investigate the possibility of PRC2 mediated Afadin methylation further, and additional mechanisms (independent of methyltransferase activity) should be considered and explored.

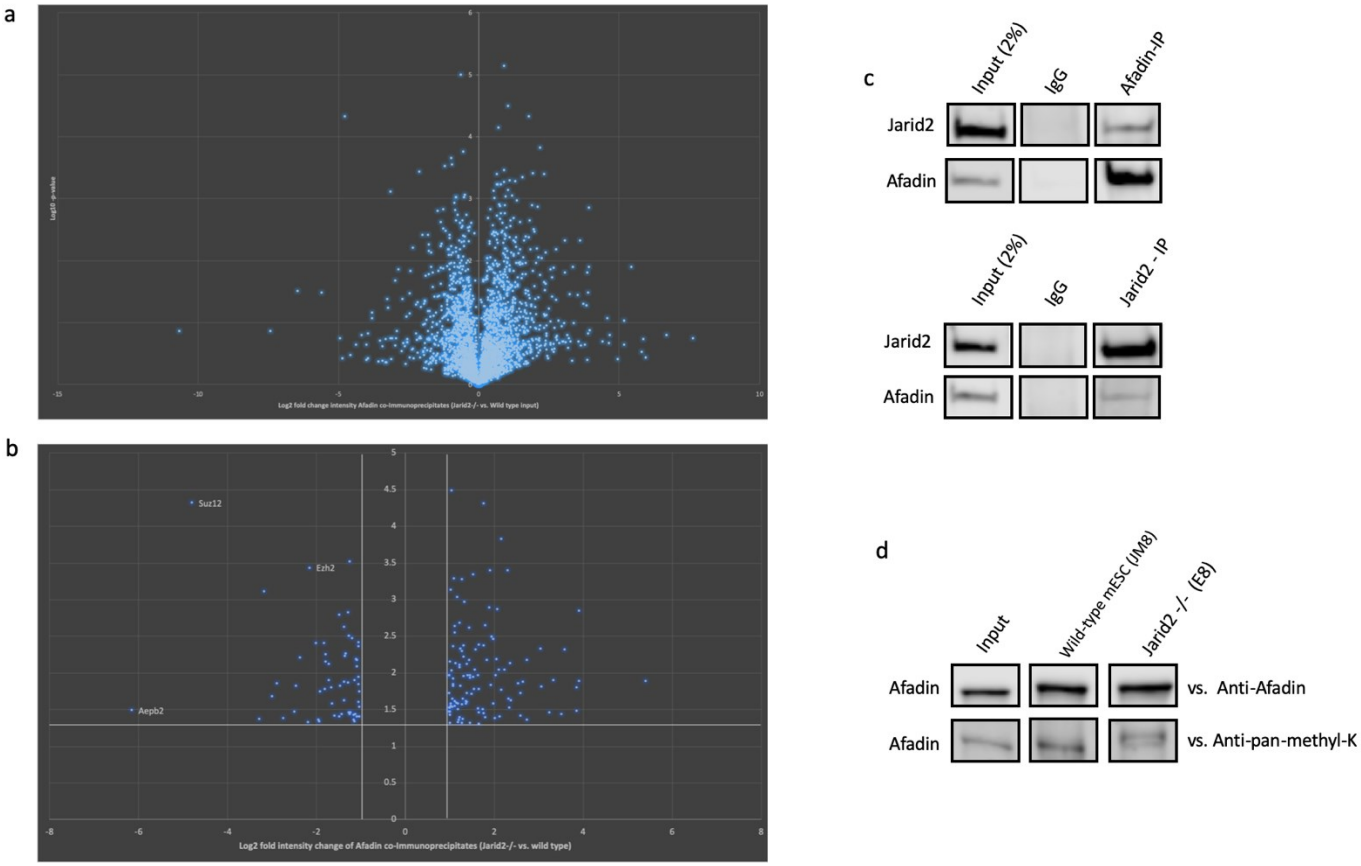

Figure 5.5. Comparison of co-Immunoprecipitates from Jarid2 null and wild-type input demonstrates reduced abundance of PRC 2.2 proteins

a. Volcano plot showing global Afadin Immunoprecipitates in Jarid2-/- mESCs relative to wild type
b. Volcano plot showing proteins co-immunoprecipitated with Afadin in Jarid2 mESCs relative to wild type, with cut off of >2-fold change in abundance and p-value <0.05. Vertical Grey lines represents 2-fold cut-off limit, horizontal grey line represents p-value <0.05 limit. Core PRC2 components highlighted, full list of proteins showing significantly reduced abundance in Afadin co-Immunoprecipitates from Jarid2-/- extracts relative to wild type are given in Table 5.4.
c. Western blot analysis of Afadin co-Immunoprecipitates (upper panels) show robust Afadin immunoprecipitation, and detectable Jarid2 staining. Conversely western blot analysis of Jarid2 co-Immunoprecipitates (lower panels) show robust Jarid2 immunoprecipitation, and weak but detectable Afadin staining.
d. Immunoprecipitation of Afadin (207 kDa), interrogated with anti-Afadin confirms successful immunoprecipitation from both Jarid2 null and wild type mESCs (upper panels). Interrogation of Immunoprecipitated Afadin with anti-pan-methyl-lysine antibody (lower panels) shows low but detectable staining.

5.5 Discussion and future perspectives

A developing facet of proteomics is the global assessment of sub-cellular protein localization, and the ability to track changes as a result of different cellular conditions (Orre et al. 2019). Using this approach, global proteomic analysis of nuclear and cytoplasmic compartment proteins has shown a relatively limited number of proteins with altered localization in the absence of Jarid2. However, I have identified a group of candidate proteins that can be investigated further. Strikingly, the core polycomb repressor complex 2 component Eed, shows a significant shift from the nuclear compartment to the cytosolic compartment in ESCs lacking Jarid2. Multiple studies have indicated that Jarid2 is a PRC2 interacting protein, with both co-immunoprecipitation (Landeira et al. 2010; Peng et al. 2009; Sanulli et al. 2015a; Shen et al. 2009), and crystallographic analysis (Kasinath et al. 2018) having shown a direct interaction between Jarid2 and Eed. Polycomb repressor complex-2 mediated H3K27me deposition patterns are altered in embryonic stem cells lacking Jarid2, however there are inconsistent reports about the extent and nature of this change. Significantly, the implication of these results is that Eed nuclear localization can to some extent be conditional on the presence of Jarid2. It has been reported that methylation of Jarid2 by PRC2 requires Eed, and this methylation event drives PRC2 catalytic activity. The suggestion that Jarid2 may be required for nuclear localization of Eed, but not other core PRC2 proteins is potentially significant, and warrants further investigation.

A further protein showing altered localization in the absence of Jarid2 is Afadin. In the absence of Jarid2, Afadin shown significant shift to the cytoplasmic compartment. Afadin is a dual residency protein, and has both cytoplasmic and nuclear functions. Cytoplasmic Afadin is a constituent of adherens junctions, and acts to the link calcium-independent cell surface

adhesion protein Nectin with the F-actin cytoskeleton. Afadin has recently been shown to interact with both E-cadherin and β-catenin at adherens junctions via αE-catenin (Sakakibara et al. 2020). An appealing prospect is that the reduced canonical Wnt signaling in mESCs lacking Jarid2, may in part result from elevated Afadin present at the adherens junction, that sequesters β-catenin, reducing the available pool to drive Wnt signaling. Further, the normalization of E-cadherin distribution observed in co-culture experiments, may alter Afadin-β-catenin binding dynamics, allowing for the rescue of canonical Wnt signaling, and sufficient canonical Wnt signaling to enable differentiation.

Previous studies in neurons have demonstrated that Afadin shuttles between the cytoplasm and the nucleus upon environmental cues, and nuclear Afadin accumulation occurs co-incident with post-translational histone modifications, specifically histone 3 phosphorylation (Sellers et al. 2018; VanLeeuwen et al. 2014). A further possibility raised by this study is that Afadin represents a Jarid2-dependent, non-histone target of PRC2, with methylation acting as a nuclear localization signal. This raises the possibility of cross-talk between PRC2-mediated histone methylation, and Afadin mediated histone phosphorylation at histone 3, coordinated by Jarid2. Further mass spectrometry-based searches of Afadin methylation searches of Afadin methylation will be required to explore this possibility and investigation of histone 3 phosphorylation profiles in the absence of Jarid2 may be informative.

6. General Discussion

Although the polycomb group proteins have well characterised roles in maintenance of gene repression, there is accumulating evidence of non-classical functions, including roles in gene activation and a broader methylation substrate specificity. There is also a body of evidence that highlights regulatory interplay between polycomb proteins and cell signalling cascades, particularly canonical Wnt signalling. Alongside these developments there has also been recent advances in our understanding of the non-classical roles of polycomb proteins in the control of differentiation and the development of cancer. Here I show that Wnt signalling is supressed in a panel of mESCs that lack core PRC2 components. Additionally, loss of Suz12 resulted in failure to differentiate, but I show this can be rescued by prior co-culture in the presence of normal E-cadherin interactions; differentiation of Suz12 null mESCs occurs concomitant with the partial restoration of Wnt signalling, and presumably in the absence of the H3K27me3 modification.

6.1. PRC2 and differentiation

The polycomb proteins are highly expressed in embryonic stem cells. While they are not essential for maintaining pluripotency in ESC cultures, and display normal self-renewal properties, PRC2 has been shown to be essential to differentiation. Mouse ESCs lacking core PRC2 components or Jarid2, fail to properly execute differentiation (Azuara et al. 2006; Aloia, Di Stefano, and Di Croce 2013; Pasini et al. 2007; Lee et al. 2006; Chamberlain, Yee, and Magnuson 2008; Landeira et al. 2010). Using mESCs lacking Suz12 as a model for PRC2 deficiency, shown again herein to have no detectable H3K27me3 modification (Hojfeldt et al.

2018; Oksuz et al. 2018), I examined the link between impaired β-catenin activity and differentiation block. A previous study had shown that these cells fail to differentiate upon treatment with an ATRA driven neuronal differentiation protocol. Pasini et al reported that mESCs lacking Suz12 showed an inability to down-regulate pluripotency markers Oct4 and Nanog, with 50-fold greater expression of pluripotency genes in Suz12-/- mESCs as compared to wild-type ESCs at day nine of differentiation. These cells also failed to express neuronal lineage markers including Nestin and Pax7 (Pasini et al. 2007). This study indicated that polycomb proteins were recruited to both activated and repressed genes upon ATRA treatment. PRC2 recruitment to repressed genes during differentiation was disturbed in the absence of Suz12, and this recruitment failure was suggested to contribute to the failure to differentiate. However, in my experiments using the same Suz12 null mESCs, I observed efficient repression of pluripotency genes Sox2 and Oct4. This discrepancy is likely to be due to the different differentiation protocols, however both studies indicate that shut-down of pluripotency gene expression may be reduced in the absence of PRC2 mediated histone H3K27me3. In keeping with the previous report, neuronal lineage markers were not induced at the mRNA and protein levels after monolayer neuronal differentiation. This is intriguing and suggests that the failure of PRC2-deficient ESCs to differentiate is the result of a failure to turn on new gene expression programs rather than turn off pluripotency genes. In keeping with this idea a study pending peer review has been recently published on bioRxiv, has shown that canonical PRC2 H3K27me3 deposition is not required for early development or differentiation (Miller, Damle, and Kingston 2020). The authors report that either treatment with the specific EZH2 methyltransferase inhibitor GSK343 titrated to ablate H3K27me3, or Crispr/Cas9 mediated mutation of the EZH2 SET domain leading to the R681C substitution, which results in failure of the H3K27me2 to H3K27me3 methylation step, does not prevent

early differentiation. Drug treated wild-type and EZH2 R681C mutant mESCs were capable of forming embryoid bodies, and differentiation in beating cardiac myocytes was observed in both conditions. Notably, H3K27me3 levels were persistently low during the differentiation protocol although some, presumably EZH1 mediated H3K27me3 was observed, this was significantly lower than observed in matched controls. Importantly, when EZH2 R681C mutant mESCs were differentiated for eight days, then challenged with monolayer ES feeder conditions they reverted to an ES phenotype with robust alkaline phosphatase activity, and the ability to form embryoid bodies. A similar result was observed after withdrawal of GSK343. This highlights the possibility that PRC2 mediated H3K27me3 might not be essential for early differentiation, but is instead required for maintenance of a stable differentiated state. These studies will require further corroboration, but the implication that PRC2's role in differentiation is for inducing gene activity as opposed to maintaining gene repression is clearly of interest.

Intriguingly my studies have convincingly shown that differentiation can be rescued in Suz12 null mESCs, following co-culture with wild-type mESCs, but only in the presence of normal E-cadherin expression. This suggests that differentiation can occur in the absence of H3K27me3, and highlights the importance of a non-classical role of PRC2 in differentiation.

6.2. PRC2 and Wnt signalling

Several lines of evidence suggest an interplay between PRC2 and canonical Wnt signalling, both in development and in malignancy. The cancer genome atlas reveals a positive correlation between EZH2 expression and β-catenin levels. Overexpression of EZH2 in cancer cell lines potentiated expression of Wnt targets, whereas knockdown of EZH2, or drug

inhibition of EZH2 methyltransferase activity results in attenuated expression of Wnt signalling targets (Wen et al. 2017; Hosogane et al. 2016). Additionally, several reports highlight a direct interaction between EZH2 and β-catenin, with forming a transcriptional activation complex with either oestrogen receptor α (Shi et al. 2007), or PAF (Jung et al. 2013), or by direct non-histone methylation of β-catenin at the K49 residue (Hoffmeyer et al. 2017; Zhu et al. 2016). Conversely, a recent report has highlighted increased EZH2 stability as a result of canonical Wnt driven expression of ubiquitin carboxyl-terminal hydrolase-1 (USP1), which suppresses ubiquitin-proteasomal degradation of EZH2 in glioma cells (Ma et al. 2019). This further highlights a complex interplay between PRC2 and β-catenin.

Our group has previously shown that Jarid2 null mESCs demonstrate low canonical Wnt signalling, and that these mESCs also display uniformly elevated Nanog expression indicative of a naïve pluripotent state (Landeira et al. 2015). The mass spectrometry analysis reported here shows a reduced total β-catenin abundance in mESCs lacking Jarid2, compared to wild type mESCs. This observation is consistent with previous data, showing reduced β-catenin activity, and suggests a possible reduced pool of β-catenin available for Wnt signalling in Jarid2 null mESCs. I also show that reduced canonical Wnt signalling is not unique to mESCs lacking the PRC2.2 component Jarid2, but is seen to a variable extent in mESCs lacking different core PRC2 components. I show that EZH2 methyltransferase inhibition also reduces canonical Wnt signalling activity as assessed by TopFlash in wild type mESCs. Notably, mESCs lacking Suz12 had reduced Wnt signalling at levels comparable to those seen in Jarid2-null mESCs. An important finding reported here is that canonical Wnt signalling was partially rescued after 72 hours of co-culture with wild-type mESCs, but only in the context of normal E-cadherin expression. Interrogation of E-cadherin in mESCs lacking Jarid2, shows aberrant patchy localisation, as opposed to the reticular pattern of staining at cell surfaces seen in

wild-type mESCs. Again, this is not unique to mESCs lacking Jarid2, but was also observed in mESCs lacking Suz12 or Eed. Our group has previously shown normalisation of E-cadherin contacts at the wild-type: mutant mESC interfaces (Landeira et al. 2015), and normalisation of cell-surface E-cadherin upon co-culture is potentially important to rescue of Wnt signalling, as β-catenin is a known interacting partner of cytosolic E-cadherin at adherens junctions. Cadherin bound β-catenin was classically thought to represent a separate pool from cytoplasmic β-catenin, which does not participate in Wnt signalling (Gottardi and Gumbiner 2004). However, it has subsequently been shown that cadherin bound β-cadherin is internalised upon dissociation of adherens junction, and will translocate to the nucleus to drive Wnt target gene expression, and it has been proposed that this may even occur in the absence of Wnt ligands (Kam and Quaranta 2009; Howard et al. 2011). Cadherin bound β-catenin has been shown to dissociate upon epithelial-mesenchymal transition (EMT), and accumulates within the cytoplasm, and contributes to canonical Wnt signalling. Importantly, E-cadherin was shown to be critical for cytoplasmic accumulation of β-catenin, and knockdown of E-cadherin by RNA interference results in loss of Wnt signalling in response to Wnt ligands (Howard et al. 2011). The authors report that despite loss of E-cadherin, β-catenin remains localised at the cell membrane, and they suggest this is due to endogenous Cadherin-6 expression, but upon induction of EMT, they observed failure of β-catenin accumulation within the cytoplasm, which they attributed to loss of E-cadherin internalisation. Here I show that E-cadherin expression and localisation is anomalous in mESCs lacking PRC2. Co-culture experiments show that partial rescue of Wnt signalling, and normalisation of E-cadherin patterning occurs in Jarid2-null ES cells at cell interface with wild-type cells.

The role of β-catenin in ES cells is complex, and context dependent (Watanabe and Dai 2011). Evidence that β-catenin supports self-renewal in mESCs include several Wnt ligands have been reported to maintain an undifferentiated state in ES cells (Singla et al. 2006; Hao et al. 2006), and depletion or chemical inhibition of GSK3B of the β-catenin destruction complex promotes self-renewal in mESCs (Doble et al. 2007; Sato et al. 2004). Subsequent studies in contrast have shown that β-catenin is dispensable for mESC formation, as several groups have generated β-catenin null mESC lines (Wray et al. 2011; Lyashenko et al. 2011; Soncin et al. 2009). Furthermore nuclear β-catenin has been shown to be required for differentiation both *in vitro* (Atlasi et al. 2013; Lyashenko et al. 2011) and *in vivo* (Huelsken et al. 2000). These opposing results have been suggested to be reconciled, as β-catenin has been shown to support self-renewal in naïve state pluripotency, and is required to prevent transition to primed pluripotency, but will drive differentiation in the primed pluripotent state (ten Berge et al. 2011; Xu et al. 2016). This model supports context-dependent consequences of canonical Wnt signalling, depending on the pluripotency landscape. However, in this study I show that mESCs lacking Jarid2 have suppressed Wnt signalling, but remain in a naïve state, something that is not in keeping with the prevailing argument that active β-catenin prevents a transition to primed pluripotency. Indeed, rescue of Wnt signalling in Jarid2 and Suz12 null mESCs through co-culture occurs coincident with the partial restoration of competency of differentiation (Landeira et al. 2015). Importantly nuclear β-catenin has been primarily implicated in mesodermal lineage commitment (Atlasi et al. 2013; Lindsley et al. 2006; Zhang et al. 2017; Bakre et al. 2007; Davidson et al. 2012). Here we show that rescue of Wnt signalling occurs concomitant to neuronal lineage commitment, with the expression of early neuronal markers readily detectable in the co-culture experiments. Intriguingly, mESCs expressing a β-catenin variant which ablates Tcf/Lef nuclear signalling and expression of

downstream Wnt targets, can rescue neuroectodermal lineage differentiation (Lyashenko et al. 2011). As a result it has been suggested that cell surface cadherin bound β-catenin may have a critical role in neuronal differentiation (Watanabe and Dai 2011). In keeping with this observation, abrogation of E-cadherin contacts in mESCs results in LIF independent self-renewal, and restoration of the β-catenin-E-Cadherin complex is essential to rescue of differentiation as re-expression of E-cadherin lacking the β-catenin binding domain in E-cadherin-/- mESCs failed to reverse the LIF independent self-renewal phenotype (Soncin et al. 2009). Taken together with results presented in this study a model whereby normalisation of E-cadherin in restoration of normal adherens junction processing, allowing cell surface β-catenin to contribute to in neuroectodermal lineage commitment (Figure 6.1).

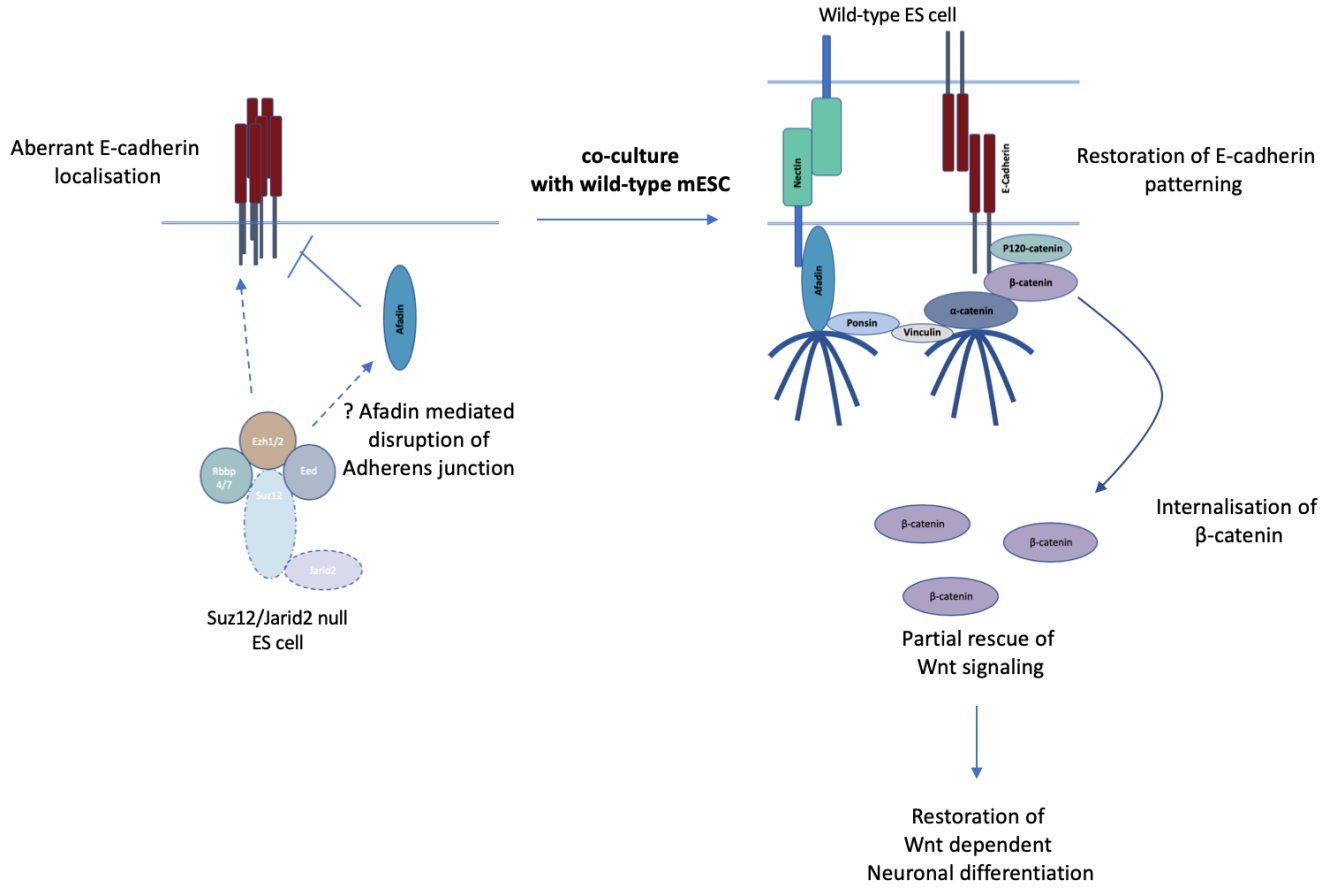

Figure 6.1. Proposed model for mechanism of restoration of Wnt signalling and neuronal differentiation in Suz12 or Jarid2 deficient mESCs following co-culture with wild-type counterparts

Schematic model outlining proposed mechanism of restoration of E-cadherin patterning through 'education' by interacting wild-type partner upon co-culturing, resulting in normalisation of adherens junction processing, internalisation of β-catenin resulting in partial rescue of Wnt signalling, with subsequent restoration of early neuronal differentiation upon monolayer neuronal differentiation challenge.

Two previous reports have highlighted β-catenin non-histone methylation substrate of Ezh2, with trimethylation reported at the lysine 49 residue (Hoffmeyer et al. 2017; Zhu et al. 2016). This has been reported to stabilise β-catenin, via impaired ubiquitination and to potentiate canonical Wnt signalling. In keeping with this report, the lysine demethylase Kdm2a/b was shown to regulate nuclear β-catenin stability (Lu et al. 2015). This is an attractive theory, as it

potentially elucidates the interplay between PRC2 and canonical Wnt signalling. Additionally, it is potentially important to cancer, as it may shed light on the observed relationship between EZH2 overexpression and Wnt signalling in malignancy, and it may represent a target for intervention in cancer. It would also would explain the reduced activity and abundance of β-catenin in mESCs lacking PRC2 as K49 methylation is proposed to stabilise β-catenin by reduced ubiquitination (Lu et al. 2015), and would explain the observed repression of Wnt signalling observed in the presence of Ezh2 drug inhibition. This mechanism however does not directly address the E-cadherin dependent rescue of canonical Wnt signalling observed in the co-culture experiments. The reports of β-catenin methylation by Ezh2 are based on immunoblotting and *in vitro* methylation assays, with one group stating they were unable to identify this modification using mass spectrometry, which was attributed to reduced trypsin digest efficiency at methylated lysine residues (Hoffmeyer et al. 2017). Against the background of this expectation, it was clear that despite substantial efforts (including alternate lysates, antibodies, digests, the presence of lysine demethylase inhibitor and two separate algorithmic searches) mass spectrometry experiments were not been able to confirm K49 methylated β-catenin in either crude extracts or immunoenriched β-catenin. The reason for this discrepancy is unclear, however the approach taken was thorough, and achieved excellent peptide coverage of the lysine 49 residue, using both the trypsin/GluC and AspN digests. Importantly, a different SMYD2 mediated K133 methylation event was however detected using this approach. This both suggests that the methodology applied was robust and may provide an explanation of the K49 methylation results reported by others.

Although not the main focus of this study, the confirmation of *in vivo* K133 methylation of β-catenin is important, and to my understanding the first report of this post-translational

modification in native β-catenin by mass spectrometry, as previous reports relied on immunoblotting, and mass spectrometry of *in vitro* methylated β-catenin (Deng et al. 2017). Methylation of β-catenin at K133 was reported to be an important nuclear localisation signal, required for efficient nuclear translocation and expression of Wnt targets in colorectal cancer cell lines, and was identified in liver cancer stem cells in this study. This modification has to my understanding not been reported in ES cells, and may have an as yet unappreciated role in stem cell function and pluripotency, and warrants further study.

6.3. Adherens junctions and PRC2

Intriguingly, several independent lines of evidence within this study highlight the adherens junction as a nexus of PRC2 mediated regulation. Adherens junctions are key cell-cell adhesion complexes, essential to cell polarity, cell migration, and development (Harris and Tepass 2010). They are composed of Cadherin and Nectin transmembrane proteins which homodimerize, and multiple cytosolic components, including α-catenin, β-catenin, P120-catenin and Afadin (Figure 1.6). Notably, unbiased mass spectrometry analysis identifies altered subcellular localisation of Afadin and reduced abundance of β-catenin. Additionally, E-cadherin, the core cadherin component of adherens junction in mESCs, has been shown to have aberrant localisation in mESCs lacking core PRC2 components or Jarid2. Strikingly, perturbation of PRC2 by loss of Suz12, or loss of Jarid2 results in mESCs with altered cell morphology, which form multiple ICMs on blastocyst injection. This suggests that PRC2 has a role in co-ordinating cell surface signals, and interruption of this allows novel cell behaviours, such as formation of independent ICMs. Adherens junctions have a well-documented role in regulating cell-cell interactions, and regulating cell migration (Etienne-Manneville 2012).

Additionally, Afadin has also been implicated in invasive behaviours in malignancy with both possible tumour suppressor function reported in pancreatic cancer (Xu, Chang, et al. 2015), and oncogene function reported in breast cancer (Tabariès et al. 2019). Specifically, loss of nuclear Afadin in pancreatic cancer cells results in enhanced expression of Snail, which cell proliferation and metastatic behaviour, and correlates with adverse clinical outcomes (Xu, Chang, et al. 2015). However, expression of Afadin in conjunction with claudin-2 has been shown to augment liver metastasis in mouse models of breast cancer. Additionally, elevated levels of Claudin2/Afadin expression in breast cancer primaries predict liver metastases, and are associated with adverse prognosis (Tabariès et al. 2019).

It is intriguing, that PRC2 seemingly functions to regulate adherens junction activity in some way. Importantly, this study highlights a potential direct interaction between PRC2 and Afadin, ostensibly mediated by Jarid2. Co-immunoprecipitation studies identify Afadin as an interacting partner of PRC2, and this interaction is ablated in the absence of Jarid2. Furthermore, altered localisation of Afadin is convincingly shown in mESCs lacking Jarid2. In addition to its role as part of the adherens junction, Afadin has an as yet poorly defined role within the nucleus. Post translational modification of Afadin has been reported to act as a nuclear localisation signal, specifically Akt mediate phosphorylation of serine residue 1718 (S1718phos) has been shown in breast cancer cells (Elloul et al. 2014). A further study has demonstrated insulin acts to phosphorylate Afadin at Serine 1795 (S1795Phos), resulting in an interaction with Histone deacetylase-6 (HDAC6) in adipocytes (Lundh et al. 2019). Furthermore, Afadin has been reported to localise to the nucleus in neurones in response to either 17β-oestradiol or N-methyl-D-aspartate (NMDA) receptor activation, and results in histone phosphorylation of Histone3 at the serine 10 residue (H3S10p), a histone modification associated with open chromatin and active transcription (VanLeeuwen et al.

2014; Sellers et al. 2018). Importantly, PRC2 in conjunction with Jarid2 may have a role in targeting Afadin to the nucleus, and loss of PRC2 or Jarid2 results in predominantly cytoplasmic Afadin. This may highlight an important non-classical role of PRC2 in co-ordinating nuclear localisation of a protein associated with antagonistic histone modifications to classical PRC2 activity.

References

'AACR Project GENIE: Powering Precision Medicine through an International Consortium'. 2017. *Cancer Discov*, 7: 818-31.

Aden, D. P., A. Fogel, S. Plotkin, I. Damjanov, and B. B. Knowles. 1979. 'Controlled synthesis of HBsAg in a differentiated human liver carcinoma-derived cell line', *Nature*, 282: 615-6.

Al-Raawi, D., R. Jones, S. Wijesinghe, J. Halsall, M. Petric, S. Roberts, N. A. Hotchin, and A. Kanhere. 2019. 'A novel form of JARID2 is required for differentiation in lineage-committed cells', *EMBO J*, 38.

Albert, M., and K. Helin. 2010. 'Histone methyltransferases in cancer', *Semin Cell Dev Biol*, 21: 209-20.

Almeida, M., G. Pintacuda, O. Masui, Y. Koseki, M. Gdula, A. Cerase, D. Brown, A. Mould, C. Innocent, M. Nakayama, L. Schermelleh, T. B. Nesterova, H. Koseki, and N. Brockdorff. 2017. 'PCGF3/5-PRC1 initiates Polycomb recruitment in X chromosome inactivation', *Science*, 356: 1081-84.

Almeida, Mafalda, Joseph S. Bowness, and Neil Brockdorff. 2020. 'The many faces of Polycomb regulation by RNA', *Current opinion in genetics & development*, 61: 53-61.

Aloia, L., B. Di Stefano, and L. Di Croce. 2013. 'Polycomb complexes in stem cells and embryonic development', *Development*, 140: 2525-34.

Anton, R., H. A. Kestler, and M. Kühl. 2007. 'Beta-catenin signaling contributes to stemness and regulates early differentiation in murine embryonic stem cells', *FEBS Lett*, 581: 5247-54.

Antonysamy, S., B. Condon, Z. Druzina, J. B. Bonanno, T. Gheyi, F. Zhang, I. MacEwan, A. Zhang, S. Ashok, L. Rodgers, M. Russell, and J. Gately Luz. 2013. 'Structural context of disease-associated mutations and putative mechanism of autoinhibition revealed by X-ray crystallographic analysis of the EZH2-SET domain', *PLoS One*, 8: e84147.

Ardehali, M. B., A. Anselmo, J. C. Cochrane, S. Kundu, R. I. Sadreyev, and R. E. Kingston. 2017. 'Polycomb Repressive Complex 2 Methylates Elongin A to Regulate Transcription', *Mol Cell*, 68: 872-84 e6.

Arnold, S. J., J. Stappert, A. Bauer, A. Kispert, B. G. Herrmann, and R. Kemler. 2000. 'Brachyury is a target gene of the Wnt/beta-catenin signaling pathway', *Mech Dev*, 91: 249-58.

Asara, J. M., H. R. Christofk, L. M. Freimark, and L. C. Cantley. 2008. 'A label-free quantification method by MS/MS TIC compared to SILAC and spectral counting in a proteomics screen', *Proteomics*, 8: 994-9.

Atlasi, Y., R. Noori, C. Gaspar, P. Franken, A. Sacchetti, H. Rafati, T. Mahmoudi, C. Decraene, G. A. Calin, B. J. Merrill, and R. Fodde. 2013. 'Wnt signaling regulates the lineage differentiation potential of mouse embryonic stem cells through Tcf3 down-regulation', *PLoS Genet*, 9: e1003424.

Aubert, Y., S. Egolf, and B. C. Capell. 2019. 'The Unexpected Noncatalytic Roles of Histone Modifiers in Development and Disease', *Trends Genet*, 35: 645-57.

Azuara, V., P. Perry, S. Sauer, M. Spivakov, H. F. Jorgensen, R. M. John, M. Gouti, M. Casanova, G. Warnes, M. Merkenschlager, and A. G. Fisher. 2006. 'Chromatin signatures of pluripotent cell lines', *Nat Cell Biol*, 8: 532-8.

Bachmann, I. M., O. J. Halvorsen, K. Collett, I. M. Stefansson, O. Straume, S. A. Haukaas, H. B. Salvesen, A. P. Otte, and L. A. Akslen. 2006. 'EZH2 expression is associated with high proliferation rate and aggressive tumor subgroups in cutaneous melanoma and cancers of the endometrium, prostate, and breast', *J Clin Oncol*, 24: 268-73.

Bakre, M. M., A. Hoi, J. C. Mong, Y. Y. Koh, K. Y. Wong, and L. W. Stanton. 2007. 'Generation of multipotential mesendodermal progenitors from mouse embryonic stem cells via sustained Wnt pathway activation', *J Biol Chem*, 282: 31703-12.

Baldi, S. 2019. 'Nucleosome positioning and spacing: from genome-wide maps to single arrays', *Essays Biochem*, 63: 5-14.

Baron, R., and M. Kneissel. 2013. 'WNT signaling in bone homeostasis and disease: from human mutations to treatments', *Nat Med*, 19: 179-92.

Bauer, M., J. Trupke, and L. Ringrose. 2016. 'The quest for mammalian Polycomb response elements: are we there yet?', *Chromosoma*, 125: 471-96.

Becker, J., and J. Wilting. 2019. 'WNT Signaling in Neuroblastoma', *Cancers (Basel)*, 11.

Béguelin, W., R. Popovic, M. Teater, Y. Jiang, K. L. Bunting, M. Rosen, H. Shen, S. N. Yang, L. Wang, T. Ezponda, E. Martinez-Garcia, H. Zhang, Y. Zheng, S. K. Verma, M. T. McCabe, H. M. Ott, G. S. Van Aller, R. G. Kruger, Y. Liu, C. F. McHugh, D. W. Scott, Y. R. Chung, N. Kelleher, R. Shaknovich, C. L. Creasy, R. D. Gascoyne, K. K. Wong, L. Cerchietti, R. L.

Levine, O. Abdel-Wahab, J. D. Licht, O. Elemento, and A. M. Melnick. 2013. 'EZH2 is required for germinal center formation and somatic EZH2 mutations promote lymphoid transformation', *Cancer Cell*, 23: 677-92.

Behjati, S., P. S. Tarpey, N. Presneau, S. Scheipl, N. Pillay, P. Van Loo, D. C. Wedge, S. L. Cooke, G. Gundem, H. Davies, S. Nik-Zainal, S. Martin, S. McLaren, V. Goodie, B. Robinson, A. Butler, J. W. Teague, D. Halai, B. Khatri, O. Myklebost, D. Baumhoer, G. Jundt, R. Hamoudi, R. Tirabosco, M. F. Amary, P. A. Futreal, M. R. Stratton, P. J. Campbell, and A. M. Flanagan. 2013. 'Distinct H3F3A and H3F3B driver mutations define chondroblastoma and giant cell tumor of bone', *Nat Genet*, 45: 1479-82.

Beltran, M., C. M. Yates, L. Skalska, M. Dawson, F. P. Reis, K. Viiri, C. L. Fisher, C. R. Sibley, B. M. Foster, T. Bartke, J. Ule, and R. G. Jenner. 2016. 'The interaction of PRC2 with RNA or chromatin is mutually antagonistic', *Genome Res*, 26: 896-907.

Berg, T., S. Thoene, D. Yap, T. Wee, N. Schoeler, P. Rosten, E. Lim, M. Bilenky, A. J. Mungall, T. Oellerich, S. Lee, C. K. Lai, P. Umlandt, A. Salmi, H. Chang, L. Yue, D. Lai, S. W. Cheng, R. D. Morin, M. Hirst, H. Serve, M. A. Marra, G. B. Morin, R. D. Gascoyne, S. A. Aparicio, and R. K. Humphries. 2014. 'A transgenic mouse model demonstrating the oncogenic role of mutations in the polycomb-group gene EZH2 in lymphomagenesis', *Blood*, 123: 3914-24.

Bernstein, B. E., T. S. Mikkelsen, X. Xie, M. Kamal, D. J. Huebert, J. Cuff, B. Fry, A. Meissner, M. Wernig, K. Plath, R. Jaenisch, A. Wagschal, R. Feil, S. L. Schreiber, and E. S. Lander. 2006. 'A bivalent chromatin structure marks key developmental genes in embryonic stem cells', *Cell*, 125: 315-26.

Biechele, S., K. Cockburn, F. Lanner, B. J. Cox, and J. Rossant. 2013. 'Porcn-dependent Wnt signaling is not required prior to mouse gastrulation', *Development*, 140: 2961-71.

Bird, A. 2002. 'DNA methylation patterns and epigenetic memory', *Genes Dev*, 16: 6-21.

Blackledge, N. P., A. M. Farcas, T. Kondo, H. W. King, J. F. McGouran, L. L. Hanssen, S. Ito, S. Cooper, K. Kondo, Y. Koseki, T. Ishikura, H. K. Long, T. W. Sheahan, N. Brockdorff, B. M. Kessler, H. Koseki, and R. J. Klose. 2014. 'Variant PRC1 complex-dependent H2A ubiquitylation drives PRC2 recruitment and polycomb domain formation', *Cell*, 157: 1445-59.

Blackledge, N. P., and R. Klose. 2011. 'CpG island chromatin: a platform for gene regulation', *Epigenetics*, 6: 147-52.

Blackledge, N. P., N. R. Rose, and R. J. Klose. 2015. 'Targeting Polycomb systems to regulate gene expression: modifications to a complex story', *Nat Rev Mol Cell Biol*, 16: 643-49.

Blanco, E., M. González-Ramírez, A. Alcaine-Colet, S. Aranda, and L. Di Croce. 2020. 'The Bivalent Genome: Characterization, Structure, and Regulation', *Trends Genet*, 36: 118-31.

Bödör, C., C. O'Riain, D. Wrench, J. Matthews, S. Iyengar, H. Tayyib, M. Calaminici, A. Clear, S. Iqbal, H. Quentmeier, H. G. Drexler, S. Montoto, A. T. Lister, J. G. Gribben, A. Matolcsy, and J. Fitzgibbon. 2011. 'EZH2 Y641 mutations in follicular lymphoma', *Leukemia*, 25: 726-9.

Böhm, J., J. K. Muenzner, A. Caliskan, B. Ndreshkjana, K. Erlenbach-Wünsch, S. Merkel, R. Croner, T. T. Rau, C. I. Geppert, A. Hartmann, A. V. Roehe, and R. Schneider-Stock. 2019. 'Loss of enhancer of zeste homologue 2 (EZH2) at tumor invasion front is correlated with higher aggressiveness in colorectal cancer cells', *J Cancer Res Clin Oncol*, 145: 2227-40.

Boyer, L. A., K. Plath, J. Zeitlinger, T. Brambrink, L. A. Medeiros, T. I. Lee, S. S. Levine, M. Wernig, A. Tajonar, M. K. Ray, G. W. Bell, A. P. Otte, M. Vidal, D. K. Gifford, R. A. Young, and R. Jaenisch. 2006. 'Polycomb complexes repress developmental regulators in murine embryonic stem cells', *Nature*, 441: 349-53.

Bracken, A. P., G. L. Brien, and C. P. Verrijzer. 2019. 'Dangerous liaisons: interplay between SWI/SNF, NuRD, and Polycomb in chromatin regulation and cancer', *Genes Dev*, 33: 936-59.

Bracken, A. P., D. Pasini, M. Capra, E. Prosperini, E. Colli, and K. Helin. 2003. 'EZH2 is downstream of the pRB-E2F pathway, essential for proliferation and amplified in cancer', *EMBO J*, 22: 5323-35.

Brockdorff, N. 2017. 'Polycomb complexes in X chromosome inactivation', *Philos Trans R Soc Lond B Biol Sci*, 372.

Brosch, M., L. Yu, T. Hubbard, and J. Choudhary. 2009. 'Accurate and sensitive peptide identification with Mascot Percolator', *J Proteome Res*, 8: 3176-81.

Burmeister, T. 2016. 'EZH2: a pleiotropic protein', *Blood*, 128: 888-9.

Caglio, G., E. Torlai Triglia, and A. Pombo. 2017. 'Keep Them Close: PRC2 Poises Enhancer-Promoter Interactions at Anterior Neuronal Genes', *Cell Stem Cell*, 20: 573-75.

Campbell, H. K., J. L. Maiers, and K. A. DeMali. 2017. 'Interplay between tight junctions & adherens junctions', *Exp Cell Res*, 358: 39-44.

Canel, M., A. Serrels, M. C. Frame, and V. G. Brunton. 2013. 'E-cadherin-integrin crosstalk in cancer invasion and metastasis', *J Cell Sci*, 126: 393-401.

Cao, Q., J. Yu, S. M. Dhanasekaran, J. H. Kim, R. S. Mani, S. A. Tomlins, R. Mehra, B. Laxman, X. Cao, J. Yu, C. G. Kleer, S. Varambally, and A. M. Chinnaiyan. 2008. 'Repression of E-cadherin by the polycomb group protein EZH2 in cancer', *Oncogene*, 27: 7274-84.

Cao, R., L. Wang, H. Wang, L. Xia, H. Erdjument-Bromage, P. Tempst, R. S. Jones, and Y. Zhang. 2002. 'Role of histone H3 lysine 27 methylation in Polycomb-group silencing', *Science*, 298: 1039-43.

Celik, H., W. K. Koh, A. C. Kramer, E. L. Ostrander, C. Mallaney, D. A. C. Fisher, J. Xiang, W. C. Wilson, A. Martens, A. Kothari, G. Fishberger, E. Tycksen, D. Karpova, E. J. Duncavage, Y. Lee, S. T. Oh, and G. A. Challen. 2018. 'JARID2 Functions as a Tumor Suppressor in Myeloid Neoplasms by Repressing Self-Renewal in Hematopoietic Progenitor Cells', *Cancer Cell*, 34: 741-56.e8.

Chamberlain, S. J., D. Yee, and T. Magnuson. 2008. 'Polycomb repressive complex 2 is dispensable for maintenance of embryonic stem cell pluripotency', *Stem Cells*, 26: 1496-505.

Chambers, I., J. Silva, D. Colby, J. Nichols, B. Nijmeijer, M. Robertson, J. Vrana, K. Jones, L. Grotewold, and A. Smith. 2007. 'Nanog safeguards pluripotency and mediates germline development', *Nature*, 450: 1230-4.

Chan, H. L., and L. Morey. 2019. 'Emerging Roles for Polycomb-Group Proteins in Stem Cells and Cancer', *Trends Biochem Sci*, 44: 688-700.

Chen, S., L. Jiao, M. Shubbar, X. Yang, and X. Liu. 2018. 'Unique Structural Platforms of Suz12 Dictate Distinct Classes of PRC2 for Chromatin Binding', *Mol Cell*, 69: 840-52.e5.

Chen, Z., P. Yang, W. Li, F. He, J. Wei, T. Zhang, J. Zhong, H. Chen, and J. Cao. 2018. 'Expression of EZH2 is associated with poor outcome in colorectal cancer', *Oncol Lett*, 15: 2953-61.

Chittock, E. C., S. Latwiel, T. C. Miller, and C. W. Müller. 2017. 'Molecular architecture of polycomb repressive complexes', *Biochem Soc Trans*, 45: 193-205.

Clevers, H. 2013. 'The intestinal crypt, a prototype stem cell compartment', *Cell*, 154: 274-84.

Clevers, H., and R. Nusse. 2012. 'Wnt/β-catenin signaling and disease', *Cell*, 149: 1192-205.

Comet, I., and K. Helin. 2014. 'Revolution in the Polycomb hierarchy', *Nat Struct Mol Biol*, 21: 573-5.

Comet, I., E. M. Riising, B. Leblanc, and K. Helin. 2016. 'Maintaining cell identity: PRC2-mediated regulation of transcription and cancer', *Nat Rev Cancer*, 16: 803-10.

Cooper, S., M. Dienstbier, R. Hassan, L. Schermelleh, J. Sharif, N. P. Blackledge, V. De Marco, S. Elderkin, H. Koseki, R. Klose, A. Heger, and N. Brockdorff. 2014. 'Targeting polycomb to pericentric heterochromatin in embryonic stem cells reveals a role for H2AK119u1 in PRC2 recruitment', *Cell Rep*, 7: 1456-70.

Cooper, S., A. Grijzenhout, E. Underwood, K. Ancelin, T. Zhang, T. B. Nesterova, B. Anil-Kirmizitas, A. Bassett, S. M. Kooistra, K. Agger, K. Helin, E. Heard, and N. Brockdorff. 2016. 'Jarid2 binds mono-ubiquitylated H2A lysine 119 to mediate crosstalk between Polycomb complexes PRC1 and PRC2', *Nat Commun*, 7: 13661.

Corces, M. R., and V. G. Corces. 2016. 'The three-dimensional cancer genome', *Curr Opin Genet Dev*, 36: 1-7.

Cox, J., M. Y. Hein, C. A. Luber, I. Paron, N. Nagaraj, and M. Mann. 2014. 'Accurate proteome-wide label-free quantification by delayed normalization and maximal peptide ratio extraction, termed MaxLFQ', *Mol Cell Proteomics*, 13: 2513-26.

Cox, J., and M. Mann. 2008. 'MaxQuant enables high peptide identification rates, individualized p.p.b.-range mass accuracies and proteome-wide protein quantification', *Nat Biotechnol*, 26: 1367-72.

Cui, K., C. Zang, T. Y. Roh, D. E. Schones, R. W. Childs, W. Peng, and K. Zhao. 2009. 'Chromatin signatures in multipotent human hematopoietic stem cells indicate the fate of bivalent genes during differentiation', *Cell Stem Cell*, 4: 80-93.

Dasgupta, M., J. K. Dermawan, B. Willard, and G. R. Stark. 2015. 'STAT3-driven transcription depends upon the dimethylation of K49 by EZH2', *Proc Natl Acad Sci U S A*, 112: 3985-90.

Davidovich, C., L. Zheng, K. J. Goodrich, and T. R. Cech. 2013. 'Promiscuous RNA binding by Polycomb repressive complex 2', *Nat Struct Mol Biol*, 20: 1250-7.

Davidson, J. S., I. M. Baumgarten, and E. H. Harley. 1986. 'Reversible inhibition of intercellular junctional communication by glycyrrhetinic acid', *Biochem Biophys Res Commun*, 134: 29-36.

Davidson, K. C., A. M. Adams, J. M. Goodson, C. E. McDonald, J. C. Potter, J. D. Berndt, T. L. Biechele, R. J. Taylor, and R. T. Moon. 2012. 'Wnt/β-catenin signaling promotes differentiation, not self-renewal, of human embryonic stem cells and is repressed by Oct4', *Proc Natl Acad Sci U S A*, 109: 4485-90.

Davidson, K. C., E. A. Mason, and M. F. Pera. 2015. 'The pluripotent state in mouse and human', *Development*, 142: 3090-9.

de Jaime-Soguero, A., W. A. Abreu de Oliveira, and F. Lluis. 2018. 'The Pleiotropic Effects of the Canonical Wnt Pathway in Early Development and Pluripotency', *Genes (Basel)*, 9.

de Napoles, M., J. E. Mermoud, R. Wakao, Y. A. Tang, M. Endoh, R. Appanah, T. B. Nesterova, J. Silva, A. P. Otte, M. Vidal, H. Koseki, and N. Brockdorff. 2004. 'Polycomb group proteins Ring1A/B link ubiquitylation of histone H2A to heritable gene silencing and X inactivation', *Dev Cell*, 7: 663-76.

De Raedt, T., E. Beert, E. Pasmant, A. Luscan, H. Brems, N. Ortonne, K. Helin, J. L. Hornick, V. Mautner, H. Kehrer-Sawatzki, W. Clapp, J. Bradner, M. Vidaud, M. Upadhyaya, E. Legius, and K. Cichowski. 2014. 'PRC2 loss amplifies Ras-driven transcription and confers sensitivity to BRD4-based therapies', *Nature*, 514: 247-51.

Deaton, A. M., and A. Bird. 2011. 'CpG islands and the regulation of transcription', *Genes Dev*, 25: 1010-22.

Delachat, A. M., N. Guidotti, A. L. Bachmann, A. C. A. Meireles-Filho, H. Pick, C. C. Lechner, C. Deluz, B. Deplancke, D. M. Suter, and B. Fierz. 2018. 'Engineered Multivalent Sensors to Detect Coexisting Histone Modifications in Living Stem Cells', *Cell Chem Biol*, 25: 51-56 e6.

Deng, X., R. Hamamoto, T. Vougiouklakis, R. Wang, Y. Yoshioka, T. Suzuki, N. Dohmae, Y. Matsuo, J. H. Park, and Y. Nakamura. 2017. 'Critical roles of SMYD2-mediated β-catenin methylation for nuclear translocation and activation of Wnt signaling', *Oncotarget*, 8: 55837-47.

Denholtz, M., G. Bonora, C. Chronis, E. Splinter, W. de Laat, J. Ernst, M. Pellegrini, and K. Plath. 2013. 'Long-range chromatin contacts in embryonic stem cells reveal a role for pluripotency factors and polycomb proteins in genome organization', *Cell Stem Cell*, 13: 602-16.

Denissov, S., H. Hofemeister, H. Marks, A. Kranz, G. Ciotta, S. Singh, K. Anastassiadis, H. G. Stunnenberg, and A. F. Stewart. 2014. 'Mll2 is required for H3K4 trimethylation on

bivalent promoters in embryonic stem cells, whereas Mll1 is redundant', *Development*, 141: 526-37.

Doble, B. W., S. Patel, G. A. Wood, L. K. Kockeritz, and J. R. Woodgett. 2007. 'Functional redundancy of GSK-3alpha and GSK-3beta in Wnt/beta-catenin signaling shown by using an allelic series of embryonic stem cell lines', *Dev Cell*, 12: 957-71.

Dorfman, David M., and Xuejun Tian. 2016. 'New insights into the mechanisms of EZH2's promotion of oncogenesis', *Translational Cancer Research*: S1057-S60.

Dowen, J. M., Z. P. Fan, D. Hnisz, G. Ren, B. J. Abraham, L. N. Zhang, A. S. Weintraub, J. Schujiers, T. I. Lee, K. Zhao, and R. A. Young. 2014. 'Control of cell identity genes occurs in insulated neighborhoods in mammalian chromosomes', *Cell*, 159: 374-87.

Dull, T., R. Zufferey, M. Kelly, R. J. Mandel, M. Nguyen, D. Trono, and L. Naldini. 1998. 'A third-generation lentivirus vector with a conditional packaging system', *J Virol*, 72: 8463-71.

Ehrlich, M. 2002. 'DNA methylation in cancer: too much, but also too little', *Oncogene*, 21: 5400-13.

Elias, J. E., and S. P. Gygi. 2007. 'Target-decoy search strategy for increased confidence in large-scale protein identifications by mass spectrometry', *Nat Methods*, 4: 207-14.

Elloul, S., D. Kedrin, N. W. Knoblauch, A. H. Beck, and A. Toker. 2014. 'The adherens junction protein afadin is an AKT substrate that regulates breast cancer cell migration', *Mol Cancer Res*, 12: 464-76.

Etienne-Manneville, S. 2012. 'Adherens junctions during cell migration', *Subcell Biochem*, 60: 225-49.

Evans, M. J., and M. H. Kaufman. 1981. 'Establishment in culture of pluripotential cells from mouse embryos', *Nature*, 292: 154-6.

Farcas, A. M., N. P. Blackledge, I. Sudbery, H. K. Long, J. F. McGouran, N. R. Rose, S. Lee, D. Sims, A. Cerase, T. W. Sheahan, H. Koseki, N. Brockdorff, C. P. Ponting, B. M. Kessler, and R. J. Klose. 2012. 'KDM2B links the Polycomb Repressive Complex 1 (PRC1) to recognition of CpG islands', *Elife*, 1: e00205.

Faust, C., A. Schumacher, B. Holdener, and T. Magnuson. 1995. 'The eed mutation disrupts anterior mesoderm production in mice', *Development*, 121: 273-85.

Filali, M., N. Cheng, D. Abbott, V. Leontiev, and J. F. Engelhardt. 2002. 'Wnt-3A/beta-catenin signaling induces transcription from the LEF-1 promoter', *J Biol Chem*, 277: 33398-410.

Fisher, A. G., M. P. H. Stumpf, and M. Merkenschlager. 2017. 'Reconciling Epigenetic Memory and Transcriptional Responsiveness', *Cell Syst*, 4: 373-74.

Flavahan, W. A., E. Gaskell, and B. E. Bernstein. 2017. 'Epigenetic plasticity and the hallmarks of cancer', *Science*, 357.

Fraichard, A., O. Chassande, G. Bilbaut, C. Dehay, P. Savatier, and J. Samarut. 1995. 'In vitro differentiation of embryonic stem cells into glial cells and functional neurons', *J Cell Sci*, 108 (Pt 10): 3181-8.

Fukuda, T., A. Tokunaga, R. Sakamoto, and N. Yoshida. 2011. 'Fbxl10/Kdm2b deficiency accelerates neural progenitor cell death and leads to exencephaly', *Mol Cell Neurosci*, 46: 614-24.

Gan, L., Y. Yang, Q. Li, Y. Feng, T. Liu, and W. Guo. 2018. 'Epigenetic regulation of cancer progression by EZH2: from biological insights to therapeutic potential', *Biomark Res*, 6: 10.

Gao, Z., J. Zhang, R. Bonasio, F. Strino, A. Sawai, F. Parisi, Y. Kluger, and D. Reinberg. 2012. 'PCGF homologs, CBX proteins, and RYBP define functionally distinct PRC1 family complexes', *Mol Cell*, 45: 344-56.

Gibcus, J. H., and J. Dekker. 2013. 'The hierarchy of the 3D genome', *Mol Cell*, 49: 773-82.

Gottardi, C. J., and B. M. Gumbiner. 2004. 'Distinct molecular forms of beta-catenin are targeted to adhesive or transcriptional complexes', *J Cell Biol*, 167: 339-49.

Green, D., A. E. Whitener, S. Mohanty, and A. C. Lekven. 2015. 'Vertebrate nervous system posteriorization: Grading the function of Wnt signaling', *Dev Dyn*, 244: 507-12.

Green, K. J., S. Getsios, S. Troyanovsky, and L. M. Godsel. 2010. 'Intercellular junction assembly, dynamics, and homeostasis', *Cold Spring Harb Perspect Biol*, 2: a000125.

Grijzenhout, A., J. Godwin, H. Koseki, M. R. Gdula, D. Szumska, J. F. McGouran, S. Bhattacharya, B. M. Kessler, N. Brockdorff, and S. Cooper. 2016. 'Functional analysis of AEBP2, a PRC2 Polycomb protein, reveals a Trithorax phenotype in embryonic development and in ESCs', *Development*, 143: 2716-23.

Gulati, N., W. Béguelin, and L. Giulino-Roth. 2018. 'Enhancer of zeste homolog 2 (EZH2) inhibitors', *Leuk Lymphoma*, 59: 1574-85.

Gunawan, M., N. Venkatesan, J. T. Loh, J. F. Wong, H. Berger, W. H. Neo, L. Y. Li, M. K. La Win, Y. H. Yau, T. Guo, P. C. See, S. Yamazaki, K. C. Chin, A. R. Gingras, S. G. Shochat, L. G. Ng, S. K. Sze, F. Ginhoux, and I. H. Su. 2015. 'The methyltransferase Ezh2 controls cell

adhesion and migration through direct methylation of the extranuclear regulatory protein talin', *Nat Immunol*, 16: 505-16.

Hansen, K. H., A. P. Bracken, D. Pasini, N. Dietrich, S. S. Gehani, A. Monrad, J. Rappsilber, M. Lerdrup, and K. Helin. 2008. 'A model for transmission of the H3K27me3 epigenetic mark', *Nat Cell Biol*, 10: 1291-300.

Hao, J., T. G. Li, X. Qi, D. F. Zhao, and G. Q. Zhao. 2006. 'WNT/beta-catenin pathway up-regulates Stat3 and converges on LIF to prevent differentiation of mouse embryonic stem cells', *Dev Biol*, 290: 81-91.

Harb, J., P. J. Lin, and J. Hao. 2019. 'Recent Development of Wnt Signaling Pathway Inhibitors for Cancer Therapeutics', *Curr Oncol Rep*, 21: 12.

Harris, T. J., and U. Tepass. 2010. 'Adherens junctions: from molecules to morphogenesis', *Nat Rev Mol Cell Biol*, 11: 502-14.

Hartsock, A., and W. J. Nelson. 2008. 'Adherens and tight junctions: structure, function and connections to the actin cytoskeleton', *Biochim Biophys Acta*, 1778: 660-9.

Hauri, S., F. Comoglio, M. Seimiya, M. Gerstung, T. Glatter, K. Hansen, R. Aebersold, R. Paro, M. Gstaiger, and C. Beisel. 2016. 'A High-Density Map for Navigating the Human Polycomb Complexome', *Cell Rep*, 17: 583-95.

He, A., X. Shen, Q. Ma, J. Cao, A. von Gise, P. Zhou, G. Wang, V. E. Marquez, S. H. Orkin, and W. T. Pu. 2012. 'PRC2 directly methylates GATA4 and represses its transcriptional activity', *Genes Dev*, 26: 37-42.

He, J., L. Shen, M. Wan, O. Taranova, H. Wu, and Y. Zhang. 2013. 'Kdm2b maintains murine embryonic stem cell status by recruiting PRC1 complex to CpG islands of developmental genes', *Nat Cell Biol*, 15: 373-84.

Herzog, V. A., A. Lempradl, J. Trupke, H. Okulski, C. Altmutter, F. Ruge, B. Boidol, S. Kubicek, G. Schmauss, K. Aumayr, M. Ruf, A. Pospisilik, A. Dimond, H. B. Senergin, M. L. Vargas, J. A. Simon, and L. Ringrose. 2014. 'A strand-specific switch in noncoding transcription switches the function of a Polycomb/Trithorax response element', *Nat Genet*, 46: 973-81.

Hoffmeyer, K., D. Junghans, B. Kanzler, and R. Kemler. 2017. 'Trimethylation and Acetylation of beta-Catenin at Lysine 49 Represent Key Elements in ESC Pluripotency', *Cell Rep*, 18: 2815-24.

Hojfeldt, J. W., A. Laugesen, B. M. Willumsen, H. Damhofer, L. Hedehus, A. Tvardovskiy, F. Mohammad, O. N. Jensen, and K. Helin. 2018. 'Accurate H3K27 methylation can be established de novo by SUZ12-directed PRC2', *Nat Struct Mol Biol*.

Holoch, D., and R. Margueron. 2017. 'Mechanisms Regulating PRC2 Recruitment and Enzymatic Activity', *Trends Biochem Sci*, 42: 531-42.

Hosogane, M., R. Funayama, M. Shirota, and K. Nakayama. 2016. 'Lack of Transcription Triggers H3K27me3 Accumulation in the Gene Body', *Cell Rep*, 16: 696-706.

Hotta, A., A. Y. Cheung, N. Farra, K. Vijayaragavan, C. A. Seguin, J. S. Draper, P. Pasceri, I. A. Maksakova, D. L. Mager, J. Rossant, M. Bhatia, and J. Ellis. 2009. 'Isolation of human iPS cells using EOS lentiviral vectors to select for pluripotency', *Nat Methods*, 6: 370-6.

Howard, S., T. Deroo, Y. Fujita, and N. Itasaki. 2011. 'A positive role of cadherin in Wnt/β-catenin signalling during epithelial-mesenchymal transition', *PLoS One*, 6: e23899.

Hoy, S. M. 2020. 'Tazemetostat: First Approval', *Drugs*, 80: 513-21.

Hu, D., A. S. Garruss, X. Gao, M. A. Morgan, M. Cook, E. R. Smith, and A. Shilatifard. 2013. 'The Mll2 branch of the COMPASS family regulates bivalent promoters in mouse embryonic stem cells', *Nat Struct Mol Biol*, 20: 1093-7.

Huang, R., X. Jin, Y. Gao, H. Yuan, F. Wang, and X. Cao. 2019. 'DZNep inhibits Hif-1α and Wnt signalling molecules to attenuate the proliferation and invasion of BGC-823 gastric cancer cells', *Oncol Lett*, 18: 4308-16.

Huang, S., Z. Wang, J. Zhou, J. Huang, L. Zhou, J. Luo, Y. Y. Wan, H. Long, and B. Zhu. 2019. 'EZH2 Inhibitor GSK126 Suppresses Antitumor Immunity by Driving Production of Myeloid-Derived Suppressor Cells', *Cancer Res*, 79: 2009-20.

Huang, Ting, Jingjing Wang, Weichuan Yu, and Zengyou He. 2012. 'Protein inference: a review', *Briefings in Bioinformatics*, 13: 586-614.

Huelsken, J., R. Vogel, V. Brinkmann, B. Erdmann, C. Birchmeier, and W. Birchmeier. 2000. 'Requirement for beta-catenin in anterior-posterior axis formation in mice', *J Cell Biol*, 148: 567-78.

Huggins, I. J., T. Bos, O. Gaylord, C. Jessen, B. Lonquich, A. Puranen, J. Richter, C. Rossdam, D. Brafman, T. Gaasterland, and K. Willert. 2017. 'The WNT target SP5 negatively regulates WNT transcriptional programs in human pluripotent stem cells', *Nat Commun*, 8: 1034.

Hughes, C. S., S. Moggridge, T. Müller, P. H. Sorensen, G. B. Morin, and J. Krijgsveld. 2019. 'Single-pot, solid-phase-enhanced sample preparation for proteomics experiments', *Nat Protoc*, 14: 68-85.

Hyun, K., J. Jeon, K. Park, and J. Kim. 2017. 'Writing, erasing and reading histone lysine methylations', *Exp Mol Med*, 49: e324.

Italiano, A. 2020. 'Targeting epigenetics in sarcomas through EZH2 inhibition', *J Hematol Oncol*, 13: 33.

Italiano, A., J. C. Soria, M. Toulmonde, J. M. Michot, C. Lucchesi, A. Varga, J. M. Coindre, S. J. Blakemore, A. Clawson, B. Suttle, A. A. McDonald, M. Woodruff, S. Ribich, E. Hedrick, H. Keilhack, B. Thomson, T. Owa, R. A. Copeland, P. T. C. Ho, and V. Ribrag. 2018. 'Tazemetostat, an EZH2 inhibitor, in relapsed or refractory B-cell non-Hodgkin lymphoma and advanced solid tumours: a first-in-human, open-label, phase 1 study', *Lancet Oncol*, 19: 649-59.

Jackstadt, Rene, Michael Charles Hodder, and Owen James Sansom. 2020. 'WNT and β-Catenin in Cancer: Genes and Therapy', *Annual Review of Cancer Biology*, 4: 177-96.

Jankowska, A. M., H. Makishima, R. V. Tiu, H. Szpurka, Y. Huang, F. Traina, V. Visconte, Y. Sugimoto, C. Prince, C. O'Keefe, E. D. Hsi, A. List, M. A. Sekeres, A. Rao, M. A. McDevitt, and J. P. Maciejewski. 2011. 'Mutational spectrum analysis of chronic myelomonocytic leukemia includes genes associated with epigenetic regulation: UTX, EZH2, and DNMT3A', *Blood*, 118: 3932-41.

Jia, N., Q. Li, X. Tao, J. Wang, K. Hua, and W. Feng. 2014. 'Enhancer of zeste homolog 2 is involved in the proliferation of endometrial carcinoma', *Oncol Lett*, 8: 2049-54.

Jiao, L., and X. Liu. 2015. 'Structural basis of histone H3K27 trimethylation by an active polycomb repressive complex 2', *Science*, 350: aac4383.

Jiao, L., M. Shubbar, X. Yang, Q. Zhang, S. Chen, Q. Wu, Z. Chen, J. Rizo, and X. Liu. 2020. 'A partially disordered region connects gene repression and activation functions of EZH2', *Proc Natl Acad Sci U S A*.

Jones, A., and H. Wang. 2010. 'Polycomb repressive complex 2 in embryonic stem cells: an overview', *Protein Cell*, 1: 1056-62.

Joshi, O., S. Y. Wang, T. Kuznetsova, Y. Atlasi, T. Peng, P. J. Fabre, E. Habibi, J. Shaik, S. Saeed, L. Handoko, T. Richmond, M. Spivakov, D. Burgess, and H. G. Stunnenberg. 2015.

'Dynamic Reorganization of Extremely Long-Range Promoter-Promoter Interactions between Two States of Pluripotency', *Cell Stem Cell*, 17: 748-57.

Jung, H. Y., S. Jun, M. Lee, H. C. Kim, X. Wang, H. Ji, P. D. McCrea, and J. I. Park. 2013. 'PAF and EZH2 induce Wnt/β-catenin signaling hyperactivation', *Mol Cell*, 52: 193-205.

Jung, J., M. R. Mysliwiec, and Y. Lee. 2005. 'Roles of JUMONJI in mouse embryonic development', *Dev Dyn*, 232: 21-32.

Jung, Y. S., and J. I. Park. 2020. 'Wnt signaling in cancer: therapeutic targeting of Wnt signaling beyond β-catenin and the destruction complex', *Exp Mol Med*, 52: 183-91.

Kahn, M. 2014. 'Can we safely target the WNT pathway?', *Nat Rev Drug Discov*, 13: 513-32.

Kalb, R., S. Latwiel, H. I. Baymaz, P. W. Jansen, C. W. Muller, M. Vermeulen, and J. Muller. 2014. 'Histone H2A monoubiquitination promotes histone H3 methylation in Polycomb repression', *Nat Struct Mol Biol*, 21: 569-71.

Kam, Y., and V. Quaranta. 2009. 'Cadherin-bound beta-catenin feeds into the Wnt pathway upon adherens junctions dissociation: evidence for an intersection between beta-catenin pools', *PLoS One*, 4: e4580.

Kaneko, S., J. Son, R. Bonasio, S. S. Shen, and D. Reinberg. 2014. 'Nascent RNA interaction keeps PRC2 activity poised and in check', *Genes Dev*, 28: 1983-8.

Kang, S. J., and T. Chun. 2020. 'Structural heterogeneity of the mammalian polycomb repressor complex in immune regulation', *Exp Mol Med*, 52: 1004-15.

Kanhere, A., K. Viiri, C. C. Araújo, J. Rasaiyaah, R. D. Bouwman, W. A. Whyte, C. F. Pereira, E. Brookes, K. Walker, G. W. Bell, A. Pombo, A. G. Fisher, R. A. Young, and R. G. Jenner. 2010. 'Short RNAs are transcribed from repressed polycomb target genes and interact with polycomb repressive complex-2', *Mol Cell*, 38: 675-88.

Kasinath, V., M. Faini, S. Poepsel, D. Reif, X. A. Feng, G. Stjepanovic, R. Aebersold, and E. Nogales. 2018. 'Structures of human PRC2 with its cofactors AEBP2 and JARID2', *Science*, 359: 940-44.

Kassis, J. A., and J. L. Brown. 2013. 'Polycomb group response elements in Drosophila and vertebrates', *Adv Genet*, 81: 83-118.

Kelly, K. F., D. Y. Ng, G. Jayakumaran, G. A. Wood, H. Koide, and B. W. Doble. 2011. 'beta-catenin enhances Oct-4 activity and reinforces pluripotency through a TCF-independent mechanism', *Cell Stem Cell*, 8: 214-27.

Kim, E., M. Kim, D. H. Woo, Y. Shin, J. Shin, N. Chang, Y. T. Oh, H. Kim, J. Rheey, I. Nakano, C. Lee, K. M. Joo, J. N. Rich, D. H. Nam, and J. Lee. 2013. 'Phosphorylation of EZH2 activates STAT3 signaling via STAT3 methylation and promotes tumorigenicity of glioblastoma stem-like cells', *Cancer Cell*, 23: 839-52.

Kim, J., Y. Lee, X. Lu, B. Song, K. W. Fong, Q. Cao, J. D. Licht, J. C. Zhao, and J. Yu. 2018. 'Polycomb- and Methylation-Independent Roles of EZH2 as a Transcription Activator', *Cell Rep*, 25: 2808-20.e4.

Kim, K. H., and C. W. Roberts. 2016. 'Targeting EZH2 in cancer', *Nat Med*, 22: 128-34.

Kim, M. S., J. Zhong, and A. Pandey. 2016. 'Common errors in mass spectrometry-based analysis of post-translational modifications', *Proteomics*, 16: 700-14.

Kim, W., G. H. Bird, T. Neff, G. Guo, M. A. Kerenyi, L. D. Walensky, and S. H. Orkin. 2013. 'Targeted disruption of the EZH2-EED complex inhibits EZH2-dependent cancer', *Nat Chem Biol*, 9: 643-50.

Kinkley, S., J. Helmuth, J. K. Polansky, I. Dunkel, G. Gasparoni, S. Fröhler, W. Chen, J. Walter, A. Hamann, and H. R. Chung. 2016. 'reChIP-seq reveals widespread bivalency of H3K4me3 and H3K27me3 in CD4(+) memory T cells', *Nat Commun*, 7: 12514.

Kinzler, K. W., M. C. Nilbert, L. K. Su, B. Vogelstein, T. M. Bryan, D. B. Levy, K. J. Smith, A. C. Preisinger, P. Hedge, D. McKechnie, and et al. 1991. 'Identification of FAP locus genes from chromosome 5q21', *Science*, 253: 661-5.

Klose, R. J., E. M. Kallin, and Y. Zhang. 2006. 'JmjC-domain-containing proteins and histone demethylation', *Nat Rev Genet*, 7: 715-27.

Komiya, Y., and R. Habas. 2008. 'Wnt signal transduction pathways', *Organogenesis*, 4: 68-75.

Konze, K. D., A. Ma, F. Li, D. Barsyte-Lovejoy, T. Parton, C. J. Macnevin, F. Liu, C. Gao, X. P. Huang, E. Kuznetsova, M. Rougie, A. Jiang, S. G. Pattenden, J. L. Norris, L. I. James, B. L. Roth, P. J. Brown, S. V. Frye, C. H. Arrowsmith, K. M. Hahn, G. G. Wang, M. Vedadi, and J. Jin. 2013. 'An orally bioavailable chemical probe of the Lysine Methyltransferases EZH2 and EZH1', *ACS Chem Biol*, 8: 1324-34.

Korinek, V., N. Barker, P. J. Morin, D. van Wichen, R. de Weger, K. W. Kinzler, B. Vogelstein, and H. Clevers. 1997. 'Constitutive transcriptional activation by a beta-catenin-Tcf complex in APC-/- colon carcinoma', *Science*, 275: 1784-7.

Kretzschmar, K., and H. Clevers. 2017. 'Wnt/β-catenin signaling in adult mammalian epithelial stem cells', *Dev Biol*, 428: 273-82.

Krysko, D. V., L. Leybaert, P. Vandenabeele, and K. D'Herde. 2005. 'Gap junctions and the propagation of cell survival and cell death signals', *Apoptosis*, 10: 459-69.

Kurek, D., A. Neagu, M. Tastemel, N. Tüysüz, J. Lehmann, H. J. G. van de Werken, S. Philipsen, R. van der Linden, A. Maas, IJcken W. F. J. van, M. Drukker, and D. Ten Berge. 2015. 'Endogenous WNT signals mediate BMP-induced and spontaneous differentiation of epiblast stem cells and human embryonic stem cells', *Stem Cell Reports*, 4: 114-28.

Landeira, D., H. Bagci, A. R. Malinowski, K. E. Brown, J. Soza-Ried, A. Feytout, Z. Webster, E. Ndjetehe, I. Cantone, H. G. Asenjo, N. Brockdorff, T. Carroll, M. Merkenschlager, and A. G. Fisher. 2015. 'Jarid2 Coordinates Nanog Expression and PCP/Wnt Signaling Required for Efficient ESC Differentiation and Early Embryo Development', *Cell Rep*, 12: 573-86.

Landeira, D., and A. G. Fisher. 2011. 'Inactive yet indispensable: the tale of Jarid2', *Trends Cell Biol*, 21: 74-80.

Landeira, D., S. Sauer, R. Poot, M. Dvorkina, L. Mazzarella, H. F. Jorgensen, C. F. Pereira, M. Leleu, F. M. Piccolo, M. Spivakov, E. Brookes, A. Pombo, C. Fisher, W. C. Skarnes, T. Snoek, K. Bezstarosti, J. Demmers, R. J. Klose, M. Casanova, L. Tavares, N. Brockdorff, M. Merkenschlager, and A. G. Fisher. 2010. 'Jarid2 is a PRC2 component in embryonic stem cells required for multi-lineage differentiation and recruitment of PRC1 and RNA Polymerase II to developmental regulators', *Nat Cell Biol*, 12: 618-24.

Larue, L., M. Ohsugi, J. Hirchenhain, and R. Kemler. 1994. 'E-cadherin null mutant embryos fail to form a trophectoderm epithelium', *Proc Natl Acad Sci U S A*, 91: 8263-7.

Laugesen, A., J. W. Højfeldt, and K. Helin. 2016. 'Role of the Polycomb Repressive Complex 2 (PRC2) in Transcriptional Regulation and Cancer', *Cold Spring Harb Perspect Med*, 6.

Laugesen, A., J. W. Højfeldt, and K. Helin. 2019. 'Molecular Mechanisms Directing PRC2 Recruitment and H3K27 Methylation', *Mol Cell*, 74: 8-18.

Lavarone, E., C. M. Barbieri, and D. Pasini. 2019. 'Dissecting the role of H3K27 acetylation and methylation in PRC2 mediated control of cellular identity', *Nat Commun*, 10: 1679.

Lee, C. H., J. R. Yu, J. Granat, R. Saldaña-Meyer, J. Andrade, G. LeRoy, Y. Jin, P. Lund, J. M. Stafford, B. A. Garcia, B. Ueberheide, and D. Reinberg. 2019. 'Automethylation of PRC2 promotes H3K27 methylation and is impaired in H3K27M pediatric glioma', *Genes Dev*, 33: 1428-40.

Lee, J. M., J. S. Lee, H. Kim, K. Kim, H. Park, J. Y. Kim, S. H. Lee, I. S. Kim, J. Kim, M. Lee, C. H. Chung, S. B. Seo, J. B. Yoon, E. Ko, D. Y. Noh, K. I. Kim, K. K. Kim, and S. H. Baek. 2012. 'EZH2 generates a methyl degron that is recognized by the DCAF1/DDB1/CUL4 E3 ubiquitin ligase complex', *Mol Cell*, 48: 572-86.

Lee, S. T., Z. Li, Z. Wu, M. Aau, P. Guan, R. K. Karuturi, Y. C. Liou, and Q. Yu. 2011. 'Context-specific regulation of NF-κB target gene expression by EZH2 in breast cancers', *Mol Cell*, 43: 798-810.

Lee, T. I., R. G. Jenner, L. A. Boyer, M. G. Guenther, S. S. Levine, R. M. Kumar, B. Chevalier, S. E. Johnstone, M. F. Cole, K. Isono, H. Koseki, T. Fuchikami, K. Abe, H. L. Murray, J. P. Zucker, B. Yuan, G. W. Bell, E. Herbolsheimer, N. M. Hannett, K. Sun, D. T. Odom, A. P. Otte, T. L. Volkert, D. P. Bartel, D. A. Melton, D. K. Gifford, R. Jaenisch, and R. A. Young. 2006. 'Control of developmental regulators by Polycomb in human embryonic stem cells', *Cell*, 125: 301-13.

Lee, W., S. Teckie, T. Wiesner, L. Ran, C. N. Prieto Granada, M. Lin, S. Zhu, Z. Cao, Y. Liang, A. Sboner, W. D. Tap, J. A. Fletcher, K. H. Huberman, L. X. Qin, A. Viale, S. Singer, D. Zheng, M. F. Berger, Y. Chen, C. R. Antonescu, and P. Chi. 2014. 'PRC2 is recurrently inactivated through EED or SUZ12 loss in malignant peripheral nerve sheath tumors', *Nat Genet*, 46: 1227-32.

Leeb, M., D. Pasini, M. Novatchkova, M. Jaritz, K. Helin, and A. Wutz. 2010. 'Polycomb complexes act redundantly to repress genomic repeats and genes', *Genes Dev*, 24: 265-76.

Lemcke, H., G. Steinhoff, and R. David. 2015. 'Gap junctional shuttling of miRNA--A novel pathway of intercellular gene regulation and its prospects in clinical application', *Cell Signal*, 27: 2506-14.

Lewis, E. B. 1978. 'A gene complex controlling segmentation in Drosophila', *Nature*, 276: 565-70.

Lewis, P. W., M. M. Müller, M. S. Koletsky, F. Cordero, S. Lin, L. A. Banaszynski, B. A. Garcia, T. W. Muir, O. J. Becher, and C. D. Allis. 2013. 'Inhibition of PRC2 activity by a gain-of-function H3 mutation found in pediatric glioblastoma', *Science*, 340: 857-61.

Li, G., R. Margueron, M. Ku, P. Chambon, B. E. Bernstein, and D. Reinberg. 2010. 'Jarid2 and PRC2, partners in regulating gene expression', *Genes Dev*, 24: 368-80.

Li, X., M. E. Gonzalez, K. Toy, T. Filzen, S. D. Merajver, and C. G. Kleer. 2009. 'Targeted overexpression of EZH2 in the mammary gland disrupts ductal morphogenesis and causes epithelial hyperplasia', *Am J Pathol*, 175: 1246-54.

Liao, J., R. Karnik, H. Gu, M. J. Ziller, K. Clement, A. M. Tsankov, V. Akopian, C. A. Gifford, J. Donaghey, C. Galonska, R. Pop, D. Reyon, S. Q. Tsai, W. Mallard, J. K. Joung, J. L. Rinn, A. Gnirke, and A. Meissner. 2015. 'Targeted disruption of DNMT1, DNMT3A and DNMT3B in human embryonic stem cells', *Nat Genet*, 47: 469-78.

Lindsley, R. C., J. G. Gill, M. Kyba, T. L. Murphy, and K. M. Murphy. 2006. 'Canonical Wnt signaling is required for development of embryonic stem cell-derived mesoderm', *Development*, 133: 3787-96.

Lindsley, R. C., B. G. Mar, E. Mazzola, P. V. Grauman, S. Shareef, S. L. Allen, A. Pigneux, M. Wetzler, R. K. Stuart, H. P. Erba, L. E. Damon, B. L. Powell, N. Lindeman, D. P. Steensma, M. Wadleigh, D. J. DeAngelo, D. Neuberg, R. M. Stone, and B. L. Ebert. 2015. 'Acute myeloid leukemia ontogeny is defined by distinct somatic mutations', *Blood*, 125: 1367-76.

Liu, W., X. Dong, M. Mai, R. S. Seelan, K. Taniguchi, K. K. Krishnadath, K. C. Halling, J. M. Cunningham, L. A. Boardman, C. Qian, E. Christensen, S. S. Schmidt, P. C. Roche, D. I. Smith, and S. N. Thibodeau. 2000. 'Mutations in AXIN2 cause colorectal cancer with defective mismatch repair by activating beta-catenin/TCF signalling', *Nat Genet*, 26: 146-7.

Liu, X., C. Wang, W. Liu, J. Li, C. Li, X. Kou, J. Chen, Y. Zhao, H. Gao, H. Wang, Y. Zhang, Y. Gao, and S. Gao. 2016. 'Distinct features of H3K4me3 and H3K27me3 chromatin domains in pre-implantation embryos', *Nature*, 537: 558-62.

Liu, Y., L. Patel, G. B. Mills, K. H. Lu, A. K. Sood, L. Ding, R. Kucherlapati, E. R. Mardis, D. A. Levine, I. Shmulevich, R. R. Broaddus, and W. Zhang. 2014. 'Clinical significance of CTNNB1 mutation and Wnt pathway activation in endometrioid endometrial carcinoma', *J Natl Cancer Inst*, 106.

Longerich, T., V. Endris, O. Neumann, E. Rempel, M. Kirchner, Z. Abadi, S. Uhrig, M. Kriegsmann, K. H. Weiss, K. Breuhahn, A. Mehrabi, T. F. Weber, L. Wilkens, B. K. Straub, A. Rosenwald, F. Schulze, B. Brors, S. Froehling, R. Pellegrino, J. Budczies, P. Schirmacher, and A. Stenzinger. 2019. 'RSPO2 gene rearrangement: a powerful driver of β-catenin activation in liver tumours', *Gut*, 68: 1287-96.

Lu, C., H. D. Han, L. S. Mangala, R. Ali-Fehmi, C. S. Newton, L. Ozbun, G. N. Armaiz-Pena, W. Hu, R. L. Stone, A. Munkarah, M. K. Ravoori, M. M. Shahzad, J. W. Lee, E. Mora, R. R. Langley, A. R. Carroll, K. Matsuo, W. A. Spannuth, R. Schmandt, N. B. Jennings, B. W. Goodman, R. B. Jaffe, A. M. Nick, H. S. Kim, E. O. Guven, Y. H. Chen, L. Y. Li, M. C. Hsu, R. L. Coleman, G. A. Calin, E. B. Denkbas, J. Y. Lim, J. S. Lee, V. Kundra, M. J. Birrer, M. C. Hung, G. Lopez-Berestein, and A. K. Sood. 2010. 'Regulation of tumor angiogenesis by EZH2', *Cancer Cell*, 18: 185-97.

Lu, L., Y. Gao, Z. Zhang, Q. Cao, X. Zhang, J. Zou, and Y. Cao. 2015. 'Kdm2a/b Lysine Demethylases Regulate Canonical Wnt Signaling by Modulating the Stability of Nuclear beta-Catenin', *Dev Cell*, 33: 660-74.

Lundh, M., P. S. Petersen, M. S. Isidor, D. N. Kazoka-Sørensen, K. Plucińska, F. Shamsi, C. Ørskov, M. Tozzi, E. L. Brown, E. Andersen, T. Ma, U. Müller, R. Barrès, V. B. Kristiansen, Z. Gerhart-Hines, Y. H. Tseng, and B. Emanuelli. 2019. 'Afadin is a scaffold protein repressing insulin action via HDAC6 in adipose tissue', *EMBO Rep*, 20: e48216.

Lyashenko, N., M. Winter, D. Migliorini, T. Biechele, R. T. Moon, and C. Hartmann. 2011. 'Differential requirement for the dual functions of beta-catenin in embryonic stem cell self-renewal and germ layer formation', *Nat Cell Biol*, 13: 753-61.

Ma, L., K. Lin, G. Chang, Y. Chen, C. Yue, Q. Guo, S. Zhang, Z. Jia, T. T. Huang, A. Zhou, and S. Huang. 2019. 'Aberrant Activation of β-Catenin Signaling Drives Glioma Tumorigenesis via USP1-Mediated Stabilization of EZH2', *Cancer Res*, 79: 72-85.

MacDonald, B. T., K. Tamai, and X. He. 2009. 'Wnt/beta-catenin signaling: components, mechanisms, and diseases', *Dev Cell*, 17: 9-26.

Mai, H., B. Zhou, L. Liu, F. Yang, C. Conran, Y. Ji, J. Hou, and D. Jiang. 2019. 'Molecular pattern of lncRNAs in hepatocellular carcinoma', *J Exp Clin Cancer Res*, 38: 198.

Majer, C. R., L. Jin, M. P. Scott, S. K. Knutson, K. W. Kuntz, H. Keilhack, J. J. Smith, M. P. Moyer, V. M. Richon, R. A. Copeland, and T. J. Wigle. 2012. 'A687V EZH2 is a gain-of-function mutation found in lymphoma patients', *FEBS Lett*, 586: 3448-51.

Mandai, K., H. Nakanishi, A. Satoh, K. Takahashi, K. Satoh, H. Nishioka, A. Mizoguchi, and Y. Takai. 1999. 'Ponsin/SH3P12: an l-afadin- and vinculin-binding protein localized at cell-cell and cell-matrix adherens junctions', *J Cell Biol*, 144: 1001-17.

Margueron, R., N. Justin, K. Ohno, M. L. Sharpe, J. Son, W. J. Drury, 3rd, P. Voigt, S. R. Martin, W. R. Taylor, V. De Marco, V. Pirrotta, D. Reinberg, and S. J. Gamblin. 2009. 'Role of

the polycomb protein EED in the propagation of repressive histone marks', *Nature*, 461: 762-7.

Martin, G. R. 1981. 'Isolation of a pluripotent cell line from early mouse embryos cultured in medium conditioned by teratocarcinoma stem cells', *Proc Natl Acad Sci U S A*, 78: 7634-8.

Mas, G., E. Blanco, C. Ballaré, M. Sansó, Y. G. Spill, D. Hu, Y. Aoi, F. Le Dily, A. Shilatifard, M. A. Marti-Renom, and L. Di Croce. 2018. 'Promoter bivalency favors an open chromatin architecture in embryonic stem cells', *Nat Genet*, 50: 1452-62.

Mas, G., and L. Di Croce. 2016. 'The role of Polycomb in stem cell genome architecture', *Curr Opin Cell Biol*, 43: 87-95.

Mazzarella, L., H. F. Jorgensen, J. Soza-Ried, A. V. Terry, S. Pearson, G. Lacaud, V. Kouskoff, M. Merkenschlager, and A. G. Fisher. 2011. 'Embryonic stem cell-derived hemangioblasts remain epigenetically plastic and require PRC1 to prevent neural gene expression', *Blood*, 117: 83-7.

McCabe, M. T., A. P. Graves, G. Ganji, E. Diaz, W. S. Halsey, Y. Jiang, K. N. Smitheman, H. M. Ott, M. B. Pappalardi, K. E. Allen, S. B. Chen, A. Della Pietra, 3rd, E. Dul, A. M. Hughes, S. A. Gilbert, S. H. Thrall, P. J. Tummino, R. G. Kruger, M. Brandt, B. Schwartz, and C. L. Creasy. 2012. 'Mutation of A677 in histone methyltransferase EZH2 in human B-cell lymphoma promotes hypertrimethylation of histone H3 on lysine 27 (H3K27)', *Proc Natl Acad Sci U S A*, 109: 2989-94.

McCabe, M. T., H. M. Ott, G. Ganji, S. Korenchuk, C. Thompson, G. S. Van Aller, Y. Liu, A. P. Graves, A. Della Pietra, 3rd, E. Diaz, L. V. LaFrance, M. Mellinger, C. Duquenne, X. Tian, R. G. Kruger, C. F. McHugh, M. Brandt, W. H. Miller, D. Dhanak, S. K. Verma, P. J. Tummino, and C. L. Creasy. 2012. 'EZH2 inhibition as a therapeutic strategy for lymphoma with EZH2-activating mutations', *Nature*, 492: 108-12.

Mendenhall, E. M., R. P. Koche, T. Truong, V. W. Zhou, B. Issac, A. S. Chi, M. Ku, and B. E. Bernstein. 2010. 'GC-rich sequence elements recruit PRC2 in mammalian ES cells', *PLoS Genet*, 6: e1001244.

Miller, Sara A., Manashree Damle, and Robert E. Kingston. 2020. 'H3K27me3 is dispensable for early differentiation but required to maintain differentiated cell identity', *bioRxiv*: 2020.06.27.175612.

Miyabayashi, T., J. L. Teo, M. Yamamoto, M. McMillan, C. Nguyen, and M. Kahn. 2007. 'Wnt/beta-catenin/CBP signaling maintains long-term murine embryonic stem cell pluripotency', *Proc Natl Acad Sci U S A*, 104: 5668-73.

Morin, R. D., M. Mendez-Lago, A. J. Mungall, R. Goya, K. L. Mungall, R. D. Corbett, N. A. Johnson, T. M. Severson, R. Chiu, M. Field, S. Jackman, M. Krzywinski, D. W. Scott, D. L. Trinh, J. Tamura-Wells, S. Li, M. R. Firme, S. Rogic, M. Griffith, S. Chan, O. Yakovenko, I. M. Meyer, E. Y. Zhao, D. Smailus, M. Moksa, S. Chittaranjan, L. Rimsza, A. Brooks-Wilson, J. J. Spinelli, S. Ben-Neriah, B. Meissner, B. Woolcock, M. Boyle, H. McDonald, A. Tam, Y. Zhao, A. Delaney, T. Zeng, K. Tse, Y. Butterfield, I. Birol, R. Holt, J. Schein, D. E. Horsman, R. Moore, S. J. Jones, J. M. Connors, M. Hirst, R. D. Gascoyne, and M. A. Marra. 2011. 'Frequent mutation of histone-modifying genes in non-Hodgkin lymphoma', *Nature*, 476: 298-303.

Morschhauser, F., G. Salles, P. McKay, H. Tilly, A. Schmitt, J. Gerecitano, P. Johnson, S. Le Gouill, M.J. Dickinson, C. Fruchart, T. Lamy, A. Chaidos, W. Jurczak, S. Opat, J. Radford, P.L. Zinzani, S. Assouline, G. Cartron, A. Clawson, N. Picazio, S. Ribich, S.J. Blakemore, J. Larus, H. Miao, P.T. Ho, and V. Ribrag. 2017. 'INTERIM REPORT FROM A PHASE 2 MULTICENTER STUDY OF TAZEMETOSTAT, AN EZH2 INHIBITOR, IN PATIENTS WITH RELAPSED OR REFRACTORY B-CELL NON-HODGKIN LYMPHOMAS', *Hematological Oncology*, 35: 24-25.

Narendra, V., P. P. Rocha, D. An, R. Raviram, J. A. Skok, E. O. Mazzoni, and D. Reinberg. 2015. 'CTCF establishes discrete functional chromatin domains at the Hox clusters during differentiation', *Science*, 347: 1017-21.

Nelson, W. J., and R. Nusse. 2004. 'Convergence of Wnt, beta-catenin, and cadherin pathways', *Science*, 303: 1483-7.

Nichols, J., and A. Smith. 2009. 'Naive and primed pluripotent states', *Cell Stem Cell*, 4: 487-92.

Niehrs, C. 2010. 'On growth and form: a Cartesian coordinate system of Wnt and BMP signaling specifies bilaterian body axes', *Development*, 137: 845-57.

Niessen, C. M., and C. J. Gottardi. 2008. 'Molecular components of the adherens junction', *Biochim Biophys Acta*, 1778: 562-71.

Nishisho, I., Y. Nakamura, Y. Miyoshi, Y. Miki, H. Ando, A. Horii, K. Koyama, J. Utsunomiya, S. Baba, and P. Hedge. 1991. 'Mutations of chromosome 5q21 genes in FAP and colorectal cancer patients', *Science*, 253: 665-9.

Niwa, H. 2007. 'How is pluripotency determined and maintained?', *Development*, 134: 635-46.

Ntziachristos, P., A. Tsirigos, P. Van Vlierberghe, J. Nedjic, T. Trimarchi, M. S. Flaherty, D. Ferres-Marco, V. da Ros, Z. Tang, J. Siegle, P. Asp, M. Hadler, I. Rigo, K. De Keersmaecker, J. Patel, T. Huynh, F. Utro, S. Poglio, J. B. Samon, E. Paietta, J. Racevskis, J. M. Rowe, R. Rabadan, R. L. Levine, S. Brown, F. Pflumio, M. Dominguez, A. Ferrando, and I. Aifantis. 2012. 'Genetic inactivation of the polycomb repressive complex 2 in T cell acute lymphoblastic leukemia', *Nat Med*, 18: 298-301.

Nusse, R., and H. Clevers. 2017a. 'Wnt/beta-Catenin Signaling, Disease, and Emerging Therapeutic Modalities', *Cell*, 169: 985-99.

Nusse, R., and H. Varmus. 2012. 'Three decades of Wnts: a personal perspective on how a scientific field developed', *EMBO J*, 31: 2670-84.

Nusse, R., and H. E. Varmus. 1982. 'Many tumors induced by the mouse mammary tumor virus contain a provirus integrated in the same region of the host genome', *Cell*, 31: 99-109.

O'Carroll, D., S. Erhardt, M. Pagani, S. C. Barton, M. A. Surani, and T. Jenuwein. 2001. 'The polycomb-group gene Ezh2 is required for early mouse development', *Mol Cell Biol*, 21: 4330-6.

Oda, H., and M. Takeichi. 2011. 'Evolution: structural and functional diversity of cadherin at the adherens junction', *J Cell Biol*, 193: 1137-46.

Okosun, J., C. Bödör, J. Wang, S. Araf, C. Y. Yang, C. Pan, S. Boller, D. Cittaro, M. Bozek, S. Iqbal, J. Matthews, D. Wrench, J. Marzec, K. Tawana, N. Popov, C. O'Riain, D. O'Shea, E. Carlotti, A. Davies, C. H. Lawrie, A. Matolcsy, M. Calaminici, A. Norton, R. J. Byers, C. Mein, E. Stupka, T. A. Lister, G. Lenz, S. Montoto, J. G. Gribben, Y. Fan, R. Grosschedl, C. Chelala, and J. Fitzgibbon. 2014. 'Integrated genomic analysis identifies recurrent mutations and evolution patterns driving the initiation and progression of follicular lymphoma', *Nat Genet*, 46: 176-81.

Oksuz, O., V. Narendra, C. H. Lee, N. Descostes, G. LeRoy, R. Raviram, L. Blumenberg, K. Karch, P. P. Rocha, B. A. Garcia, J. A. Skok, and D. Reinberg. 2018. 'Capturing the Onset of PRC2-Mediated Repressive Domain Formation', *Mol Cell*, 70: 1149-62.e5.

Okumura, N., H. Akutsu, T. Sugawara, T. Miura, Y. Takezawa, A. Hosoda, K. Yoshida, J. K. Ichida, M. Yamada, T. Hamatani, N. Kuji, K. Miyado, Y. Yoshimura, and A. Umezawa. 2013. 'beta-catenin functions pleiotropically in differentiation and tumorigenesis in mouse embryo-derived stem cells', *PLoS One*, 8: e63265.

Olsson, L., S. Zettermark, A. Biloglav, A. Castor, M. Behrendtz, E. Forestier, K. Paulsson, and B. Johansson. 2016. 'The genetic landscape of paediatric de novo acute myeloid leukaemia as defined by single nucleotide polymorphism array and exon sequencing of 100 candidate genes', *Br J Haematol*, 174: 292-301.

Orkin, S. H., J. Wang, J. Kim, J. Chu, S. Rao, T. W. Theunissen, X. Shen, and D. N. Levasseur. 2008. 'The transcriptional network controlling pluripotency in ES cells', *Cold Spring Harb Symp Quant Biol*, 73: 195-202.

Orre, L. M., M. Vesterlund, Y. Pan, T. Arslan, Y. Zhu, A. Fernandez Woodbridge, O. Frings, E. Fredlund, and J. Lehtiö. 2019. 'SubCellBarCode: Proteome-wide Mapping of Protein Localization and Relocalization', *Mol Cell*, 73: 166-82.e7.

Ott, H. M., A. P. Graves, M. B. Pappalardi, M. Huddleston, W. S. Halsey, A. M. Hughes, A. Groy, E. Dul, Y. Jiang, Y. Bai, R. Annan, S. K. Verma, S. D. Knight, R. G. Kruger, D. Dhanak, B. Schwartz, P. J. Tummino, C. L. Creasy, and M. T. McCabe. 2014. 'A687V EZH2 is a driver of histone H3 lysine 27 (H3K27) hypertrimethylation', *Mol Cancer Ther*, 13: 3062-73.

Ozawa, M., H. Baribault, and R. Kemler. 1989. 'The cytoplasmic domain of the cell adhesion molecule uvomorulin associates with three independent proteins structurally related in different species', *EMBO J*, 8: 1711-7.

Pachano, T., G. Crispatzu, and A. Rada-Iglesias. 2019. 'Polycomb proteins as organizers of 3D genome architecture in embryonic stem cells', *Brief Funct Genomics*, 18: 358-66.

Paro, R. 1995. 'Propagating memory of transcriptional states', *Trends Genet*, 11: 295-7.

Pasini, D., A. P. Bracken, J. B. Hansen, M. Capillo, and K. Helin. 2007. 'The polycomb group protein Suz12 is required for embryonic stem cell differentiation', *Mol Cell Biol*, 27: 3769-79.

Pasini, D., A. P. Bracken, M. R. Jensen, E. Lazzerini Denchi, and K. Helin. 2004. 'Suz12 is essential for mouse development and for EZH2 histone methyltransferase activity', *EMBO J*, 23: 4061-71.

Pasini, D., P. A. Cloos, J. Walfridsson, L. Olsson, J. P. Bukowski, J. V. Johansen, M. Bak, N. Tommerup, J. Rappsilber, and K. Helin. 2010. 'JARID2 regulates binding of the Polycomb repressive complex 2 to target genes in ES cells', *Nature*, 464: 306-10.

Pasini, D., and L. Di Croce. 2016. 'Emerging roles for Polycomb proteins in cancer', *Curr Opin Genet Dev*, 36: 50-8.

Patsialou, A., D. Wilsker, and E. Moran. 2005. 'DNA-binding properties of ARID family proteins', *Nucleic Acids Res*, 33: 66-80.

Peng, J. C., A. Valouev, T. Swigut, J. Zhang, Y. Zhao, A. Sidow, and J. Wysocka. 2009. 'Jarid2/Jumonji coordinates control of PRC2 enzymatic activity and target gene occupancy in pluripotent cells', *Cell*, 139: 1290-302.

Pereira, C. F., F. M. Piccolo, T. Tsubouchi, S. Sauer, N. K. Ryan, L. Bruno, D. Landeira, J. Santos, A. Banito, J. Gil, H. Koseki, M. Merkenschlager, and A. G. Fisher. 2010. 'ESCs require PRC2 to direct the successful reprogramming of differentiated cells toward pluripotency', *Cell Stem Cell*, 6: 547-56.

Perkins, D. N., D. J. Pappin, D. M. Creasy, and J. S. Cottrell. 1999. 'Probability-based protein identification by searching sequence databases using mass spectrometry data', *Electrophoresis*, 20: 3551-67.

Petrova, Y. I., L. Schecterson, and B. M. Gumbiner. 2016. 'Roles for E-cadherin cell surface regulation in cancer', *Mol Biol Cell*, 27: 3233-44.

Pfisterer, U., A. Kirkeby, O. Torper, J. Wood, J. Nelander, A. Dufour, A. Björklund, O. Lindvall, J. Jakobsson, and M. Parmar. 2011. 'Direct conversion of human fibroblasts to dopaminergic neurons', *Proc Natl Acad Sci U S A*, 108: 10343-8.

Pieters, T., and F. van Roy. 2014. 'Role of cell-cell adhesion complexes in embryonic stem cell biology', *J Cell Sci*, 127: 2603-13.

Piunti, A., and A. Shilatifard. 2016. 'Epigenetic balance of gene expression by Polycomb and COMPASS families', *Science*, 352: aad9780.

Plass, C., S. M. Pfister, A. M. Lindroth, O. Bogatyrova, R. Claus, and P. Lichter. 2013. 'Mutations in regulators of the epigenome and their connections to global chromatin patterns in cancer', *Nat Rev Genet*, 14: 765-80.

Pombo, A., and N. Dillon. 2015. 'Three-dimensional genome architecture: players and mechanisms', *Nat Rev Mol Cell Biol*, 16: 245-57.

Popovic, R., E. Martinez-Garcia, E. G. Giannopoulou, Q. Zhang, Q. Zhang, T. Ezponda, M. Y. Shah, Y. Zheng, C. M. Will, E. C. Small, Y. Hua, M. Bulic, Y. Jiang, M. Carrara, R. A. Calogero, W. L. Kath, N. L. Kelleher, J. P. Wang, O. Elemento, and J. D. Licht. 2014. 'Histone methyltransferase MMSET/NSD2 alters EZH2 binding and reprograms the myeloma epigenome through global and focal changes in H3K36 and H3K27 methylation', *PLoS Genet*, 10: e1004566.

Puda, A., J. D. Milosevic, T. Berg, T. Klampfl, A. S. Harutyunyan, B. Gisslinger, E. Rumi, D. Pietra, L. Malcovati, C. Elena, M. Doubek, M. Steurer, N. Tosic, S. Pavlovic, P. Guglielmelli, L. Pieri, A. M. Vannucchi, H. Gisslinger, M. Cazzola, and R. Kralovics. 2012. 'Frequent deletions of JARID2 in leukemic transformation of chronic myeloid malignancies', *Am J Hematol*, 87: 245-50.

Qi, W., K. Zhao, J. Gu, Y. Huang, Y. Wang, H. Zhang, M. Zhang, J. Zhang, Z. Yu, L. Li, L. Teng, S. Chuai, C. Zhang, M. Zhao, H. Chan, Z. Chen, D. Fang, Q. Fei, L. Feng, L. Feng, Y. Gao, H. Ge, X. Ge, G. Li, A. Lingel, Y. Lin, Y. Liu, F. Luo, M. Shi, L. Wang, Z. Wang, Y. Yu, J. Zeng, C. Zeng, L. Zhang, Q. Zhang, S. Zhou, C. Oyang, P. Atadja, and E. Li. 2017. 'An allosteric PRC2 inhibitor targeting the H3K27me3 binding pocket of EED', *Nat Chem Biol*, 13: 381-88.

Qiao, E., D. Chen, Q. Li, W. Feng, X. Yu, X. Zhang, L. Xia, J. Jin, and H. Yang. 2019. 'Long noncoding RNA TALNEC2 plays an oncogenic role in breast cancer by binding to EZH2 to target p57(KIP2) and involving in p-p38 MAPK and NF-κB pathways', *J Cell Biochem*, 120: 3978-88.

Radulescu, S., R. A. Ridgway, J. Cordero, D. Athineos, P. Salgueiro, R. Poulsom, J. Neumann, A. Jung, S. Patel, J. Woodgett, N. Barker, D. M. Pritchard, K. Oien, and O. J. Sansom. 2013. 'Acute WNT signalling activation perturbs differentiation within the adult stomach and rapidly leads to tumour formation', *Oncogene*, 32: 2048-57.

Ramakrishnan, A. B., and K. M. Cadigan. 2017. 'Wnt target genes and where to find them', *F1000Res*, 6: 746.

Reddington, J. P., S. M. Perricone, C. E. Nestor, J. Reichmann, N. A. Youngson, M. Suzuki, D. Reinhardt, D. S. Dunican, J. G. Prendergast, H. Mjoseng, B. H. Ramsahoye, E. Whitelaw, J. M. Greally, I. R. Adams, W. A. Bickmore, and R. R. Meehan. 2013.

'Redistribution of H3K27me3 upon DNA hypomethylation results in de-repression of Polycomb target genes', *Genome Biol*, 14: R25.

Reya, T., and H. Clevers. 2005. 'Wnt signalling in stem cells and cancer', *Nature*, 434: 843-50.

Riising, E. M., I. Comet, B. Leblanc, X. Wu, J. V. Johansen, and K. Helin. 2014. 'Gene silencing triggers polycomb repressive complex 2 recruitment to CpG islands genome wide', *Mol Cell*, 55: 347-60.

Rinn, J. L., M. Kertesz, J. K. Wang, S. L. Squazzo, X. Xu, S. A. Brugmann, L. H. Goodnough, J. A. Helms, P. J. Farnham, E. Segal, and H. Y. Chang. 2007. 'Functional demarcation of active and silent chromatin domains in human HOX loci by noncoding RNAs', *Cell*, 129: 1311-23.

Roose, J., G. Huls, M. van Beest, P. Moerer, K. van der Horn, R. Goldschmeding, T. Logtenberg, and H. Clevers. 1999. 'Synergy between tumor suppressor APC and the beta-catenin-Tcf4 target Tcf1', *Science*, 285: 1923-6.

Rose, N. R., E. C. Woon, A. Tumber, L. J. Walport, R. Chowdhury, X. S. Li, O. N. King, C. Lejeune, S. S. Ng, T. Krojer, M. C. Chan, A. M. Rydzik, R. J. Hopkinson, K. H. Che, M. Daniel, C. Strain-Damerell, C. Gileadi, G. Kochan, I. K. Leung, J. Dunford, K. K. Yeoh, P. J. Ratcliffe, N. Burgess-Brown, F. von Delft, S. Muller, B. Marsden, P. E. Brennan, M. A. McDonough, U. Oppermann, R. J. Klose, C. J. Schofield, and A. Kawamura. 2012. 'Plant growth regulator daminozide is a selective inhibitor of human KDM2/7 histone demethylases', *J Med Chem*, 55: 6639-43.

Rothberg, J. L. M., H. B. Maganti, H. Jrade, C. J. Porter, G. A. Palidwor, C. Cafariello, H. L. Battaion, S. T. Khan, T. J. Perkins, R. F. Paulson, C. Y. Ito, and W. L. Stanford. 2018. 'Mtf2-PRC2 control of canonical Wnt signaling is required for definitive erythropoiesis', *Cell Discov*, 4: 21.

Rowley, M. J., and V. G. Corces. 2018. 'Organizational principles of 3D genome architecture', *Nat Rev Genet*, 19: 789-800.

Roy, A. L., and R. S. Conroy. 2018. 'Toward mapping the human body at a cellular resolution', *Mol Biol Cell*, 29: 1779-85.

Rubinfeld, B., I. Albert, E. Porfiri, C. Fiol, S. Munemitsu, and P. Polakis. 1996. 'Binding of GSK3beta to the APC-beta-catenin complex and regulation of complex assembly', *Science*, 272: 1023-6.

Sagar, G. D., and D. M. Larson. 2006. 'Carbenoxolone inhibits junctional transfer and upregulates Connexin43 expression by a protein kinase A-dependent pathway', *J Cell Biochem*, 98: 1543-51.

Sakakibara, S., K. Mizutani, A. Sugiura, A. Sakane, T. Sasaki, S. Yonemura, and Y. Takai. 2020. 'Afadin regulates actomyosin organization through αE-catenin at adherens junctions', *J Cell Biol*, 219.

Sanchez-Vega, F., M. Mina, J. Armenia, W. K. Chatila, A. Luna, K. C. La, S. Dimitriadoy, D. L. Liu, H. S. Kantheti, S. Saghafinia, D. Chakravarty, F. Daian, Q. Gao, M. H. Bailey, W. W. Liang, S. M. Foltz, I. Shmulevich, L. Ding, Z. Heins, A. Ochoa, B. Gross, J. Gao, H. Zhang, R. Kundra, C. Kandoth, I. Bahceci, L. Dervishi, U. Dogrusoz, W. Zhou, H. Shen, P. W. Laird, G. P. Way, C. S. Greene, H. Liang, Y. Xiao, C. Wang, A. Iavarone, A. H. Berger, T. G. Bivona, A. J. Lazar, G. D. Hammer, T. Giordano, L. N. Kwong, G. McArthur, C. Huang, A. D. Tward, M. J. Frederick, F. McCormick, M. Meyerson, E. M. Van Allen, A. D. Cherniack, G. Ciriello, C. Sander, and N. Schultz. 2018. 'Oncogenic Signaling Pathways in The Cancer Genome Atlas', *Cell*, 173: 321-37.e10.

Sano, M., D. R. Driscoll, W. E. DeJesus-Monge, B. Quattrochi, V. A. Appleman, J. Ou, L. J. Zhu, N. Yoshida, S. Yamazaki, T. Takayama, M. Sugitani, N. Nemoto, D. S. Klimstra, and B. C. Lewis. 2016. 'Activation of WNT/β-Catenin Signaling Enhances Pancreatic Cancer Development and the Malignant Potential Via Up-regulation of Cyr61', *Neoplasia*, 18: 785-94.

Sanulli, S., N. Justin, A. Teissandier, K. Ancelin, M. Portoso, M. Caron, A. Michaud, B. Lombard, S. T. da Rocha, J. Offer, D. Loew, N. Servant, M. Wassef, F. Burlina, S. J. Gamblin, E. Heard, and R. Margueron. 2015a. 'Jarid2 Methylation via the PRC2 Complex Regulates H3K27me3 Deposition during Cell Differentiation', *Mol Cell*, 57: 769-83.

Saramäki, O. R., T. L. Tammela, P. M. Martikainen, R. L. Vessella, and T. Visakorpi. 2006. 'The gene for polycomb group protein enhancer of zeste homolog 2 (EZH2) is amplified in late-stage prostate cancer', *Genes Chromosomes Cancer*, 45: 639-45.

Sarungbam, J., N. Agaram, S. Hwang, C. Lu, L. Wang, J. Healey, and M. Hameed. 2016. 'Symplastic/pseudoanaplastic giant cell tumor of the bone', *Skeletal Radiol*, 45: 929-35.

Sato, N., L. Meijer, L. Skaltsounis, P. Greengard, and A. H. Brivanlou. 2004. 'Maintenance of pluripotency in human and mouse embryonic stem cells through activation of Wnt signaling by a pharmacological GSK-3-specific inhibitor', *Nat Med*, 10: 55-63.

Sbirkov, Y., C. Kwok, A. Bhamra, A. J. Thompson, V. Gil, A. Zelent, and K. Petrie. 2017. 'Semi-Quantitative Mass Spectrometry in AML Cells Identifies New Non-Genomic Targets of the EZH2 Methyltransferase', *Int J Mol Sci*, 18.

Scelfo, A., A. Piunti, and D. Pasini. 2015. 'The controversial role of the Polycomb group proteins in transcription and cancer: how much do we not understand Polycomb proteins?', *FEBS J*, 282: 1703-22.

Schoenfelder, S., R. Sugar, A. Dimond, B. M. Javierre, H. Armstrong, B. Mifsud, E. Dimitrova, L. Matheson, F. Tavares-Cadete, M. Furlan-Magaril, A. Segonds-Pichon, W. Jurkowski, S. W. Wingett, K. Tabbada, S. Andrews, B. Herman, E. LeProust, C. S. Osborne, H. Koseki, P. Fraser, N. M. Luscombe, and S. Elderkin. 2015. 'Polycomb repressive complex PRC1 spatially constrains the mouse embryonic stem cell genome', *Nat Genet*, 47: 1179-86.

Schrode, N., N. Saiz, S. Di Talia, and A. K. Hadjantonakis. 2014. 'GATA6 levels modulate primitive endoderm cell fate choice and timing in the mouse blastocyst', *Dev Cell*, 29: 454-67.

Schuettengruber, B., H. M. Bourbon, L. Di Croce, and G. Cavalli. 2017. 'Genome Regulation by Polycomb and Trithorax: 70 Years and Counting', *Cell*, 171: 34-57.

Schwartz, L. H., S. Litière, E. de Vries, R. Ford, S. Gwyther, S. Mandrekar, L. Shankar, J. Bogaerts, A. Chen, J. Dancey, W. Hayes, F. S. Hodi, O. S. Hoekstra, E. P. Huang, N. Lin, Y. Liu, P. Therasse, J. D. Wolchok, and L. Seymour. 2016. 'RECIST 1.1-Update and clarification: From the RECIST committee', *Eur J Cancer*, 62: 132-7.

Schwartz, Y. B., and V. Pirrotta. 2013. 'A new world of Polycombs: unexpected partnerships and emerging functions', *Nat Rev Genet*, 14: 853-64.

Schwartzentruber, J., A. Korshunov, X. Y. Liu, D. T. Jones, E. Pfaff, K. Jacob, D. Sturm, A. M. Fontebasso, D. A. Quang, M. Tönjes, V. Hovestadt, S. Albrecht, M. Kool, A. Nantel, C. Konermann, A. Lindroth, N. Jäger, T. Rausch, M. Ryzhova, J. O. Korbel, T. Hielscher, P. Hauser, M. Garami, A. Klekner, L. Bognar, M. Ebinger, M. U. Schuhmann, W. Scheurlen, A. Pekrun, M. C. Frühwald, W. Roggendorf, C. Kramm, M. Dürken, J. Atkinson, P. Lepage, A. Montpetit, M. Zakrzewska, K. Zakrzewski, P. P. Liberski, Z. Dong, P. Siegel, A. E. Kulozik, M. Zapatka, A. Guha, D. Malkin, J. Felsberg, G.

Reifenberger, A. von Deimling, K. Ichimura, V. P. Collins, H. Witt, T. Milde, O. Witt, C. Zhang, P. Castelo-Branco, P. Lichter, D. Faury, U. Tabori, C. Plass, J. Majewski, S. M. Pfister, and N. Jabado. 2012. 'Driver mutations in histone H3.3 and chromatin remodelling genes in paediatric glioblastoma', *Nature*, 482: 226-31.

Score, J., C. Hidalgo-Curtis, A. V. Jones, N. Winkelmann, A. Skinner, D. Ward, K. Zoi, T. Ernst, F. Stegelmann, K. Döhner, A. Chase, and N. C. Cross. 2012. 'Inactivation of polycomb repressive complex 2 components in myeloproliferative and myelodysplastic/myeloproliferative neoplasms', *Blood*, 119: 1208-13.

Segditsas, S., and I. Tomlinson. 2006. 'Colorectal cancer and genetic alterations in the Wnt pathway', *Oncogene*, 25: 7531-7.

Sellers, K. J., I. A. Watson, R. E. Gresz, P. Raval, and D. P. Srivastava. 2018. 'Cyto-nuclear shuttling of afadin is required for rapid estradiol-mediated modifications of histone H3', *Neuropharmacology*, 143: 153-62.

Serio, R. N. 2014. 'Wnt of the two horizons: putting stem cell self-renewal and cell fate determination into context', *Stem Cells Dev*, 23: 1975-90.

Sexton, T., and G. Cavalli. 2015. 'The role of chromosome domains in shaping the functional genome', *Cell*, 160: 1049-59.

Shapiro, L., and W. I. Weis. 2009. 'Structure and biochemistry of cadherins and catenins', *Cold Spring Harb Perspect Biol*, 1: a003053.

Shen, X., W. Kim, Y. Fujiwara, M. D. Simon, Y. Liu, M. R. Mysliwiec, G. C. Yuan, Y. Lee, and S. H. Orkin. 2009. 'Jumonji modulates polycomb activity and self-renewal versus differentiation of stem cells', *Cell*, 139: 1303-14.

Shi, B., J. Liang, X. Yang, Y. Wang, Y. Zhao, H. Wu, L. Sun, Y. Zhang, Y. Chen, R. Li, Y. Zhang, M. Hong, and Y. Shang. 2007. 'Integration of estrogen and Wnt signaling circuits by the polycomb group protein EZH2 in breast cancer cells', *Mol Cell Biol*, 27: 5105-19.

Sineva, G. S., and V. A. Pospelov. 2014. 'beta-Catenin in pluripotency: adhering to self-renewal or Wnting to differentiate?', *Int Rev Cell Mol Biol*, 312: 53-78.

Singla, D. K., D. J. Schneider, M. M. LeWinter, and B. E. Sobel. 2006. 'wnt3a but not wnt11 supports self-renewal of embryonic stem cells', *Biochem Biophys Res Commun*, 345: 789-95.

Smith, A. G., and M. L. Hooper. 1987. 'Buffalo rat liver cells produce a diffusible activity which inhibits the differentiation of murine embryonal carcinoma and embryonic stem cells', *Dev Biol*, 121: 1-9.

Sneeringer, C. J., M. P. Scott, K. W. Kuntz, S. K. Knutson, R. M. Pollock, V. M. Richon, and R. A. Copeland. 2010. 'Coordinated activities of wild-type plus mutant EZH2 drive tumor-associated hypertrimethylation of lysine 27 on histone H3 (H3K27) in human B-cell lymphomas', *Proc Natl Acad Sci U S A*, 107: 20980-5.

Snijders, A. P., M. L. Hung, S. A. Wilson, and M. J. Dickman. 2010. 'Analysis of arginine and lysine methylation utilizing peptide separations at neutral pH and electron transfer dissociation mass spectrometry', *J Am Soc Mass Spectrom*, 21: 88-96.

Sokol, S. Y. 2011. 'Maintaining embryonic stem cell pluripotency with Wnt signaling', *Development*, 138: 4341-50.

Son, M. Y., H. Choi, Y. M. Han, and Y. S. Cho. 2013. 'Unveiling the critical role of REX1 in the regulation of human stem cell pluripotency', *Stem Cells*, 31: 2374-87.

Soncin, F., L. Mohamet, D. Eckardt, S. Ritson, A. M. Eastham, N. Bobola, A. Russell, S. Davies, R. Kemler, C. L. Merry, and C. M. Ward. 2009. 'Abrogation of E-cadherin-mediated cell-cell contact in mouse embryonic stem cells results in reversible LIF-independent self-renewal', *Stem Cells*, 27: 2069-80.

Song, H., Z. Yu, X. Sun, J. Feng, Q. Yu, H. Khan, X. Zhu, L. Huang, M. Li, M. T. S. Mok, A. S. L. Cheng, Y. Gao, and H. Feng. 2018. 'Androgen receptor drives hepatocellular carcinogenesis by activating enhancer of zeste homolog 2-mediated Wnt/β-catenin signaling', *EBioMedicine*, 35: 155-66.

Staal, F. J., F. Famili, L. Garcia Perez, and K. Pike-Overzet. 2016. 'Aberrant Wnt Signaling in Leukemia', *Cancers (Basel)*, 8.

Stazi, G., C. Zwergel, A. Mai, and S. Valente. 2017. 'EZH2 inhibitors: a patent review (2014-2016)', *Expert Opin Ther Pat*, 27: 797-813.

Steinhart, Z., and S. Angers. 2018. 'Wnt signaling in development and tissue homeostasis', *Development*, 145.

Stewart, S. A., D. M. Dykxhoorn, D. Palliser, H. Mizuno, E. Y. Yu, D. S. An, D. M. Sabatini, I. S. Chen, W. C. Hahn, P. A. Sharp, R. A. Weinberg, and C. D. Novina. 2003. 'Lentivirus-delivered stable gene silencing by RNAi in primary cells', *Rna*, 9: 493-501.

Stock, J. K., S. Giadrossi, M. Casanova, E. Brookes, M. Vidal, H. Koseki, N. Brockdorff, A. G. Fisher, and A. Pombo. 2007. 'Ring1-mediated ubiquitination of H2A restrains poised RNA polymerase II at bivalent genes in mouse ES cells', *Nat Cell Biol*, 9: 1428-35.

Su, I. H., A. Basavaraj, A. N. Krutchinsky, O. Hobert, A. Ullrich, B. T. Chait, and A. Tarakhovsky. 2003. 'Ezh2 controls B cell development through histone H3 methylation and Igh rearrangement', *Nat Immunol*, 4: 124-31.

Sudo, T., T. Utsunomiya, K. Mimori, H. Nagahara, K. Ogawa, H. Inoue, S. Wakiyama, H. Fujita, K. Shirouzu, and M. Mori. 2005. 'Clinicopathological significance of EZH2 mRNA expression in patients with hepatocellular carcinoma', *Br J Cancer*, 92: 1754-8.

Szemes, M., A. Greenhough, Z. Melegh, S. Malik, A. Yuksel, D. Catchpoole, K. Gallacher, M. Kollareddy, J. H. Park, and K. Malik. 2018. 'Wnt Signalling Drives Context-Dependent Differentiation or Proliferation in Neuroblastoma', *Neoplasia*, 20: 335-50.

Tabariès, S., A. McNulty, V. Ouellet, M. G. Annis, M. Dessureault, M. Vinette, Y. Hachem, B. Lavoie, A. Omeroglu, H. G. Simon, L. A. Walsh, S. Kimbung, I. Hedenfalk, and P. M. Siegel. 2019. 'Afadin cooperates with Claudin-2 to promote breast cancer metastasis', *Genes Dev*, 33: 180-93.

Takeuchi, T., Y. Yamazaki, Y. Katoh-Fukui, R. Tsuchiya, S. Kondo, J. Motoyama, and T. Higashinakagawa. 1995. 'Gene trap capture of a novel mouse gene, jumonji, required for neural tube formation', *Genes Dev*, 9: 1211-22.

Tavares, L., E. Dimitrova, D. Oxley, J. Webster, R. Poot, J. Demmers, K. Bezstarosti, S. Taylor, H. Ura, H. Koide, A. Wutz, M. Vidal, S. Elderkin, and N. Brockdorff. 2012. 'RYBP-PRC1 complexes mediate H2A ubiquitylation at polycomb target sites independently of PRC2 and H3K27me3', *Cell*, 148: 664-78.

Tee, W. W., and D. Reinberg. 2014. 'Chromatin features and the epigenetic regulation of pluripotency states in ESCs', *Development*, 141: 2376-90.

ten Berge, D., D. Kurek, T. Blauwkamp, W. Koole, A. Maas, E. Eroglu, R. K. Siu, and R. Nusse. 2011. 'Embryonic stem cells require Wnt proteins to prevent differentiation to epiblast stem cells', *Nat Cell Biol*, 13: 1070-5.

Tian, X., Z. Liu, B. Niu, J. Zhang, T. K. Tan, S. R. Lee, Y. Zhao, D. C. Harris, and G. Zheng. 2011. 'E-cadherin/β-catenin complex and the epithelial barrier', *J Biomed Biotechnol*, 2011: 567305.

Tomasetti, C., L. Marchionni, M. A. Nowak, G. Parmigiani, and B. Vogelstein. 2015. 'Only three driver gene mutations are required for the development of lung and colorectal cancers', *Proc Natl Acad Sci U S A*, 112: 118-23.

Turner, B. M. 2002. 'Cellular memory and the histone code', *Cell*, 111: 285-91.

Tyanova, S., T. Temu, A. Carlson, P. Sinitcyn, M. Mann, and J. Cox. 2015. 'Visualization of LC-MS/MS proteomics data in MaxQuant', *Proteomics*, 15: 1453-6.

Tyanova, S., T. Temu, P. Sinitcyn, A. Carlson, M. Y. Hein, T. Geiger, M. Mann, and J. Cox. 2016. 'The Perseus computational platform for comprehensive analysis of (prote)omics data', *Nat Methods*, 13: 731-40.

van Kruijsbergen, I., S. Hontelez, and G. J. Veenstra. 2015. 'Recruiting polycomb to chromatin', *Int J Biochem Cell Biol*, 67: 177-87.

van Mierlo, G., G. J. C. Veenstra, M. Vermeulen, and H. Marks. 2019. 'The Complexity of PRC2 Subcomplexes', *Trends Cell Biol*, 29: 660-71.

VanLeeuwen, J. E., I. Rafalovich, K. Sellers, K. A. Jones, T. N. Griffith, R. Huda, R. J. Miller, D. P. Srivastava, and P. Penzes. 2014. 'Coordinated nuclear and synaptic shuttling of afadin promotes spine plasticity and histone modifications', *J Biol Chem*, 289: 10831-42.

Varambally, S., S. M. Dhanasekaran, M. Zhou, T. R. Barrette, C. Kumar-Sinha, M. G. Sanda, D. Ghosh, K. J. Pienta, R. G. Sewalt, A. P. Otte, M. A. Rubin, and A. M. Chinnaiyan. 2002. 'The polycomb group protein EZH2 is involved in progression of prostate cancer', *Nature*, 419: 624-9.

Vasanthakumar, A., D. Xu, A. T. Lun, A. J. Kueh, K. P. van Gisbergen, N. Iannarella, X. Li, L. Yu, D. Wang, B. R. Williams, S. C. Lee, I. J. Majewski, D. I. Godfrey, G. K. Smyth, W. S. Alexander, M. J. Herold, A. Kallies, S. L. Nutt, and R. S. Allan. 2017. 'A non-canonical function of Ezh2 preserves immune homeostasis', *EMBO Rep*, 18: 619-31.

Vaswani, R. G., V. S. Gehling, L. A. Dakin, A. S. Cook, C. G. Nasveschuk, M. Duplessis, P. Iyer, S. Balasubramanian, F. Zhao, A. C. Good, R. Campbell, C. Lee, N. Cantone, R. T. Cummings, E. Normant, S. F. Bellon, B. K. Albrecht, J. C. Harmange, P. Trojer, J. E. Audia, Y. Zhang, N. Justin, S. Chen, J. R. Wilson, and S. J. Gamblin. 2016. 'Identification of (R)-N-((4-Methoxy-6-methyl-2-oxo-1,2-dihydropyridin-3-yl)methyl)-2-methyl-1-(1-(1-(2,2,2-trifluoroethyl)piperidin-4-yl)ethyl)-1H-indole-3-carboxamide (CPI-1205), a Potent and Selective Inhibitor of Histone Methyltransferase EZH2, Suitable for Phase I Clinical Trials for B-Cell Lymphomas', *J Med Chem*, 59: 9928-41.

Veeman, M. T., D. C. Slusarski, A. Kaykas, S. H. Louie, and R. T. Moon. 2003. 'Zebrafish prickle, a modulator of noncanonical Wnt/Fz signaling, regulates gastrulation movements', *Curr Biol*, 13: 680-5.

Veltri, A., C. Lang, and W. H. Lien. 2018. 'Concise Review: Wnt Signaling Pathways in Skin Development and Epidermal Stem Cells', *Stem Cells*, 36: 22-35.

Venkatesan, N., J. F. Wong, K. P. Tan, H. H. Chung, Y. H. Yau, E. Cukuroglu, A. Allahverdi, L. Nordenskiold, J. Goke, S. Geifman-Shochat, V. C. L. Lin, M. S. Madhusudhan, and I. H. Su. 2018. 'EZH2 promotes neoplastic transformation through VAV interaction-dependent extranuclear mechanisms', *Oncogene*, 37: 461-77.

Venkatesan, N., J. F. Wong, K. P. Tan, H. H. Chung, Y. H. Yau, E. Cukuroglu, A. Allahverdi, L. Nordenskiöld, J. Göke, S. Geifman-Shochat, V. C. L. Lin, M. S. Madhusudhan, and I. H. Su. 2018. 'EZH2 promotes neoplastic transformation through VAV interaction-dependent extranuclear mechanisms', *Oncogene*, 37: 461-77.

Verkaar, F., K. M. Cadigan, and R. van Amerongen. 2012. 'Celebrating 30 years of Wnt signaling', *Sci Signal*, 5: mr2.

Verma, S. K., X. Tian, L. V. LaFrance, C. Duquenne, D. P. Suarez, K. A. Newlander, S. P. Romeril, J. L. Burgess, S. W. Grant, J. A. Brackley, A. P. Graves, D. A. Scherzer, A. Shu, C. Thompson, H. M. Ott, G. S. Aller, C. A. Machutta, E. Diaz, Y. Jiang, N. W. Johnson, S. D. Knight, R. G. Kruger, M. T. McCabe, D. Dhanak, P. J. Tummino, C. L. Creasy, and W. H. Miller. 2012. 'Identification of Potent, Selective, Cell-Active Inhibitors of the Histone Lysine Methyltransferase EZH2', *ACS Med Chem Lett*, 3: 1091-6.

Vidal, M., and K. Starowicz. 2017. 'Polycomb complexes PRC1 and their function in hematopoiesis', *Exp Hematol*, 48: 12-31.

Vieux-Rochas, M., P. J. Fabre, M. Leleu, D. Duboule, and D. Noordermeer. 2015. 'Clustering of mammalian Hox genes with other H3K27me3 targets within an active nuclear domain', *Proc Natl Acad Sci U S A*, 112: 4672-7.

Virani, S., J. A. Colacino, J. H. Kim, and L. S. Rozek. 2012. 'Cancer epigenetics: a brief review', *Ilar j*, 53: 359-69.

Visvader, J. E., and G. J. Lindeman. 2012. 'Cancer stem cells: current status and evolving complexities', *Cell Stem Cell*, 10: 717-28.

Vogelstein, B., N. Papadopoulos, V. E. Velculescu, S. Zhou, L. A. Diaz, Jr., and K. W. Kinzler. 2013. 'Cancer genome landscapes', *Science*, 339: 1546-58.

Voigt, P., G. LeRoy, W. J. Drury, 3rd, B. M. Zee, J. Son, D. B. Beck, N. L. Young, B. A. Garcia, and D. Reinberg. 2012. 'Asymmetrically modified nucleosomes', *Cell*, 151: 181-93.

Voigt, P., W. W. Tee, and D. Reinberg. 2013. 'A double take on bivalent promoters', *Genes Dev*, 27: 1318-38.

Voncken, J. W., B. A. Roelen, M. Roefs, S. de Vries, E. Verhoeven, S. Marino, J. Deschamps, and M. van Lohuizen. 2003. 'Rnf2 (Ring1b) deficiency causes gastrulation arrest and cell cycle inhibition', *Proc Natl Acad Sci U S A*, 100: 2468-73.

Wagner, R. T., X. Xu, F. Yi, B. J. Merrill, and A. J. Cooney. 2010. 'Canonical Wnt/beta-catenin regulation of liver receptor homolog-1 mediates pluripotency gene expression', *Stem Cells*, 28: 1794-804.

Wan, Y. C. E., J. Liu, and K. M. Chan. 2018. 'Histone H3 Mutations in Cancer', *Curr Pharmacol Rep*, 4: 292-300.

Wang, G., W. W. Wu, Z. Zhang, S. Masilamani, and R. F. Shen. 2009. 'Decoy methods for assessing false positives and false discovery rates in shotgun proteomics', *Anal Chem*, 81: 146-59.

Wang, H., S. Ge, G. Qian, W. Li, J. Cui, G. Wang, A. R. Hoffman, and J. F. Hu. 2015. 'Restoration of IGF2 imprinting by polycomb repressive complex 2 docking factor SUZ12 in colon cancer cells', *Exp Cell Res*, 338: 214-21.

Wang, L., J. L. Brown, R. Cao, Y. Zhang, J. A. Kassis, and R. S. Jones. 2004. 'Hierarchical recruitment of polycomb group silencing complexes', *Mol Cell*, 14: 637-46.

Wang, R., J. Liang, H. Jiang, L. J. Qin, and H. T. Yang. 2008. 'Promoter-dependent EGFP expression during embryonic stem cell propagation and differentiation', *Stem Cells Dev*, 17: 279-89.

Wang, X., Y. Long, R. D. Paucek, A. R. Gooding, T. Lee, R. M. Burdorf, and T. R. Cech. 2019. 'Regulation of histone methylation by automethylation of PRC2', *Genes Dev*, 33: 1416-27.

Wang, X., R. D. Paucek, A. R. Gooding, Z. Z. Brown, E. J. Ge, T. W. Muir, and T. R. Cech. 2017. 'Molecular analysis of PRC2 recruitment to DNA in chromatin and its inhibition by RNA', *Nat Struct Mol Biol*, 24: 1028-38.

Wassef, M., and R. Margueron. 2017. 'The Multiple Facets of PRC2 Alterations in Cancers', *J Mol Biol*, 429: 1978-93.

Watanabe, K., and X. Dai. 2011. 'A WNTer revisit: new faces of β-catenin and TCFs in pluripotency', *Sci Signal*, 4: pe41.

Weinberg, D. N., C. D. Allis, and C. Lu. 2017. 'Oncogenic Mechanisms of Histone H3 Mutations', *Cold Spring Harb Perspect Med*, 7.

Weinberger, L., M. Ayyash, N. Novershtern, and J. H. Hanna. 2016. 'Dynamic stem cell states: naive to primed pluripotency in rodents and humans', *Nat Rev Mol Cell Biol*, 17: 155-69.

Weiner, A., D. Lara-Astiaso, V. Krupalnik, O. Gafni, E. David, D. R. Winter, J. H. Hanna, and I. Amit. 2016. 'Co-ChIP enables genome-wide mapping of histone mark co-occurrence at single-molecule resolution', *Nat Biotechnol*, 34: 953-61.

Weinstein, J. N., E. A. Collisson, G. B. Mills, K. R. Shaw, B. A. Ozenberger, K. Ellrott, I. Shmulevich, C. Sander, and J. M. Stuart. 2013. 'The Cancer Genome Atlas Pan-Cancer analysis project', *Nat Genet*, 45: 1113-20.

Wen, Y., J. Cai, Y. Hou, Z. Huang, and Z. Wang. 2017. 'Role of EZH2 in cancer stem cells: from biological insight to a therapeutic target', *Oncotarget*, 8: 37974-90.

Wolf, D., M. Rodova, E. A. Miska, J. P. Calvet, and T. Kouzarides. 2002. 'Acetylation of beta-catenin by CREB-binding protein (CBP)', *J Biol Chem*, 277: 25562-7.

Wood, L. D., D. W. Parsons, S. Jones, J. Lin, T. Sjöblom, R. J. Leary, D. Shen, S. M. Boca, T. Barber, J. Ptak, N. Silliman, S. Szabo, Z. Dezso, V. Ustyanksky, T. Nikolskaya, Y. Nikolsky, R. Karchin, P. A. Wilson, J. S. Kaminker, Z. Zhang, R. Croshaw, J. Willis, D. Dawson, M. Shipitsin, J. K. Willson, S. Sukumar, K. Polyak, B. H. Park, C. L. Pethiyagoda, P. V. Pant, D. G. Ballinger, A. B. Sparks, J. Hartigan, D. R. Smith, E. Suh, N. Papadopoulos, P. Buckhaults, S. D. Markowitz, G. Parmigiani, K. W. Kinzler, V. E. Velculescu, and B. Vogelstein. 2007. 'The genomic landscapes of human breast and colorectal cancers', *Science*, 318: 1108-13.

Worsdorfer, P., S. Maxeiner, C. Markopoulos, G. Kirfel, V. Wulf, T. Auth, S. Urschel, J. von Maltzahn, and K. Willecke. 2008. 'Connexin expression and functional analysis of gap junctional communication in mouse embryonic stem cells', *Stem Cells*, 26: 431-9.

Wray, J., T. Kalkan, S. Gomez-Lopez, D. Eckardt, A. Cook, R. Kemler, and A. Smith. 2011. 'Inhibition of glycogen synthase kinase-3 alleviates Tcf3 repression of the pluripotency network and increases embryonic stem cell resistance to differentiation', *Nat Cell Biol*, 13: 838-45.

Wu, G., A. Broniscer, T. A. McEachron, C. Lu, B. S. Paugh, J. Becksfort, C. Qu, L. Ding, R. Huether, M. Parker, J. Zhang, A. Gajjar, M. A. Dyer, C. G. Mullighan, R. J. Gilbertson, E. R. Mardis, R. K. Wilson, J. R. Downing, D. W. Ellison, J. Zhang, and S. J. Baker. 2012. 'Somatic histone H3 alterations in pediatric diffuse intrinsic pontine gliomas and non-brainstem glioblastomas', *Nat Genet*, 44: 251-3.

Wu, H., H. Zeng, A. Dong, F. Li, H. He, G. Senisterra, A. Seitova, S. Duan, P. J. Brown, M. Vedadi, C. H. Arrowsmith, and M. Schapira. 2013. 'Structure of the catalytic domain of EZH2 reveals conformational plasticity in cofactor and substrate binding sites and explains oncogenic mutations', *PLoS One*, 8: e83737.

Wu, X., J. V. Johansen, and K. Helin. 2013. 'Fbxl10/Kdm2b recruits polycomb repressive complex 1 to CpG islands and regulates H2A ubiquitylation', *Mol Cell*, 49: 1134-46.

Xu, B., D. M. On, A. Ma, T. Parton, K. D. Konze, S. G. Pattenden, D. F. Allison, L. Cai, S. Rockowitz, S. Liu, Y. Liu, F. Li, M. Vedadi, S. V. Frye, B. A. Garcia, D. Zheng, J. Jin, and G. G. Wang. 2015. 'Selective inhibition of EZH2 and EZH1 enzymatic activity by a small molecule suppresses MLL-rearranged leukemia', *Blood*, 125: 346-57.

Xu, K., Z. J. Wu, A. C. Groner, H. H. He, C. Cai, R. T. Lis, X. Wu, E. C. Stack, M. Loda, T. Liu, H. Xu, L. Cato, J. E. Thornton, R. I. Gregory, C. Morrissey, R. L. Vessella, R. Montironi, C. Magi-Galluzzi, P. W. Kantoff, S. P. Balk, X. S. Liu, and M. Brown. 2012. 'EZH2 oncogenic activity in castration-resistant prostate cancer cells is Polycomb-independent', *Science*, 338: 1465-9.

Xu, Y., R. Chang, Z. Peng, Y. Wang, W. Ji, J. Guo, L. Song, C. Dai, W. Wei, Y. Wu, X. Wan, C. Shao, and L. Zhan. 2015. 'Loss of polarity protein AF6 promotes pancreatic cancer metastasis by inducing Snail expression', *Nat Commun*, 6: 7184.

Xu, Z., A. M. Robitaille, J. D. Berndt, K. C. Davidson, K. A. Fischer, J. Mathieu, J. C. Potter, H. Ruohola-Baker, and R. T. Moon. 2016. 'Wnt/β-catenin signaling promotes self-renewal and inhibits the primed state transition in naïve human embryonic stem cells', *Proc Natl Acad Sci U S A*, 113: E6382-e90.

Yamagishi, Makoto, Makoto Hori, Dai Fujikawa, Daisuke Honma, Nobuaki Adachi, Takeo Ohsugi, Kazumi Nakano, Makoto Nakashima, Seiichiro Kobayashi, Masako Iwanaga, Atae Utsunomiya, Seiji Okada, Kunihiro Tsukasaki, Kensei Tobinai, Kazushi Araki, Toshiki Watanabe, and Kaoru Uchimaru. 2016. 'Development and Molecular Analysis

of Synthetic Lethality By Targeting EZH1 and EZH2 in Non-Hodgkin Lymphomas', *Blood*, 128: 462-62.

Yan, J., B. Dutta, Y. T. Hee, and W. J. Chng. 2019. 'Towards understanding of PRC2 binding to RNA', *RNA Biol*, 16: 176-84.

Yan, J., B. Li, B. Lin, P. T. Lee, T. H. Chung, J. Tan, C. Bi, X. T. Lee, V. Selvarajan, S. B. Ng, H. Yang, Q. Yu, and W. J. Chng. 2016. 'EZH2 phosphorylation by JAK3 mediates a switch to noncanonical function in natural killer/T-cell lymphoma', *Blood*, 128: 948-58.

Yan, J., S. B. Ng, J. L. Tay, B. Lin, T. L. Koh, J. Tan, V. Selvarajan, S. C. Liu, C. Bi, S. Wang, S. N. Choo, N. Shimizu, G. Huang, Q. Yu, and W. J. Chng. 2013. 'EZH2 overexpression in natural killer/T-cell lymphoma confers growth advantage independently of histone methyltransferase activity', *Blood*, 121: 4512-20.

Yap, D. B., J. Chu, T. Berg, M. Schapira, S. W. Cheng, A. Moradian, R. D. Morin, A. J. Mungall, B. Meissner, M. Boyle, V. E. Marquez, M. A. Marra, R. D. Gascoyne, R. K. Humphries, C. H. Arrowsmith, G. B. Morin, and S. A. Aparicio. 2011. 'Somatic mutations at EZH2 Y641 act dominantly through a mechanism of selectively altered PRC2 catalytic activity, to increase H3K27 trimethylation', *Blood*, 117: 2451-9.

Ying, Q. L., M. Stavridis, D. Griffiths, M. Li, and A. Smith. 2003. 'Conversion of embryonic stem cells into neuroectodermal precursors in adherent monoculture', *Nat Biotechnol*, 21: 183-6.

Yu, J. R., C. H. Lee, O. Oksuz, J. M. Stafford, and D. Reinberg. 2019. 'PRC2 is high maintenance', *Genes Dev*, 33: 903-35.

Yu, W., L. Yang, T. Li, and Y. Zhang. 2019. 'Cadherin Signaling in Cancer: Its Functions and Role as a Therapeutic Target', *Front Oncol*, 9: 989.

Yuan, W., M. Xu, C. Huang, N. Liu, S. Chen, and B. Zhu. 2011. 'H3K36 methylation antagonizes PRC2-mediated H3K27 methylation', *J Biol Chem*, 286: 7983-9.

Zhan, T., N. Rindtorff, and M. Boutros. 2017. 'Wnt signaling in cancer', *Oncogene*, 36: 1461-73.

Zhang, H., M. J. Zeitz, H. Wang, B. Niu, S. Ge, W. Li, J. Cui, G. Wang, G. Qian, M. J. Higgins, X. Fan, A. R. Hoffman, and J. F. Hu. 2014. 'Long noncoding RNA-mediated intrachromosomal interactions promote imprinting at the Kcnq1 locus', *J Cell Biol*, 204: 61-75.

Zhang, J., L. Ding, L. Holmfeldt, G. Wu, S. L. Heatley, D. Payne-Turner, J. Easton, X. Chen, J. Wang, M. Rusch, C. Lu, S. C. Chen, L. Wei, J. R. Collins-Underwood, J. Ma, K. G. Roberts, S. B. Pounds, A. Ulyanov, J. Becksfort, P. Gupta, R. Huether, R. W. Kriwacki, M. Parker, D. J. McGoldrick, D. Zhao, D. Alford, S. Espy, K. C. Bobba, G. Song, D. Pei, C. Cheng, S. Roberts, M. I. Barbato, D. Campana, E. Coustan-Smith, S. A. Shurtleff, S. C. Raimondi, M. Kleppe, J. Cools, K. A. Shimano, M. L. Hermiston, S. Doulatov, K. Eppert, E. Laurenti, F. Notta, J. E. Dick, G. Basso, S. P. Hunger, M. L. Loh, M. Devidas, B. Wood, S. Winter, K. P. Dunsmore, R. S. Fulton, L. L. Fulton, X. Hong, C. C. Harris, D. J. Dooling, K. Ochoa, K. J. Johnson, J. C. Obenauer, W. E. Evans, C. H. Pui, C. W. Naeve, T. J. Ley, E. R. Mardis, R. K. Wilson, J. R. Downing, and C. G. Mullighan. 2012. 'The genetic basis of early T-cell precursor acute lymphoblastic leukaemia', *Nature*, 481: 157-63.

Zhang, M., Y. Wang, S. Jones, M. Sausen, K. McMahon, R. Sharma, Q. Wang, A. J. Belzberg, K. Chaichana, G. L. Gallia, Z. L. Gokaslan, G. J. Riggins, J. P. Wolinksy, L. D. Wood, E. A. Montgomery, R. H. Hruban, K. W. Kinzler, N. Papadopoulos, B. Vogelstein, and C. Bettegowda. 2014. 'Somatic mutations of SUZ12 in malignant peripheral nerve sheath tumors', *Nat Genet*, 46: 1170-2.

Zhang, T., S. Cooper, and N. Brockdorff. 2015. 'The interplay of histone modifications - writers that read', *EMBO Rep*, 16: 1467-81.

Zhang, X., Y. Chen, Y. Ye, J. Wang, H. Wang, G. Yuan, Z. Lin, Y. Wu, Y. Zhang, and X. Lin. 2017. 'Wnt signaling promotes hindgut fate commitment through regulating multi-lineage genes during hESC differentiation', *Cell Signal*, 29: 12-22.

Zhang, X., and X. He. 2013. 'PAF makes it EZ(H2) for β-catenin transactivation', *Mol Cell*, 52: 157-8.

Zhang, Z., A. Jones, C. W. Sun, C. Li, C. W. Chang, H. Y. Joo, Q. Dai, M. R. Mysliwiec, L. C. Wu, Y. Guo, W. Yang, K. Liu, K. M. Pawlik, H. Erdjument-Bromage, P. Tempst, Y. Lee, J. Min, T. M. Townes, and H. Wang. 2011. 'PRC2 complexes with JARID2, MTF2, and esPRC2p48 in ES cells to modulate ES cell pluripotency and somatic cell reprogramming', *Stem Cells*, 29: 229-40.

Zhao, J., T. K. Ohsumi, J. T. Kung, Y. Ogawa, D. J. Grau, K. Sarma, J. J. Song, R. E. Kingston, M. Borowsky, and J. T. Lee. 2010. 'Genome-wide identification of polycomb-associated RNAs by RIP-seq', *Mol Cell*, 40: 939-53.

Zhao, J., B. K. Sun, J. A. Erwin, J. J. Song, and J. T. Lee. 2008. 'Polycomb proteins targeted by a short repeat RNA to the mouse X chromosome', *Science*, 322: 750-6.

Zhao, Y., and O. N. Jensen. 2009. 'Modification-specific proteomics: strategies for characterization of post-translational modifications using enrichment techniques', *Proteomics*, 9: 4632-41.

Zheng, H., B. Huang, B. Zhang, Y. Xiang, Z. Du, Q. Xu, Y. Li, Q. Wang, J. Ma, X. Peng, F. Xu, and W. Xie. 2016. 'Resetting Epigenetic Memory by Reprogramming of Histone Modifications in Mammals', *Mol Cell*, 63: 1066-79.

Zhu, P., Y. Wang, G. Huang, B. Ye, B. Liu, J. Wu, Y. Du, L. He, and Z. Fan. 2016. 'lnc-beta-Catm elicits EZH2-dependent beta-catenin stabilization and sustains liver CSC self-renewal', *Nat Struct Mol Biol*, 23: 631-9.

Zingg, D., J. Debbache, S. M. Schaefer, E. Tuncer, S. C. Frommel, P. Cheng, N. Arenas-Ramirez, J. Haeusel, Y. Zhang, M. Bonalli, M. T. McCabe, C. L. Creasy, M. P. Levesque, O. Boyman, R. Santoro, O. Shakhova, R. Dummer, and L. Sommer. 2015. 'The epigenetic modifier EZH2 controls melanoma growth and metastasis through silencing of distinct tumour suppressors', *Nat Commun*, 6: 6051.

Żylicz, J. J., A. Bousard, K. Žumer, F. Dossin, E. Mohammad, S. T. da Rocha, B. Schwalb, L. Syx, F. Dingli, D. Loew, P. Cramer, and E. Heard. 2019. 'The Implication of Early Chromatin Changes in X Chromosome Inactivation', *Cell*, 176: 182-97.e23.

Appendices

Buffers

FACS collection buffer;

Phosphate buffered saline supplemented with 10% fetal calf serum, 100U/ml penicillin/100μg/ml streptomycin; filtered 45μM prior to use

FACS sort buffer;

Phosphate buffered saline supplemented with 1% fetal calf serum, 1mM EDTA, 25mM HEPES pH 7.6; filtered 45μM prior to use

Fractionation buffer;

10mM HEPES, 10mM KCl, 1.5mM MgCl2, 0.34M sucrose, 10%v/v glycerol, 1mM DTT, 0.1% v/v TRITON X-100, 1x cOmplete protease inhibitor cocktail

Immunofluorescence Blocking buffer;

Phosphate buffered saline supplemented with 2.5% w/v bovine serum albumin fraction V, 0.05% TWEEN20, and 10% fetal calf serum

Immunofluorescence Permiabilisation buffer;

Phosphate buffered saline supplemented with 0.2% TRITON X-100

Immunofluorescence wash buffer;

Phosphate buffered saline supplemented with 0.2%w/v BSA fraction V + 0.05%v/v TWEEN 20

Laemmli buffer;

2% w/v sodium dodecyl sulphate (SDS), 10% v/v glycerol, 0.002% bromophenol blue, 0.06M TRIS HCl pH 6.8, 5%v/v 2-mercaptoethanol

Mass spectrometry wash buffer;

20mM HEPES pH7.6, 150mmol NaCl, 1.5mM $MgCl_2$ 0.2mM EDTA, 0.02% NP40 alternate

Mass spectrometry elution buffer;

100mM Glycine, pH2.3 (Adjusted with 1M hydrochloric acid)

Mass spectrometry denaturing buffer;

80mM TRIS HCl (pH 6.8), 2%w/v SDS, 100mM DTT

Tris buffered saline (TBS);

50mM TRIS HCL (pH 7.5), 150mM sodium chloride

TBST;

50mM TRIS HCL (pH 7.5), 150mM sodium chloride, 0.1%v/v TWEEN20

Protein Identification	Gene Identification	Mean WT intensity	Mean Jarid-/- intensity	Relative intensity	Lo2 relative intensity	P-value	log10-p
Zinc finger protein AEBP2	Aebp2	3.82E+06	2.68E+08	0.014	-6.133	0.033	1.483
Polycomb protein Suz12	Suz12	4.42E+07	1.21E+09	0.036	-4.779	0.000	4.314
Doublesex- and mab-3-related transcription factor 1	Dmrt1	3.37E+07	3.25E+08	0.104	-3.271	0.043	1.367
Poly [ADP-ribose] polymerase 12	Parp12	1.82E+07	1.63E+08	0.112	-3.161	0.001	3.105
Plaktophilin 2	Pkp2	7.39E+07	5.86E+08	0.126	-2.987	0.021	1.668
Y-box-binding protein 2	Ybx2	1.20E+07	8.79E+07	0.136	-2.877	0.014	1.847
BAG family molecular chaperone regulator 5	Bag5	2.36E+07	1.57E+08	0.150	-2.735	0.043	1.370
DNA repair protein RAD50	Rad50	6.18E+07	3.43E+08	0.180	-2.474	0.034	1.465
Ubiquitin carboxyl-terminal hydrolase 22	Usp22	2.24E+07	1.22E+08	0.184	-2.444	0.015	1.821
E3 ubiquitin-protein ligase TRIM21	Trim21	2.89E+07	1.48E+08	0.195	-2.356	0.006	2.200
Ribonuclease P protein subunit p20	Pop7	6.46E+06	2.92E+07	0.222	-2.174	0.048	1.319
Histone-lysine N-methyltransferase EZH2	Ezh2	1.20E+08	5.27E+08	0.228	-2.130	0.000	3.429
Transcription elongation factor, mitochondrial	Tefm	1.19E+08	4.75E+08	0.250	-1.998	0.004	2.402
39S ribosomal protein L45, mitochondrial	Mrpl45	2.17E+07	8.30E+07	0.261	-1.936	0.045	1.348
Notchless protein homolog 1	Nle1	2.32E+07	8.74E+07	0.265	-1.915	0.047	1.329
Protein SOX-15	Sox15	1.07E+07	4.01E+07	0.267	-1.903	0.018	1.739
Coiled-coil domain-containing protein 160	Ccdc160	8.37E+07	2.93E+08	0.286	-1.805	0.004	2.399
Pre-mRNA-splicing factor SLU7	Slu7	1.40E+08	4.85E+08	0.288	-1.794	0.017	1.769
39S ribosomal protein L12, mitochondrial	Mrpl12	2.12E+08	7.25E+08	0.292	-1.777	0.006	2.250
39S ribosomal protein L10, mitochondrial	Mrpl10	4.60E+07	1.57E+08	0.292	-1.774	0.007	2.149
POZ/BTB and AT hook containing zinc-finger protein	Patz1	4.21E+07	1.37E+08	0.308	-1.698	0.013	1.891
Probable ATP-dependent RNA helicase DDX10	Ddx10	2.06E+08	6.69E+08	0.309	-1.697	0.008	2.113
ATP-dependent RNA helicase DHX8	Dhx8	5.91E+08	1.86E+09	0.318	-1.651	0.016	1.795
Methenyltetrahydrofolate synthase domain-containing protein	Mthfsd	8.86E+07	2.74E+08	0.323	-1.632	0.027	1.569
Receptor expression-enhancing protein	Reep2	9.63E+06	2.87E+07	0.336	-1.574	0.039	1.404
Aspartate--tRNA ligase, mitochondrial	Dars2	1.29E+07	3.58E+07	0.361	-1.471	0.002	2.789
Double-strand break repair protein MRE11A	Mre11a	2.24E+08	6.18E+08	0.363	-1.463	0.040	1.403
Complement component 1 Q subcomponent-binding protein	C1qbp	4.03E+09	1.10E+10	0.367	-1.447	0.015	1.819
Envoplakin	Evpl	2.07E+07	5.52E+07	0.375	-1.416	0.037	1.427
Tuftelin	Tuft1	1.76E+08	4.54E+08	0.388	-1.367	0.014	1.867
Monocarboxylate transporter 4	Slc16a3	5.49E+07	1.41E+08	0.390	-1.358	0.002	2.616
ELAV-like protein 2	Elavl2	1.37E+08	3.50E+08	0.391	-1.356	0.024	1.614
U3 small nucleolar RNA-associated protein 14 homolog A	Utp14a	6.22E+08	1.58E+09	0.394	-1.345	0.006	2.228
Titin	Ttn	6.59E+08	1.65E+09	0.400	-1.323	0.006	2.257
Caspase activity and apoptosis inhibitor 1	Caap1	5.65E+07	1.36E+08	0.414	-1.272	0.014	1.865
Protein lin-28 homolog A	Lin28a	2.04E+09	4.91E+09	0.416	-1.264	0.002	2.814
Serine/threonine-protein phosphatase 4 regulatory subunit 3B	Smek2	5.05E+06	1.21E+07	0.419	-1.255	0.003	2.501
BMS1 ribosome biogenesis protein	Bms1	5.73E+08	1.36E+09	0.421	-1.248	0.036	1.449
PIN2/TERF1-interacting telomerase inhibitor 1	Pinx1	7.92E+07	1.85E+08	0.428	-1.225	0.000	3.511
39S ribosomal protein L44, mitochondrial	Mrpl44	4.28E+07	9.91E+07	0.431	-1.213	0.035	1.452
Protein unc-80 homolog	Unc80	2.84E+08	6.45E+08	0.441	-1.181	0.003	2.468
Peptidyl-tRNA hydrolase ICT1, mitochondrial	Ict1	8.58E+07	1.89E+08	0.454	-1.139	0.038	1.423
Serine/threonine-protein phosphatase 6 regulatory subunit 3	Ppp6r3	1.44E+08	3.17E+08	0.455	-1.135	0.044	1.358
AF4/FMR2 family member 4	Aff4	3.39E+08	7.43E+08	0.456	-1.132	0.047	1.332
Caprin-2	Caprin2	2.34E+07	5.11E+07	0.459	-1.124	0.013	1.898
BAG family molecular chaperone regulator 4	Bag4	2.51E+07	5.42E+07	0.463	-1.110	0.038	1.426
Pre-mRNA-splicing factor CWC25 homolog	Cwc25	1.09E+08	2.32E+08	0.470	-1.088	0.007	2.175
Transmembrane protein 201	Tmem201	1.48E+07	3.13E+07	0.473	-1.080	0.008	2.083
pre-rRNA processing protein FTSJ3	Ftsj3	3.09E+09	6.47E+09	0.477	-1.069	0.040	1.398
Transcription elongation factor SPT6	Supt6h	4.22E+08	8.82E+08	0.478	-1.064	0.007	2.171
Pericentriolar material 1 protein	Pcm1	7.23E+08	1.48E+09	0.488	-1.036	0.004	2.357
Forkhead box K1	Foxk1	1.12E+08	2.29E+08	0.488	-1.035	0.012	1.934
Multiple myeloma tumor-associated protein 2 homolog	Mmtag2	1.63E+08	3.33E+08	0.489	-1.032	0.014	1.843
Signal recognition particle 14 kDa protein	Srp14	2.79E+08	5.68E+08	0.490	-1.029	0.004	2.409
Centrosomal protein of 131 kDa	Cep131	2.32E+08	4.72E+08	0.490	-1.028	0.026	1.592
39S ribosomal protein L1, mitochondrial	Mrpl1	1.75E+08	3.54E+08	0.494	-1.017	0.018	1.743
Protein FAM195B	Fam195b	1.01E+08	2.03E+08	0.496	-1.013	0.040	1.399
A-kinase anchor protein 1	Akap1	4.90E+08	9.88E+08	0.496	-1.011	0.030	1.530

Supplementary table 1. Proteins identified as significantly reduced in Afadin co-immunoprecipitation experiments in the absence of Jarid2.

Afadin co-immunoprecipitates from Jarid2-null mESCs relative to immunoprecipitates from wild-type mESCs. Proteins with >2 fold decrease in abundance, and p value <0.05.

Plasmids

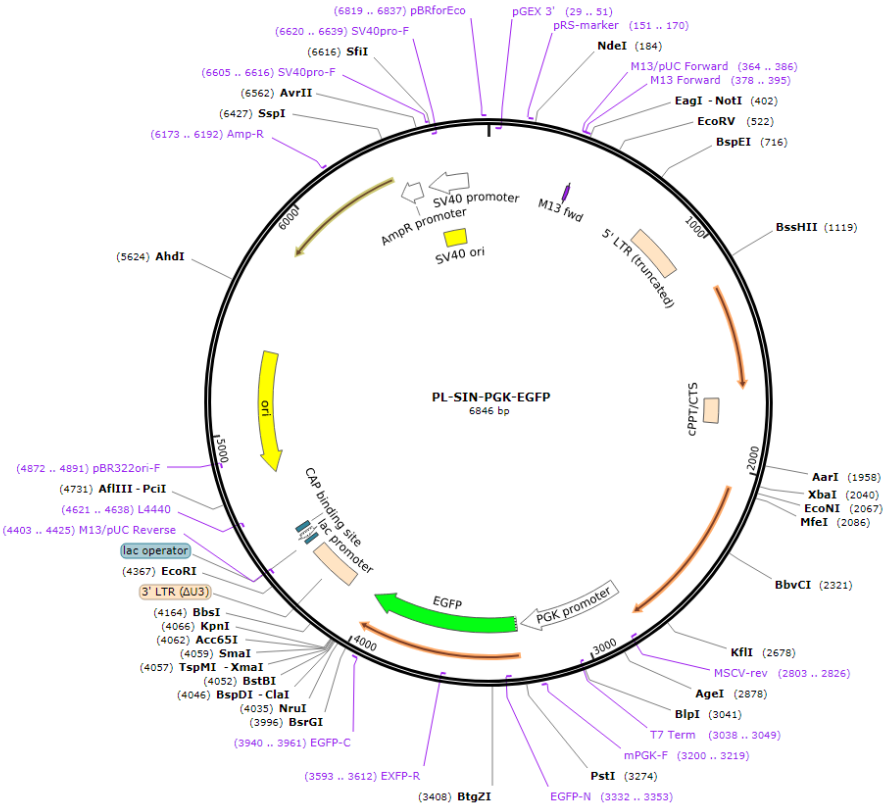
PL-SIN-PGK-EGFP
6846 bp
(6819 .. 6837) pBRforEco
pGEX 3' (29 .. 51)
(6620 .. 6639) SV40pro-F
pRS-marker (151 .. 170)
(6616) SfiI
NdeI (184)
(6605 .. 6616) SV40pro-F
M13/pUC Forward (364 .. 386)
M13 Forward (378 .. 395)
(6562) AvrII
EagI - NotI (402)
(6427) SspI
EcoRV (522)
(6173 .. 6192) Amp-R
BspEI (716)
BssHII (1119)
(5624) AhdI
AarI (1958)
XbaI (2040)
EcoNI (2067)
MfeI (2086)
BbvCI (2321)
KflI (2678)
MSCV-rev (2803 .. 2826)
AgeI (2878)
BlpI (3041)
T7 Term (3038 .. 3049)
mPGK-F (3200 .. 3219)
PstI (3274)
EGFP-N (3332 .. 3353)
(3408) BtgZI
(3593 .. 3612) EXFP-R
(3940 .. 3961) EGFP-C
(4164) BbsI
(4066) KpnI
(4062) Acc65I
(4059) SmaI
(4057) TspMI - XmaI
(4052) BstBI
(4046) BspDI - ClaI
(4035) NruI
(3996) BsrGI
(4403 .. 4425) M13/pUC Reverse
(4621 .. 4638) L4440
(4731) AflIII - PciI
(4872 .. 4891) pBR322ori-F
lac operator
(4367) EcoRI
3' LTR (ΔU3)
SV40 promoter
AmpR promoter
SV40 ori
M13 fwd
5' LTR (truncated)
cPPT/CTS
ori
CAP binding site
lac promoter
EGFP
PGK promoter
1000
2000
3000
4000
5000
6000

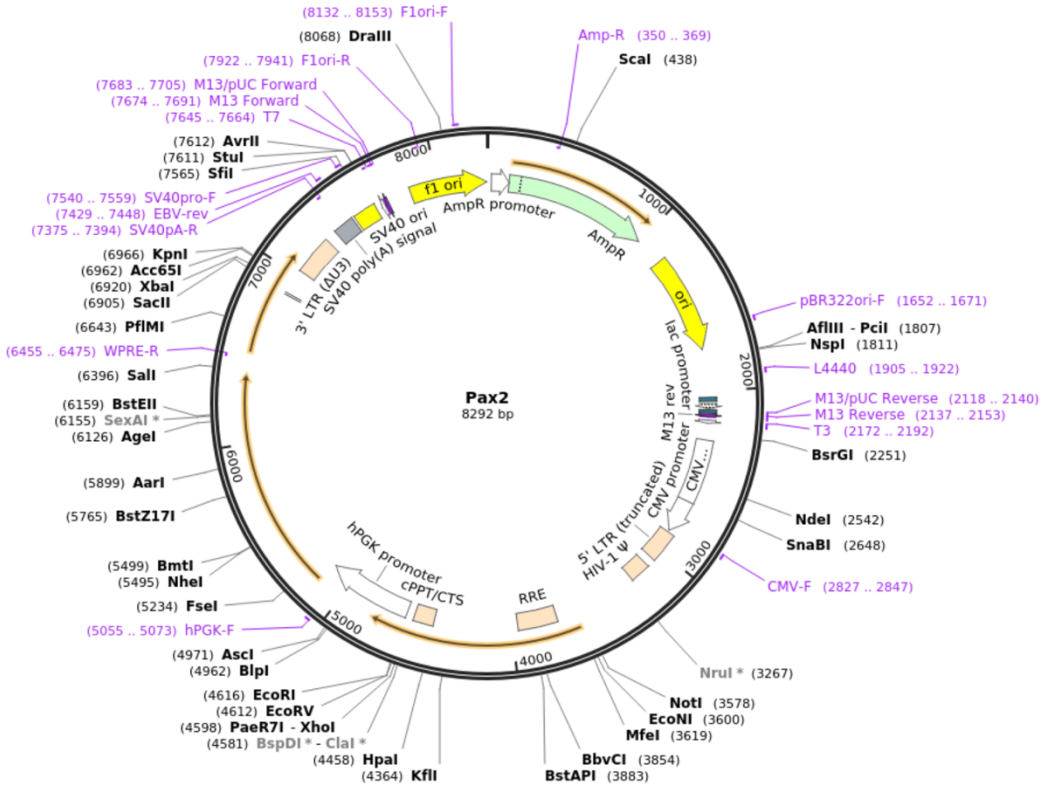
Pax2
8292 bp
(8132 .. 8153) F1ori-F
(8068) DraIII
Amp-R (350 .. 369)
ScaI (438)
(7922 .. 7941) F1ori-R
(7683 .. 7705) M13/pUC Forward
(7674 .. 7691) M13 Forward
(7645 .. 7664) T7
(7612) AvrII
(7611) StuI
(7565) SfiI
(7540 .. 7559) SV40pro-F
(7429 .. 7448) EBV-rev
(7375 .. 7394) SV40pA-R
(6966) KpnI
(6962) Acc65I
(6920) XbaI
(6905) SacII
(6643) PflMI
(6455 .. 6475) WPRE-R
(6396) SalI
(6159) BstEII
(6155) SexAI *
(6126) AgeI
(5899) AarI
(5765) BstZ17I
(5499) BmtI
(5495) NheI
(5234) FseI
(5055 .. 5073) hPGK-F
(4971) AscI
(4962) BlpI
(4616) EcoRI
(4612) EcoRV
(4598) PaeR7I - XhoI
(4581) BspDI * - ClaI *
(4458) HpaI
(4364) KflI
BbvCI (3854)
BstAPI (3883)
MfeI (3619)
EcoNI (3600)
NotI (3578)
NruI * (3267)
CMV-F (2827 .. 2847)
SnaBI (2648)
NdeI (2542)
BsrGI (2251)
T3 (2172 .. 2192)
M13 Reverse (2137 .. 2153)
M13/pUC Reverse (2118 .. 2140)
L4440 (1905 .. 1922)
NspI (1811)
AflIII - PciI (1807)
pBR322ori-F (1652 .. 1671)
f1 ori
AmpR promoter
AmpR
ori
lac promoter
M13 rev
CMV promoter
5' LTR (truncated) HIV-1 ψ
RRE
hPGK promoter
cPPT/CTS
SV40 ori
SV40 poly(A) signal
3' LTR (ΔU3)
1000
2000
3000
4000
5000
6000
7000
8000

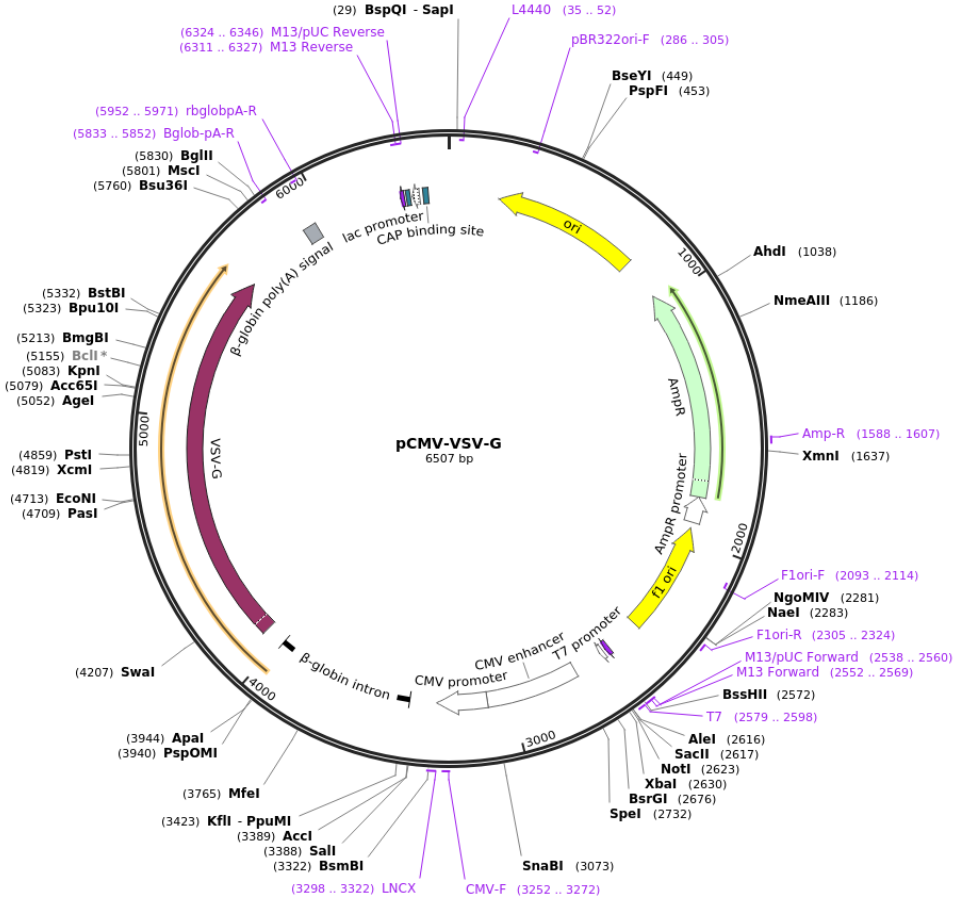
pCMV-VSV-G
6507 bp
(29) BspQI - SapI
L4440 (35 .. 52)
pBR322ori-F (286 .. 305)
BseYI (449)
PspFI (453)
AhdI (1038)
NmeAIII (1186)
Amp-R (1588 .. 1607)
XmnI (1637)
F1ori-F (2093 .. 2114)
NgoMIV (2281)
NaeI (2283)
F1ori-R (2305 .. 2324)
M13/pUC Forward (2538 .. 2560)
M13 Forward (2552 .. 2569)
BssHII (2572)
T7 (2579 .. 2598)
AleI (2616)
SacII (2617)
NotI (2623)
XbaI (2630)
BsrGI (2676)
SpeI (2732)
SnaBI (3073)
CMV-F (3252 .. 3272)
(3298 .. 3322) LNCX
(3322) BsmBI
(3388) SalI
(3389) AccI
(3423) KflI - PpuMI
(3765) MfeI
(3940) PspOMI
(3944) ApaI
(4207) SwaI
(4709) PasI
(4713) EcoNI
(4819) XcmI
(4859) PstI
(5052) AgeI
(5079) Acc65I
(5083) KpnI
(5155) BclI*
(5213) BmgBI
(5323) Bpu10I
(5332) BstBI
(5760) Bsu36I
(5801) MscI
(5830) BglII
(5833 .. 5852) Bglob-pA-R
(5952 .. 5971) rbglobpA-R
(6311 .. 6327) M13 Reverse
(6324 .. 6346) M13/pUC Reverse
lac promoter
CAP binding site
ori
AmpR
AmpR promoter
f1 ori
T7 promoter
CMV enhancer
CMV promoter
β-globin intron
β-globin poly(A) signal
VSV-G
1000
2000
3000
4000
5000
6000


M50 Super 8x TOPFlash
4984 bp
Kpnl (0)
Eco53kI (4)
SacI (6)
AscI - BssHII (117)
NheI (129)
BmtI (133)
TspMI - XmaI (134)
SmaI - SrfI (136)
PaeR7I - XhoI (140)
BglII (144)
EcoRI (179)
HindIII (214)
NcoI - StyI (247)
KasI (281)
NarI (282)
SfoI (283)
PluTI (285)
LucNrev (315 .. 333)
PfoI * (356)
BstBI (418)
BsrGI (739)
BclI * (829)
SphI (912)
XcmI (984)
EcoO109I - PpuMI (1428)
SgrAI (1677)
FseI (1922)
EBV-rev (1953 .. 1972)
SV40pA-R (2007 .. 2026)
HpaI (2063)
BsaBI * (2164)
BamHI (2165)
SalI (2171)
AccI (2172)
PshAI (2236)
AfeI (2297)
L4440 (2311 .. 2328)
PciI (2421)
(2562 .. 2581) pBR322ori-F
(2837) AlwNI
(3314) AhdI
(3375) BsaI
(3462) NmeAIII
(3486) AseI
(3864 .. 3883) Amp-R
(3913) XmnI
(4320 .. 4339) F1ori-R
(4458) BtgZI
(4463) BsaAI
(4466) DraIII
(4530 .. 4551) F1ori-F
(4812) NotI
(4921 .. 4940) RVprimer3
(4970) BsgI
(4980) Acc65I
pause site
minP
Kozak sequence
luciferase
SV40 poly(A) signal
ori
AmpR promoter
AmpR
f1 ori
500
1000
1500
2000
2500
3000
3500
4000
4500

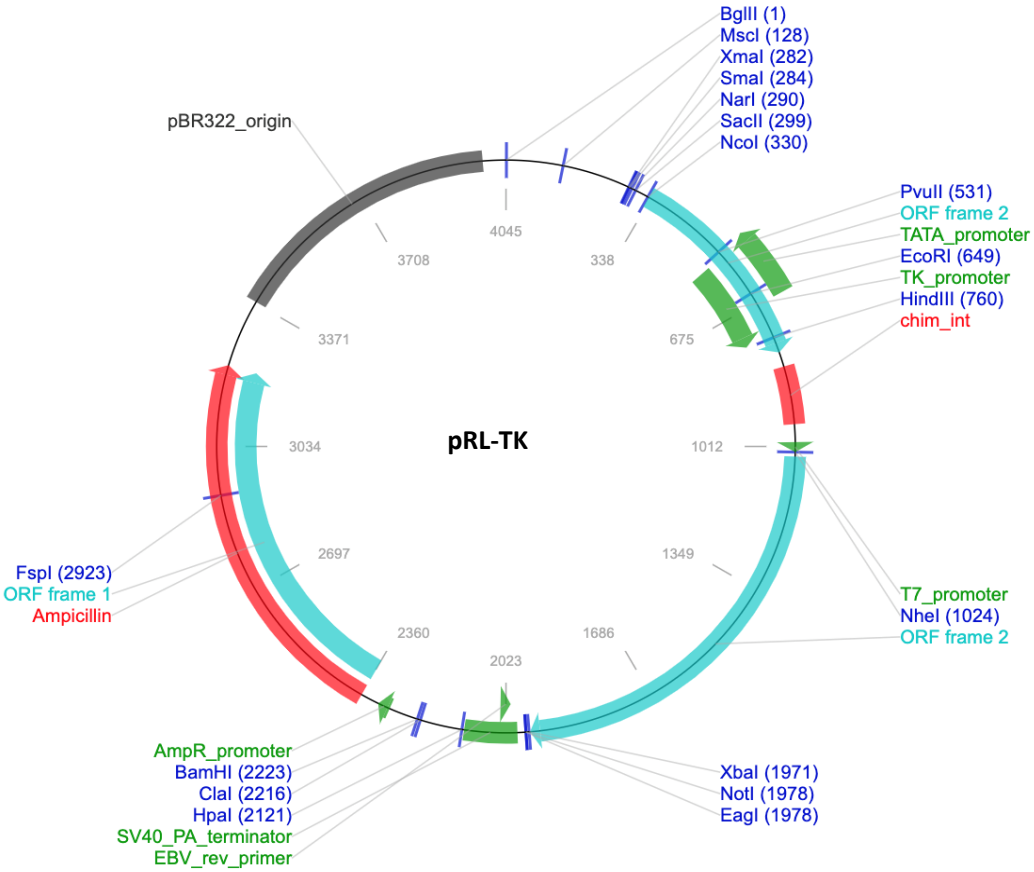
pRL-TK
BglII (1)
MscI (128)
XmaI (282)
SmaI (284)
NarI (290)
SacII (299)
NcoI (330)
PvuII (531)
ORF frame 2
TATA_promoter
EcoRI (649)
TK_promoter
HindIII (760)
chim_int
T7_promoter
NheI (1024)
ORF frame 2
XbaI (1971)
NotI (1978)
EagI (1978)
AmpR_promoter
BamHI (2223)
ClaI (2216)
HpaI (2121)
SV40_PA_terminator
EBV_rev_primer
FspI (2923)
ORF frame 1
Ampicillin
pBR322_origin
4045
338
675
1012
1349
1686
2023
2360
2697
3034
3371
3708